MAGNETOM Flash

The Magazine of MR

Issue Number 3/2007
RSNA Edition

SIEMENS

Women's Health

Dynamic VIEWS, Inter-VIEWS, RADIANT and Tim
Page 16

Use of MRI in Detecting Clinically and Mammographically Occult Ductal Carcinoma In Situ. Two Case Reports
Page 24

Diffusion-weighted Imaging in Breast MRI
Page 28

MR Spectroscopy of the Breast
Pages 38 and 41

Clinical

Prostate Cancer
Page 48

7 Tesla MR – Musculoskeleteal Imaging
Page 96

Exceeding the Limits with *syngo* TimCT
Page 6

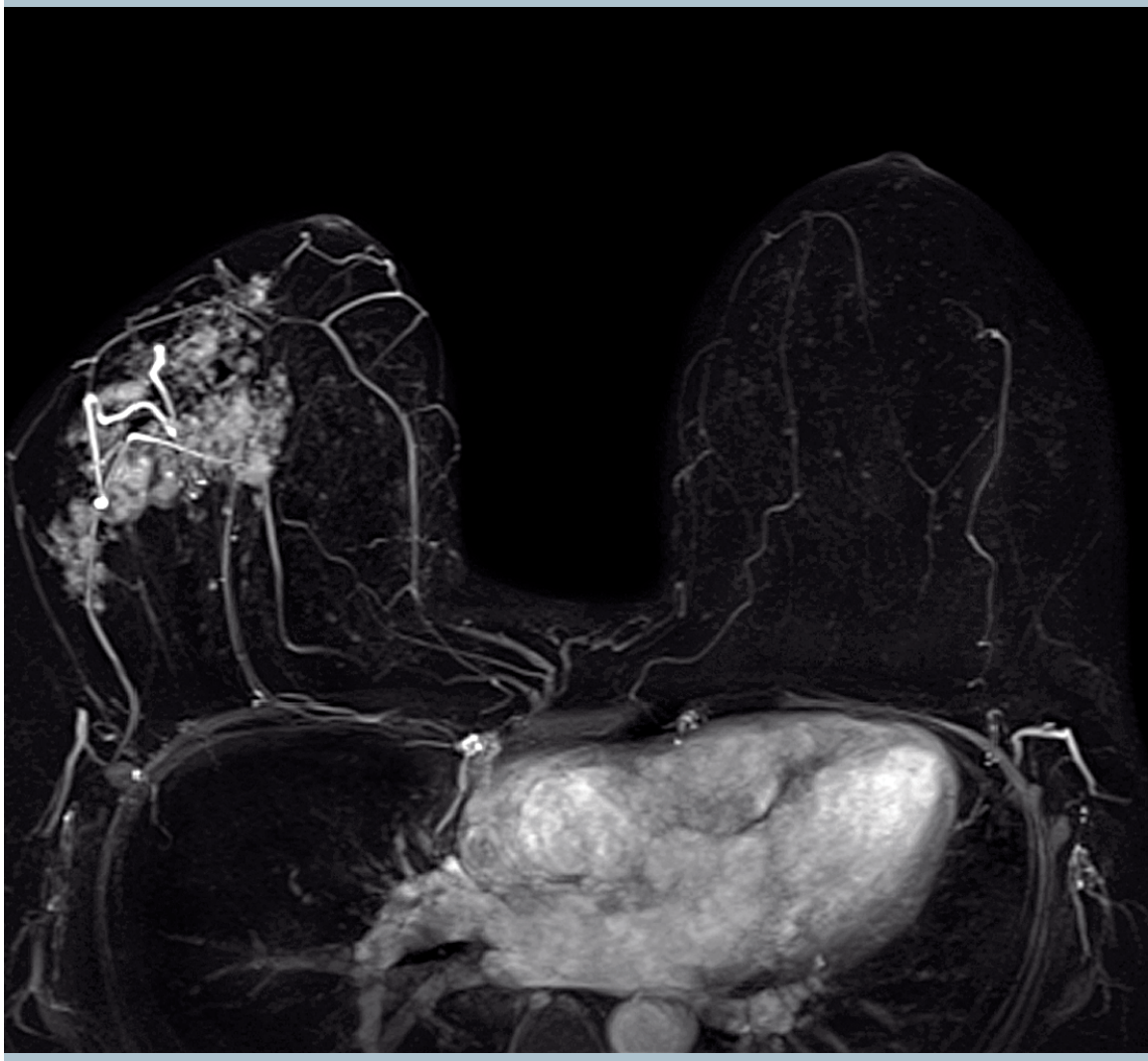

37

Dear MAGNETOM user,

MAGNETOM ESSENZA is possibly the most affordable 1.5 Tesla system today, not only for its price, but also for its low-cost of installation, operation and maintenance. For this issue of MAGNETOM Flash we have created an image gallery that gives proof of the ESSENZA's image quality for head to toe routine clinical imaging.
Breast MRI is an excellent supplemental tool to mammography to help diagnose breast cancer. In this issue we present examples of state-of-the-art breast imaging including diffusion techniques and spectroscopy to enhance the diagnostic power of this technique.
While the impact of MRI is increasing every other day in the evaluation of breast cancer, the excellent article from Dr. Padhani (page 48) gives an overall view of MR prostate imaging techniques and the possible combination of anatomical and functional imaging of the prostate. Don't miss the amazing orthopedic imaging results from 7 Tesla on page 96.

Enjoy reading the Flash.

A. Nejat Bengi, M.D.

MAGNETOM Flash is part of Life, Siemens' unique customer care solution that helps you get the most from your investment. With its programs and services Life sharpens your skills so you can see optimal clinical value. It provides the support you need to maximize productivity and it assures that as technology changes, you will always be at the cutting edge.

The Editorial Team

We appreciate your comments.
Please contact us at magnetomworld.med@siemens.com

A. Nejat Bengi, M.D.
Editor in Chief

Antje Hellwich
Associate Editor

Dagmar Thomsik-Schröpfer,
Ph.D., MR Marketing-Products,
Erlangen, Germany

Cécile Mohr, Ph.D.
Head of Market Segment
Management, Erlangen

Heike Weh,
Clinical Data Manager,
Erlangen, Germany

Bernhard Baden,
Clinical Data Manager,
Erlangen, Germany

Peter Kreisler, Ph.D.
Collaborations & Applications,
Erlangen, Germany

Milind Dhamankar, M.D.
Director, MR Product
Marketing, Malvern, USA

Kathleen Giannini,
US Installed Base Manager,
Malvern, PA, USA

Gary R. McNeal, MS (BME)
Advanced Application Specialist,
Cardiovascular MR Imaging
Hoffman Estates, USA

Dr. Sunil Kumar S.L.
Senior Manager Applications,
Canada

Tony Enright, Ph.D.
Asia Pacific Collaborations,
Australia

Content

Technology

6 Exceeding the Limits with *syngo* TimCT

Image Gallery

12 Image Gallery: The Beauty of Life

Clinical Women's Health

16 Dynamic VIEWS, InterVIEWS, RADIANT and Tim: Advanced MR Techniques for Breast Cancer Imaging

24 Use of MRI in Detecting Clinically an Mammographically Occult Ductal Carcinoma in Situ. Two Case Reports

28 Diffusion-Weighted Imaging in Breast MRI – An Easy Way to Improve Specificity

33 Potential Role of Multi b Factor Diffusion-weighted Imaging of the Breast

38 Quantification of Total Choline in Breast Tumors using *syngo* GRACE and PRISMA: Initial Experience at 1.5T

41 ^{1}H MR Spectroscopy of the Breast

44 *syngo* GRACE

46 Case Report: Role of MRI Imaging in a Gynecological Emergency of Ectopic Pregnancy

Clinical Abdomen/Pelvis

48 Prostate Cancer – Meeting Clinical Needs by Advanced MRI at Diagnosis and on Follow-Up

60 The Clinical Advantages of T2-weighted MR Imaging in the Female Pelvis with *syngo* BLADE

63 3D MR Cholangiopancreatography and Volume Rendering: a Perfect Liaison

70 Both Morphological and Functional Assessments of Congenital Urinary Tract Abnormality using 3D Sequences

Clinical Neurology

74 Clinical Applications of Diffusion Tensor Imaging

88 Indian Experience with *syngo* SWI at 3T MAGNETOM Trio, A Tim System

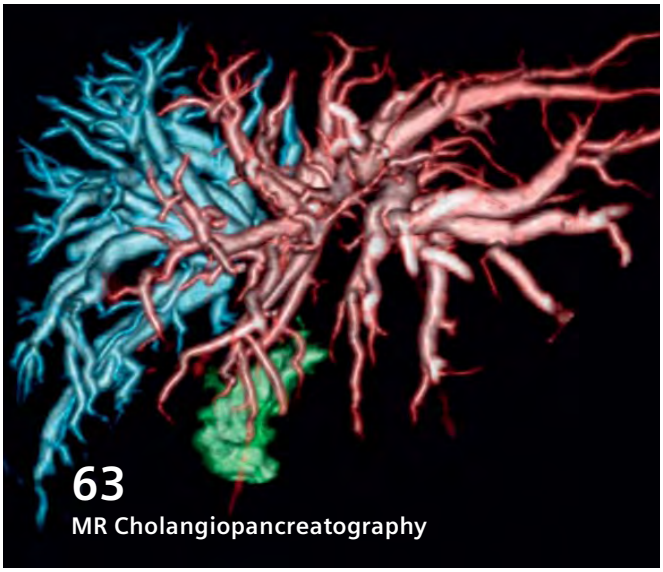

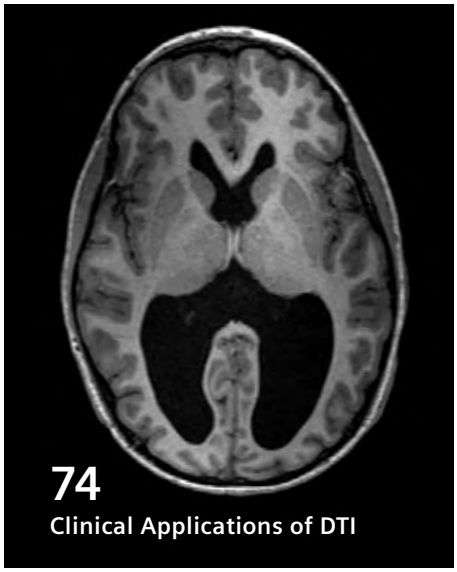

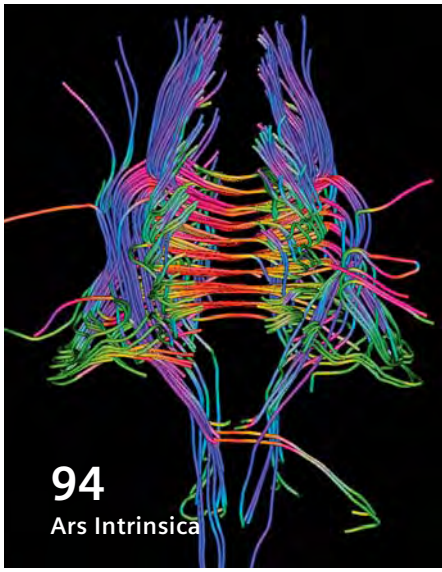

Image Gallery

94 Image Gallery Ars Intrinsica

Clinical Orthopedics

96 7 Tesla MR – Musculo-skeletal Imaging

Clinical Cardiovascular

100 High Spatial and Temporal Resolution MRA of the Entire Peripheral Vascular System Using a New 3D Time-Resolved MRA Technique (*syngo* TWIST)

102 High Spatial and Temporal Resolution MRA in Acute Aortic Dissection

Clinical → How I do it

104 MR Mammography: How I Do it

107 Improved Planning Strategies for Reduced Imaging Time

110 Neuro 3D – A Clinical Exam

114 Fat Suppression in the Abdomen

Product News

120 70 cm Bore in Clinical Practice: Why It Works

129 Tim proves to be a Total improvement

Image Gallery

148 7T Musculoskeletal (MSK) Imaging

Life

150 Innovations '07: Siemens Annual Education Symposium for Technologists and IT Customers

152 "ars intrinsica" – MR images in another setting

"The future is here. It's just not widely distributed yet." (William Ford Gibson)

Exceeding the Limits with *syngo* TimCT

Arnd-Oliver Schaefer, M.D.; Tobias Baumann, M.D.; Mathias Langer, M.D.

Department of Diagnostic Radiology, University Hospital Freiburg, Germany

Based on sliding multislice (SMS) technique *syngo* TimCT Oncology* is on the way to revolutionize axial moving-table MR imaging. The adoption of commercially-available sequences with their typical contrasts in combination with seamless data acquisition around the isocenter of the magnet and automatic coil switching render this technique extremely attractive for oncologic whole-body work-up. Besides image quality, one of the most striking features of TimCT Oncology is time efficiency. Technical refinements like motion correction and online reconstruction help to minimize artifacts. Our own investigations clearly point out the high diagnostic accuracy of the procedure which has been used for oncologic staging since the end of 2005. Experiences with Sliding Multislice are available for whole-body staging of rectal cancer, gynecologic malignancies, prostate cancer, breast cancer, lung cancer, gastrointestinal stromal tumors (GIST), plasmocytoma, lymphomas and for diagnostic work-up of patients with Crohn's disease.

In MAGNETOM Flash issue no. 1/2007 we previously reported on technical aspects and initial results of sliding multislice moving-table MRI [1, 2]. Concerning abdominal tumor staging our data was so encouraging that in a first step a shift in rectal cancer work-up could be established at our institution [3, 4]. Additionally, the technique has also gained acceptance as an imaging tool for patients with Crohn's disease.

Have we already reached the top of the ladder?

Certainly not. In a second step our investigations focused on extending the procedure to the lungs in order to obtain a real one-stop-shop imaging for tumor patients. For pulmonary nodule detection the free-breathing TIRM sequence from the SMS protocol was compared to multislice CT as the reference standard with unexpected results. The study identified a total of 321 nodules. On a per-patient basis the sensitivity and specificity for pulmonary nodule detection with the free-breathing TIRM were 81.8% and 94.7% respectively. Receiver operating characteristic (ROC) analysis revealed high values of specificity ranging between 91.6% and 99.1% with average mean sensitivities above 90.2% for lesions larger than 3 mm in diameter and accuracies over 94.5%. Noteworthy, the technique can be utilized almost independently of patient compliance. All clinically-relevant lung lesions are distinguishable and thus can be monitored during follow-up.

What are our opinions about *syngo* TimCT Oncology to date?

The major benefit of this technology represents seamless imaging from head to thighs within a few minutes acquiring 2 different image contrasts. Consequently, the procedure is easily applicable as an adjunct to dedicated high-resolution MRI for local tumor staging especially in patients with pelvic malignancies. Patient repositioning and stepwise examination for whole body coverage are completely omitted. The disadvantage of inferior lesion characterization using SMS technique instead of standard MRI will be removed in the near future by implementation of additional image contrasts and continual technical optimization. From a user's point of view sliding multislice moving-table MRI embedded in the upcoming *syngo* TimCT Oncology package has meanwhile reached a high degree of practicability and substantial acceptance. TimCT Oncology represents a cutting-edge technology for cancer staging with whole-body MRI and has the potential to dramatically improve patient workflow.

*Works in progress (WIP). The information about this product is preliminary. The product is under development and not commercially available in the U.S., and its future availability cannot be ensured.

References

1 Fautz HP, Kannengiesser SA. Sliding Multislice (SMS): a new technique for minimum FOV usage in axial continuously moving-table acquisitions. Magn Reson Med 2006;55:363–370.

2 Fautz HP, Honal M, Saueressig U, Schaefer O, Kannengiesser SA. Artifact reduction in moving-table acquisitions using parallel imaging and multiple averages. Magn Reson Med 2007;57:226–232.

3 Schaefer O, Langer M. etection of recurrent rectal cancer with CT, MRI and PET/CT. Eur Radiol 2007;17:2044–2054.

4 Schafer AO, Baumann T, Pache G, Wiech T, Langer M. Preoperative staging of rectal cancer. Radiologe 2007 [Epub].

Female with pulmonary metastatic extraskeletal mesenchymal chondrosarcoma of the heel.

Combined local high-resolution MRI of the ankle and *syngo* TimCT Oncology for M-staging.
Subsequent thoracic multislice computed tomography (MSCT).

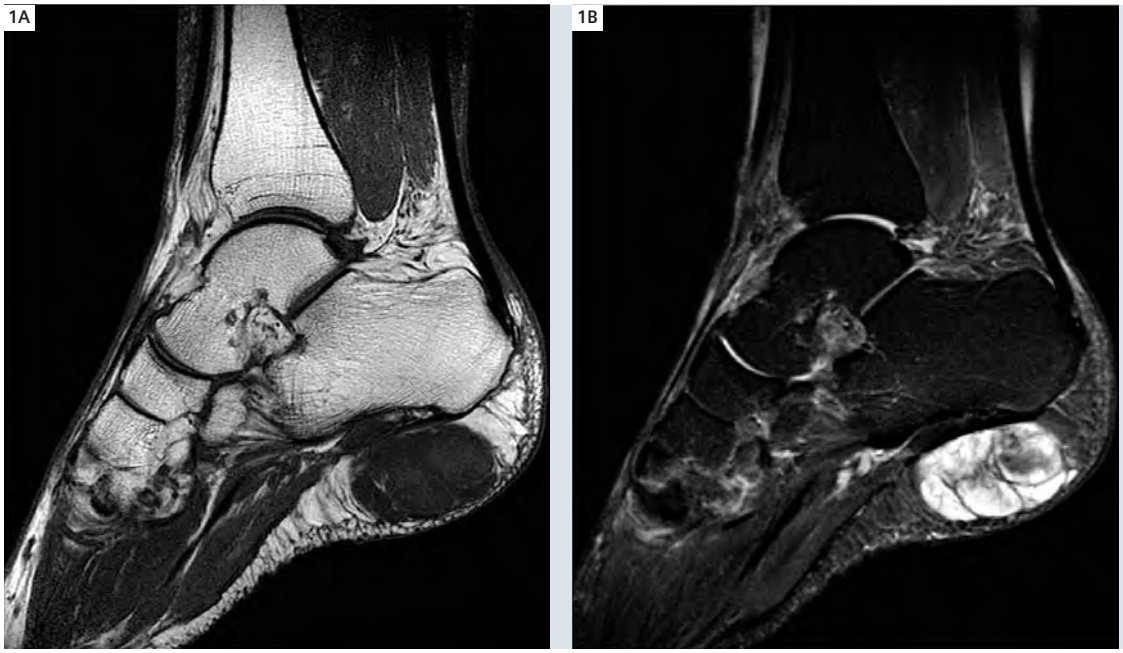

1 Sagittal T1-weighted TSE and TIRM images reveal the primary tumor within the subcutaneous tissue of the right heel.

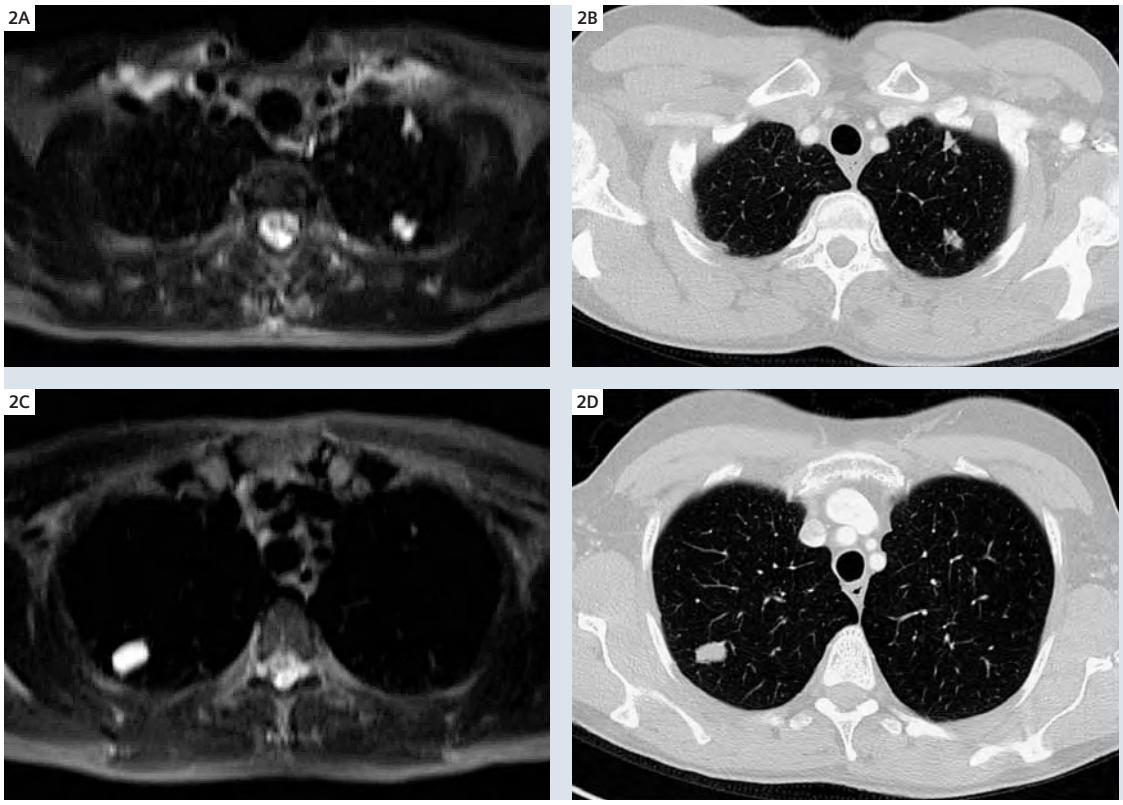

2 Axial sliding multislice free-breathing TIRM images and corresponding MSCT images demonstrate multiple pulmonary metastases.

Continued on page 8

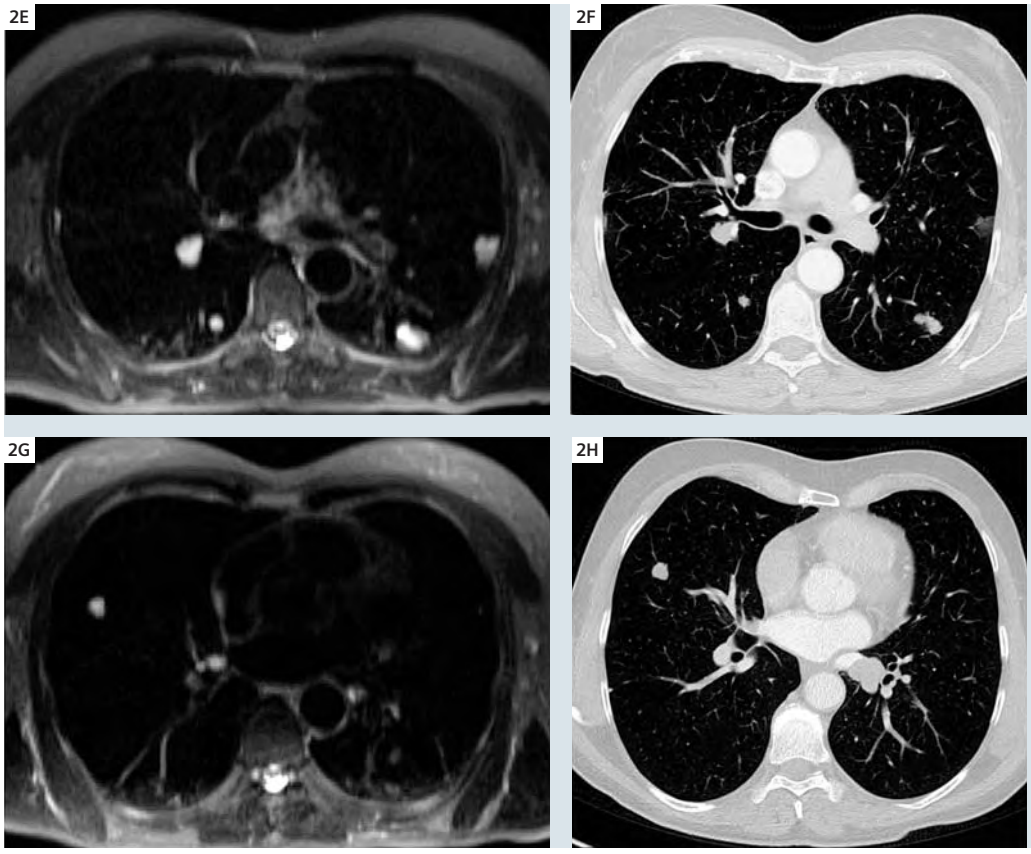

2 Axial sliding multislice free-breathing TIRM images and corresponding MSCT images demonstrate multiple pulmonary metastases.

Female with FIGO (International Federation of Gynecology and Obstetrics) stage IV left ovarian cancer:

Peritoneal carcinosis with subileus, ascites, pleural effusions and lymph node metastases.
Combined local and M-staging performing dedicated pelvic and MR imaging with *syngo* TimCT Oncology.

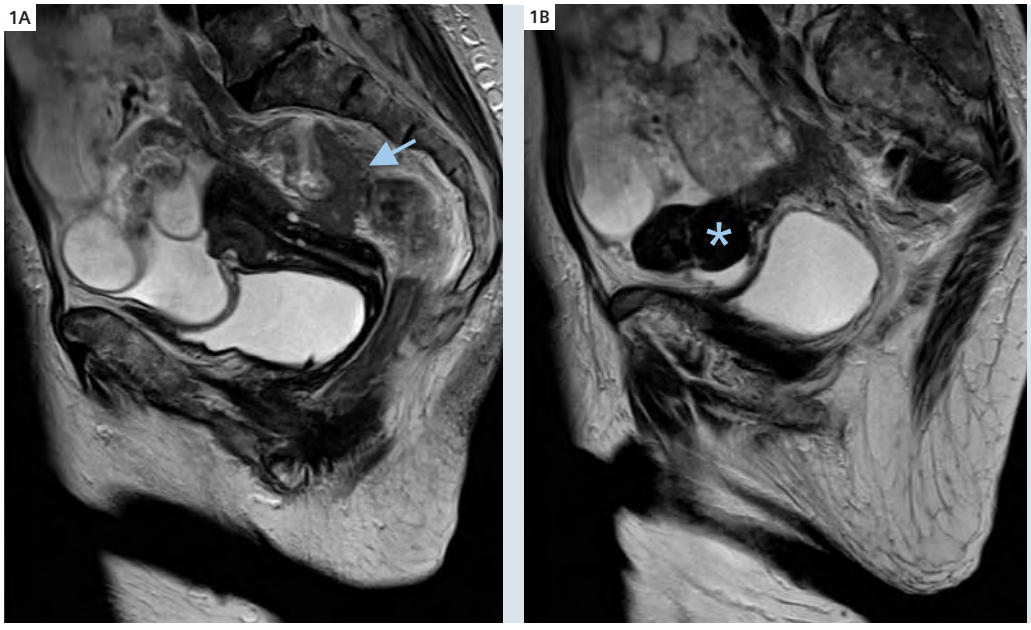

1 On the sagittal and axial T2-weighted TSE images detection of a low-signal left ovarian carcinoma (asterisk), an advanced peritoneal carcinosis (arrow), a left iliac lymph node metastasis (arrow), ascites and subileus.

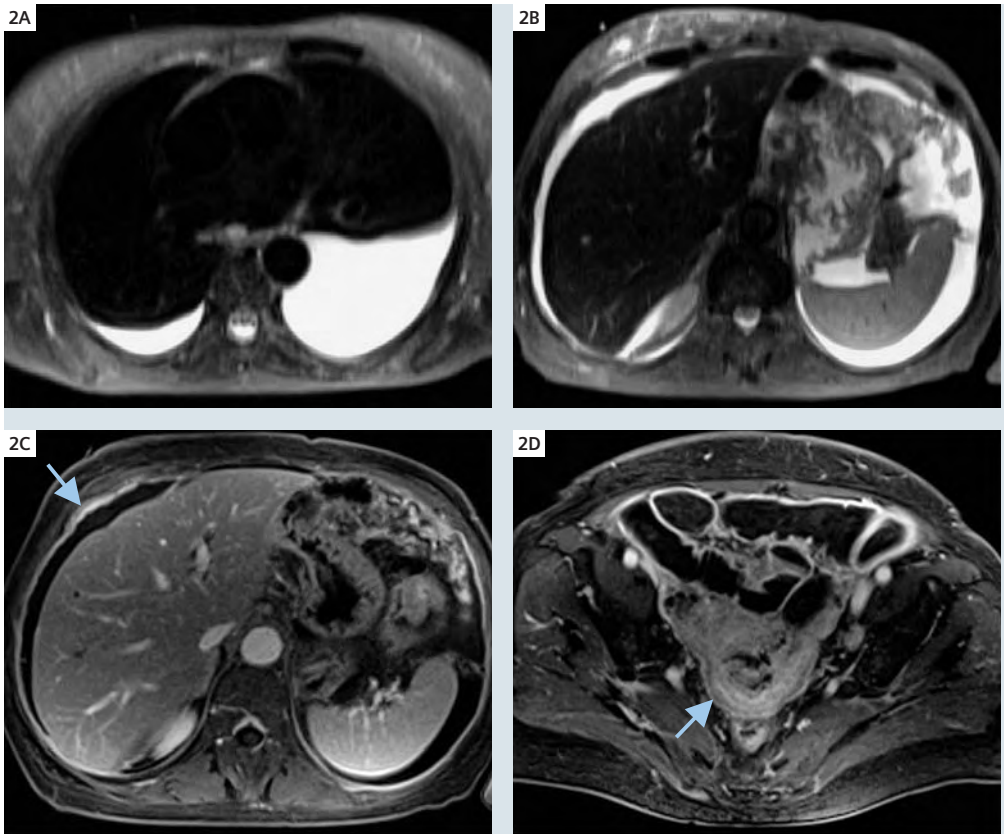

2 Axial sliding multislice free-breathing TIRM and contrast-enhanced breathhold FLASH-2D images reveal pleural effusions, ascites and peritoneal carcinosis (arrows).

Male with recurrent prostate cancer, initially pT4N1. Moving-table staging using *syngo* TimCT Oncology.

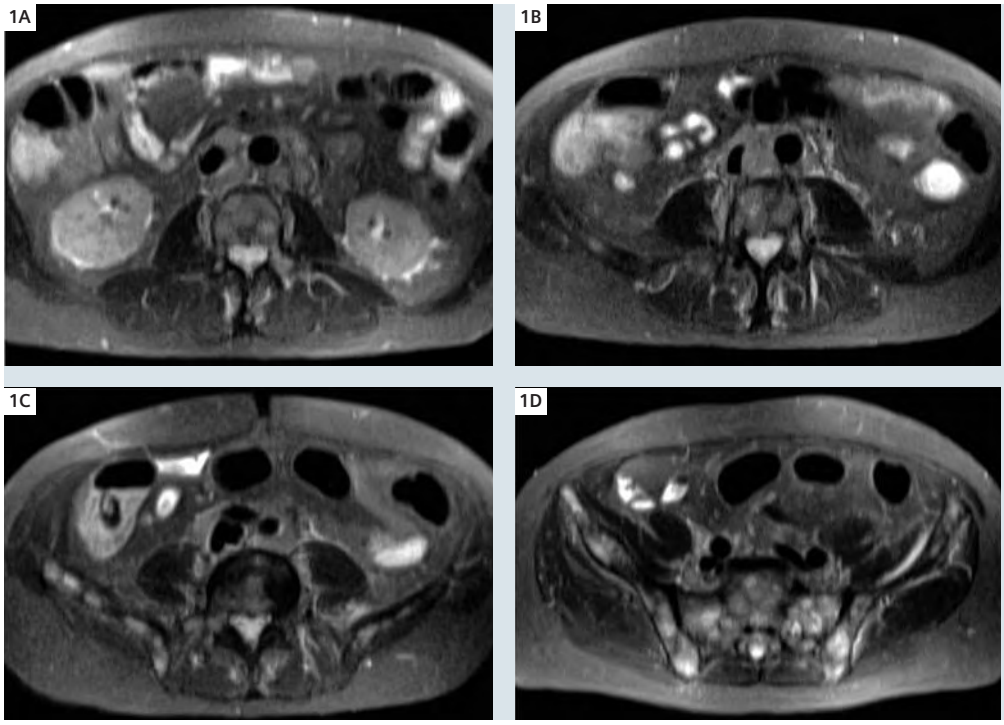

1 Axial sliding multislice free-breathing TIRM images show retroperitoneal lymph node metastases and extensive bone infiltration.

Continued on page 10

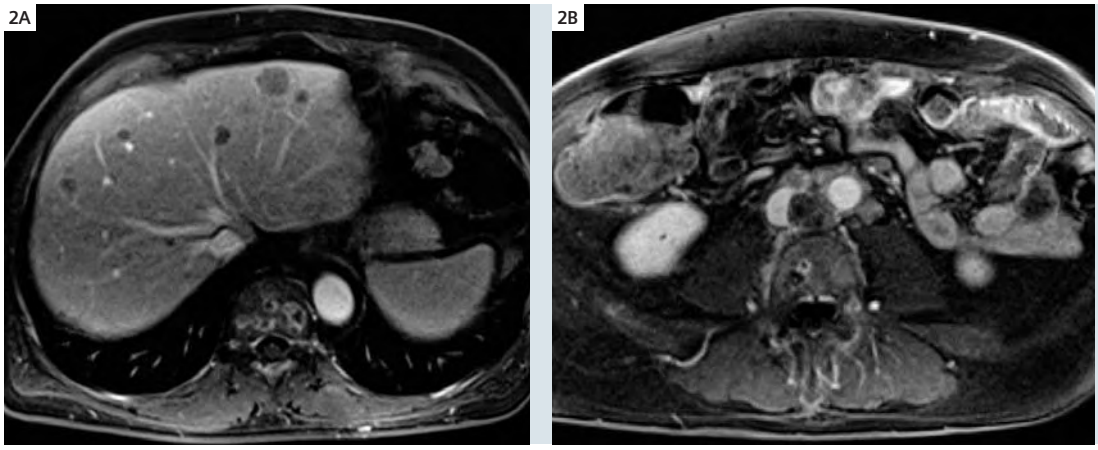

2 On the axial sliding multislice contrast-enhanced breathhold FLASH-2D images liver metastases are apparent. The confluent retroperitoneal lymph node metastases causing compression of the inferior vena cava.

Male with stage cT3N2M1 neuroendocrine cacinoma of the rectum. Diffuse hepatic and osseous metastatic disease, soft tissue metastases. Combined local and M-staging using *syngo* TimCT Oncology.

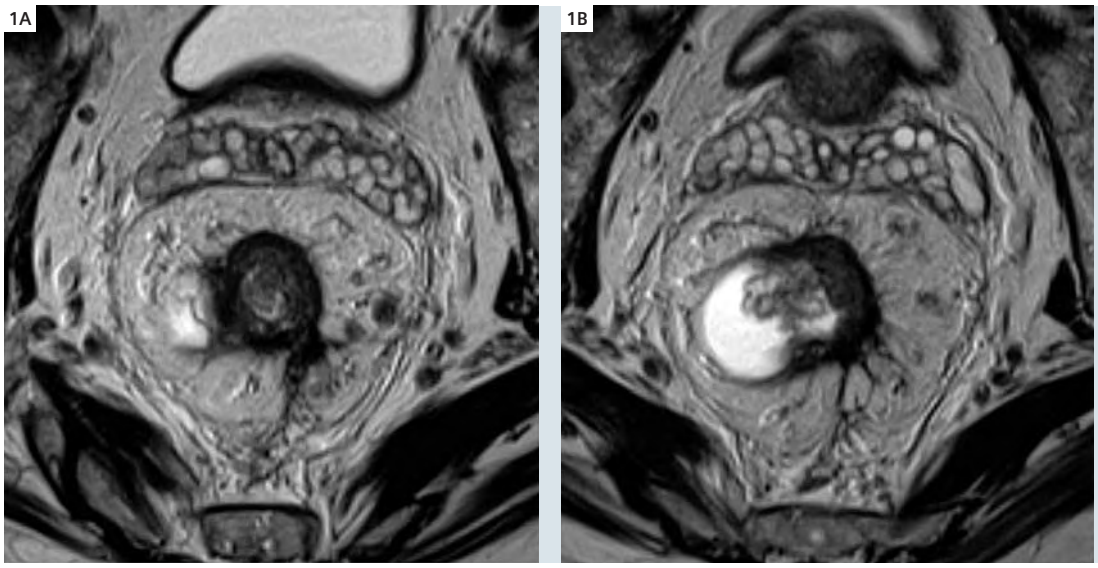

1 Axial T2-weighted TSE images demonstrate stenosing, wall-exceeding rectal cancer with adjacent mesorectal lymph node metastases.

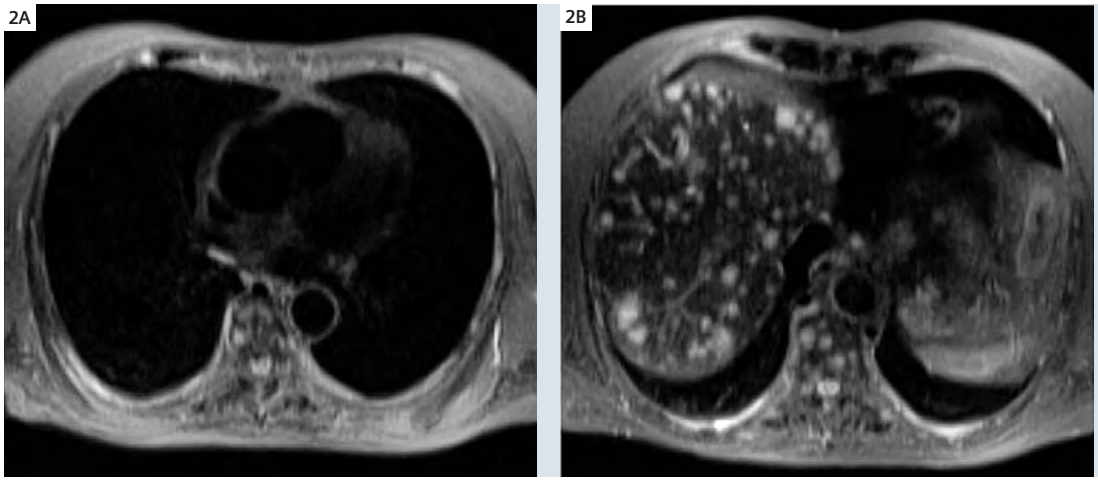

2 Axial sliding multislice free-breathing TIRM images show normal lung, diffuse bright-signal liver metastases, multiple bone metastases and a small metastasis in the erector spinae muscle (arrow in Fig. 2D).

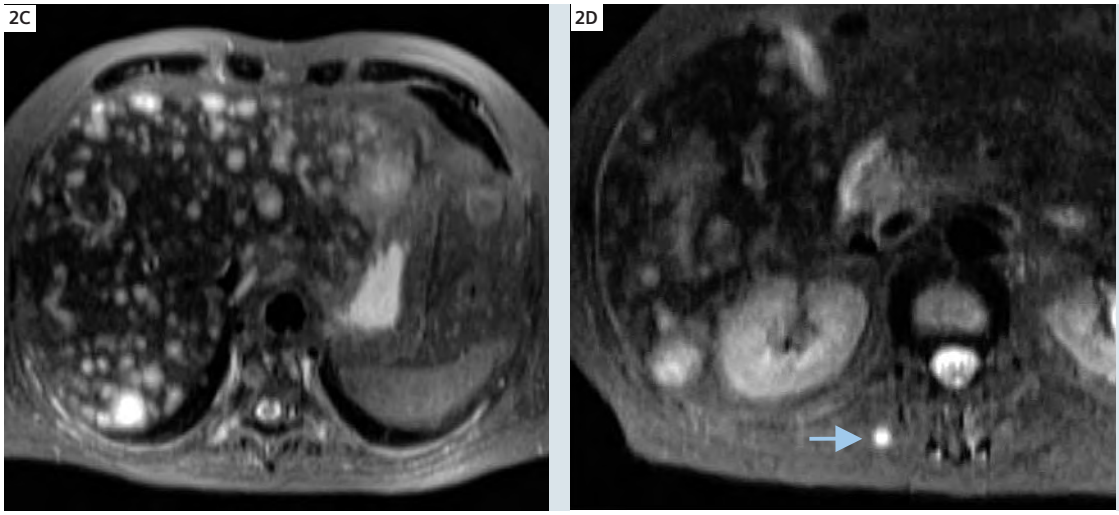

2 Axial sliding multislice free-breathing TIRM images show normal lung, diffuse bright-signal liver metastases, multiple bone metastases and a small metastasis in the erector spinae muscle (arrow).

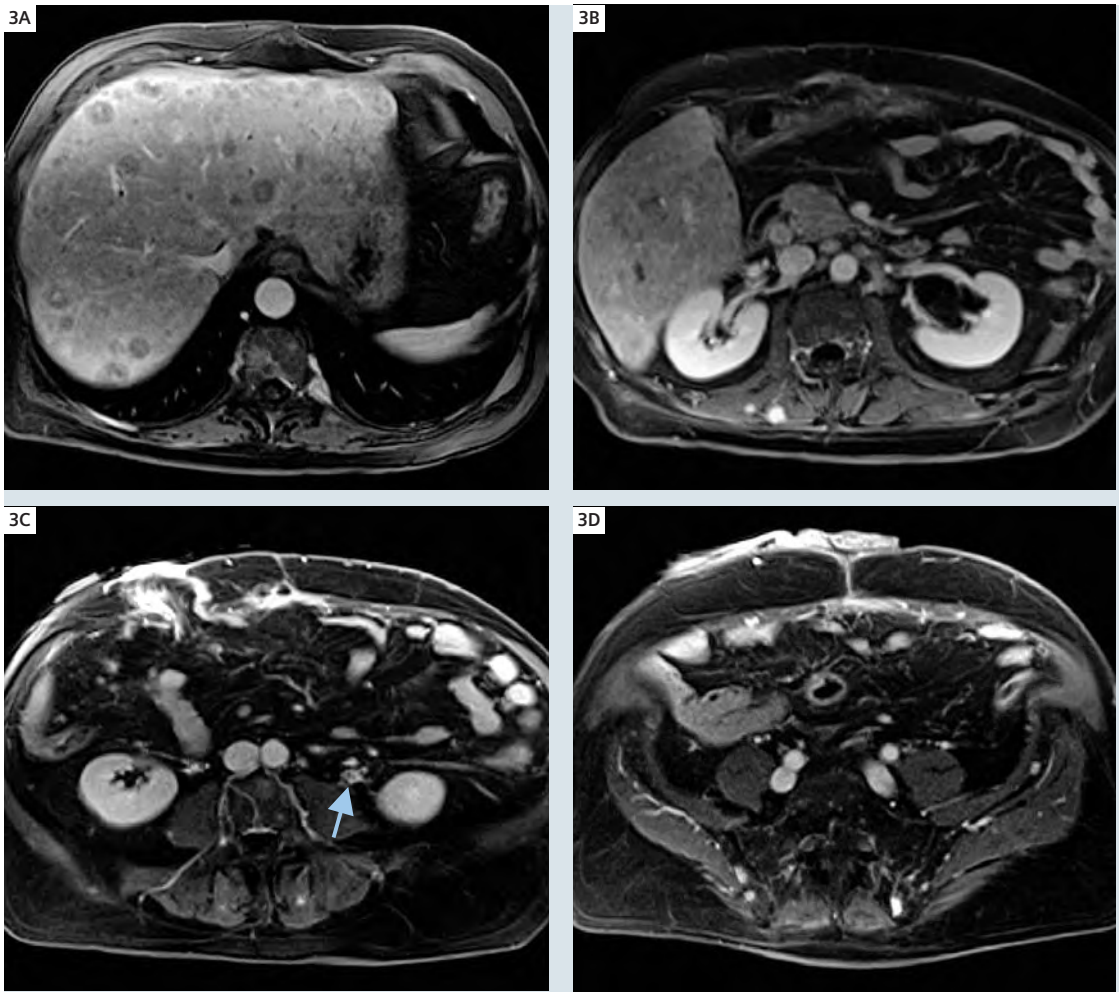

3 Axial sliding multislice contrast-enhanced breathhold FLASH-2D images reveal liver metastases, left hydronephrosis due to ureteral infiltration (arrow), small metastases in the erector spinae muscle and hypervascular bone metastases.

The Beauty of Life

Hui-Cheng Cheng, M.D., Ph.D.

VGH Healthtech International, Taiwan

Goal

Besides medical application and scientific research, MRI can also be used to engrave lives and to inspire imagination. We have tried to explore and present the beauty of life through MR imaging.

Materials and Methods

MR imaging by clinical scanner (MAGNETOM Symphony, A Tim System, Siemens, Erlangen, Germany) utilizing the knee coil was performed for the following objects:

Fruit: Acquired in T2-weighted imaging technique, 3D fast imaging by steady state free-precession (TrueFISP) (TR/TE = 8.14/4.07 ms; flip angle = 50°; FoV = 160 mm; matrix = 320 x 320; slice thickness = 0.2–0.4 mm; average = 1).

Flowers: Acquired in T1-weighted imaging technique, 3D volumetric interpolated breathhold magnetic resonance imaging (VIBE) (TR/TE = 9.35/4.76 ms; flip angle = 120; FoV = 160 mm; matrix = 512 x 512; slice thickness = 0.2-0.4 mm; average = 2). Flowers and plants were soaked in diluted (1:100) 0.5M Gadodiamide (Omniscan, Amersham Health, Cork, Ireland) for 1–2 days before scanning.

Seashells: Acquired in T1-weighted imaging technique, the sequences and the parameters used were as in Flowers. The objects were soaked in diluted (1:100) 0.5M Gadodiamide before scanning.
All the images had been postprocessed by using Maximum Intensity Projection (MIP), MultiPlanar Reconstruction (MPR) or 3D Volume Rendering Technique (VRT).

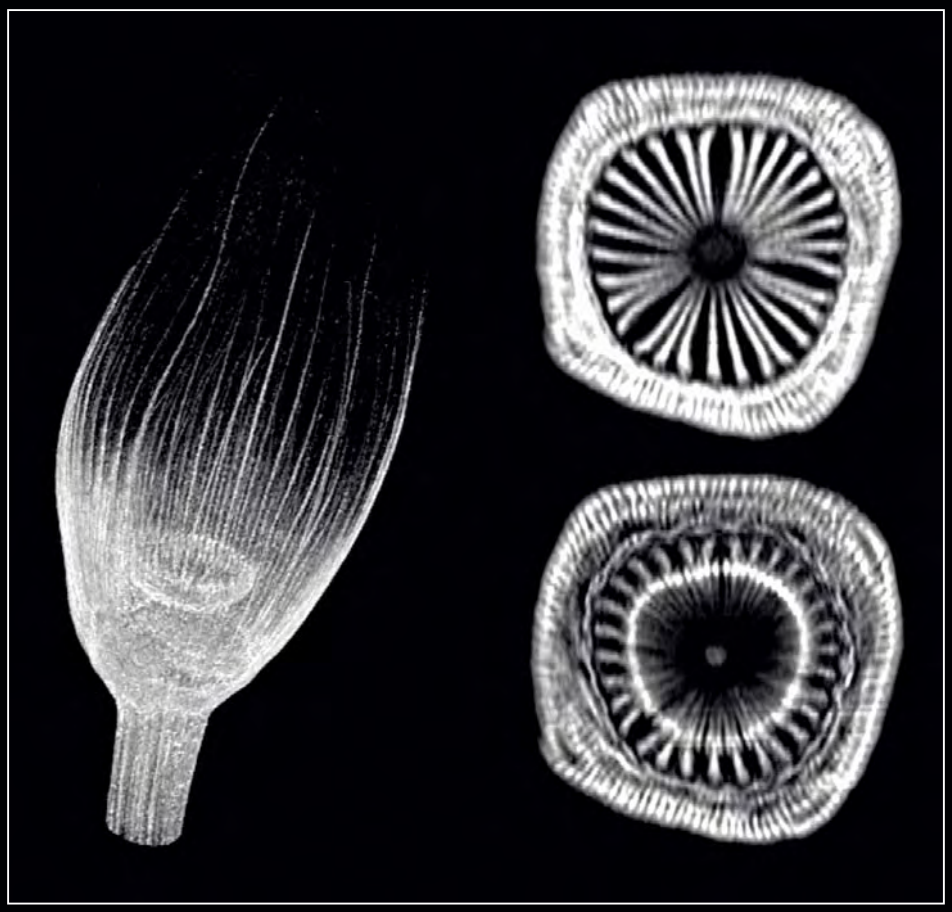

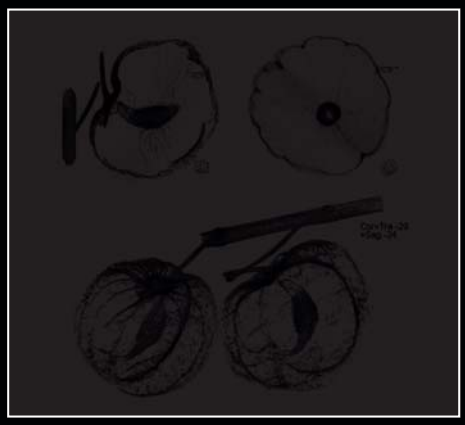

Discussion

Fruits generally have more water content, better to be acquired by T2-weighted imaging. 3D TrueFISP provides fast T2-weighted images with high resolution and good signal-to-noise ratio (SNR). But to be able to show the veins in the petals, stamen and stigma of a flower, soaking in diluted gadolinium before scanning is needed so that the flowers could enhance when using 3D VIBE. However, some flowers do not uptake gadolinium readily, such as sunflower and rose. Seashell has unique spiral skeleton that is exceptional and intriguing. The seashell does not have any water element to be visualized in MR imaging. Placing the objects in diluted gadolinium solution provides negative contrast during scanning with both 3D TrueFISP and 3D VIBE. The results of TrueFISP were superior in SNR but had less field homogeneity. We also tried fly-through technique to navigate the inside of a seashell.

Conclusion

The 3D data set allows to demonstrate the superficial and internal details of the objects thereby enabling us to photograph nature in a very unique way. MRI can provide an additional perspective to reveal the beauty of life, which we have not yet experienced.

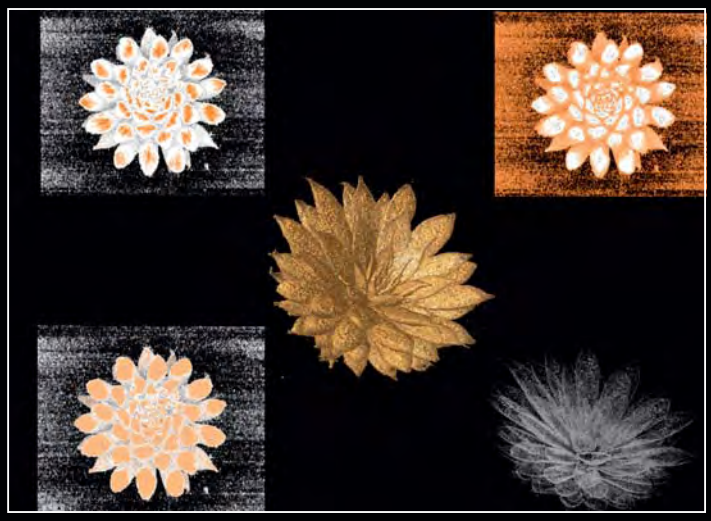

Dynamic VIEWS, InterVIEWS, RADIANT and Tim: Advanced MR Techniques for Breast Cancer Imaging

Bruce A. Porter, M.D., FACR[1]; Helmuth Schultze-Haakh, Ph.D.[2]

[1]*First Hill Diagnostic Imaging – Swedish Medical Center, Seattle, Washington, USA*
[2]*Siemens Medical Solutions USA, Inc., Cypress, CA, USA*

Introduction

In the early 1990's initial clinical applications of magnetic resonance imaging of the breast, relied either on a series of low-resolution dynamic (kinetic) images or longer, high-resolution (morphologic) images to differentiate benign from malignant processes. Current MR equipment, however, allows a hybrid technique, providing both kinetic data and high-resolution morphologic information in one exam. VIEWS: Volume Imaging with Enhanced Water Signal, developed for Siemens MR systems, is a high-resolution 3-dimensional gradient-echo acquisition technique with fat suppression. The hybrid form combines time limited acquisitions, DynamicVIEWS, and an additional higher resolution acquisition interspersed between the DynamicVIEWS: InterVIEWS. The kinetic and morphologic approaches each have their individual strengths and limitations; however, the combination of these methods provides functional information (enhancement curves) and thin section, high-resolution 3D data sets with great anatomic detail, thus improving characterization of enhancing masses. This report illustrates the complementarity of these two methods and the current status of MR breast imaging, with a focus on key situations where this unique exam impacts, often substantially, clinical care of patients with known or suspected breast cancer.

Case 1: Multicentric and occult contralateral invasive breast cancer

This 48-year-old woman, a health care provider herself, noticed a new density in her left breast. Her mammograms were extremely dense, with no indication of cancer, asymmetrical masses, or malignant-type calcifications, even in retrospect. An ultrasound-guided biopsy of the palpable lesion revealed a high-grade infiltrating ductal carcinoma. She was referred for MR of the breasts to determine the extent of tumor and for staging. On MR, in addition to the known 1.3 cm tumor in the lower inner quadrant of the left breast (Fig. 1A), a second suspicious, spiculated 0.6 cm lesion with rapid washout kinetics was detected in the posterior upper inner quadrant; this was subsequently confirmed with ultrasound. Additionally, in the con-

1A Axial full maximum intensity projection (MIP) from the first post-contrast subtraction images reveals the known cancer in the medial left breast and a smaller suspicious finding posteriorly (arrow). Additionally a markedly vascular, unsuspected, contralateral (right) cancer was detected.

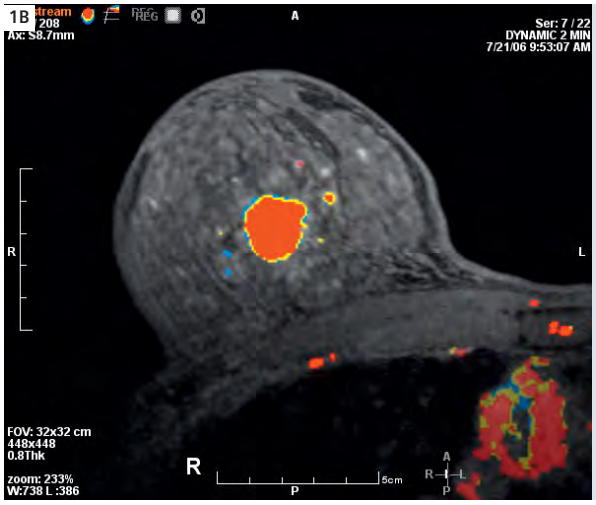

1B CAD parametric image documents in red the rapid enhancement and washout kinetics of the right breast cancer and of a small satellite lesion medially.

1C High quality oblique MIP image is possible from the dynamic images because of thin sections and good in-plane resolution, and the use of interpolation. The second left cancer is subtle on this image, but visible near the chest wall (arrow).

tralateral (right) breast a markedly enhancing 2 cm clinically and mammographically occult tumor was detected and confirmed at subsequent mastectomy. The DynamicVIEWS series provides not only kinetic data for parametric analysis using a CAD system (Confirma, Inc.) as seen in figure 1B, but also has resolution sufficient to produce detailed oblique Maximum Intensity Projection (MIP) images (Fig. 1C) for correlation with MLO (medial lateral oblique) mammograms.

Comment

The patient elected bilateral mastectomies; the left breast cancer (known) was determined to be Stage 1, whereas several small tumor nodules were found in the sentinel lymph node on the right, resulting in a Stage 2 classification. Hence, the occult contralateral tumor was not only larger than the presenting mass, but already involved the axillary lymph nodes.

Case 2: MR of the breasts for preoperative planning

A 32-year-old woman noted a firm mass, nipple retraction, and diminished milk production in her right breast during lactation. Ultrasound demonstrated a 2.2 cm solid mass, and mammography revealed micro-calcifications of the "casting-type" over 5 cm in extent (Fig. 2A). Biopsy confirmed mixed infiltrating ductal and in situ carcinoma, as suspected.

MR was requested to determine extent of the tumor, to assess the contralateral breast, and for staging. The axial maximum intensity projection (MIP) images (Fig. 2B) and corresponding parametric images (Fig. 2C) revealed a markedly vascular, irregular mass with malignant enhancement, and large draining veins involving the majority of the central right breast. High-resolution InterVIEWS images (Fig. 2D) revealed a mixed pattern, with a spiculated, solid 2.3 cm invasive mass, surrounded by a mixed solid and ductal enhancement consistent with high-grade in situ carcinoma, which was confirmed by mastectomy. The MR findings, readily understood by the patient, allowed her and her surgeon to determine together that mastectomy was clearly the appropriate surgical therapy. Pre-operative breast MR is a very helpful communication tool for the surgeon to discuss treatment options with the patient, to determine the extent of tumor, and to decrease the requirement for surgical re-excision for inadequate or positive surgical margins [Ref: Beatty and Porter].

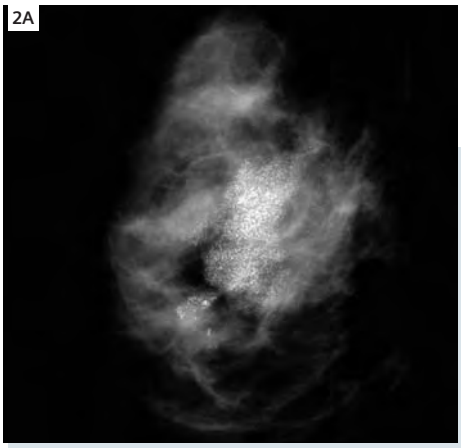

2A Right medial lateral oblique (MLO) mammogram shows extensive malignant calcifications in the mid breast to upper outer quadrant.

2B The extent of tumor is even greater than suspected on the abnormal mammogram, with regional malignant enhancement and large asymmetrical veins. The left breast has a few physiological foci, but is negative for cancer.

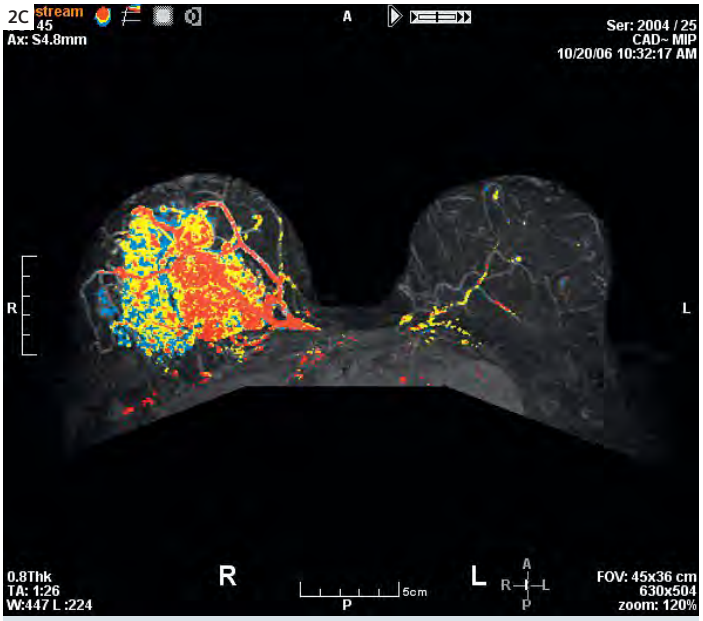

2C Parametric enhancement images dramatically document the markedly abnormal vascularity that is characteristic of such high-grade and potentially lethal tumors.

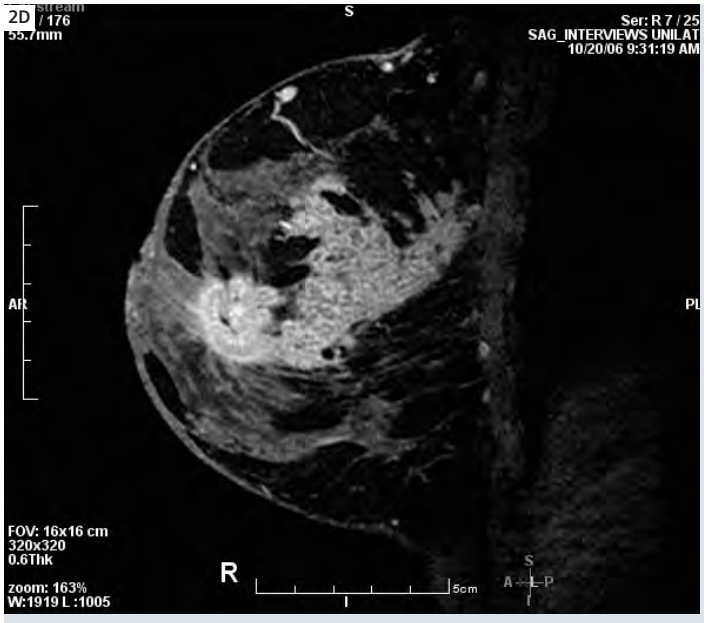

2D,E Right breast: two images from the same uni-lateral, sagittal InterVIEWS series at different slice locations. The invasive cancer is mass-like and more anterior, whereas the in situ tumor extends almost to the chest wall and is partly solid and partly ductal in appearance.

Case 3:
Prior history of breast cancer: detection of clinically and mammographically occult, early breast cancer

A 43-year-old woman with a history of left breast carcinoma and mastectomy 5 years earlier was undergoing annual mammographic and MR surveillance for contralateral disease. She had a very strong family history of breast cancer. Recent mammograms were negative. However, a new clumped and ductal morphologic pattern of enhancement was noted on the MIP images in the axial and oblique projections (Figs. 3A, 3B). These findings were not present on a prior MR exam 2 years earlier. CAD analysis revealed a mixed pattern of persistent and plateau-type enhancement, within a small spiculated nodule and adjacent branching, ductal-type enhancement in the central right breast, also well seen on the high resolution InterVIEWS images (Fig. 3C).
Due to the malignant morphologic and kinetic features, this was considered MR BIRADS (Breast Imaging Reporting and Data System) category 5 and MR-guided biopsy was undertaken, following a negative directed ultrasound of this region. The biopsy revealed high-grade in situ carcinoma. Subsequent mastectomy confirmed a small (5 mm) focus of low-grade invasive ductal cancer and surrounding in situ carcinoma, solid type with high nuclear grade. The patient elected mastectomy and had negative lymph nodes at surgery.

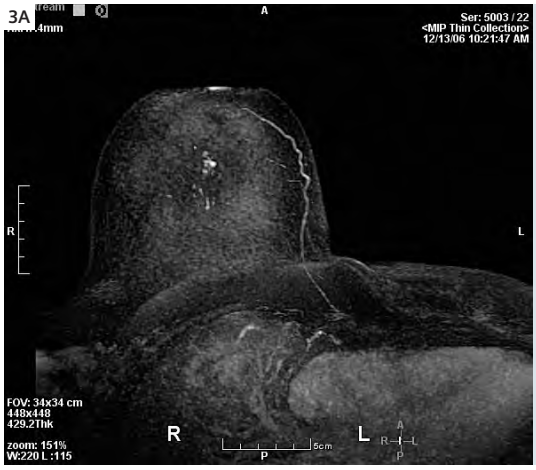

3A Axial 2 minute subtraction MIP of the remaining right breast shows a clumped abnormality not seen on a prior MR of 2 years earlier Mammogram was negative in this area, as was ultrasound.

3B Right oblique MIP better portrays the ductal pattern and anatomic detail that leads to a diagnosis of probable malignancy.

3C The high resolution sagittal InterVIEWS image shows a small mass with a neighboring linear enhancement with ductal distribution. Subtle spiculations can be identified, characteristic of an invasive malignancy.

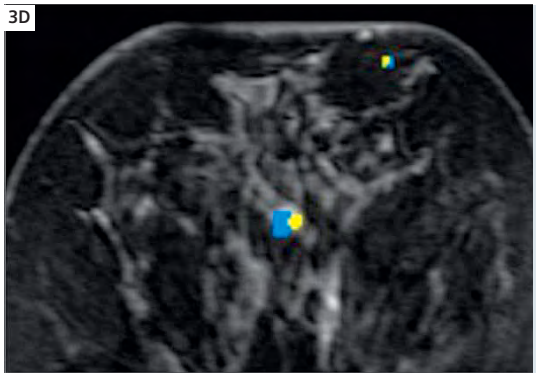

3D CAD image revealed mixed persistent and plateau type enhancement (blue and yellow, respectively) in the nodule in agreement with the morphologic assessment.

4A Axial MIP displays a normal left breast and multiple circumscribed nodules in the right breast.

4B An oblique MIP reveals and better shows that there are 4 small masses and one larger nodule.

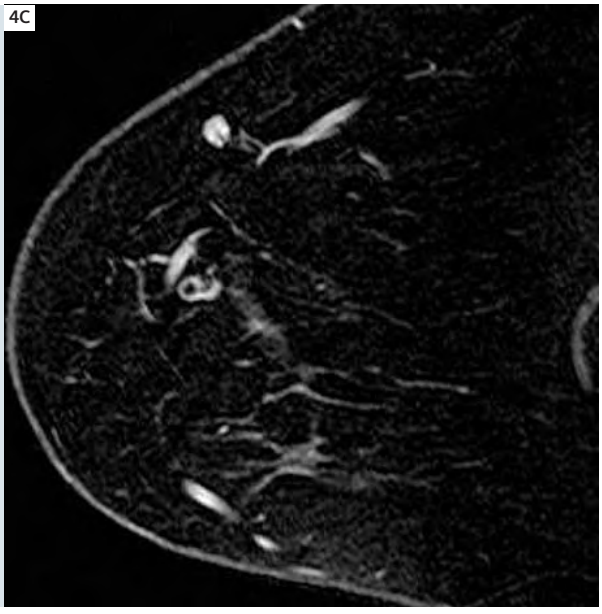

4C Sagittal 0.64 mm thick InterVIEWS image has sufficiently high resolution to diagnose these as benign intramammary lymph nodes.

Case 4: Very high resolution, 3-dimensional imaging improves characterization of benign enhancing breast masses

A 52-year-old woman with heterogeneously dense breasts, and who had a sister with breast cancer, had increasingly prominent nodular densities in the right breast on mammography, with no clear ultrasound correlate; she was then referred for MR due to her history and a problematic mammogram. MIP subtraction images (Figs. 4A, 4B) showed four small (4–8 mm) well-circumscribed, reniform masses with clearly visualized fatty hila and benign type kinetics: characteristics of benign intramammary lymph nodes. The near isotropic voxels (0.64 x 0.5 x 0.5 mm) and consequent very high resolution of the InterVIEWS images (Fig. 4C) allows detailed radial (RADIANT = RADial Imaging Around Nipple or Tumor) reconstructions at 1.5 degree intervals (Fig. 4D); this technique provided even greater diagnostic confidence. A classification of MR BIRADS category 2, benign, was given for the nodes.

The extremely thin slice thickness is also key to high quality multiplanar and radial images. This allows delineation of the full and complete surface margin and internal architecture of an adjacent fibroadenoma (Fig. 4E), using 1.5 mm RADIANT reconstructions at 1.5 degree intervals. There was very clear delineation of typical non-enhancing internal septations. Radial imaging, with the axis on the center of the lesion, allows assessment of the entire surface, to demonstrate that it is smooth, without angular, spiculated, or irregular margins; this supports the conclusion that this mass is benign, and biopsy confirmed a fibroadenoma.

The resolution on this exam is so extremely fine that the capillaries and venules feeding and draining the lymph nodes are readily appreciated on both source images and especially well on cine review of the

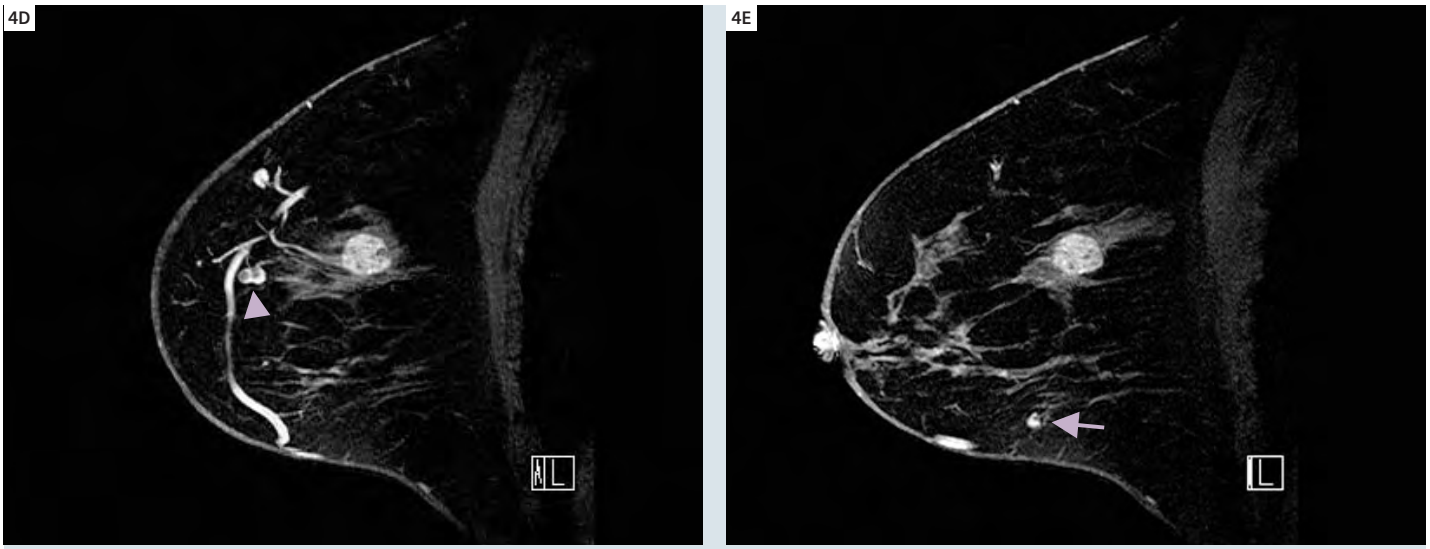

4D,E Oblique sagittal RADIANT images with a thin-MIP thickness of 1.5 mm better delineates the vascular structures, hilar fat of the nodes (arrow head, dark section is fat), and the larger mass posteriorly. Note the extremely fine anatomic detail from this reconstructed image. The non-enhancing internal septations of the biopsy proven fibroadenoma are clearly seen. The fourth node is very small but is well seen inferiorly in 4E (arrow).

RADIANT image set. In breast imaging, proper characterization of a lesion based upon morphology requires detailed visualization of the entire surface of any suspected mass, lest a small area of irregularity, possibly indicating malignancy, be missed. The InterVIEWS technique, with image acquisition at the time of maximal cancer enhancement and minimal background enhancement, improves lesion characterization, based upon morphologic features. When combined with benign enhancement kinetics, greater diagnostic confidence is achieved. If histologic confirmation is required (as was suggested for the larger lesion), ultrasound or MR-guided biopsy can be performed, but the number of MR biopsies can be reduced with such high-resolution, detailed imaging.

Case 5:
Tumor, node, metastases (TNM) staging with MR: breast and body imaging

A palpable firmness in the upper outer right breast brought a 58-year-old woman to medical attention; mammograms were very dense, interpreted as negative, and an ultrasound showed a 1.2 x 1.1 cm hypoechoic mass that on biopsy was an intermediate grade infiltrating ductal cancer. MR of the breast and a whole body staging study were requested. The breast exam revealed extensive infiltration of virtually the entire right upper outer quadrant with mixed invasive and intraductal carcinoma (Figs. 5A, B, C). Additionally, abnormal axillary lymph nodes were detected from level I to level III (Fig. 5D) with no internal mammary, supraclavicular, or cervical adenopathy.

5A Extensive malignancy with nodular, mass-like and diffuse enhancement is seen to involve much of the lateral right breast on this axial MIP; the left breast is negative for tumor.

5B Again, the availability of high quality oblique images, similar to mammographic MLO projections, complements the CC-like axial MIP images for localization of the cancer and estimation of its extent.

5C Sagittal InterVIEWS at 2.5 minutes post-injection produces high contrast between the cancer and the normal background dense parenchyma. Preciswee timing is critical to regularly achieve such detailed tumor visualization in dense breasts.

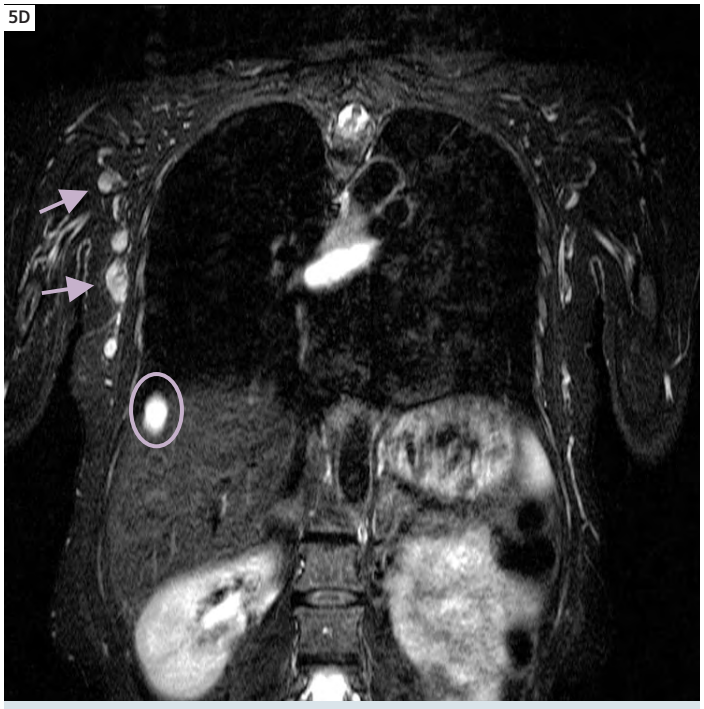

5D "Whole body" coronal imaging with STIR detects suspicious lymph nodes in the right axilla in levels 1 and 2 on this image (arrows); more extensive nodal disease was noted on other images. A fluid-containing cyst is seen in the liver (orange outline) and another in the mediastinum (center).

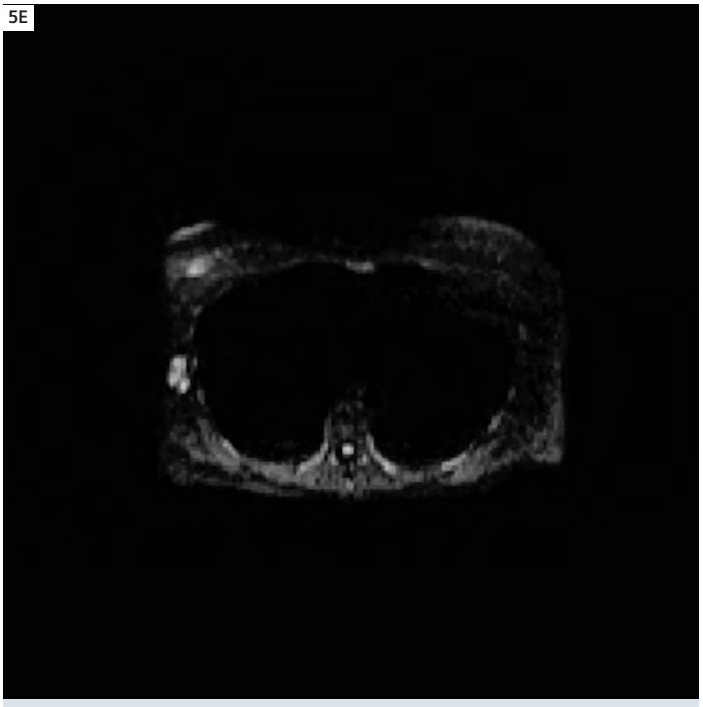

5E Axial diffusion image, with B value of 250, detects suspicious signal in the confirmed malignant axillary nodes. Diffusion images are sensitive to pathology, but lower in resolution.

Ultrasound-guided fine-needle aspiration (FNA) of a selected axillary node, with abnormal signal on diffusion imaging (Fig. 5E) confirmed malignancy. A high signal, sharply demarcated hepatic cyst and a gallstone were seen in the liver, and in addition a 1.5 cm solitary metastasis to the anterior right lobe of the liver on whole body imaging (Fig. 5F); this was confirmed on PET-CT and by follow-up studies showing progression. As suspected, despite intensive chemotherapy, the tumor has progressed and this patient has not done well.

Comments

Marked improvement in software, gradient amplifiers, and coils now allows a clinically effective hybrid breast MR technique that combines the strengths of the dynamic/kinetic approach and morphologic imaging in one examination. The extent of invasive and in situ carcinomas is readily appreciated, improving preoperative planning and diminishing the need for reoperation, and improving staging as well [Beatty and Porter]. The addition of "whole-body" MR adds further to the clinical value and effectiveness of MR as a breast cancer staging tool for not only the size of the tumor within the breast (T-classification), but also for detection of nodal and extra-nodal metastatic disease (N and M classifications).

There has been much recent emphasis on the great sensitivity of MR imaging for surveillance of high-risk patients such as breast cancer gene carriers, or women with a greater than 20–25% lifetime risk of developing breast cancer (ACS Guidelines). High-risk patients are effectively monitored with this technique, and small tumors with a better prognosis can be diagnosed early.

Additionally, MR detection of contralateral tumors markedly affects patient morbidity, management* and surgical decision-making, and decreases the cost of patient care and the potential risk from an occult cancer undetected by conventional methods. Recent publications indicate that MR detects occult contralateral cancers in at least 3% of cases [Lehman]. This, by itself, is a major reason why MR of the breast should be considered in any woman with a newly diagnosed breast carcinoma, particularly if breast conservation is considered. Other higher-risk patient groups are being identified, for which MR may play a crucial role in early detection of small cancers, as seen in Case 3. Recent reports show great improvements in detection of in situ cancers with better technology as well [Kuhl, Lancet].

Though the current capabilities of contrast-enhanced breast MR and body imaging are certainly very impressive, hardware and software advances in MR are continuing and improvements in exam methodology, CAD assessment and interpretation can also be expected. This examination is technically and interpretatively challenging, and therefore the training of radiologists and technologists in this vitally important procedure, with its unique clinical capability, is required and ongoing.

5F

5F Coronal body staging STIR study detected a lesion in the mid liver (arrow) of lower signal than the cyst seen in 5E, but abnormal and confirmed as an early hepatic metastasis. Note the edema (high signal) in the edematous right breast tissue and skin in a tumor that had lympho-vascular invasion on pathology.

References

1 Beatty J, Porter B. Contrast-enhanced breast magnetic resonance imaging: the surgical perspective. Am J Surg 193;5:600-605.

2 Kuhl CK, Schrading S, Bieling HB, Wardelmann E, et al. MRI for diagnosis of pure ductal carcinoma in situ: a prospective observational study. Lancet 2007;370:485-92.

3 Lehman CD, Gatsonis C, Kuhl CK, Hendrick RE, et al. MRI evaluation of the contralateral breast in women with recently diagnosed breast cancer. N Engl J Med 356;13:1295-1303, March 29, 2007.

4 Saslow D, Boetes C, Burke W, Harms S, et al. American Cancer Society Guidelines for Breast Screening with MRI as an Adjunct to Mammography. CA Cancer J Clin 2007;57:75-89.

*Works in progress (WIP). The information about this product is preliminary. The product is under development and not commercially available in the U.S., and its future availability cannot be ensured.

Use of MRI in Detecting Clinically and Mammographically Occult Ductal Carcinoma In Situ. Two Case Reports*

Gladys Lo, M.D.; Polly SY Cheung, M.D.

Hong Kong Sanatorium and Hospital, Hong Kong

Reproduced with permission from the Hong Kong Academy of Medicine.

Abstract

We would like to report on two cases where breast MRI examination has changed clinical management. Breast MRI is now recognized as an indispensable adjunctive examination to mammography and ultrasound.

In each of the two cases described, breast MRI had shown unsuspected extensive mammographic and ultrasound occult ductal carcinoma in situ (DCIS). In each of these cases, the planned breast conserving surgery was changed to mastectomy. The success of breast conservation treatment depends on removal of all tumor with clear margins at the time of surgery. MRI is now considered to be the most sensitive method to evaluate the extent of breast cancer. Breast MRI has very high sensitivity for invasive carcinoma (near 100%), and recent studies show the specificity of high-risk patients at 93–99%. MRI may well prove to be an important adjunctive examination in patients who have dense breasts or extensive fibrocystic change.

Introduction

Although breast MRI has been available for over a decade, it is only recently becoming recognized as an indispensable adjunct to examination of the breast after mammography and ultrasound. Several key factors contribute to this, Firstly, breast MRI protocol is approaching standardization. Secondly, high resolution images are now routinely obtained with 1.5 Tesla and especially with 3 Tesla scanners. Thirdly, MRI breast biopsy devices are now commercially available. Most breast MRI examinations are completed in 30 minutes. Since November 2005, we have been performing breast MRI examinations on a 3 Tesla MRI scanner. 3 Tesla imaging gives increased signal to noise compared to 1.5 Tesla scanners. In addition, it performs well with parallel imaging techniques (iPAT) which gives very high resolution images without increasing the scan time.

Case 1

A 52-year-old female first noticed some thickening in the left breast upper outer quadrant in 2003. Mammogram and ultrasound at that time was normal. Increasing density was noted in May 2005 but ultrasound showed no particular masses. In November 2006 a repeat mammogram showed two areas of opacity in the upper outer quadrant (Fig. 1A). Breast ultrasound was entirely normal (Fig. 1B). Physical examination showed mild thickening at the left 2 o'clock. Fine-needle aspiration (FNA) of the thickening however showed cancer cells. Core needle biopsy confirmed invasive ductal carcinoma. In view of the discordant findings between mammogram and ultrasound, breast MRI was performed to exclude multicentric disease. MRI scan showed 2 spiculated masses in the upper outer quadrant corresponding to the areas of architectural distortion on the mammogram (Fig. 1C). These masses measured 0.7 x 1.5 x 1.3 cm and 0.8 x 1.5 x 1 cm. The signal intensity-time graph showed rapid uptake of contrast with washout for lesion 1 and rapid uptake of contrast with plateau for lesion 2. These features are diagnostic of carcinoma.

Separate from these 2 lesions, there is a large segmental area with nodular and linear clumped enhancement through-out the lower quadrant of the left breast. These findings are compatible with extensive DCIS with and without invasive component (Fig. 1D).

Because of the extensive and multicentric disease seen on MRI, the initially planned breast conserving surgery was switched to mastectomy.

The patient underwent left skin sparing total mastectomy, sentinel node biopsy, axillary dissection and transverse rectus abdominis muculocutaneous (TRAM) flap reconstruction in January 2007. Pathology showed extensive intraduct carcinoma (EIC) measuring 7 cm in diameter, with 5 foci of invasion, largest measuring 1.8 cm grade II, multifocal lymphovascular invasion, 2 of the resected axillary nodes showed metastasis.

In summary the patient had stage IIA carcinoma of left breast $T1_{c(m)}N_1aM_0$ ER200 PR200 PI 6% c-erbB2 w+. She received adjuvant chemotherapy, radiotherapy and hormonal therapy following surgery.

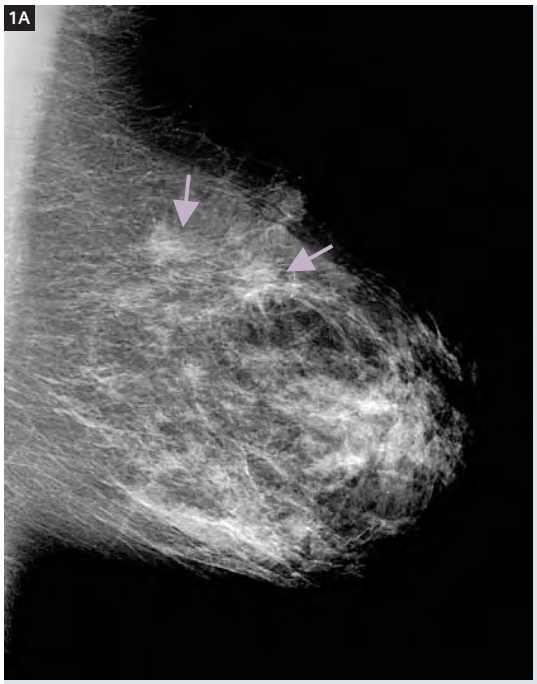

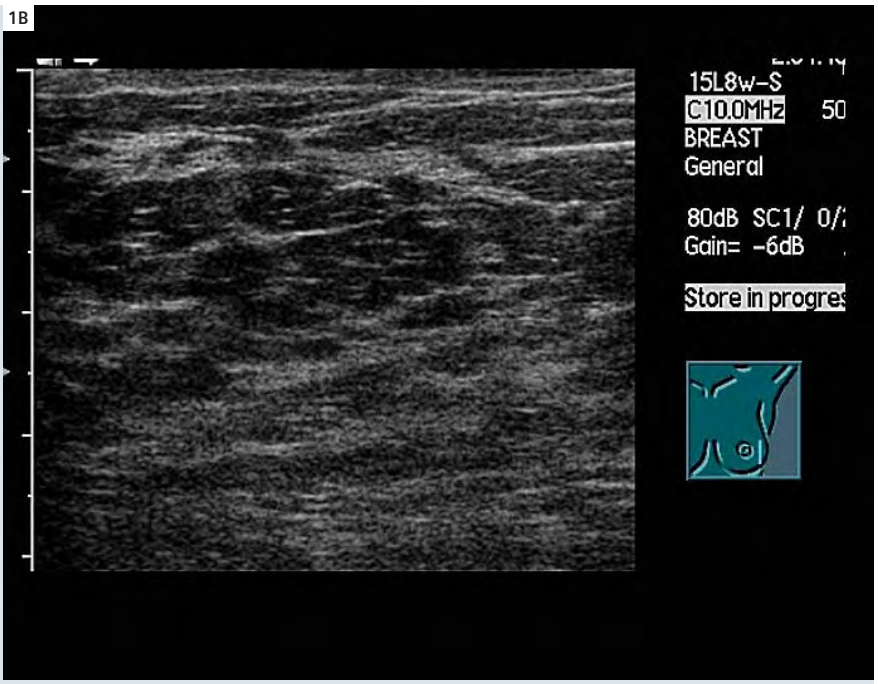

1A Left MLO mammogram shows 2 opacities in the upper quadrant of the left breast.

1B Ultrasound of the left breast is normal.

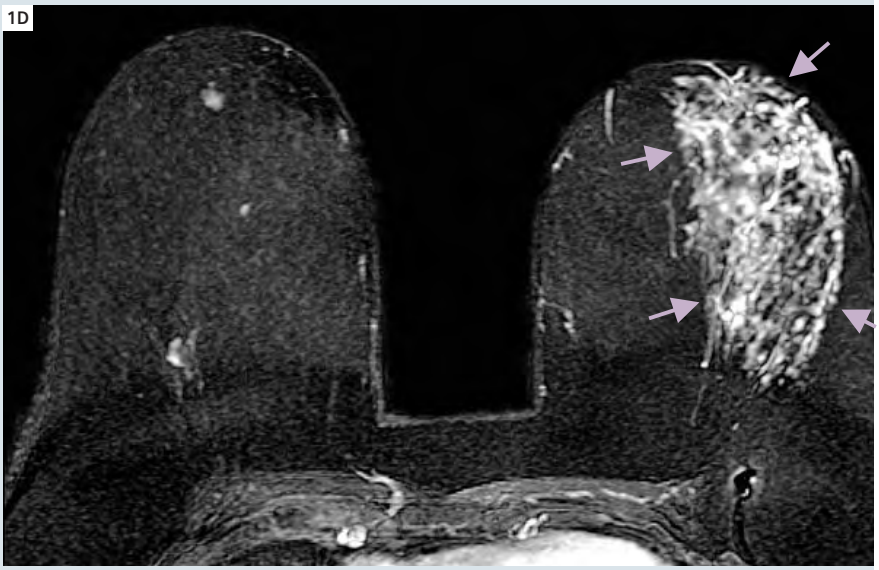

1C MRI: post-contrast sagittal T1-weighted image with fat saturation shows 2 spiculated masses in the upper quadrant and segmental enhancement in the lower quadrant.

1D MRI: post-contrast axial T1-weighted subtracted scan shows segmental linear and nodular clumped enhancement in lower outer quadrant of the left breast.

2A

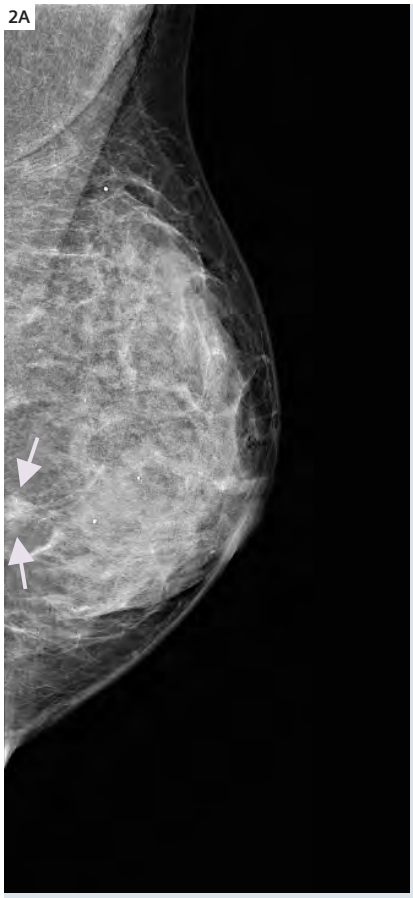

2B

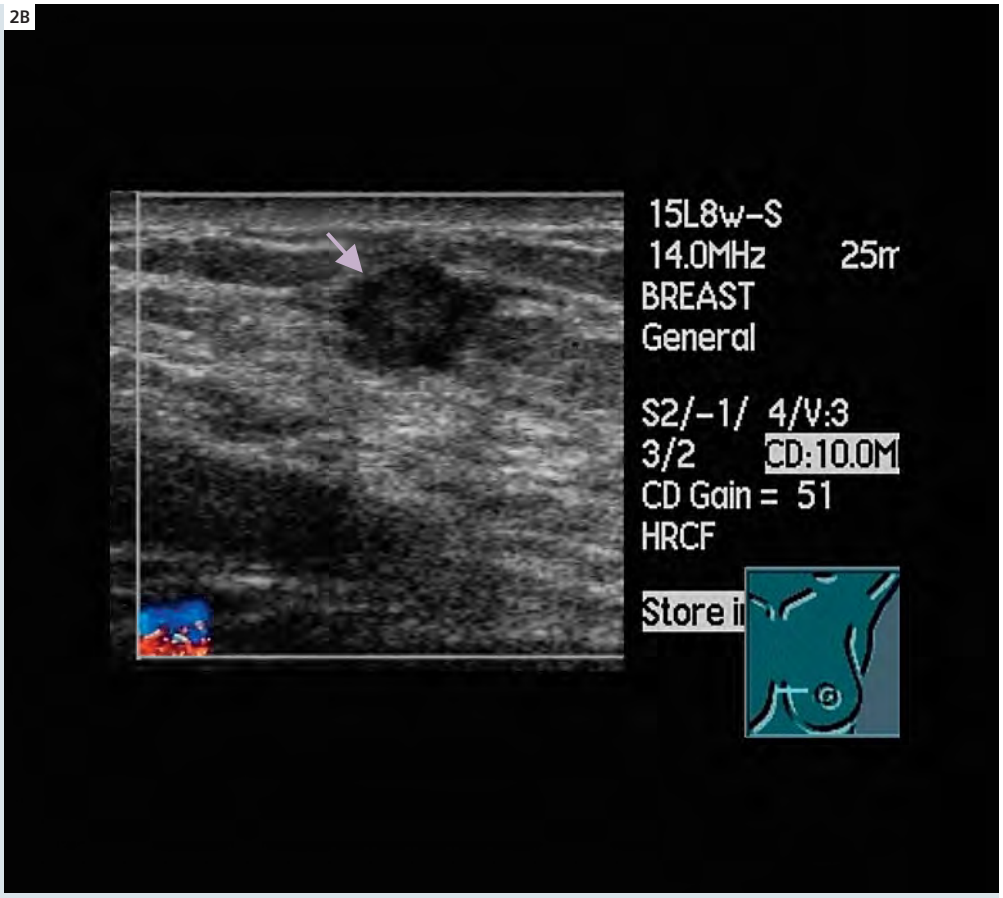

2A Left MLO mammogram shows asymmetric density at 9 o'clock.

2B Ultrasound of the left breast shows hypoechoic mass at 9 o'clock.

2C

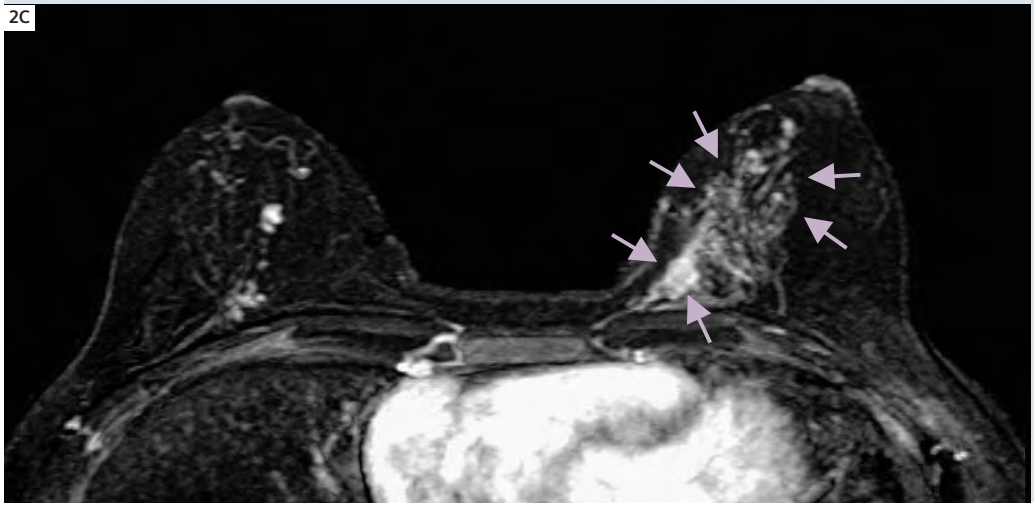

2C Post-contrast axial T1-weighted image with fat saturation shows at 9 o'clock a rim enhancing mass and segmental linear enhancement at the medial lower quadrant of the left breast.

Case 2

A 37-year-old female first noticed a left breast lump in January 2007. The mammogram showed asymmetric density in the left breast at 9 o'clock position with bilateral scattered benign and coarse microcalcifications in both breasts (Fig. 2A). Ultrasound showed a hypoechoic shadow measuring 8 x 6 x 8 mm at 9 o'clock position of the left breast (Fig. 2B) with a cyst at 10 o'clock position. There is also a cyst in the right breast. The left 9 o'clock mass on ultrasound was highly suspicious for cancer and was also confirmed on FNA. In view of the surrounding benign appearing shadow on ultrasound, breast MRI was performed which showed the index lesion in the left breast at 9 o'clock position to be highly compatible with carcinoma, measuring 1.1 cm. It also showed extensive intraductal enhancement involving 6 o'clock to 10 o'clock area measuring 2.3 x 6 cm (Fig. 2C). Because of the MRI findings, the initially planned umpectomy was changed to mastectomy. Left skin sparing total mastectomy and sentinel node biopsy with TRAM flap reconstruction was performed in February 2007. Pathology showed 0.8 cm grade III invasive ductal carcinoma at L9h position, associated with an 8 x 2.8 x 1.3 cm area of ductal carcinoma in situ (DCIS), sentinel node biopsy was negative for metastasis. In summary the patient had stage I carcinoma of the left breast $T_{1b}N_0M_0$ ER170 PR180 PI 8% c-erbB2 strongly+. She was put on Tamoxifen as adjuvant therapy.

Discussion

The success of breast conservation treatment depends on removal of all tumor with clear margins at the time of surgery. Any residual tumor will increase the chance of recurrence even after radiation therapy [1]. Surgeons are sometimes faced with reoperations on patients who appear to be suitable for breast conserving surgery with clinical, mammographic and ultrasound assessments. Often, these are intraduct carcinoma with no apparent mass formation and do not produce microcalcifications on mammogram. Multifocal (more than 1 tumor in 1 quadrant) and multicentric tumor (tumor in more than 1 quadrant) occur in 6 to 34% of breast cancer cases [2].

MRI is now considered to be the most sensitive method to evaluate the extent of breast cancer [3]. It is superior to mammography and ultrasound. Breast MRI has very high sensitivity of 90% or more for breast cancer and near 100% sensitivity for invasive breast carcinoma [4, 5]. Recent literature studying high risk groups such as those with BRCA1 and BRCA2 genes show specificity of 93 to 99% [6]. This is achieved by using a dedicated breast coil and meticulous techniques. Lesions are analyzed by their morphology as well as their enhancement characteristics [7, 8]. The sensitivity of MRI in detecting DCIS is lower probably because of various subtypes. Menell and colleagues report a sensitivity of 88% [9]. Traditionally mammography has been used to evaluate DCIS showing areas of suspicious microcalcifications. However, mammography frequently underestimates the size of tumor and as much as 60% of breast cancer do not form microcalcifications. MRI can detect DCIS with microcalcifications as well as DCIS without microcalcifications. In the two cases presented, the areas of extent DCIS did not show any microcalcification and were mammographic and ultrasound occult. Our two case reports illustrate the use of breast MRI to fully evaluate the extent of breast cancer before definitive surgery, thus avoiding multiple reoperations due to unexpected positive tumor margins from clinically occult extensive DCIS.

Conclusion

It is yet to be evaluated whether MRI should be a routine procedure before all breast cancer surgery. It may prove to be a useful adjunct in preoperative assessment in young breast cancer patients who often have dense breasts, where mammographic accuracy is reduced. It may also be useful in patients with fibrocystic breast change, showing multiple indeterminate shadows on ultrasound, as illustrated in Case Two. When there are discordant findings on clinical, mammographic and ultrasound appearance, MRI will provide more information on breast cancer assessment, as illustrated in Case One. The cost of breast MRI may be a concern. However, the cost becomes insignificant compared to multiple reoperations.

*Some of the concepts and information presented in this paper are based on research and are not commercially available in the U.S.

References

1 Dershaw David, Magnetic Resonance Imaging as a Clinical Tool. Morris Elizabeth, Liberman Laura, Breast MRI: diagnosis and intervention, New York, Springer – Science & Business Media 2005.

2 Liberman Laura, Percutaneous Magnetic Resonance Imaging Guided breast biopsy, Morris Elizabeth, Liberman Laura, Breast MRI: diagnosis and intervention, New York, Springer – Science & Business Media 2005.

3 Hlawatsch A, Teifke A, Schmidt M , Thelen M. Preoperative assessment of breast cancer: sonography versus MR imaging. AJR Am J Roentgenol. 2002; 179:1493-1501.

4 Orel Susan Greenstein MD, MR Imaging of the breast, MRI Clinics of North America Vol 9 #2, May 2001.

5 Heywang-Kobrunner SH, Heinig A, Pickuth D, et al. Internventional MRI of the breast: lesion localisatio and biopsy. Eur Radiol. 2000; 10:36-45.

6 Warner, E Plewes D, Hill K et al. Surveillance of BRCA1 and BRAC2 mutation carriers with magnetic resonance imaging, ultrasound, mammography and clinical breast examination. JAMA 2004; 292:1317-1325.

7 Morris Elizabeth A, Breast Magnetic Resonance Imaging. Morris Elizabeth, Liberman Laura, Breast MRI: diagnosis and intervention, New York, Springer – Science & Business Media 2005.

8 Kuhl Christiane K., Dynamic Breast Magnetic Resonance Imaging, Morris Elizabeth, Liberman Laura, Breast MRI: diagnosis and intervention, New York, Springer – Science & Business Media 2005.

9 Menell JH, Morris EA, Dershaw DD et al. Determination of presence and extent pure ductal carcinoma in situ by mammography and MR. AARS 2003 (presented).

Diffusion-Weighted Imaging in Breast MRI* – An Easy Way to Improve Specificity

Dr. Evelyn Wenkel, M.D.[1]; Dr. Christian Geppert, Ph.D.[2]; Prof. Dr. Michael Uder, M.D.[1]; Dr. Berthold Kiefer, Ph.D.[2]; Prof. Dr. Werner Bautz, M.D.[1]; Dr. Rolf Janka, M.D.[1]

[1] *University Hospital Erlangen, Radiology, Erlangen, Germany*
[2] *Siemens Medical Solutions, Erlangen, Germany*

Introduction

Classic breast magnetic resonance imaging (MRI) is based on the enhancement pattern of lesions in dynamic breast MRI, and morphologic changes [1–3]. With these two criteria breast MRI has a sensitivity of about 85–99% in detecting malignant breast lesions [1–10]. However, there is an overlap of these criteria with benign lesions which leads to a reported specificity of about 40 to 80% [1, 10, 11]. There is an increasing number of congress abstracts and published studies that the specificity of breast MRI could be increased using diffusion-weighted (DW) sequences [12–16]. DW MRI is based on the principle that random motion of molecules during the interval of excitation and signal measurement reduces the amplitude of the resulting signal. The application of appropriate pulse sequences (using, for example, bipolar gradient pulses in one or several directions) allows the measurement of the signal cancellation due to diffusion in the given direction. While normal tissue exhibits gross signal loss, areas with restricted motion of molecules like densely packed tumor cells show less signal loss and become bright in diffusion-weighted images. The value of the diffusion of water in tissue is called the apparent diffusion coefficient (ADC). Based on the diffusion-weighted images an ADC map can be calculated which shows the ADC value of each voxel in every slice. Restricted water movement in tumors with high cellularity leads to smaller ADC values [13]. In some organs, especially the brain, the direction of the diffusion contains important information which can be used, for example, for tracking of fibers by diffusion tensor imaging in many directions. However, in tumor clusters the diffusion is vastly restricted in every direction and therefore it is sufficient to measure DWI of the breast in just one orientation. In most applications the diffusion gradients are integrated in echo planar imaging (EPI) sequences which exhibit high signal intensity in areas with restricted diffusion as well as in fatty tissue. Furthermore, the fat signal is displaced in the direction of the chemical shift as compared to the water signal. This makes fat saturation techniques necessary to identify

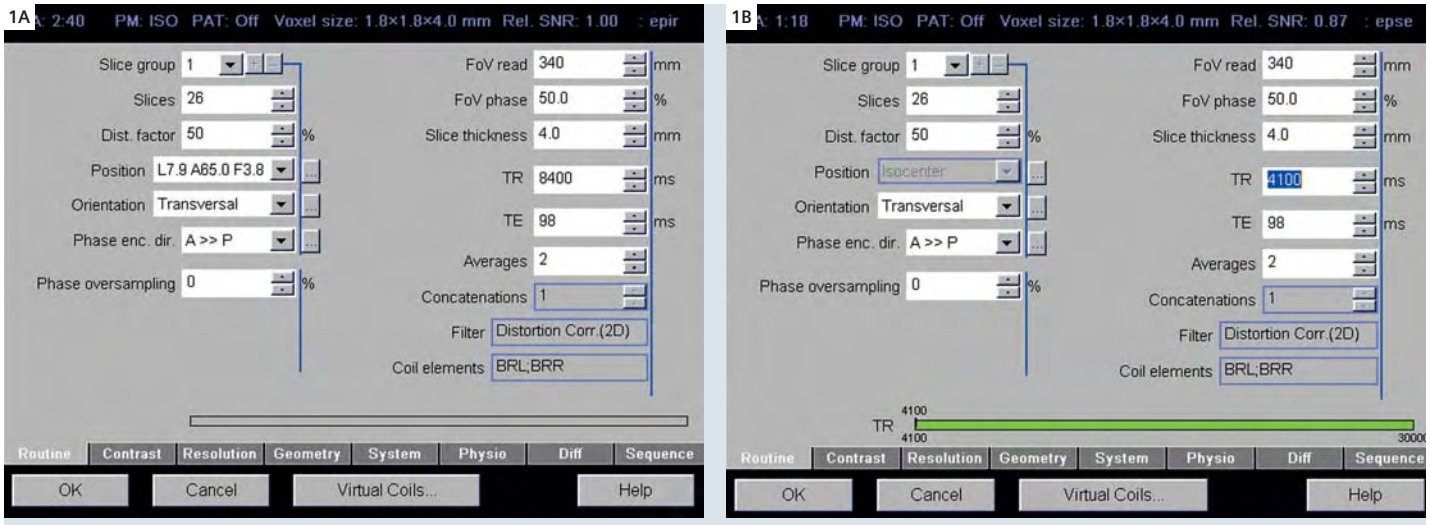

1 Sequence card of the diffusion-weighted EPI STIR **(A)** and the diffusionweighted EPI fs sequence **(B)**.

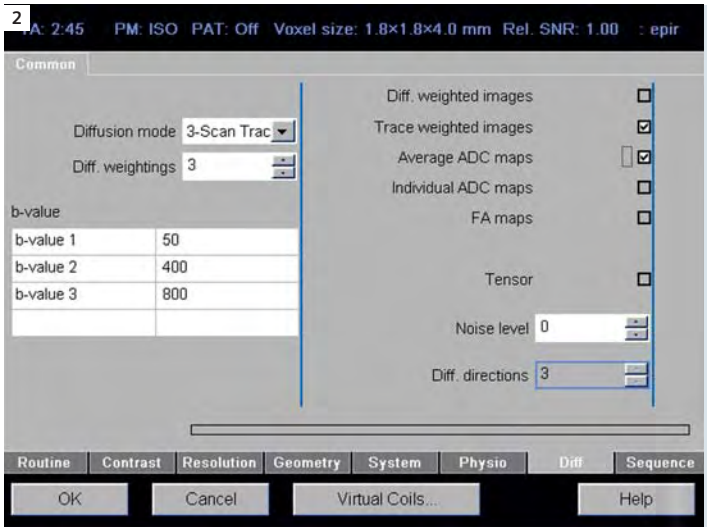

2 Parameters in the diffusion card.

the lesions in the diffusion-weighted images. There are two main possibilities for fat saturation: spectral fat saturation (fs) and a 180° pre-pulse with a short inversion time (STIR or TIRM).
In *syngo* MR B13 both methods can be applied. In our setup we acquire the DW images in axial slice orientation using echo planar imaging pulse sequences incorporating diffusion gradients. TR/TE/TI for the inversion recovery diffusion-weighted EPI (DW EPI STIR) are 8400/98/180 ms (Fig. 1A). The fat saturated diffusion weighted EPI (DW EPI fs) pulse sequence is scanned with a TR = 4100 ms and a TE = 98 msec (Fig.1B). Both sequences are acquired with a FoV of 340 x 170 mm, matrix: 192 x 96 and a slice thickness of 4 mm. We apply the DW sequences prior to the dynamic scan as the T1 relaxation due to the contrast agent will cause changes to the inversion of the tissue and thus can have a strong impact. All DW measurements were acquired with two averages of 26 slices and b-values of 50, 400 and 800 using 3-scan trace calculation, i.e. the sum of the diagonal elements D_{xx}, D_{yy} and D_{zz} of the diffusion tensor is calculated for each slice position and b-value (Fig. 2). With the MAGNETOM Avanto scanner the DW EPI STIR takes 2:40 minutes while DW EPI fs is performed in 1:18 minute. ADC maps are calculated automatically on the basis of the b50, b400 and b800 images using the scanner software. As mentioned above we suppose that a diffusion gradient in just one direction would also lead to sufficient results.

Image interpretation

Image interpretation starts like conventional breast MRI. If a lesion is visualized in the dynamic scan (Fig. 3) it has to be identified in the corresponding slice of the diffusion weighted images. As a second step, a region-of-interest (ROI) is drawn in the centre of the lesion on the b-800 DWI and copied to the ADC map (Fig. 4). The scanner software provides the mean value within the ROI which equals the ADC value (multiplied by 10^{-3} mm²/s). If the lesion is not visible in the b-800 images, the location of the lesion can be identified in the b-400 or b-50 image. Where the lesion is not visible in the b-50, b-400 or the b-800 image the ADC value cannot be evaluated. Lesions smaller than 5 mm and lesions with central necrosis and an enhancing rim smaller than 5 mm are often hard to delineate in the DWI or lead to wrong ADC values. So we do not recommend evaluating such lesions with DWI.

Results of DWI of the breast

In a pilot study with 56 patients and 69 histologically proven lesions > 5 mm only 5/69 lesions could not be evaluated with DW-MRI [17]. Three of these five lesions were not visible in the DWI sequences and therefore could not be matched with the ADC map. Histology of these lesions were one septated invasive lobular carcinoma with two tumor portions of 9 and 6 mm, one recurrent invasive ductal carcinoma with a maximum diameter of 10 mm in the MRI and one tubulolobular invasive carcinoma with 7 mm. In two patients the DWI images were not evaluable due to patient movement. ADC values were finally measured in 51 women (age 50

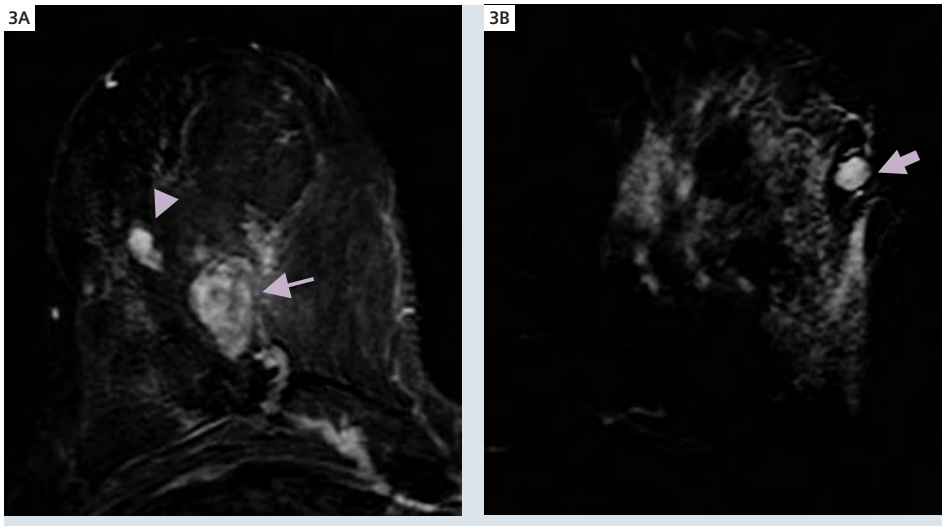

3 Your diagnosis? Subtraced image of the dynamic contrast enhanced sequence: **(A)** 45- year-old woman with a palpable mass and two suspicious lesions with blurred borders. The bigger one with inhomogeneous contrast enhancement (small arrow) and a smaller non-palpable lesion with nearly homogenous enhancement. **(B)** 41-year-old woman with a suspicious lesion in mammography and a sharp lined lesion in the outer-upper quadrant (big arrow).

Table 1: Histology of 69 lesions with DW sequences

Histology, N = 69	IDC	ILC	DCIS	Rare	FA	FD	BP	total
Evaluated	39	6	1	3	8	6	1	64
Not evaluated	2	2	0	1	0	0	0	5

IDC: invasive ductal carcinoma, ILC: invasive lobular carcinoma, DCIS: ductal carcinoma in situ, Rare: rare malignant tumors (medullary, tubular carcinoma, carcinosarcoma, angiosarcoma), FA: fibroadenoma, FD: fibrocystic disease, BP: benign phylloides tumor.

Table 2: Apparent diffusion coefficient (ADC) values (10^{-3} mm²/s) of all evaluated lesions (b = benign, m = malignant) in both MR diffusion weighted sequences

			ADC values (10^{-3} mm²/s)							
	n		Mean ± SD		Maximum		Minimum		95% CI	
	b	m	b	m	b	m	b	m	b	m
DW EPI STIR	15	45	1.92 ± 0.53	0.91 ± 0.24	3.20	1.43	1.10	0.35	1.62-2.22	0.83-0.98
DW EPI fs	15	49	1.76 ± 0.42	0.90 ± 0.18	2.58	1.19	1.21	0.34	1.53-2.00	0.85-0.96

SD: Standard deviation, EPI STIR: echo planar imaging with short time inversion recovery, EPI fs: echo planar imaging with spectral fat saturation.

years ± 15 years) with 64 focal mass lesions (15 benign, 49 malignant).
The mean longest diameter of the evaluated lesions was 17 ± 10 mm (benign 17 ± 10 mm, malignant lesions 17 ± 10 mm). The size of the ROI for the ADC value calculation was 24 ± 11 mm² (benign 27 ± 13 mm², malignant lesions 23 ± 10 mm²). There was no statistical difference of the size of the lesions or the ROI between benign or malignant masses. In the DW EPI STIR sequence the ADC values of 4 lesions could not be evaluated correctly due to patient movement between the b-50 and the b-800 sequence. So the ADC values of 60 lesions in the DW EPI STIR sequence and 64 lesions in the DW EPI fs sequence were evaluated (table 2). Lesion delineation was significantly better in the EPI fs sequence than in the EPI STIR sequence.
The mean ADC values were 1.92 ± 0.53 and 1.76 ± 0.42 x 10^{-3} mm²/s in benign lesions (DW EPI STIR and, DW EPI fs), and 0.91 ± 0.24 and 0.90 ± 0.18 x 10^{-3} mm²/s in malignant lesions, respectively. There was a highly significant difference in ADC values between benign and malignant lesions in both DW sequences. In the DW EPI STIR sequence the range of the ADC values of benign lesions was 1.10 – 3.20 x 10^{-3} mm²/s (95% CI: 1.62 – 2.22 x 10^{-3} mm²/s) and in malignant lesions 0.35 – 1.43 x 10^{-3} mm²/s (95% CI: 0.83 – 0.98 x 10^{-3} mm²/s, table 2). Assuming a threshold of 1.26 x 10-3 mm²/s for the DW EPI STIR sequence, 1/15 benign lesion and 1/45 malignant lesion would be misdiagnosed. In the DW EPI fs sequence the range of ADC values of benign lesions was 1.21 – 2.58 x 10^{-3} mm²/s (95% CI: 1.53 – 2.00 x 10^{-3} mm²/s) and of malignant lesions 0.34 –1.19 x 10^{-3} mm²/s (95% CI: 0.85 – 0.96 x 10^{-3} mm²/s) . There was no overlap in the ADC values of benign and malignant lesions in the DW EPI fs sequence.

Discussion

Detection of breast lesions has become more sensitive in mammography, ultrasound and MRI due to technical developments in the last years. Digital mammography seems to be more sensitive for breast lesion detection in dense breasts [18]. Higher spatial resolution leads to higher detection rates in ultrasound [19] and MRI.
However, the characterization of the detected lesions can be difficult. Up to now breast MRI is analyzed according to morphologic criteria, the enhancement kinetics and the T2 characteristic of breast lesions. However, all these criteria show an overlap between benign and malignant lesions [2, 4, 20-22]. In this situation an additional feature to characterize suspicious lesions would be helpful in order to decrease the number of invasive breast procedures. Prior studies with breast MRI and DWI have already addressed this question and show promising results [13-15]. In our study we compared two different DW sequences, an EPI STIR sequence and an EPI sequence with spectral fat saturation. Both DW sequences revealed a significant difference between ADC values of malignant and benign breast lesions. Comparing both sequences there was no overlap between the ADC values of benign and malignant breast lesions in the DW

sequence with spectral fat saturation. Assuming a threshold of 1.26 x 10^{-3} mm^2/s, 2/60 lesions (1 benign and 1 malignant) would have been misclassified in the DW EPI STIR sequence.

In our opinion placement of the ROI is the crucial point in analyzing DWI. In most prior studies the ROI was placed with direct reference to the subtracted images of the dynamic contrast enhanced sequence. However, the spatial localization of a lesion in the dynamic contrast enhanced sequence is not necessarily the same as in the DW images due to distortion of echo planar images or patient movement between the DW sequence and the dynamic contrast enhanced sequence. Especially in small lesions this may lead to inadequate placement of the ROI. To overcome this problem the easiest and possibly more exact method to evaluate the ADC value is to localize the lesion in the contrast enhanced sequence, match it with the corresponding lesion in the DWI, select a ROI in the DWI and copy this ROI to the ADC map (Fig. 4). Using this method, lesion delineation in the DW sequence plays an important role for ADC measurement. In terms of lesion delineation the EPI fs sequence was significantly better than the EPI STIR sequence. This can be explained with the reduced signal-to-noise ratio (SNR) with inversion recovery as opposed to fat saturation.

Lesion delineation may also have an impact on the ADC map. Calculating the ADC map is a voxel per voxel analysis in the b-50, b-400 and b-800 DWI. A good delineation of the lesion in all three DW measurements should result in a sharp edged and homogenous ADC map of this lesion and vice versa. In our study the better lesion delineation in the DW EPI fs sequence corresponded with a significant lower standard deviation within the ROI in the ADC measurements.

There are some limitations of DW MRI of the breast. Patient movement between the acquisitions of the three DW sequences leads to wrong ADC values. In our study four lesions scanned with the EPI STIR

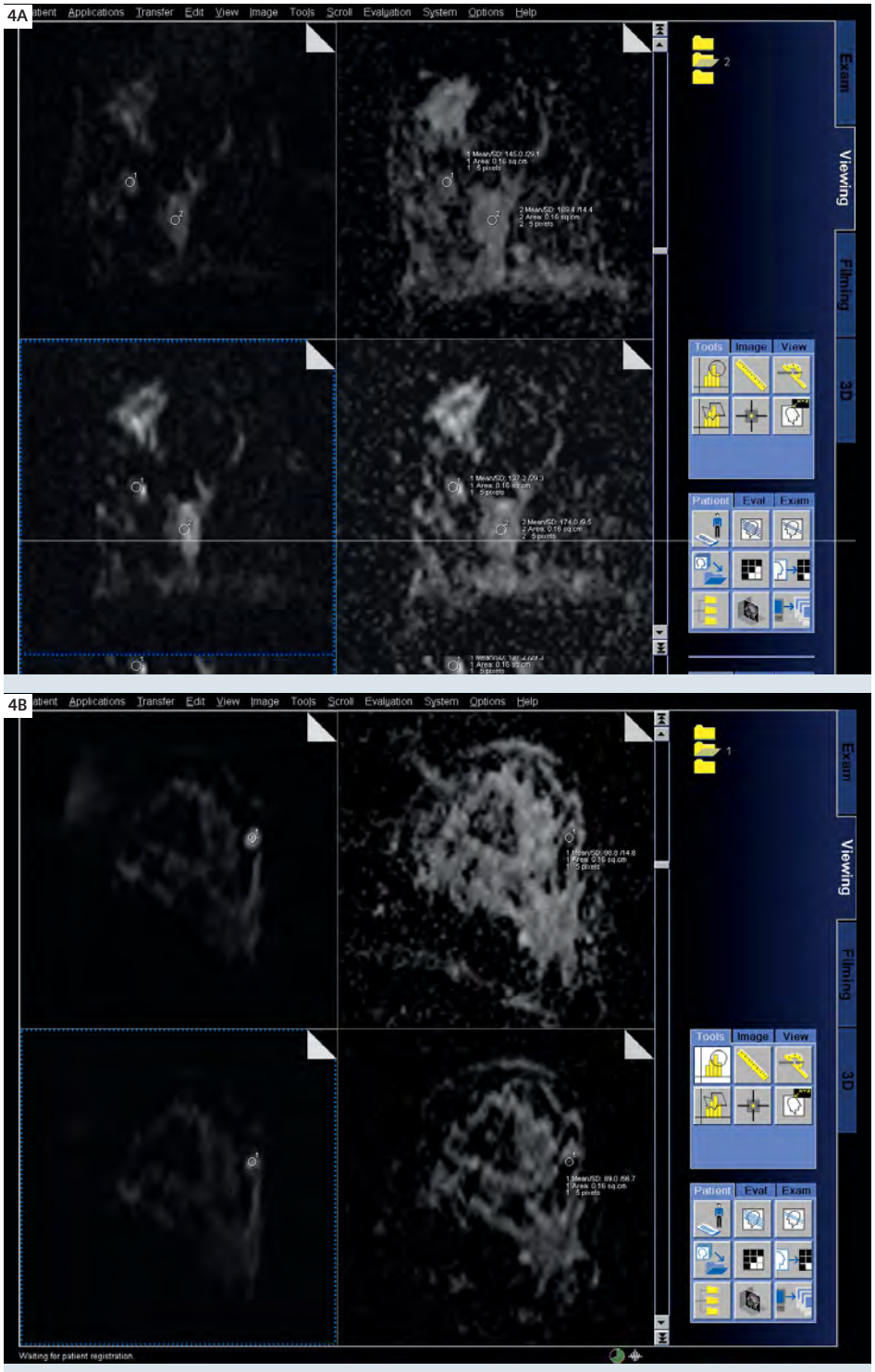

4 DWI (b=800, left side) of the corresponding lesions in figure 3 and the calculated ADC-maps (right side). Upper row: DW EPI fs, lower row DW EPI STIR. A region of interest was drawn in the centre of the lesions and copied in the ADC-map. **(A)** The ADC value of the bigger lesion reveals 1,7 x 10^{-3} mm^2/s and the EPI fs and EPI STIR sequence. The ADC value of the smaller lesion is 1.5 x 10^{-3} mm^2/s (EPI fs) and 1.4 x 10^{-3} mm^2/s (EPI STIR). Histology of both lesions was a fibroadenoma. **(B)** The ADC value of the solitary lesion is 1.0 and 0.9 x 10^{-3} mm^2/s (DW EPI fs and DW EPI STIR) Histology of the lesion was an invasive ductal carcinoma.

sequence were excluded from the evaluation due to patient movement. The reason for this may be the longer acquisition time of the EPI STIR sequence compared to the EPI fs sequence (2 min 40 s vs. 1 min 18 s) which makes patient movement more likely. But even under optimal circumstances DWI can fail to categorize breast lesions. Some lesions cannot be visualized in the DWI and therefore the exact localization of the ROI in the ADC map cannot be determined. In our study 3/69 lesions were not visualized in DWI and could not be evaluated. This ratio would be higher if lesions smaller than 5 mm had been analyzed. However, according to Liberman et al. there is a low likelihood of cancer in lesions smaller than 5 mm [23]. Malignant lesions with central necrosis often show high ADC values in the area of necrosis [24, 25] and the rim of the lesion may be too thin for correct ROI placement. Non focal mass lesions as often seen in DCIS may not be categorized correctly with DWI even with a small ROI due to diffuse tumor spread and partial volume effects [15]. Carcinoma with very high signal intensities in T2-weighted images – like mucinous tumors – could result in misleading ADC values due to different tumor cell packing compared to classic intraductal breast cancer [26]. Despite these limitations DWI of the breast provides additional information to characterize focal breast lesions in a fast and easy way and will hopefully help to reduce invasive procedures.

*Some of the concepts and information presented in this paper are based on research and are not commercially available in the U.S.

Conclusion

DW MRI of the breast with EPI fs and EPI STIR sequences has a high potential to differentiate between benign and malignant breast lesions. Due to significantly better lesion delineation, better selectivity and shorter acquisition time the DW EPI fs sequence is superior.

The authors: Dr. Evelyn Wenkel M.D. (left) and Dr. Rolf Janka, M.D. (right) from the University Hospital Erlangen, Radiology, Erlangen, Germany.

References

1 Macura KJ, Ouwerkerk R, Jacobs MA, et al. Patterns of enhancement on breast MR images: interpretation and imaging pitfalls. Radiographics 2006; 26:1719-1734; quiz 1719.
2 Schnall MD, Blume J, Bluemke DA, et al. Diagnostic architectural and dynamic features at breast MR imaging: multicenter study. Radiology 2006; 238:42-53.
3 Szabo BK, Aspelin P, Wiberg MK, et al. Dynamic MR imaging of the breast. Analysis of kinetic and morphologic diagnostic criteria. Acta Radiol 2003; 44:379-386.
4 Bluemke DA, Gatsonis CA, Chen MH, et al. Magnetic resonance imaging of the breast prior to biopsy. Jama 2004; 292:2735-2742.
5 Wiener JI, Schilling KJ, Adami C, et al. Assessment of suspected breast cancer by MRI: a prospective clinical trial using a combined kinetic and morphologic analysis. AJR Am J Roentgenol 2005; 184:878-886.
6 Bedrosian I, Mick R, Orel SG, et al. Changes in the surgical management of patients with breast carcinoma based on preoperative magnetic resonance imaging. Cancer 2003; 98:468-473.
7 Heywang-Kobrunner SH, Bick U, Bradley WG, Jr., et al. International investigation of breast MRI: results of a multicentre study (11 sites) concerning diagnostic parameters for contrast-enhanced MRI based on 519 histopathologically correlated lesions. Eur Radiol 2001; 11:531-546.
8 Kaiser WA. [Magnetic resonance tomography of the breast. The results of 253 examinations]. Dtsch Med Wochenschr 1989; 114:1351-1357.
9 Kinkel K, Helbich TH, Esserman LJ, et al. Dynamic high-spatial-resolution MR imaging of suspicious breast lesions: diagnostic criteria and interobserver variability. AJR Am J Roentgenol 2000; 175:35-43.
10 Kuhl CK, Mielcareck P, Klaschik S, et al. Dynamic breast MR imaging: are signal intensity time course data useful for differential diagnosis of enhancing lesions? Radiology 1999; 211:101-110.
11 Fischer U, Kopka L and Grabbe E. Breast carcinoma: effect of preoperative contrast-enhanced MR imaging on the therapeutic approach. Radiology 1999; 213:881-888.
12. Sinha S, Lucas-Quesada FA, Sinha U, et al. In vivo diffusion-weighted MRI of the breast: potential for lesion characterization. J Magn Reson Imaging 2002; 15:693-704.
13 Guo Y, Cai YQ, Cai ZL, et al. Differentiation of clinically benign and malignant breast lesions using diffusion-weighted imaging. J Magn Reson Imaging 2002; 16:172-178.
14 Rubesova E, Grell AS, De Maertelaer V, et al. Quantitative diffusion imaging in breast cancer: a clinical prospective study. J Magn Reson Imaging 2006; 24:319-324.
15 Woodhams R, Matsunaga K, Iwabuchi K, et al. Diffusion-weighted imaging of malignant breast tumors: the usefulness of apparent diffusion coefficient (ADC) value and ADC map for the detection of malignant breast tumors and evaluation of cancer extension. J Comput Assist Tomogr 2005; 29:644-649.
16 Kuroki Y, Nasu K, Kuroki S, et al. Diffusion-weighted imaging of breast cancer with the sensitivity encoding technique: analysis of the apparent diffusion coefficient value. Magn Reson Med Sci 2004; 3:79-85.
17 Wenkel E, Geppert C, Schulz-Wendtland R, et al. Diffusion weighted imaging in breast MRI comparison of two different pulse sequences. Acad Radiol 2007; 14:1077-1083.
18 Pisano ED, Gatsonis C, Hendrick E, et al. Diagnostic performance of digital versus film mammography for breast-cancer screening. N Engl J Med 2005; 353:1773-1783.
19 Schulz-Wendtland R, Bock K, Aichinger U, et al. [Ultrasound examination of the breast with 7.5 MHz and 13 MHz-transducers: scope for improving diagnostic accuracy in complementary breast diagnostics?]. Ultraschall Med 2005; 26:209-215.
20 Bartella L, Liberman L, Morris EA, et al. Nonpalpable mammographically occult invasive breast cancers detected by MRI. AJR Am J Roentgenol 2006; 186:865-870.
21 Kuhl CK, Klaschik S, Mielcarek P, et al. Do T2 weighted pulse sequences help with the differential diagnosis of enhancing lesions in dynamic breast MRI? J Magn Reson Imaging 1999; 9:187-196.
22 Nunes LW, Schnall MD and Orel SG. Update of breast MR imaging architectural interpretation model. Radiology 2001; 219:484-494.
23 Liberman L, Mason G, Morris EA, et al. Does size matter? Positive predictive value of MRI-detected breast lesions as a function of lesion size. AJR Am J Roentgenol 2006; 186:426-430.
24 Chang SC, Lai PH, Chen WL, et al. Diffusion-weighted MRI features of brain abscess and cystic or necrotic brain tumors: comparison with conventional MRI. Clin Imaging 2002; 26:227-236.
25 Dorenbeck U, Butz B, Schlaier J, et al. Diffusion-weighted echo-planar MRI of the brain with calculated ADCs: a useful tool in the differential diagnosis of tumor necrosis from abscess? J Neuroimaging 2003; 13:330-338.
26 Kawashima M, Tamaki Y, Nonaka T, et al. MR imaging of mucinous carcinoma of the breast. AJR Am J Roentgenol 2002; 179:179-183.

Potential Role of Multi b Factor Diffusion-Weighted Imaging of the Breast*

Mitsuhiro Tozaki, M.D.[1], Katsuya Maruyama[2]

[1]*Breast Center, Kameda Medical Center, Chiba, Japan*
[2]*Siemens-Asahi Medical Technologies LTD., Tokyo, Japan*

Introduction

Diffusion-weighted imaging (DWI) is characterized by extremely high contrast resolution, and it has been applied to diagnose early-stage cerebral infarction. When used to image the body, however, strong artifacts are created by the non-uniformity of the magnetic field. Recent development of MR technology has nearly overcome this obstacle and enabled the clinical application of diffusion-weighted imaging. DWI has shown great promise in the detection of any tumor type throughout the entire body.

Regarding breast DWI, the potential role of apparent diffusion coefficient (ADC) value in characterizing breast lesions has been reported. In the preliminary results, the ADC value may be an effective parameter in distinguishing between benign and malignant breast lesions because tumor cellularity has a significant influence on the ADC values. On the other hand, the VIBE (volumetric interpolated breathhold examination) sequence with iPAT (integrated parallel acquisition techniques), which allows high-spatial-resolution images with isotropic voxels to be obtained, improves the quality of breast MR examinations dramatically (Table and Figs. 1–3). Following this development, it is debatable whether DWI of the breast is useful or not in routine clinical MR examinations.

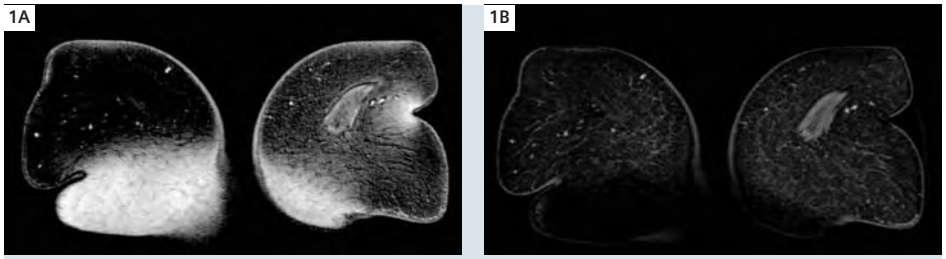

1 Breast measurements with the VIBE sequence and Fat Sat using CHESS **(A)** and SPAIR **(B)**. SPAIR utilizes adiabatic fat suppression pulses which have also been optimized with respect to their frequency selective profile. Thus the sensitivity to B1-inhomogeneities is reduced.

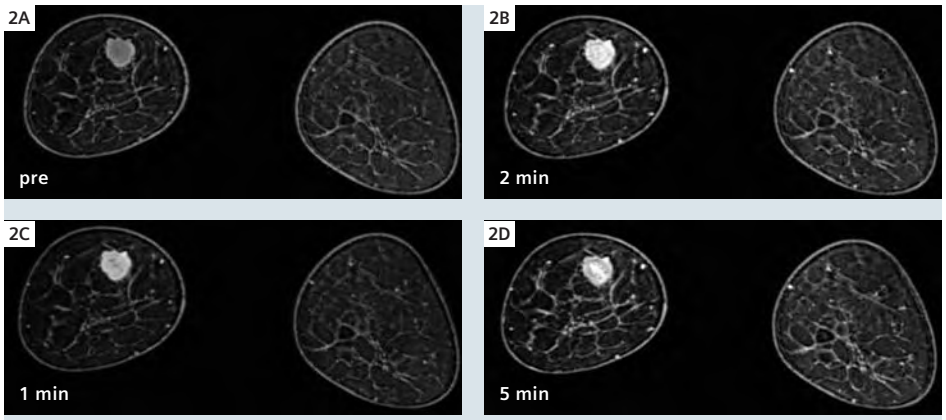

2 Dynamic protocol using VIBE with iPAT: High resolution 3D dynamic acquisitions with fat saturation (SPAIR) using a PAT factor of 2. Both breasts were examined in the coronal plane on the first, second, and fifth-phase dynamic images.

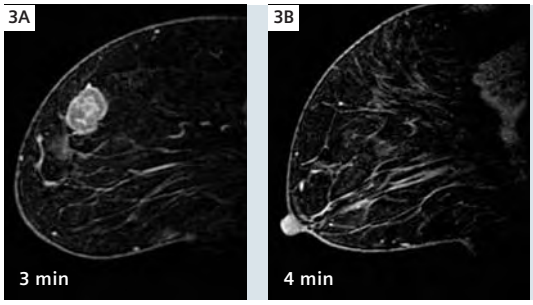

3 High resolution imaging using VIBE without iPAT in the same patient as Fig. 2: Bilateral breasts were sagittally examined on images obtained in the third **(A)** and fourth phases **(B)**. **(A)** Right breast. **(B)** Left breast.

The impact of DWI

Tumor detection

Unfortunately, there was no evidence that sensitivity and accuracy of breast cancer detection by DWI are higher than

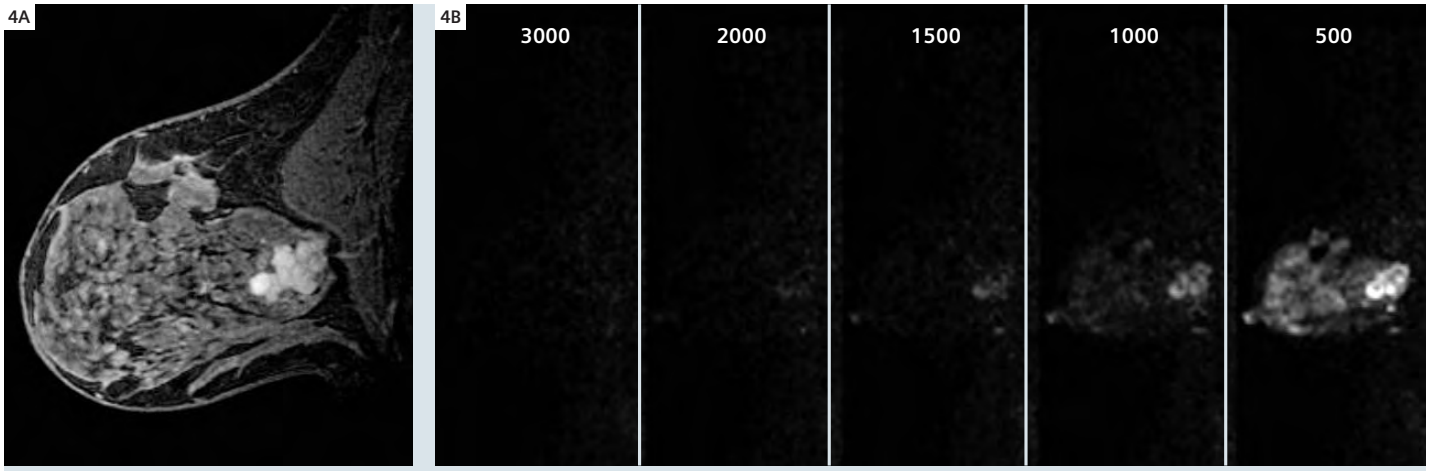

4 Sagittal MPR images of diffusion-weighted imaging, showing a fibroadenoma. This benign tumor appears hyperintense on b 500–1500 images.

that by standard contrast-enhanced MRI. In fact, it is insufficient to detect small breast cancer or ductal carcinoma in situ (DCIS). Tumor angiogenesis and increasing cellularity are developed simultaneously in breast cancer. However, the detection of the presence of angiogenesis by perfusion MR imaging using Gd-DTPA contrast agent is more sensitive than that of the degree of increasing cellularity by DWI. In these circumstances, screening MRI without the use of contrast agent has come up for discussion in Japan. Breast cancer is the leading cause of cancer deaths among Japanese women, and among this group it tends to occur in the late forties. Because the limitations of X-ray mammography are well known in dense breast tissue, screening for breast cancer with ultrasound has just started in Japan. One of the current problems of screening ultrasound is that too many benign hypoechoic nodules are depicted. In our hospital, the clinical usefulness of non-contrast MRI that combines DWI and T1-, T2-weighted imaging has been investigated prospectively for the patients with equivocal or suspicious findings on screening ultrasound.

Differential analysis: multi b factor DWI

Regarding the differentiation between benign and malignant lesions, the ADC value may be an effective parameter. Up to the present, only the diagnostic cut-off value of ADC has been evaluated and discussed. However, there is the overlap in ADC values. We try to make categorization using multi b factor DWI. In the differen-

Table 1: Protocols

	sequence	orientation	voxel size	TA	TE	TR
localizer	gre	3 orientation	2.1x1.6x6mm	0:35	4,22	9,2
t1_fl3d_cor_in-phase_FS(-)	fl3d_vibe	coronal	1x1x3mm	0:52	4,76	8
t2_tse_sag_R_fs_SPAIR	tse_rst_ire	sag (right)	0.6x0.6x3mm	1:18	97	4780
t2_tse_sag_L_fs_SPAIR	tse_rst_ire	sag (left)	0.6x0.6x3mm	1:18	97	4780
DWI_ep2d_cor_fs_SPAIR	ep2d_diff_pace	coronal	3x3x3mm	2:24	96	8000
Dyn_t1_fl3d_vibe_cor_fs_SPAIR	fl3d_vibe	coronal	1x0.7x0.9mm	1:00 x 3	2,29	5,23
t1_fl3d_vibe_sag_R_fs_SPAIR	fl3d_vibe	sag (right)	0.6x0.6x1.2mm	1:00	2,22	4:04
t1_fl3d_vibe_sag_L_fs_SPAIR	fl3d_vibe	sag (left)	0.6x0.6x1.2mm	1:00	2,22	4:04
Delay_t1_fl3d_vibe_cor_SPAIR	fl3d_vibe	coronal	1x0.7x0.9mm	1:00	2,29	5,23
svs_se_ub2_270_breast	svs_se_ub2	transversal	15x15x15mm	7:01	270	1620

tial diagnosis of breast lesions, categorization of the lesions, such as ACR-BI-RADS and scoring system (Göttingen score, Jena score, and MARIBS (Magnetic Resonance Imaging in Breast Screening)), is essential. In our hospital we perform categorization visually based on multi-b-factor DWI, always applying the same window level and width (Figs. 4, 5).

Monitoring the therapeutic response
After one or two cycles of chemotherapy there are substantial changes in the contrast enhancement pattern, which are observed even before measurable changes of the tumor size occur. However, contrast enhancement patterns may lead to misleading findings and false-negative results due to the effects of chemotherapeutic agents. In contrast, DWI and ^{1}H MR spectroscopy show great promise in the observation of the direct effects of chemotherapeutic agents. ^{1}H MR spectroscopy is a promising molecular-based method, although the chemotherapeutic changes can be observed within a limited region (single voxel) that, in advanced cases, may be smaller than the breast cancer itself. We believed that DWI has additional information in monitoring the therapeutic response of locally advanced breast can-

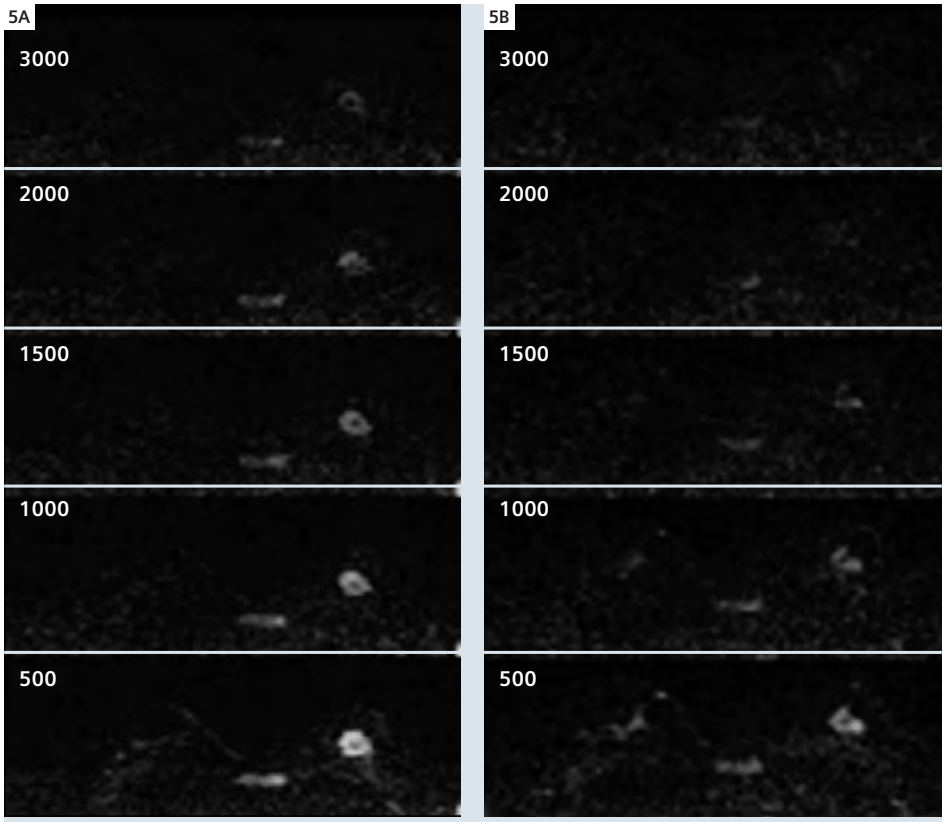

5 Transeverse MPR images of diffusion-weighted imaging, showing a breast cancer in the left breast. DWI before **(A)** and after **(B)** chemotherapy. Signal intensity and size of the tumor are reduced after chemotherapy.

FA	FoV read	FoV phase	slice thickness (mm)	matrix (base resolution)	matrix (phase resolution)	iPAT (Acce)	Fat Sat	band width
20	400	100	6	256	75%	off	off	230
25	330	100	3	320	100%	GRAPPA (2)	off	320
150(refo)	160	100	3	256	100%	off	SPAIR	300
150(refo)	160	100	3	256	100%	off	SPAIR	300
3scan-trace	330	100	3	110	100%	GRAPPA (2)	SPAIR	1684*
12	330	100	0,9	448	71%	GRAPPA (2)	SPAIR	430**
15	160	100	1,2	256	100%	off	SPAIR	390
15	160	100	1,2	256	100%	off	SPAIR	390
12	330	100	0,9	448	71%	GRAPPA (2)	SPAIR	430
90							spectral suppresion	1000

*b1=500,b2=1000,b3=1500,b4=2000,b5=3000; **pre+ 2 measurements

cer patients (Fig. 5). In addition, diffusion-weighted images are thought to be a useful guide for placing a volume of interest (VOI) within a breast tumor in order to measure the 1H MR spectrum.
There is, however, a pitfall in the use of ADC values. Figure 6 shows a patient with breast cancer before and after neoadjuvant chemotherapy. Before chemotherapy, cancer was visible on b 3000 images and had a low ADC value (0.69 x 10^{-3} mm^2/s). After chemotherapy, the cancer decreased in size as observed on both contrast-enhanced MRI and DWI. The lesion was visible on b 2000 images and had an ADC value (0.64 x 10^{-3} mm^2/s) similar to the pre-therapy value. Despite the decrease in tumor size due to the chemotherapeutic effect, cellularity changes within the lesion were of variable degree (Fig. 6). In short, decreasing cellularity of breast cancer has occurred inhomogeneously within the tumor and may be independent useful information, compared with morphology and vascular permeability.

Conclusion

It is debatable whether DWI of the breast is useful or not in the clinical MR examinations. However, DWI is the only sequence able to visualize breast cancers with a high rate on non- or pre-contrast enhanced MRI. We should continuously evaluate the potential role and limitations of this Cellularity-weighted Imaging. Further investigation and prospective study incorporating the visual assessment of multi b factor DWI is necessary.

*Some of the concepts and information presented in this paper are based on research and are not commercially available in the U.S.

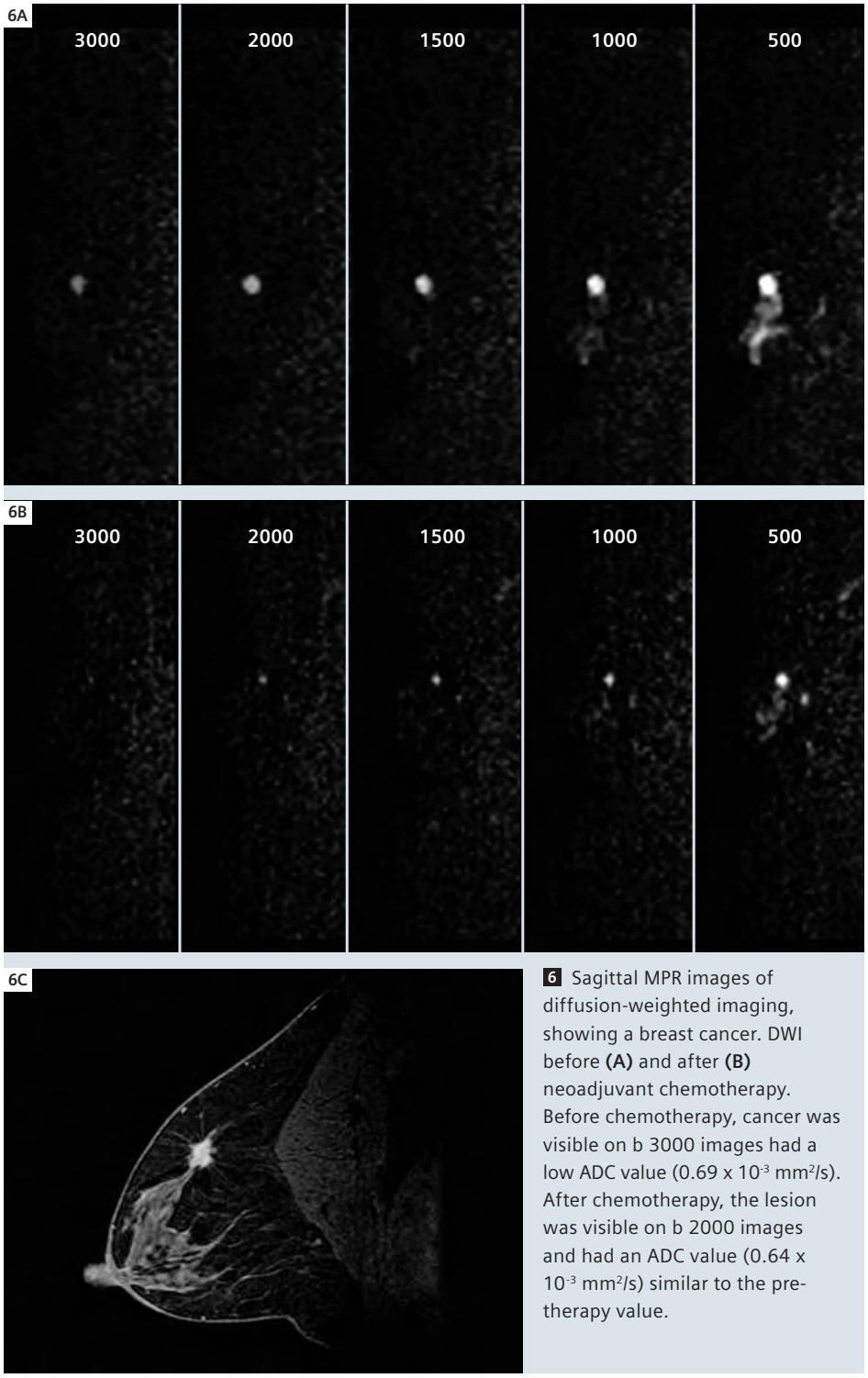

6 Sagittal MPR images of diffusion-weighted imaging, showing a breast cancer. DWI before **(A)** and after **(B)** neoadjuvant chemotherapy. Before chemotherapy, cancer was visible on b 3000 images had a low ADC value (0.69 x 10^{-3} mm^2/s). After chemotherapy, the lesion was visible on b 2000 images and had an ADC value (0.64 x 10^{-3} mm^2/s) similar to the pre-therapy value.

Am I getting the best care?

Breast Care Solutions. A comprehensive approach – covering every step of the way.

Every breast cancer patient is different. That's why we provide you with a wide product portfolio, covering every step in breast care. Benefit from clearest image quality or anatomical and functional information. And deliver treatment with utmost precision. For women. For health. For life. **www.siemens.com/healthcare +49 69 797 6420**

Answers for life.

SIEMENS

CC-Z1055-2-7600

Quantification of Total Choline in Breast Tumors using *syngo* GRACE and PRISMA: Initial Experience at 1.5T

M. Lemort[1]; S. L. Chao[1]; M. Radermecker[1]; R. Demeure[2]

[1]*Institut Jules Bordet, Comprehensive Cancer Center, Department of Medical Imaging, MR Unit, Brussels, Belgium*
[2]*Siemens Medical Solutions Belgium*

Introduction

Choline is a metabolite that is relatively simple to observe using MR 1H spectroscopy and is recognized as a metabolic marker of active tumor tissue. What is observed with MR Spectroscopy (MRS) is a compound effect of the presence of not only choline but also choline derivatives such as phosphocholine, phosphatidylcholine, glucophosphocholine... Usually, the observed MRS signal is referred as tCho for "total choline".
The mechanisms of the accumulation of choline in cancer cells are not fully understood. Choline together with glucose transport and phosphorylation may be stimulated in breast cancer cells, due to up regulation of choline kinase and transporter genes [1]. It leads to an intracellular accumulation of phosphocholine. This can be observed dynamically using choline labelled with an isotopic marker or statically trough measurement of the choline content of tumor. MRS may achieve this measurement noninvasively. Accumulation of choline derivatives is a rapid phenomenon in cancer cells. So, the variation of tissue tCho contents may prove to be a short-term indicator of the level of tumor activity and/or viability. To evaluate choline as a marker of response to treatment, quantification of the metabolite is needed, and has to be repeated with good reproducibility. This raises specific problems in clinical spectroscopy.

We implemented a clinical quantitative technique using the *syngo* GRACE spectroscopy method, an internal water reference method and PRISMA* for spectroscopy post-processing, to assess the concentration of tCho in breast cancer, and its measurement error. PRISMA* is a PC standalone WIP package (Siemens Medical Solutions, Erlangen, Germany) for spectroscopy post-processing in the time domain. The method is robust, fully automatic and includes quality assessment.
We report our initial experience using this protocol for quantitative single voxel ^{1}H spectroscopy of breast tumors during neo-adjuvant chemotherapy.

*WIP. Works in Progress: This information about this product is preliminary. The product is under development and not commercially available in the U.S., and its future availability cannot be ensured.

Method

For quantification we used an internal reference as described by Meisamy et al. [2] at 4T, where [tCho] is derived from the water molal concentration
Where:
$f_{T1} = 1 - \exp(-TR/T1)$; $f_{T2} = \exp(-TE/T2)$;
η = number of 1H nuclei per molecule (2 for water and 18 for tCho)
MW = molecular weight
A = amplitude of measured signal

The clinical application of this method requires that:

1. All scans have to be acquired from the same voxel, and in the same coil sensitivity condition.
2. The T1 and T2 of tCho may be fixed by reference values obtained on preliminary experiments.
3. The water T2 or A0 (full relaxed amplitude) is measured in each experiment,
4. The correction for water T1 is eliminated by approximating full relaxation condition at TR of 6s for the water unsuppressed acquisitions.
5. The measured tissue water content is assumed to be mono-compartmental and relatively insensitive to change.

The *syngo* GRACE application for breast spectroscopy offers the capability to perform a single voxel acquisition of a breast lesion in less than 10 minutes.
We did the MRS acquisitions during routine breast MRI examinations also including coronal T2-weighted images, coronal 3D FLASH dynamic series, high-resolution fat-suppressed, MT prepared 3D T1-weighted

$$[tCho] = \frac{10^6}{MW_{water}} \left(\frac{\eta\, f_{T1}\, f_{T2}}{A}\right)_{water} \left(\frac{A}{\eta\, f_{T1}\, f_{T2}}\right)_{tCho} \quad (mmol/kg)$$

FLASH sequence and targeted diffusion-weighted imaging (DWI) with ADC map [3].

The acquisition scheme was as follows:

Step 1: Localizer reference images

- Using thin MIP reconstruction, the 3D subtraction data set is reformatted into 3 orthogonal plans centered on the lesion;
- these images are stored in an new series and loaded in the exam localizer when opening the MRS protocol.
- Before MRS, a patient positioning scout is acquired in each reference plan.

Step 2: Voxel planning

- The measurement voxel is adjusted to cover the maximum of the contrast-enhanced lesion, with a minimum of adipose tissue inclusion in each plane,
- 6 OVS bands are positioned at the voxel borders.
- For horizontal MRS the last acquisition should be used to facilitate the same repositioning, and voxel size should be readjusted following the above criteria, as the lesion may change with response to therapy.

Step 3: Shim adjustment

- The best result of 2 consecutive auto-shim should be used to improve the FWHW of the water magnitude spectrum to less than 24 Hz using linear shims manually.
- At visual inspection, if the water is less than twice the fat amplitude, the size and/or position of the voxel should be readjusted.

Step 4: tCho acquisition

- The *syngo* GRACE protocol was applied with a TR/TE = 1500/135 ms and NS = 192.

Step 5: tCho and water-reference acquisition

- During tCho acquisition, the same measurement protocol is appended to queue and modified without altering the voxel adjustment, obtaining 5 water-reference scans at different echo time (TE = 50, 75, 100, 125, 150), with water and fat suppression turned off, TR of 6000 ms and 4 repetitions.

Step 6: Patient position check

- After MRS acquisition, the positioning scout is restarted to check for patient immobility.

Figures 1 and 2 show results in typical patients.

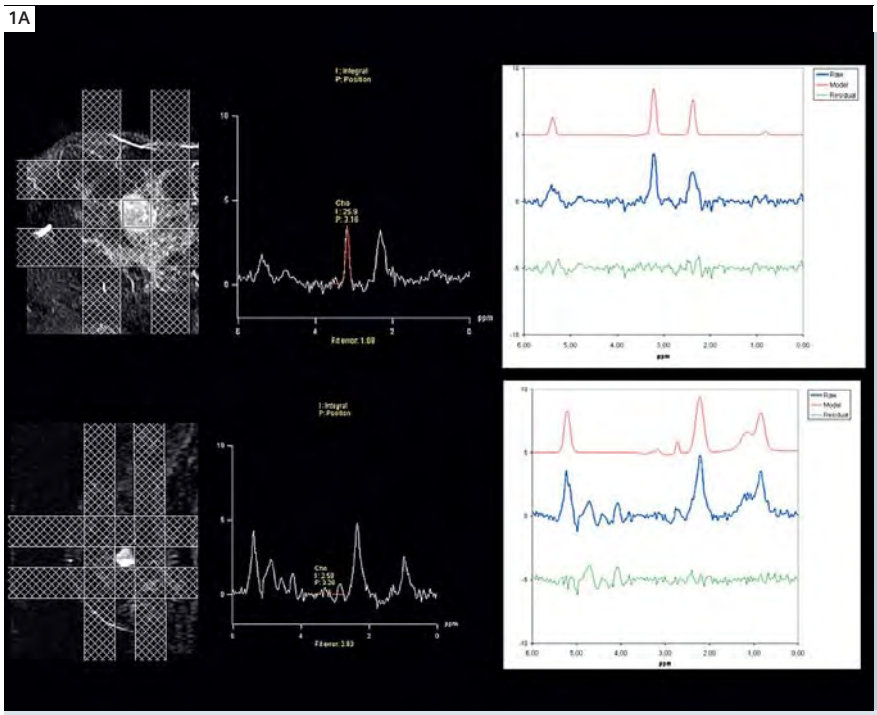

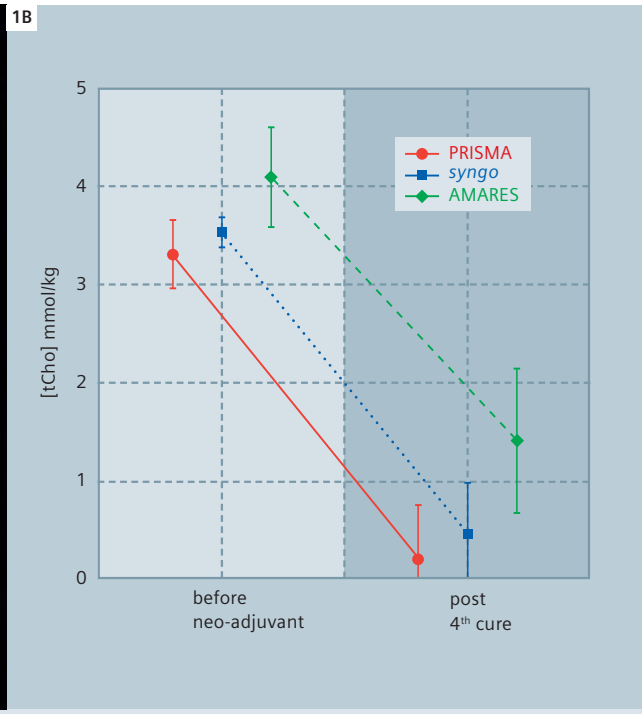

1 47-year-old patient with an invasive ductal carcinoma in the left breast, 4 cm in size, treated with neoadjuvant chemotherapy (Taxotère®). Figure 1A shows the localizer, spectrum and PRISMA output at baseline (upper row) and after 4 courses of chemotherapy (lower row). The size is clearly reduced (1.4 cm) and the sample volume had to be reduced accordingly. The calculated [tCho] at baseline was 2.35 (+- 0.42) mMol/kg. After the end of treatment (4 courses), the Cho peak is in the range of background noise. Figure 1B shows the graph of [tCho] calculated using the PRISMA and two other processing methods (MRUI/AMARES [4] and basic *syngo* processing).

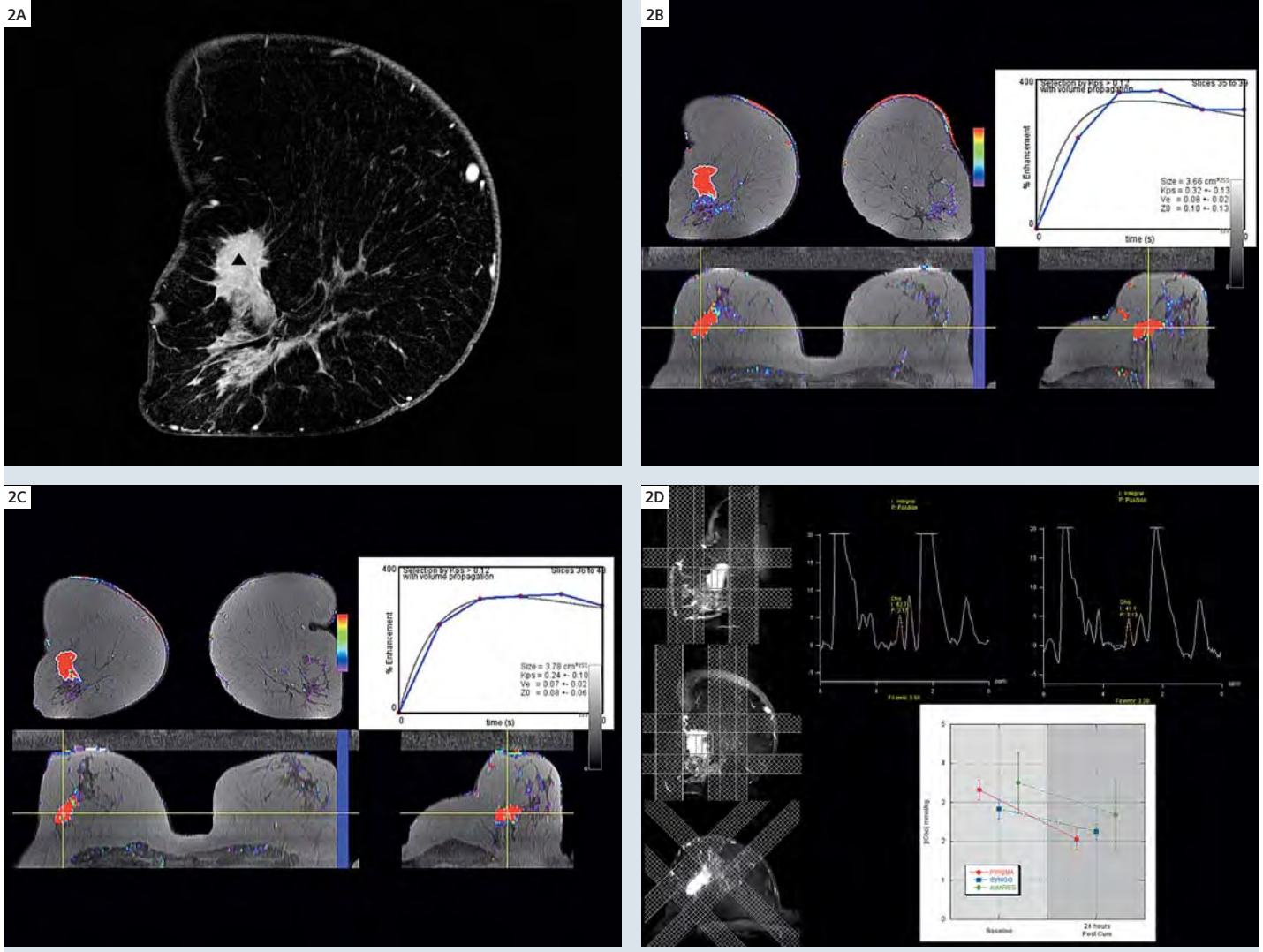

2 41-year-old patient with an invasive ductal carcinoma in the right breast, 3 cm diameter, with no palpable lymphadenopathy. On the baseline MR examination the targeted HR, MTC prepared, fat suppressed T1-weighted FLASH sequence **(Fig. 2A)** shows a mass in the right outer quadrants with a typical, spiculated appearance (black triangle). The DCE-MRI analysis using a pharmacokinetic model **(Fig. 2B)** shows a hypervascularized tumor with a transfer constant (Kps) markedly increased and numerous voxels with a washout phenomenon. 24 hours after the first course of neoadjuvant chemotherapy with FEC (Fluorouracil, Epirubicin, Cyclophosphamide), there is a marked reduction of the Kps values without significant reduction in size **(Fig. 2C)**. The spectrum **(Fig. 2D)** shows a clearly visible tCho peak. The calculated [tCho] using PRISMA at baseline was 3.32 (+- 0.27) mMol/kg. 24 hours after the first FEC course there is a reduced tCho peak with a calculated [tCho] at 2.05 (+- 0.27) mMol/kg. Figure 2D also shows the graph of [tCho] calculated using the PRISMA and two other processing methods (MRUI/AMARES and basic *syngo* processing).

Conclusion

Our first experience with quantitative single voxel MRS of tCholine in breast tumors using *syngo* GRACE and PRISMA at 1.5T is encouraging regarding both the feasability in the clinical setting and the ability to show a significant decrease in tCho contents as early as 24 hours after initiation of chemotherapy. Provided that a rigorous method is applied, the technique does not require high field nor special harware. Quantitative MRS gives an insight into the metabolic changes of tumor tissue and may be less related to microenvironmental changes than the vascular changes reflected by DCE*-MRI. As such, it may contribute to the definition of new surrogate markers for treatment response assessment. Prospective series are needed to assess the prognostic reliability of this marker.

References and suggested reading

1 G. Eliyahu, T. Kreizman, H. Degani. Phosphocholine as a biomarker of breast cancer: molecular and biochemical studies Int J Cancer, 2007, 120(8):1721-30.

2 Sina Meisamy, Patrick J. Bolan, Eva H. Baker, Robin L. Bliss, Evin Gulbahce, Lenore I. Everson, Michael T. Nelson, Tim H. Emory, Todd M. Tuttle, Douglas Yee, and Michael Garwood. Neoadjuvant Chemotherapy of Locally Advanced Breast Cancer: Predicting Response with in Vivo ^{1}H MR Spectroscopy – A Pilot Study at 4 T Radiology 2004; 233: 424-431.

3 E. Rubesova, A.S. Grell, V. De Maertelaer, S.L. Chao, T.Metens, M.Lemort. Quantitative diffusion imaging in breast cancer: a clinical prospective study J Magn Reson Imaging. 2006 Aug;24(2):319-24.

4 van den Boogaart, A., Van Hecke, P., Van Huffel, S., Graveron-Demilly, D., van Ormondt, D., de Beer, R. MRUI: a graphical user interface for accurate routine MRS data analysis. In: Proceedings of the ESMRMB 13th Annual Meeting, Prague, p. 318, 1996.

* WIP Works in progress. The information about this product is preliminary. The product ist under development and not commercially available in the U.S., and its future availability cannot be ensured.

^{1}H MR Spectroscopy of the Breast*

Mitsuhiro Tozaki, M.D.[1], Katsuya Maruyama[2]

[1]*Breast Center, Kameda Medical Center, Chiba, Japan*
[2]*Siemens-Asahi Medical Technologies LTD., Tokyo, Japan*

Introduction

Breast MRI has emerged as a highly sensitive modality for the imaging of breast tumors, although its specificity remains variable, ranging from 30% to 80%. To improve the specificity, detailed assessment of lesion morphology using three-dimensional MR imaging and of kinetic patterns depicted using dynamic protocols may be useful. In addition, new characterizations of tumor cellularity on diffusion-weighted imaging and of tumor metabolism on ^{1}H MR spectroscopy can be obtained in routine clinical breast MRI examinations.

In vivo ^{1}H MR spectroscopy of the breast, actually molecular information obtained in a non-invasive manner, has demonstrated that Choline (Cho) can be detected in breast cancers, whereas Cho is generally undetectable in normal breast tissue. Increased levels of composite Cho compounds is thought to be an indicator of the activity of breast neoplasms and of the viability of breast cancers. Therefore, breast MR spectroscopy has shown great promise as a way to differentiate between benign and malignant lesions, and to gauge the effect of chemotherapeutic agents in patients with locally advanced breast cancer.

To date, there has been no large dataset with which to evaluate the clinical usefulness of in vivo breast ^{1}H MR spectroscopy. Recent technical improvements in breast MR spectroscopy and in the stability of the obtained spectra, even on 1.5T MR equipment, make it possible to investigate breast MR spectroscopy worldwide. In our hospital more than 200 breast MRI examinations are performed each month, and more than 600 breast MR spectroscopy (MRS) exams have been obtained in six months.

Sequence description

The breast spectroscopy sequence** is a spin-echo sequence with the following added capabilities: spectral suppression pulses, up to 8 regional saturation bands for outer volume suppression, physiological triggering, online frequency correction, extended voxel dimension limits, and multi-channel data combination.

Spectral suppression

By the spectral suppression method, transverse magnetization is selectively dephased before and after the second spin-echo pulse. The quality of spectral suppression can be visualized by the following simulated frequency response profile of our numerically optimized pulses: Magnetization components of Mxy = -1 are dephased; components of Mxy = 1 are rephased. This method of spectral suppression has been described as "MEGA" or double "BASING". The parameters shown in Fig. 1 work well for breast spectroscopy where the peaks of interest are between 2.5 and 3.5 ppm. With the centre of the lipid suppression pulse being at 1.3 ppm (4.7–3.4) and the width of the suppres-

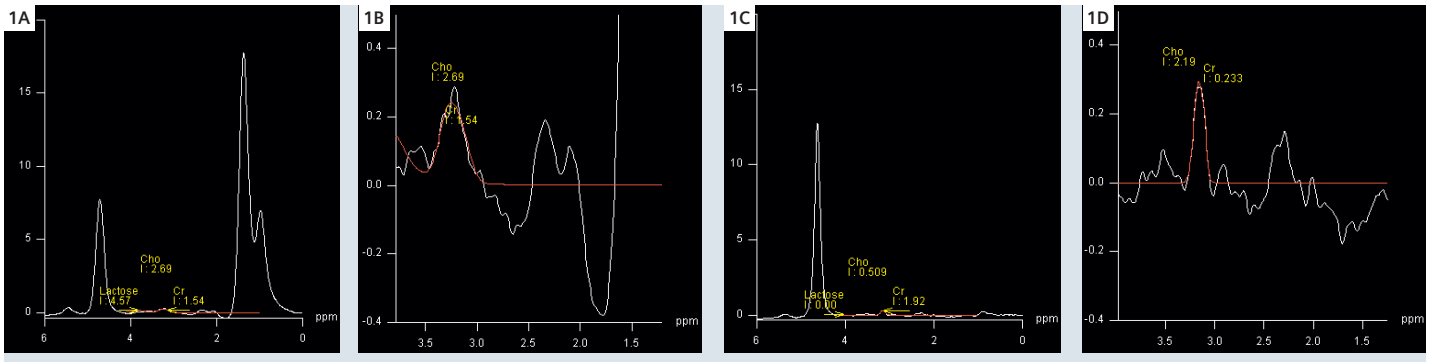

1 MR Spectra of breast cancer without **(A and B)** and with **(C and D)** lipid suppression. SVS TE = 270, voxel size 15 x 15 x 15 mm^{3}, TA = 7 min. **(B)** and **(D)** are displayed spectra from 1.2 to 4.0 ppm of **(A)** and **(C)**. Choline peak is detected more clearly in **(D)** than in **(B)**.

*Some of the concepts and information in this paper are based on research and are not commercially available in the U.S.

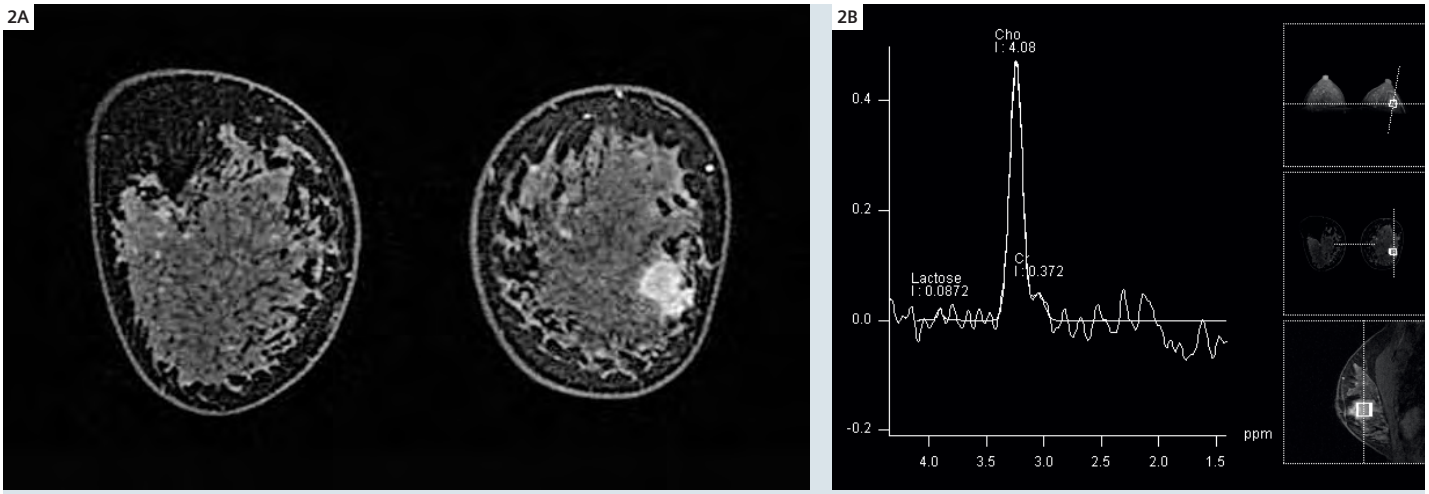

2 High resolution 3D dynamic imaging, showing a breast cancer in the right breast. SVS spectra from a biopsy proven invasive breast cancer acquired on a MAGNETOM Avanto. ^{1}H MR spectroscopy proved to be quite sensitive for detecting invasive carcinoma.

sion pulse being 1.55 ppm, signals in the spectral range of 0.5–2.1 ppm are suppressed.

Online frequency correction

The sequence includes online frequency correction, implemented within the reconstruction program, and the correction requires a water peak for inline shifting. Therefore, to ensure sufficient water signal, use the water suppression setting "Weak water suppression" and a longer "WET recovery delay," the delay between the WET schema and the excitation.

Post-processing

Filter: Hanning, width 400 ms, Zero filling: 2048, Baseline: polynomial order: 6, Phase correction: manual or auto using choline; Note that a bias is introduced by phasing a single signal. Curve fitting: calculation range: 1.6 ppm: choline.

Differential analysis

Regarding the differentiation between benign and malignant breast lesions, we report several promising results. In malignant lesions, ^{1}H MR spectroscopy achieved a high overall sensitivity (more than 80%) (Fig. 2). Moreover, ^{1}H MR spectroscopy proved to be quite sensitive for detecting invasive carcinoma from sarcoma and ductal carcinoma in situ. In ductal carcinoma in situ, the limited number of cases until now has been investigated with lower sensitivity, while most benign tumors were negative on ^{1}H MR spectroscopy. However, false positive cases were sometimes experienced (Fig. 3). With the ongoing development of MR technology and breast matrix coils, detection of weak Cho peaks in benign lesions is increasing, and the specificity may be decreasing. In the near future, technology to determine the quantity of composite Cho compounds may be needed.

Monitoring the therapeutic response

Another potential application of ^{1}H MR spectroscopy is in the assessment of the response to neoadjuvant chemotherapy. Contrast-enhancement patterns may lead to misleading findings and false-negative results due to the effects of chemotherapeutic agents. In contrast, ^{1}H MR spectroscopy and diffusion-weighted imaging are demonstrating great promise in the evaluation of the direct effects of chemotherapeutic agents. The presence of a Cho peak in breast cancer may reflect the increased cell proliferation, with a decrease in this peak after treatment reflecting decreased viability of the tumor (Fig. 4). In short, metabolic changes observable by ^{1}H MR spectroscopy are predictive of subsequent clinical response. We believe that early changes in the Cho peak after one or two cycles of neoadjuvant chemotherapy are important information for the decision to continue treatment. Furthermore, the same measurement protocol is required for each follow-up examination. Using the Phoenix functionality of the *syngo* software, the same parameters and voxel size (15 x 15 x 15 mm^{3}) are ensured for all measurements.

Conclusion

Recent technical improvements in breast MR spectroscopy, including special software to reduce large lipid signals, have made it possible to obtain stable spectra even on 1.5T MR equipment. Clinical investigations using breast MR spectroscopy have just begun; however, the technique has already shown great promise in the MR diagnosis of breast lesions and in the therapeutic decision for patients with breast cancers. With further development and the assessment of Cho quantity in the tumor, breast MR spectroscopy may be helpful in the elucidation of the biology of breast cancer.

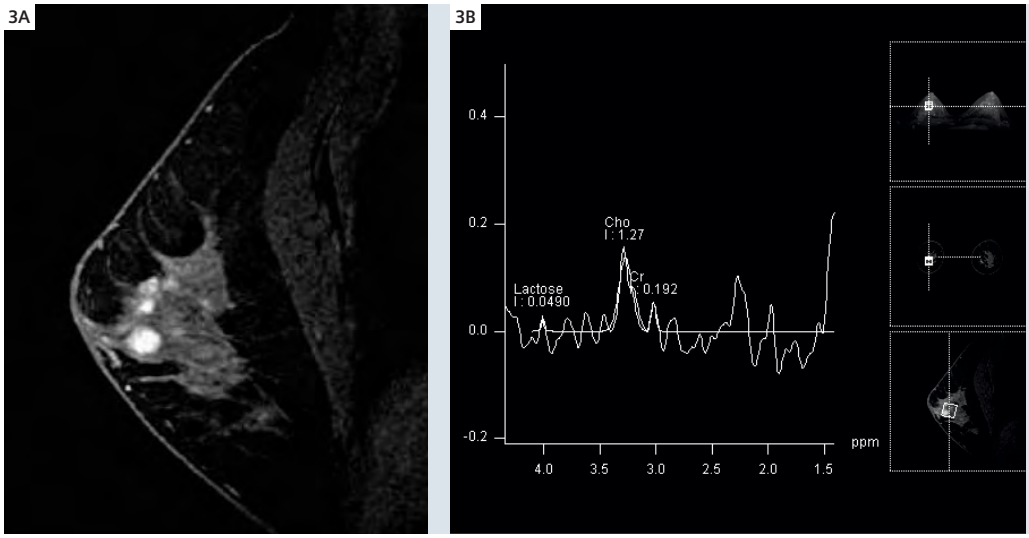

3 SVS spectra showing weak Cho peak from a biopsy proven fibroadenoma. False positive cases occur.

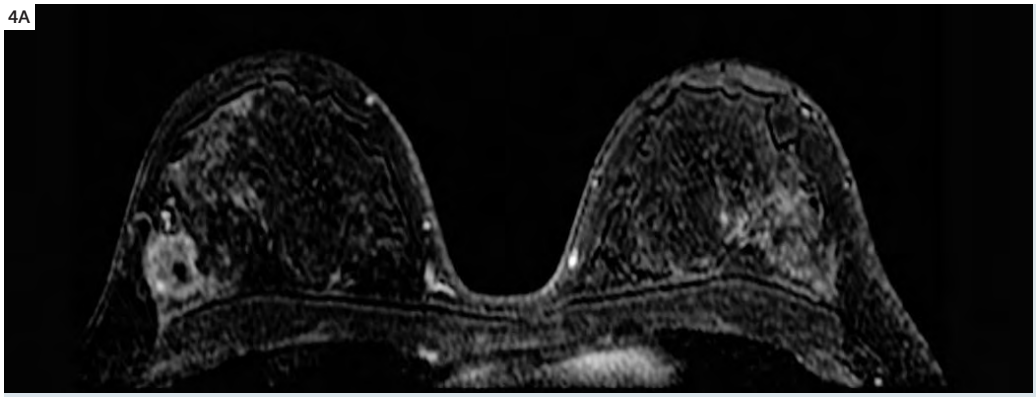

4 Transverse MPR images of high resolution 3D dynamic imaging, showing a breast cancer in the right breast **(A)**.

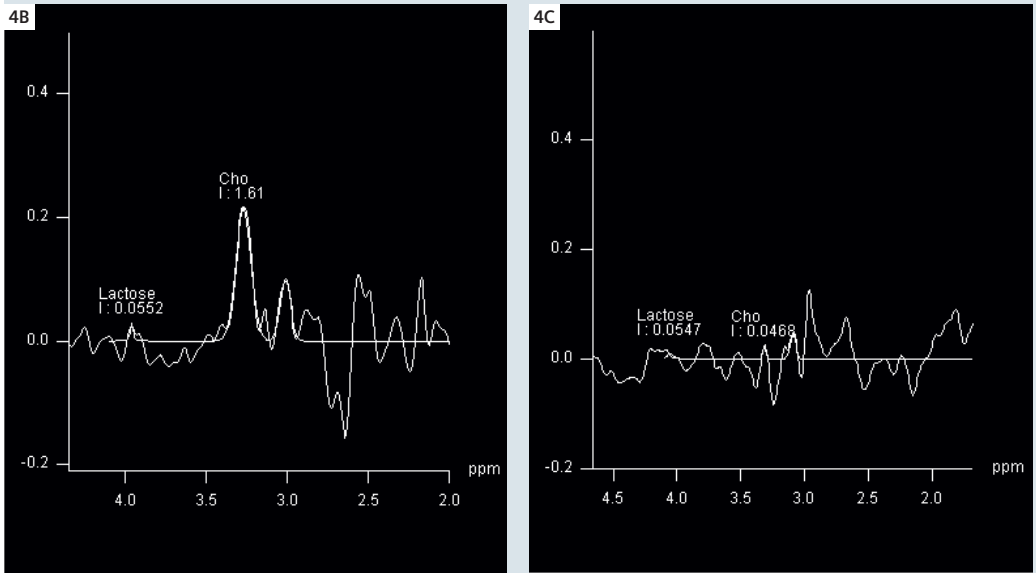

SVS Spectra before **(B)** and after **(C)** neoadjuvant chemotherapy. Metabolic changes observable by ^{1}H MR spectroscopy are predictive of subsequent clinical response.

**WIP – Work in progress. This information about this product is preliminary. The product is under development and not commercially available in the U.S., and its future availability cannot be ensured.

syngo GRACE

Sheila Christ, B.S., RT (R) (CT) (MR)

Senior Clinical Education Specialist, Siemens Medical Solutions, Cary, NC, USA

Introduction

Breast cancer is the second leading cause of cancer death in women. In 2007 approximately 40,460 women and 450 men will die from breast cancer per the American Cancer Society. With the improvements in MR technology, *syngo* GRACE is a valuable diagnostic tool for breast cancer with an easy workflow process.

syngo GRACE

GRACE (GeneRAlized breast speCtroscopy Exam) makes it possible to examine breast lesions on a molecular level, using the ^{1}H MR spectroscopy (MRS) single voxel spectroscopy (SVS) technology.
Choline acts as biomarker in breast spectroscopy. The choline metabolite in healthy breast tissue is usually negligible. A visible higher choline signal in the spectrum can be correlated with mailignant biopsy results. However, choline levels may be visible in the lactating breast.

Clinical values

By using *syngo* GRACE, the radiologist can use a noninvasive method of differentiating between benign and malignant lesions. This can eliminate the need for the biopsy of a tumor.
Monitoring therapeutic efficacy is essential in the management of cancer patients. The tCho concentration of the spectrum can serve as an indicator for predicting clinical response to chemotherapy.
GRACE can help improve identification of possible vital residues after chemotherapy and preoperative intervention.
The following examples show tumor spectrum of breast cancer before, and during chemotherapy. Biopsy correlates with high choline signal in the spectrum.

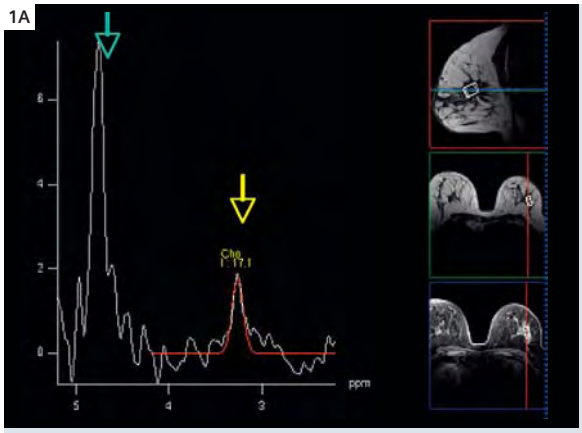

1A Spectrum shows a high choline peak prior to chemotherapy.

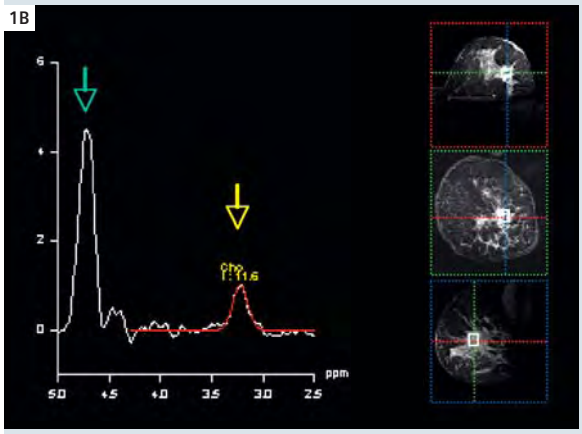

1B Choline signal appears reduced after second cycle of chemotherapy.

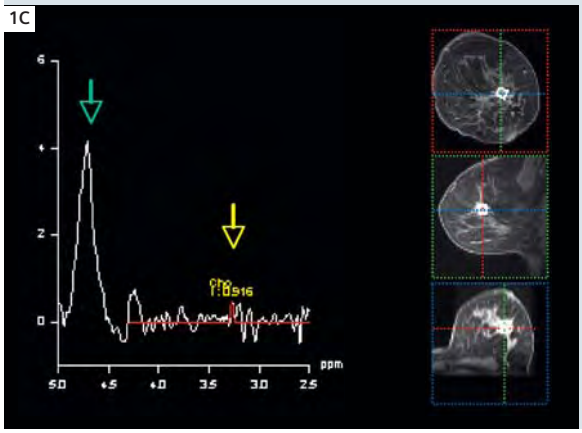

1C Almost no choline signal is seen after the last (sixth) cycle of chemotherapy.

Images courtesy of Prof. T. J. Vogl, University of Frankfurt/Main, Germany.

Quantification with external reference

The Siemens Breast Matrix coil has a reference solution present in the coil housing for the normalization of the choline signal relative to saline. The choline signal is automatically normalized with an additional measurement of the reference sample signal.

Quantification with internal reference

An additional possibility for normalizing the choline signal consists of an internal reference measurement. For this purpose, you can perform a fast, non-water suppressed measurement in the tumor with an identical voxel position and size. However, the internal reference method is not considered clinically sound for controlling the course of therapies.

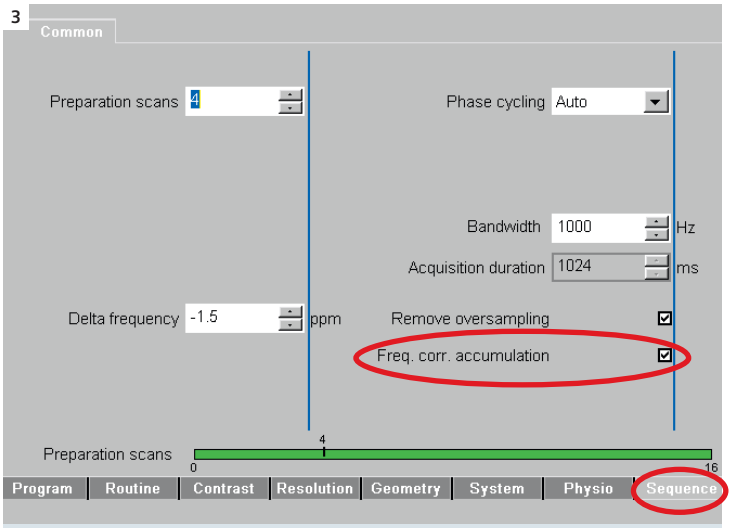

3 Another new feature of the sequence is the Inline frequency correction which can minimize respiratory artifacts.

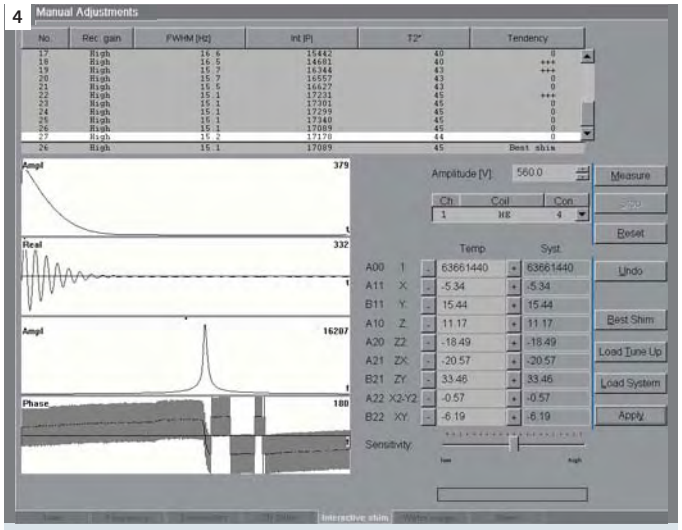

4 The shimming in breast MR spectroscopy.

Breast MRS setup

Position the patient in the prone position in the breast coil, with careful fixation of the breast. It is helpful to use the subtraction images for voxel positioning.
Voxel size should be adapted to the tumor size. If the voxel size is too large and if there is poor positioning of the voxel; then fat signal is superimposed on the choline signal.

Sequences

GRACE uses the svs_se sequence with spectral lipid suppression and weak water suppression. By using the spectral lipid suppression, this reduces the effect of lipid on the choline signal. The weak water suppression leaves a residual water peak; this allows you to include the water line in various post-processing functions.

Shim

Semi-automatic shimming is the method of choice for *syngo* GRACE pre-scan adjustments (Fig. 4). With your protocol open, select the options-adjustments, from the display window pop up, select the show tab. In the bottom right corner of the window select invalidate all then adjust all. Wait until the adjustments are complete (the system will communicate with you in the bottom left corner of the window). To confirm how well the shim adjusted, select the interactive shim tab, then measure (this begins an endless measurement), check FWHM and T2* in the top box, the FWHM must be equal to or less than 25 Hz, the smaller the number the better the shim. If the FWHM is greater than 25 Hz FWHM, adjust the linear terms X,Y, and Z separately using the +/- keys until the above criteria for FWHM is achieved. Select stop, best shim and apply. Close the adjustments window and apply the sequence.

Post processing normalization

A known reference quantity is required when normalizing the tCholine signal as part of breast spectroscopy (Fig. 5). The breast signal is normalized using an additionally measured reference data set. The reference data is acquired by doing a fast SVS measurement without water suppression. If you are using the Siemens Breast Matrix coil in the housing there is an external probe filled with sodium chloride combined with a nitrate preservative. The normalization algorithmic step is applied in the frequency domain.

Conclusion

syngo GRACE is a valuable diagnostic tool to classify lesions and to help predict the response to therapy. The application is optimized for the Siemens Breast Matrix coil that is equipped with a reference probe utilized during imaging. GRACE has an easy workflow process with semi-automatic shimming and normalization post processing.

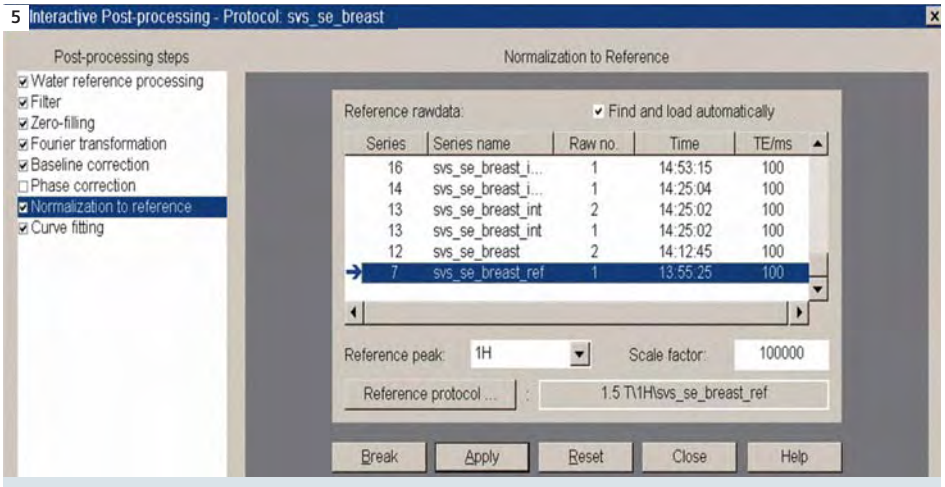

5 Post processing normalization.

Case Report: Role of MRI Imaging in a Gynecological Emergency of Ectopic Pregnancy

Dr. N. Dahmen, M.D.

Klinik St. Josef, St. Vith, Belgium

Patient history

A 16-year-old female presented in our emergency room with complaints of intermittent abdominal pain for more than one month. Biology tests revealed anemia, augmented neutrophyle leucocytes and an inflammatory condition. Ultrasound examination showed a large pelvic hemoperitoneum. As the patient was in a stable condition, an MRI exam was performed.

Sequence details

1. Coronal and transverse T2-weighted Turbo Spin Echo (tse) with *syngo* BLADE to reduce respiratory motion of the pelvis. TR/TE = 4000/106, FoV of 280 mm (FoV phase 100%), 30 slices of 3.5 mm coronal, 5 mm transverse, 2 concats, base resolution 320 (phase resolution 100%), BW = 363 Hz/pixel, TF = 35, echo spacing = 5.88 ms, no fatsat, TA = 2 min 18 s
2. Transverse T1-weighted tse with fatsat, TR/TE = 434/12, FoV = 280 (FoV phase 75%), Base resolution 448 (phase resolution 75%), TF = 3, fatsat
3. Transverse T2-weighted tse with *syngo* BLADE, using fatsat
4. T1-weighted transverse VIBE in pre and post contrast in 3 planes at different injection times: TR/TE = 4.68/2.17, FoV coronal = 400 mm (FoV phase 100%), FoV transverse/sagittal = 320 (FoV phase 75%), 72 slices of 2 mm (cor) and 40 slices of 3 mm (tra/sag), flip angle 12°, base resolution 320 (phase resolution 66%, slice resolution 64%), BW = 400 Hz/pixel, fatsat, breathhold

Results

After realization of the tse_BLADE T2-weighted sequences, a hemoperitoneum and a mass – of which the 'onion-tunic' is clearly depicted – is seen in the adnexal area. After gadolinium injection, late injection phases show peripheral contrast uptake of the mass and a slow uptake of a tubular structure.
This finding was suggestive of a peritoneal abortion of an ectopic pregnancy (also called extra uterine pregnancy) with reactional salpingitis on the right and a hemoperitoneum as result of venous rupture. The right Fallopian tube is intact without rupture.

Discussion

Ectopic pregnancy (EP) as detected after T2 tse BLADE sequences. Application of the BLADE technique reduces artefacts, originating from peristaltic movement and reducing respiratory movements of the frontal fat layer. Consequently, saturation bands are no longer used. BLADE sequences have a shorter acquisition time and permit a final diagnosis in a very short time. In the future, these sequences can be used as unique T2 sequence in a fast, pre operative phase, insofar as the vital condition of the patient is not in danger. The T2-weighted BLADE sequences should be completed by fast, dynamic T1-weighted VIBE sequences in search of active bleeding.

Conclusion

The abortion of ectopic pregnancy was confirmed by laboratory tests, showing a positive ß-hCG (human Chorionic Gonadotropin hormon), and through Pathology. No salpingo-ophorectomy had to be performed.
The T2-weighted *syngo* BLADE sequence, in combination with T1-weighted dynamic VIBE imaging is a good emergency gynecological protocol.

1 Coronal T2-weighted TSE sequence with *syngo* BLADE: the fundus of the uterus, right adnexal and an ectopic pregnancy (EP) with abortion in the peritoneum.

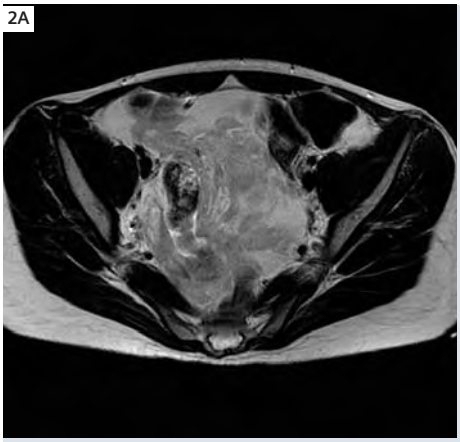

2A Transverse T2-weighted Turbo Spin Echo (tse) sequence with *syngo* BLADE: EP with hemoperitoneum.

2B Transverse T2-weighted tse with *syngo* BLADE: hemoperitoneum, right adnexal, round ligament, large ligament and posterior part of the mass.

3A Coronal VIBE post contrast: contrast uptake of the right adnexal and around the expulsion material, showing a slow bleeding tubo-ovarian vasculature.

3B Transverse VIBE late post contrast: ring enhancement of the expulsion material, showing a tubo-ovarian bleeding.

3C Contrast uptake of the large ligament and of the right adnexal, in contact with peritoneal abortion of ectopic conception material.

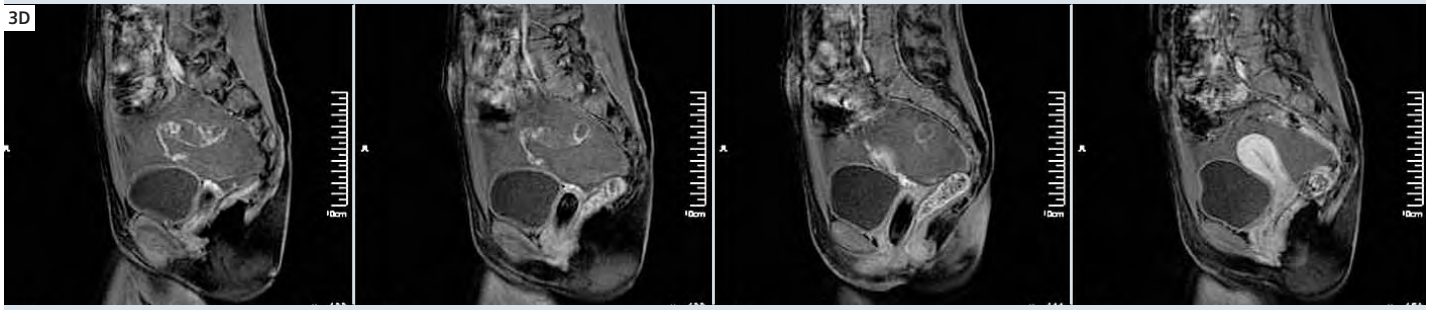

3D Sagittal VIBE post contrast: enhancement of the right adnexal with active bleeding, causing the hemoperitoneum.

Prostate Cancer – Meeting Clinical Needs by Advanced MRI at Diagnosis and on Follow-Up

Dr. Anwar R. Padhani, M.D.[1,2]; Dr. Clare Allen, M.D.[3]

[1]*Paul Strickland Scanner Centre, Mount Vernon Cancer Centre, Northwood, Middlesex, United Kingdom*
[2]*Synarc Inc., San Francisco, CA, USA*
[3]*Department of Imaging, University College Hospital, London, United Kingdom*

Introduction

Carcinoma of the prostate is the commonest form of human carcinoma, found at autopsy in 30% of men at the age of 50 and in over 80% of men in their 90s. Worldwide, more than 650,000 men are diagnosed with the disease each year accounting for a 10th of all new male cancers. In Europe, the lifetime risk of being diagnosed with prostate cancer is approximately 1 in 13. In 2006, an estimated 234,460 American men were newly diagnosed with prostate cancer, and over 30,000 died of the disease. There is a close association between recent increases in the incidence of prostate cancer and the use of transurethral resection of the prostate (TURP) for treating obstructive lower urinary tract symptoms due to presumed benign prostatic hyperplasia (BPH) and more recently with serum prostatic serum antigen (PSA) testing. Whether there is a real increase in incidence or not, the number of cases of prostate cancer will rise further as the population at risk (older men) grows with lengthening of life expectancy. With the increased use of PSA testing, it has been noted that there has been a gradual downward stage migration (increased incidence of early disease) with the discovery of carcinomas that are possibly not life threatening. Prostate carcinoma thus represents a significant challenge for men's health. This fact has been recently recognized by the US Congress with the recent introduction of the Prostate Research Imaging and Men's Education (PRIME) act. This act, the first to directly support imaging technologies and in vivo diagnostics for the detection, diagnosis and treatment of prostate cancer, seeks to authorise an investment of USD 600 million over five years to combat this deadly disease with related educational efforts to raise public awareness. There are considerable limitations in current diagnostic and therapy pathways for prostate cancer patients. Only moderate tumor and nodal staging accuracies of imaging tests has resulted in the patchy adoption of MRI into routine patient management particularly at new diagnosis. The fact that prostate cancer is often multicentric and poorly depicted by non-invasive tests has resulted in whole organ rather than specific tumor-directed therapy. With downward stage migration, it is increasingly unclear whether it is necessary to actively treat all diagnosed cases. There is debate on what constitutes clinically important disease encapsulated by the disparity between the approximate 30–40% prevalence of histological prostate cancer in men older than 50 years of age and the 8% of cancers that become clinically significant or the 3% lifetime risk for death from this disease. Since therapies are not without their sometimes devastating complications, there is increasing patient pressure for more minimally invasive and more effective therapeutic approaches. In this context it is clear that focal ablations (so-called "male lumpectomy") will play increasingly important management roles (examples include photodynamic therapy (PDT), cryotherapy, high-intensity focused ultrasound (HIFU) and high-dose rate brachytherapy). The usage and future success of these treatments will depend on the identification of clinically significant focal disease (the dominant intra-prostatic lesion (DIL) also called index lesion and the absence of extra prostatic disease (see box for additional clarification of these terms). Additionally, new therapeutic approaches include prophylactic nodal radiotherapy with the intensity modulation (IMRT) require the accurate mapping of the location of pelvic lymph nodes for the eradication of metastases. In the future, patient therapy will be more personalized taking into consideration not only the extent of local disease but also assessments of biological aggressiveness as well as patient and physician preferences. It is in these contexts that this paper describes the current and future roles of MRI in prostate cancer patient management. The approach is from the perspective of the patient pathway describing clinical and research requirements at each stage and the authors' opinions on the roles of morphological and functional imaging in order to overcome current bottlenecks in prostate cancer management. The opinions expressed

Terminology

Localised prostate cancer can be stratified into risk groups using combinations of clinical findings, histopathology using the Gleason grading system and presenting serum prostate specific antigen level (PSA). General risk categories for prostate cancer are given in table 1. Many readers will be unfamiliar with some of the terminology pertaining to prostate cancer management. These concepts are used in different ways by clinicians and pathologists and the authors' current understanding of these terms is as follows:

Dominant intraprostatic lesion (DIL) also called Index lesion: This is a vague term used in the radiotherapy/surgical literature referring to the major focus of disease in terms of tumor volume, the goal being to focally ablate these regions as part of whole prostate gland therapy.

Clinically insignificant disease: Small-volume prostate cancers (usually 0.5 ml or less) without elements of Gleason grade pattern 4 or 5. By definition these tumors are non-palpable and confined to the prostate gland. However, since many prostate cancer deaths occur more than 10 years after the initial diagnosis, the biological behavior of small-volume prostate cancers may become important in patients with relatively long post-diagnosis life expectancies.

Clinically significant disease in non-palpable (T1c) prostate cancer: These tumors are often risk stratified by well-established prognostic factors (Gleason score [GS], pretreatment serum PSA level, and percent positive biopsy findings [%+Bx]) because these factors predict biological aggressiveness.

High risk: GS = 8-10 or PSA level > 20 ng/mL; or GS = 7 or PSA level > 10–20 ng/mL and > 50%+Bx – these patients have a historical four-year PSA control of 10% to 30% after definitive therapy.

Intermediate risk: GS = 7, PSA level > 10–20 ng/mL, and 34%–50%+Bx. These patients have a historical four-year PSA control of 50% to 60% after definitive therapy.

Significant disease can also be based on age and GS. Antiticipated prostate cancer mortality greater than 30% to 50% also includes patients with GS = 7 and age 70 years, and GS = 6 and age 65 years.

represent the views of the authors based on literature reviews and personal experiences. Recommendations given are partly dependent on our subjective assessments of ease of imaging acquisition, analysis and interpretations.

Roles and current limitations of MRI in clinical practice

From the outset it should be recognised that MRI for newly diagnosed cancer patients is not universally accepted nor used. However, the majority of urological surgeons and radiotherapists agree that the following patients should have MRI at first diagnosis:

1. Symptomatic patients: MRI has an important contributing role in determining tumor extent, detecting complications and planning treatment.
2. Patients at higher risk of local / metastatic spread: a current consensus definition of risk groups for prostate cancer patients is given in table 1.
3. Potential surgical candidates where Partin tables suggest the risk of extra-prostatic disease (level of risk is debated but probably > 30% – depending on radiological expertise).
4. Patients with palpable apical tumors. Patients with advanced or metastatic disease need not always undergo detailed local staging with MRI.

It is to be noted that clinical requirements change at various points of the prostate cancer patient's journey and questions for MRI to address are correspondingly altered (Table 2). So for example when MRI is used for newly diagnosed patients, the objectives for its usage are:

1. To delineate the intra- and extra-prostatic extent of the local disease. Here, the key first distinction is organ confinement versus extra-prostatic disease.
2. Prostatic cancer is often multifocal, and the detection of the dominant prostatic cancer nodule or index lesion is becoming important for therapy planning (for definition see box).
3. To detect the presence of cancer at the prostatic apex; this is an important consideration for patients being considered for surgical therapy.
4. To detect the presence and location (intra- versus extra-pelvic) of metastatic nodal involvement.
5. To detect the presence of bone metastases.
6. To detect the presence of complications of urinary tract obstruction.

Years of experience shows that morphological (T2-weighted) MRI has many limitations for the evaluation of the prostate gland. We have come to recognize that tumor volume and distribution is often underestimated because not all tumors are visible and small tumors are not consistently shown. Confounding effects occur because there are other causes of low signal intensity in the peripheral gland

* Works in progress (WIP). The information about this product is preliminary. The product is under development and not commercially available in the U.S., and its future availability cannot be ensured.

Table 1: UK National Comprehensive Cancer Network (NCCN) definitions of risk for prostate cancer (2005)

Low Risk	T1-T2a and Gleason Score 2–6 and PSA < 10 ng/ml
Intermediate Risk[1]	T2b-T2b or Gleason Score 7 or PSA 10–20 ng/ml
High Risk[1]	T3a or Gleason Score 8–10 or PSA > 20 ng/ml

[1] Patients with multiple adverse factors may be shifted into the next higher group. Note: T3a/b and T4 disease is not organ confined.

Table 2: The prostate cancer patient journey and contribution of MRI in patient care

			Treatment of initial disease*								Treatment of relapsed disease	
				Curative intent								
Clinical Journey begins here	**Suspect cancer**	**Stage known cancer**	**Initial observation (deferred therapy)**	**Surgery**	**Ablative therapies (HIFU, PDT, cryotherapy brachytherapy)**	**External beam radiotherapy to prostate ± pelvic nodes**	**Palliative**	**Monitoring effectiveness of therapy**	**Surveillance of treated disease**	**Suspect relapse**	**Local salvage**	**Palliative**
Clinical scenario	Raised PSA with negative biopsy TRUS and or biopsies	Cancer diagnosed and confirmed by biopsy	Small volume Low aggressiveness	Organ confinement No tumour at prostatic apex No metastases	Organ confinement No metastases	Usually includes neo-adjuvant hormones	Usually hormonal therapy ± RT	Usually after focal therapies	Rare to use imaging in this role (Serum PSA surveillance)	Significant rise in serum PSA	Disease is localised and salvage is possible	Disease is not localised and salvage is impossible
Clinical (C) or Research (R) requirements	Define tumour location and size for targeted biopsy (C)	TNM stage (C) Define dominant lesion (C) Define lesion aggressiveness (C/R) Therapy planning (C)	Confirm organ confinement (C) Document size (C) Depict lesion aggressiveness (C/R)	Detect adverse features (C) Target pelvic nodal dissection (C)	Define dominant lesion location and size (C/R)	Confirm confinement to pelvis (C) Nodal mapping (C/R)	Define extent of nodal & distant metastases (C) Requirements for local palliation (C)	Treatment verification (R) Define volume and extent of residual disease (R)	Detect active disease in absence of significant PSA rise (R)	Identify site and volume of recurrence (C)	Define extent of local disease and absence of metastases (C)	Define extent of of relapsed disease and complications (C) Requirements for local metastases (C)
Contribution made by MRI[1]												
Morphology	+++	+++	+++	+++	+++	+++	++	+++	++	+++	+++	+++
Additional MRI biopsy	+	0	+	0	0	0	0	+	+	++	++	0
Lymphography	0	++	+++	+++	+++	+++	+	0	0	++	++	0
MRSI	+++	+	++	++	+	+	+	0	+++	++	+	0
DW-MRI	+++	++	+++	++	++	++	+	+	++	+++	++	0
Data fusion	++	++	+	++	++	++	0	0	+	+	++	0
DCE-MRI	+++	+	+++	++	+	+	0	+++	+++	+++	+++	0
BOLD-MRI	0	+	0	0	+	+	+	+	0	+	0	0

[1] These authors' opinions are based on literature reviews, personal experiences and recommendations are partly dependent on subjective assessments of ease of imaging data acquisition, analysis and interpretations. *The imaging recommendations are for the purpose of planning therapy.
0 = No requirement; + = possible requirement; ++ = probably indicated; +++ = definite indication

(scars, prostatitis, haemorrhage and therapy effects) and central gland tumors can be particularly difficult to see in the presence of benign prostate hyperplasia (BPH). Conventionally it was thought that these were unimportant limitations as key therapeutic decisions were based on tumor extent (simply organ confinement or not) but we know that MRI also has a restricted ability to distinguish organ confined disease from early T3 disease resulting in great staging variability from center to center. Furthermore the clinical situation has changed because it is now increasingly important to depict the index lesion/DIL for the application of minimally invasive treatments which may (or may not) be used in combination with conventional approaches. As we move into the arena of personalised patient-oriented therapy, imaging assessments will need to become more comprehensive and accurate, depicting not only the extent of local disease but also assessing biological aggressiveness (by depicting tumor grade other biological important features such as the presence and extent of tumor hypoxia, increased vascularisation and proliferation rate). Beyond local tumor assessments, our current ability to accurately depict nodal metastatic disease is also limited by the use of morphological criteria based mainly on size evaluations. There is a high incidence of reactive pelvic lymph node enlargement and it is well described that adenocarcinoma prostate metastases are of small volume (microscopic) and therefore may be found in normal sized lymph nodes. There is a high incidence of nodal spread to surgically non-sampled sites at pelvic lymph node dissection (PLND). Therefore future assessments of prostate cancer patients will also include more accurate depiction of the presence and extent of nodal metastatic disease.

Overcoming limitations with advanced MRI techniques

Over recent years tremendous experience has been gained in functional MRI techniques and it is becoming increasingly clear that they may be able to address some of the bottlenecks in prostate cancer patient management. New techniques which include dynamic contrast enhanced MRI (DCE-MRI), diffusion-weighted MR imaging (DW-MRI), proton MR spectroscopic imaging (MRSI) and blood oxygen level dependent MR imaging (BOLD-MRI) are making the transition from academic investigation to routine clinical usage. The progress made by each technique in the transition to clinical practice varies, but important lessons on their potential uses and limitations are known. With the advent of faster sequences performed on high-performance, high field strength MRI scanners it is possible to combine morphological and multiple functional prostatic imaging into a more comprehensive evaluation with only a small additional time penalty. Since the limitations of each technique are often non-overlapping it is recommended that multiple functional imaging techniques are used for making diagnoses and therapeutic decisions at various stages of the clinical cancer journey as recommended in tables 2 and 3. The biological basis of observations on these techniques is discussed briefly with appropriate references for interested readers. Examples of multifunctional imaging use in clinically suspected cancer at diagnosis and after definitive treatment are shown in the figures.

Dynamic contrast enhanced MRI (DCE-MRI) using small molecular weight gadolinium chelates enables non-invasive imaging characterization of prostatic vascularity. Established clinical roles in prostate gland include lesion detection and localization, for tumor staging and for the detection of suspected tumour recurrence [1]. **Diffusion-weighted MRI** (DW-MRI) is a technique that displays information about the extent and direction of random water motion in tissues. DW-MRI provides information on extracellular space tortuosity, tissue cellularity and the integrity of cellular membranes. Clinical data indicates a number of potential roles in prostate cancer including lesion localisation and characterisation and determination of the lesion aggressiveness [2]. Diffusion MRI images should always be interpreted by integration of morphology, high b-value (> 750 sec/mm^2) signal appearances and on ADC maps. This is because the calculated ADC values are dependent on the range of b-values used with additional errors arising from noise in very high b-value images. **MR spectroscopic imaging** (MRSI) of the prostate depicts the altered metabolism associated with prostate cancer. Normal prostatic glandular tissues shows high citrate levels whereas prostate cancer is characterised by high levels of choline. Studies to date suggest that MRSI might provide information that could be used to increase staging accuracy for less experienced readers and thereby reduce inter-observer variability, improve the non-invasive assessment of tumour location (although a recent American College of Radiology Imaging Network (ACRIN) study was inconclusive) and provides guidance for directing biopsies and focal therapies [3, 4]. The primary source of image contrast on **Blood Oxygen Level Dependent** MRI is endogenous, paramagnetic deoxyhaemoglobin which increases the transverse relaxation rate (R2*) of water in blood and surrounding tissues and thus BOLD-MRI is sensitive to pO2 within and in tissues adjacent to perfused vessels. BOLD-MRI does

Continued on page 59 .

* Works in progress (WIP). The information about this product is preliminary. The product is under development and not commercially available in the U.S., and its future availability cannot be ensured.

1 Rising PSA levels with repeated negative TRUS biopsies.
This 56-year-old male patient had 3 negative transrectal ultrasound (TRUS) guided biopsies for rising serum PSA levels over 2–3 years. In May 2006 the PSA level was 5.8 and now it had risen to 14.6 ng/ml. A multifunctional study was undertaken. Morphology, DW-MRI, DCE-MRI and MRSI examinations were all obtained within a 1-hour examination time on Siemens 1.5T MAGNETOM Symphony scanner with Tim (Total imaging matrix) capability using surface coils only. Evaluations of data obtained were done on Siemens Leonardo Workstation (MMWP) using Viewing, MRP with fusion, MeanCurve and Spectroscopy Taskcards.

1A Viewing TaskCard. Top-Left: T2-weigthed image shows some low signal in the peripheral zone at the base of the prostate gland in the midline. No central gland abnormality is shown.
Top-right: ADC map (calculated from b-value 0t, 50t, 100t, 250t, 500t and 750t images) shows restricted diffusion in the left central gland measuring 1.3 cm (arrow).
Bottom-left: Fusion image (b 1200 trace+T2-weighted) with 50% opacity confirms that the restricted diffusion is co-located in the left central gland indicating high cellularity.

1A

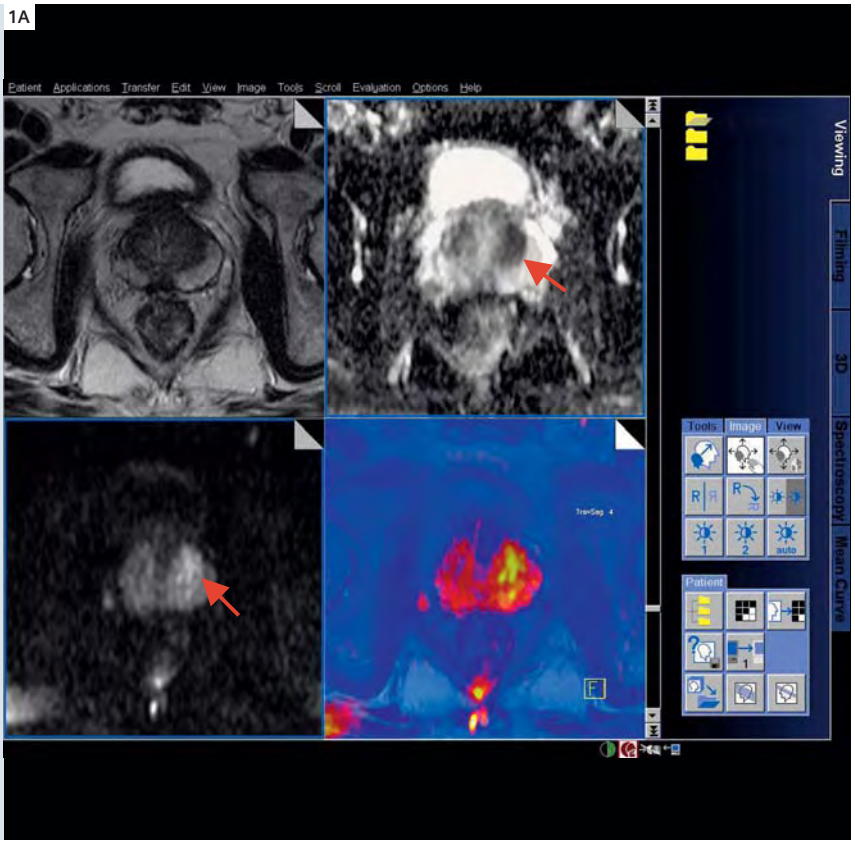

1B MPR TaskCard. Anatomical and functional images are co-localised using advanced, non-rigid software algorithms with false colour overlays of high b-value (b1200t) images. The TaskCard shows the prostate in 3 planes and indicates the site of high cellularity which can be used to indicate where to biopsy and can guide focal therapies.

1B

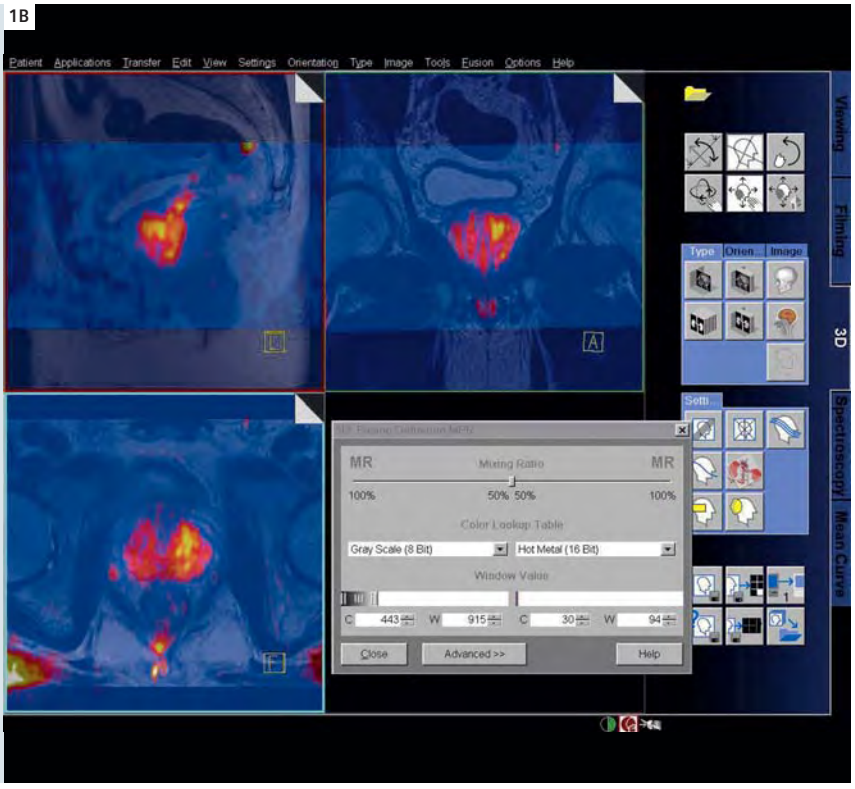

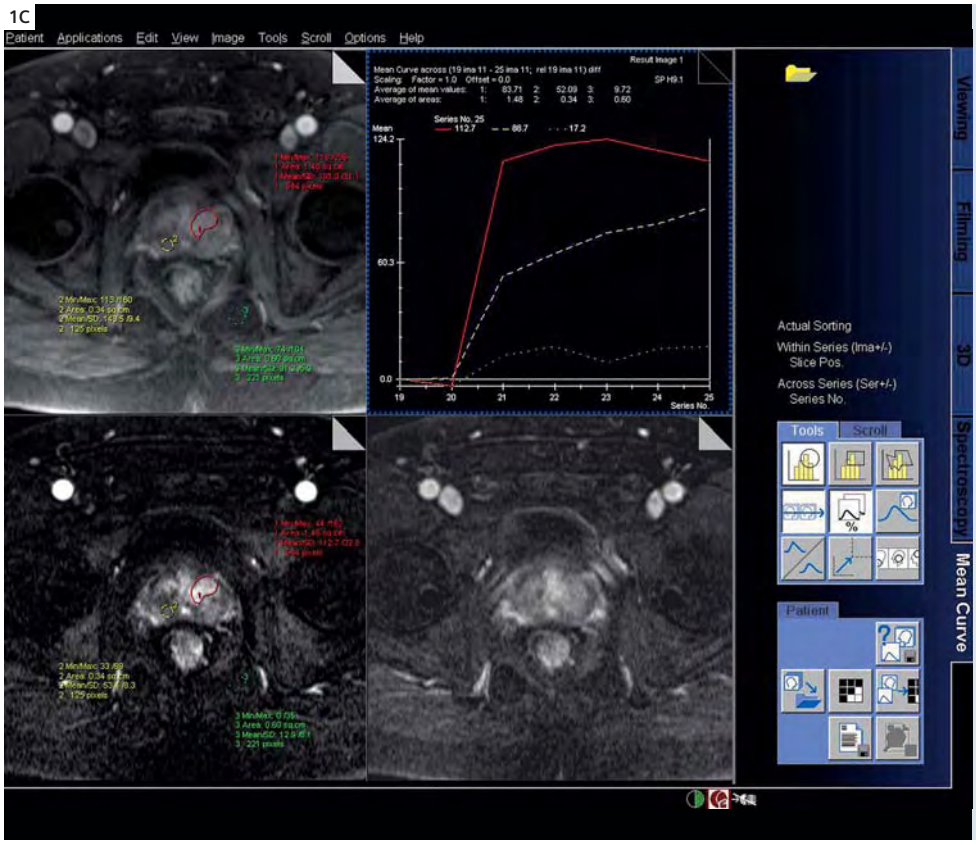

1C The MeanCurve TaskCard can be used to analyze dynamic contrast enhanced images (DCE-MRI). High spatial resolution DCE-MRI data were acquired every 30 seconds (twice before and 5 times post 0.1 mmol/kg Gd-DTPA).
Top-left: Regions of interest (ROIs) are placed in the region of the restricted diffusion (red ROI), in the right peripheral zone (yellow ROI) and in ischio-rectal fat.
Top-Right: Graphic depiction of contrast-enhancement with time shows marked early enhancement of the mass in the left central zone with some wash-out (red line).
Bottom-left: Subtraction image depicts more clearly the enhancing regions and can be used to place ROIs.
Bottom-right: Late post contrast enhanced T1-weighted image with fat-suppression. The area of high enhancement is difficult to see.

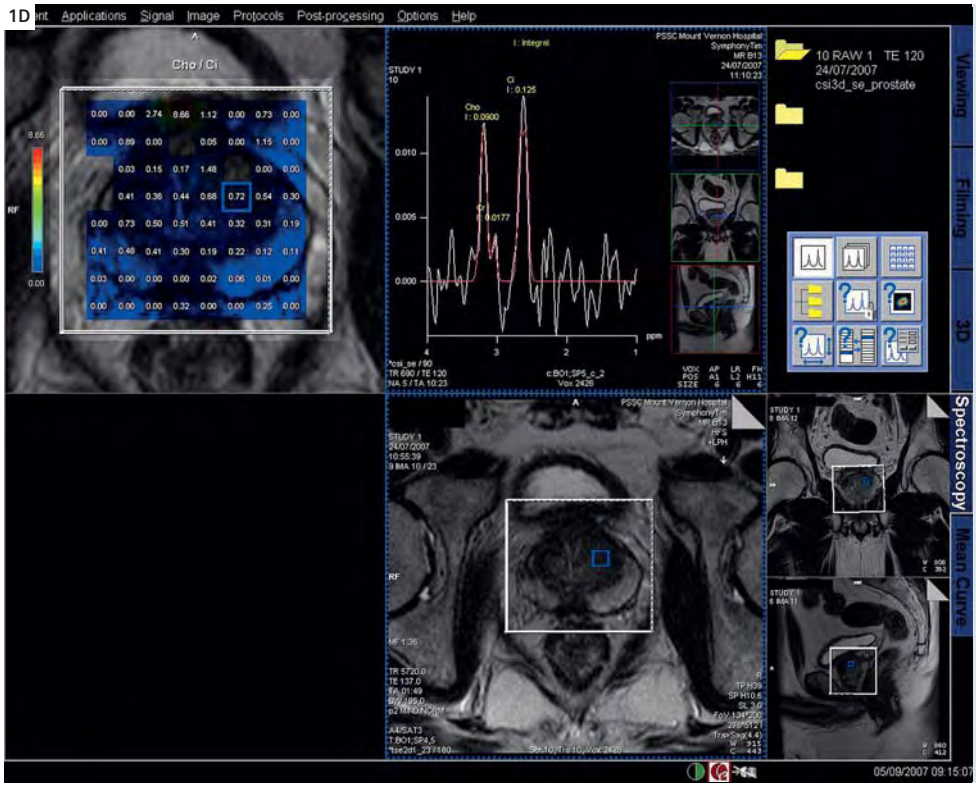

1D Spectroscopy TaskCard. MR spectroscopic imaging (5 x 5 mm voxel) from the left central gland lesion shows abnormal spectrum with high choline and low citrate levels (Choline: citrate ration: 0.72). The information obtained with these tools indicates a highly suspicious lesion suggestive of prostate cancer in the left central gland (mass, high cellularity, high perfusion and abnormal metabolism). This area was specifically targeted for biopsy and a cancer was diagnosed.

* Works in progress (WIP). The information about this product is preliminary. The product is under development and not commercially available in the U.S., and its future availability cannot be ensured.

2 Tumor recurrence following radiotherapy
72-year old male patient with prostate cancer previously treated (4 years prior) with radio-therapy for prostate cancer for T3a/b disease but now with rising serum PSA levels (5.4 ng/ml).

2A Top-Left: T2-weighted image showing a 2 cm mass posterior arising from the peripheral gland of the prostate breaching the mesorectal fascia indenting but not invading the rectum.
Top-Right: ADC map (from b0-750t images) showing marked restriction of water diffusion in relation to the mass behind the prostate.
Bottom-right: b 1200 trace image shows hyperintensity of the tumor recurrence; note that the treated prostate gland is not hyperintense.
Bottom-left: Fusion image (b1200 trace + T2-weighted) with 50% opacity confirms that the restricted diffusion is co-located in the recurrent tumor.

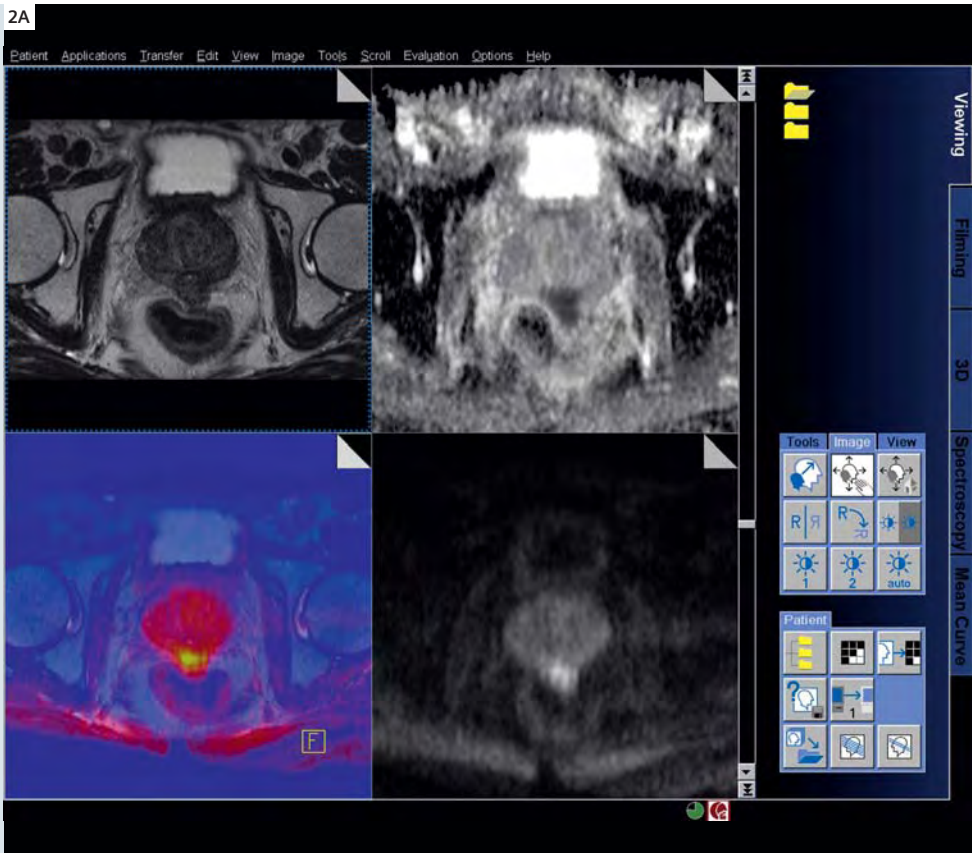

2B Anatomical and functional imaging are co-localised using advanced, non-rigid software algorithms with color overlays of high b-value (b1200t) images in the **MPR TaskCard.** The opacity of the color overlays can be adjusted to optimise data display.

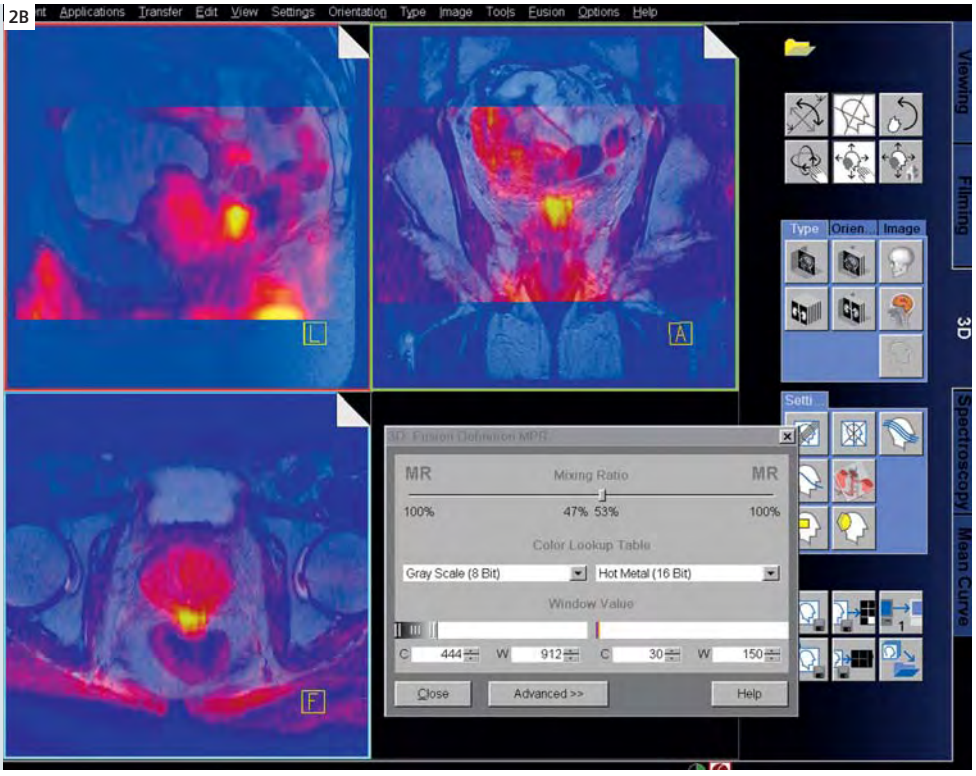

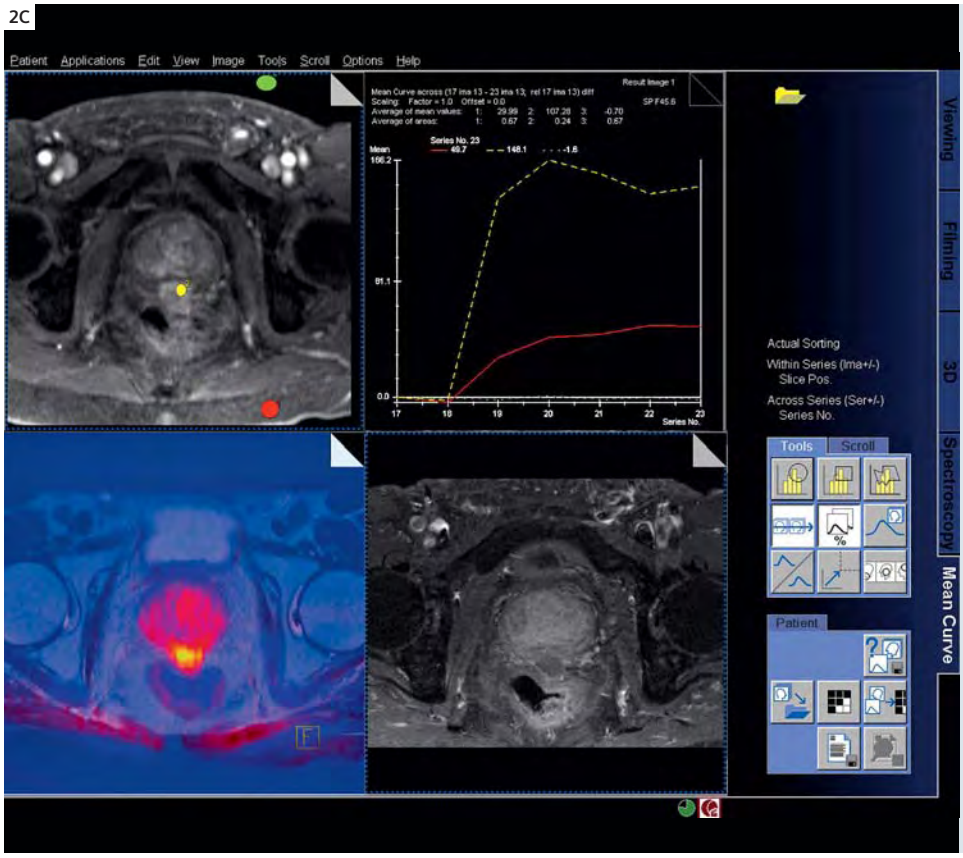

2C This is an example of how the **MeanCurve TaskCard** can be used to analyze dynamic contrast enhanced images (DCE-MRI). High spatial resolution DCE-MRI data were acquired every 30 seconds (twice before and 5 times post 0.1 mmol/kg Gd-DTPA).
Top-left: Regions of interest (ROIs) are placed on the edge of the recurrence (yellow), in fat (red) and in air (green) on the 60 seconds post contrast image.
Top-right: Graphic depiction of contrast-enhancement with time shows marked early enhancement of the tumor recurrence with some wash-out (yellow line).
Bottom-left: Axial fusion image (b 1200 trace + T2-weighted) with 50% opacity.
Bottom-right: Late post contrast enhanced T1-weighted image with fat-suppression. The tumor recurrence is difficult to see.

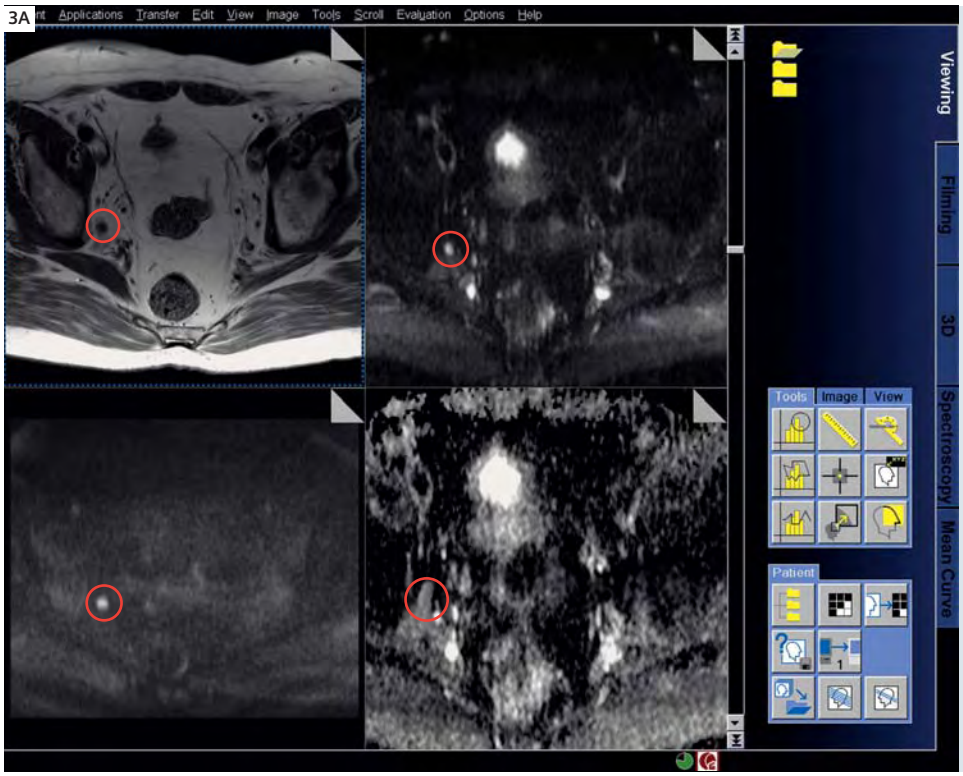

3 **Nodal evaluation with diffusion-weighted MRI**
72-year-old male patient with new diagnosis of prostate cancer. This is the same patient as in figure 5.

3A **Top-left**: There is an equivocally enlarged lymph node (7 mm) in the right internal iliac region (circled).
Top-right: on b0 images, the lymph node is difficult to see because of adjacent hyper-intensity in vascular structures. Note the hyperintense signal in the bladder anteriorly.
Bottom-left: b 1400 trace image shows persistent hyperintensity of the lymph node; all other pelvic structures are no longer hyper-intense.
Bottom-right: ADC maps show moderate restriction of water diffusion in the node (1170 x 10^{-5} mm^2/s). Taken together these findings are suggestive of metastatic invasion.

*Works in progress (WIP). The information about this product is preliminary. The product is under development and not commercially available in the U.S., and its future availability cannot be ensured.

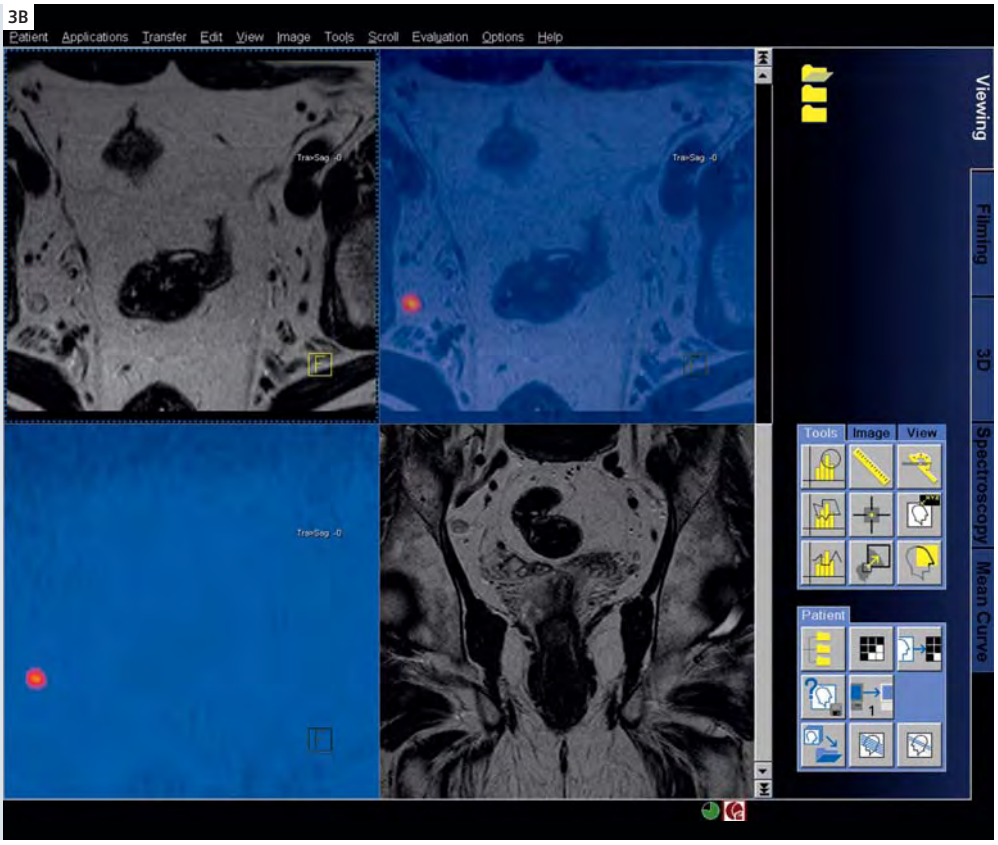

3B **Top-left** and **bottom-right:** T2-weighted images confirm the anatomical location of the lymph node in the right internal iliac region. **Top-right** and **bottom-left:** Fusion images (b 1400 trace + T2-weighted) with 50% and 100% opacities, confirms that the restricted diffusion is co-located in the lymph node.

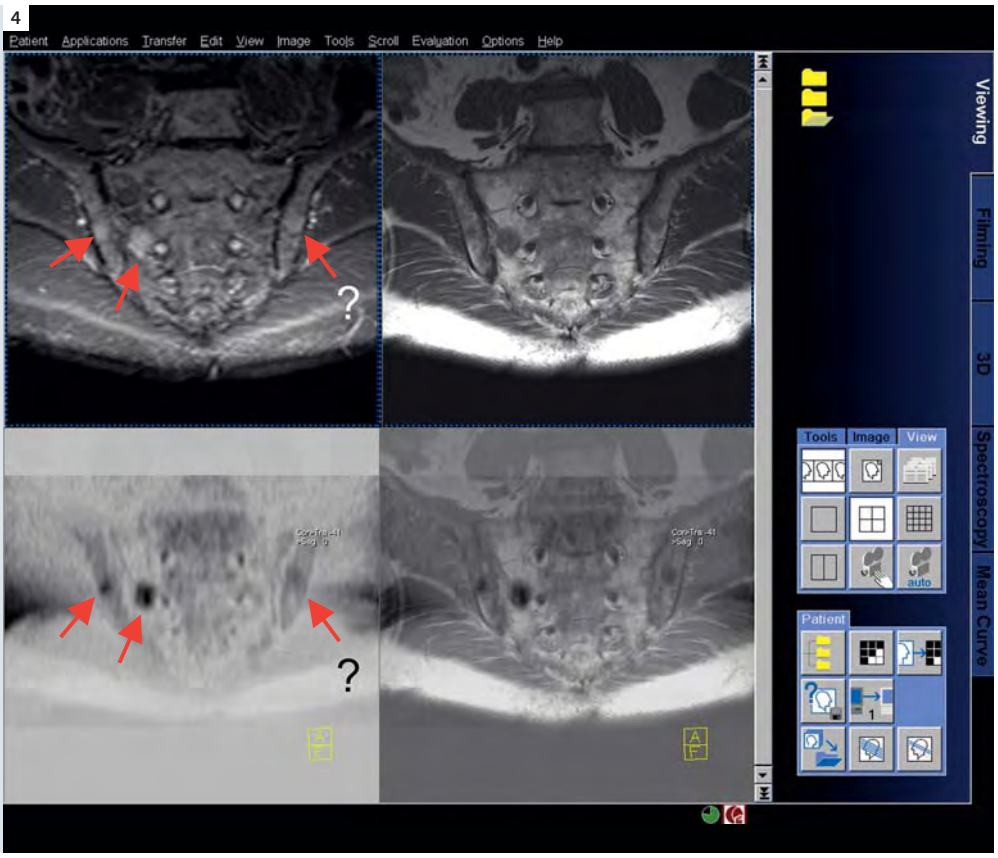

4 **Bone marrow evaluation with diffusion-weighted MRI**
75-year-old male patient with prostate cancer previously treated with radiotherapy for prostate cancer but now with rising PSA levels (2.4 ng/ml). The bone scan was negative and no enlarged lymph nodes were seen. The treated prostate gland had normal appearances post radiotherapy. There are 2 equivocal lesions seen in the bone marrow of the right hemipelvis (straight arrows) with a possible 3rd lesion on the left side shown on the STIR and T1-weighted sequences **(top-left** and **top-right)**. **Bottom-left** and **bottom-right:** Fusion images (b 1200 trace + T1-weighted) with 50% and 100% opacities (inverted grey-scale), confirms that the restricted diffusion is co-located in the 2 right sided abnormalities (ADC map not shown). These appearances are highly suggestive of cellular tissues within the bone marrow and therefore of metastases as being the cause of rising PSA levels.

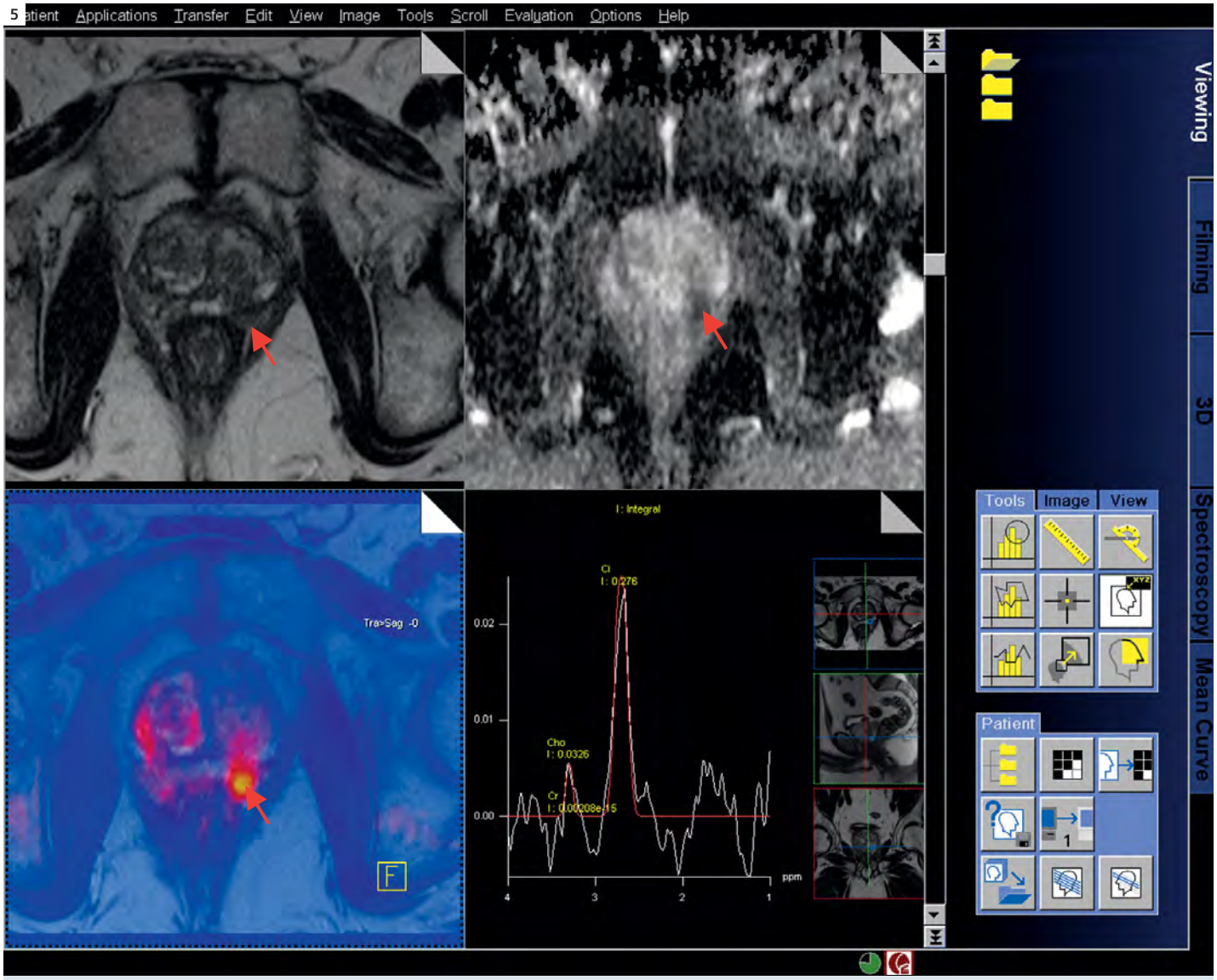

5 Discordance between DW-MRI and MRSI
This is the same patient as figure 3. 72-year-old male with new diagnosis of prostate cancer.
Top-left: The T2-weighted image shows moderate volume extra-capsular disease (T3A) with obliteration of the recto-prostatic angle (arrow).
Top-right: ADC map shows marked restriction of water diffusion in the region of the tumor.
Bottom-left: Fusion image (b 1000 trace + T2-weighted) confirms extraprostatic disease.
Bottom-right: MRSI (5 x 5mm voxel) shows normal spectrum with high citrate and low choline peaks in tumor.

*Works in progress (WIP). The information about this product is preliminary. The product is under development and not commercially available in the U.S., and its future availability cannot be ensured.

Table 3: MRI techniques and their usage in prostate cancer patients

Technique (Siemens Tools)	Basis of usage	Indications	Authors' opinions on indication[1]
Morphology (Viewing TaskCard)	Depiction of the tumor extent	At almost every stage of the patient journey (not routinely used for very early stage cancers nor for very advanced disease)	+++
MRI biopsy (None specific)	To obtain histological material targeting a lesion/area Rarely to direct focal treatments to a specified region	Not routinely indicated. Used when cancer is suspected, TRUS biopsies are negative and) MRI depicts suspicious lesion(s)	+
Lymphography with lymph node specific contrast agent (Sinerem/Combidex*) (Lymph Node TaskCard) *Contrast agent not yet approved (Dec 07) but expected soon	To improve the accuracy of nodal staging	Remains to be decided but will include one or more of the following: ■ For newly diagnosed patients who are potentially curable (regardless of therapy modality) taking into account age and volume of disease (including small volume T3 disease) ■ >15% risk for nodal metastases ■ Gleason ≥7 (≥ 4+3) ■ PSA >10 ng/ml regardless of histological grade ■ For nodal mapping prior to IMRT or for targeted, extended PLND ■ PSA relapse – provided local relapse is excluded and bone scan is negative **and** in whom salvage pelvic radiotherapy therapy is being considered	+++
Proton MRSI (Spectroscopy TaskCard)	For depicting the intraprostatic tumor extent For assessing lesion aggressiveness (complementary information to DW-MRI and DCE-MRI and should be used together where possible)	■ For depicting and confirming the location of the primary prostate cancer ■ PSA relapse when bone scan is negative and in whom salvage therapy is being considered	++ ++
DW-MRI (ADC tool)	For depicting the intraprostatic tumour extent (complementary information to DW-MRI and DCE-MRI and should be used together where possible)	■ For depicting and confirming the location of the primary prostate cancer ■ PSA relapse when bone scan is negative and in whom salvage therapy is being considered	++ +++
DCE-MRI with mean curve analysis (DCE and mean curve TaskCards)	For depicting the intraprostatic tumour extent (complementary information to DW-MRI and DCE-MRI and should be used together where possible)	■ For depicting and confirming the location of the primary prostate cancer ■ For monitoring response to hormonal therapy ■ For the assessment of the effectiveness of focal therapies (eg PDT, HIFU) ■ PSA relapse when bone scan is negative and in whom salvage therapy is being considered	++ + +++ +++
Data fusion (MPR TaskCard with fusion option)	Combining & displaying morphological with functional imaging	To aid in the co-localisation for data presentation purposes and for therapy planning. Very useful when used with proton-MRS and DWI.	+++
BOLD-MRI (No specific task card)	To map prostate cancer hypoxia. Used in combination with techniques that map the location of tumours	Could be used for focal ablative therapies as well as radiotherapy planning for boosting dose delivery to hypoxic regions.	+

[1] These authors' opinions are based on literature reviews, personal experiences and recommendations are partly dependent on subjective assessments of ease of imaging data acquisition, analysis and interpretations
0 = No requirement; + = possible requirement; ++ = probably indicated; +++ = definite indication

not measure pO2 directly and in order to be able to correctly interpret BOLD images it is necessary to know or to determine the distribution of blood volume in tissues. Recent data suggests that BOLD-MRI can be used to generate probability biomaps of prostate tumor hypoxia and when combined with DW-MRI and DCE-MRI may be used to target hypoxic prostate tumor regions with focal therapies such as high dose rate brachytherapy, cryotherapy as well as HIFU [5, 6].

MR lymphography using the intravenously administered contrast agent Ferumoxatan-10 has emerged as a powerful new tool for the evaluation of nodal involvement. Much research attesting to its accuracy for nodal characterisation (including the detection of micrometastases) has appeared in the literature, although efficacy data relating to changing patient management and altering clinical outcomes remains generally lacking [7, 8]. Approval of this contrast agent in Europe is expected soon. Two basic strategies have been explored for **MRI guided prostate gland biopsy:** (1) co-registration of previously acquired diagnostic MR imaging to interventional TRUS or open scanner MR images, and (2) stereotactic needle interventions within conventional diagnostic scanners using careful patient positioning or the aid of simple manipulators. Such techniques can be used for needle-based interventions for prostate cancer, including biopsy, brachytherapy, and thermal therapy.

Conclusions

As we move into the early 21st century it is clear that the prostate cancer imaging landscape will change radically. One challenge that radiologists will face is how to communicate complex multifunctional information to clinicians looking after patients. One method is to use **fusion tools** which allows anatomical and functional imaging to be co-localised using advanced, non-rigid software algorithms which can also be extremely useful for the purpose of data presentation, analysis, biopsy and therapy planning (examples are shown in figures). Standardized MRI reporting systems depicting graphically the location of abnormalities with the relative confidence of diagnostic radiologists will be needed to accurately convey complex information to clinicians. When using such toolbox multifunctional imaging approaches for prostate cancer it is often found that the results obtained are not always concordant (for example, morphology, DW-MRI, DCE-MRI may suggest the presence of tumor and MRSI does not – see figure 5 for an example case). The latter is not really surprising as these techniques are depicting different biological processes. The relative weighting to be placed on each component of a comprehensive exanimation in a given clinical situation will require sophisticated bioinformatics approaches where imaging data will be analysed with co-located immunohistochemistry, gene expression profiles and other biomarker data. We anticipate that fusion of functional imaging and other biomarker data will yield more robust and more effective tumor signatures. Thus, multi-spectral analysis of imaging data represents the new bioinformatics challenge of the early 21st century in prostate cancer.

References and suggested reading

1 Alonzi R, Padhani AR, Allen C. Dynamic contrast enhanced MRI in prostate cancer. Eur J Radiol. 2007 Sep;63(3):335-50.

2 Koh DM, Collins DJ. Diffusion-weighted MRI in the body: applications and challenges in oncology. AJR Am J Roentgenol. 2007 Jun;188(6):1622-35.

3 Zapotoczna A, Sasso G, Simpson J, Roach M 3rd. Current role and future perspectives of magnetic resonance spectroscopy in radiation oncology for prostate cancer. Neoplasia. 2007 Jun;9(6):455-63.

4 Claus FG, Hricak H, Hattery RR. Pretreatment evaluation of prostate cancer: role of MR imaging and 1H MR spectroscopy. Radiographics. 2004 Oct; 24 Suppl 1:S167-80.

5 Hoskin PJ, Carnell DM, Taylor NJ, Smith RE, Stirling JJ, Daley FM, Saunders MI, Bentzen SM, Collins DJ, d'Arcy JA, Padhani AP. Hypoxia in prostate cancer: correlation of BOLD-MRI with pimonidazole immunohistochemistry-initial observations. Int J Radiat Oncol Biol Phys. 2007 Jul 15;68(4):1065-71.

6 Padhani AR, Krohn KA, Lewis JS, Alber M. Imaging oxygenation of human tumours. Eur Radiol. 2007 Apr;17(4):861-72.

7 Harisinghani MG, Barentsz J, Hahn PF, Deserno WM, Tabatabaei S, van de Kaa CH, de la Rosette J, Weissleder R. Non-invasive detection of clinically occult lymph-node metastases in prostate cancer. N Engl J Med. 2003 Jun 19;348(25):2491-9.

8 Saksena MA, Saokar A, Harisinghani MG. Lymphotropic nanoparticle enhanced MR imaging (LNMRI) technique for lymph node imaging. Eur J Radiol. 2006 Jun;58(3):367-74

*Works in progress (WIP). The information about this product is preliminary. The product is under development and not commercially available in the U.S., and its future availability cannot be ensured.

The Clinical Advantages of T2-weighted MR Imaging in the Female Pelvis with *syngo* BLADE

Takashi Koyama; Koji Fujimoto; Kaori Togashi

Kyoto University Graduate School of Medicine, Kyoto, Japan

Introduction

syngo BLADE is a non-Cartesian data acquisition technique that has been applied for motion correction in brain imaging. In *syngo* BLADE, the echo trains in each TR are acquired in the same way as in a conventional turbo spin-echo sequence. Each echo train is made up like a blade, and the blade rotates to fill k-space. This trajectory makes the BLADE sequence motion insensitive.

Although the artifacts from respiratory motion are limited in the female pelvic region, motion artifacts from the abdominal wall and intestine degrade MR images. In this article, we would like to show the advantages and limitations of BLADE technique compared to turbo spin-echo T2-weighted imaging (T2WI) of the female pelvic region, introducing our recent study that was presented at the ISMRM meeting in Berlin, Germany in 2007. In our study, we compared sagittal T2WI with BLADE (TR/TE = 6760-9500/113) and T2WI with conventional acquisition (TR/TE = 3730/105-120) in 34 subjects, including 6 healthy volunteers (age: 28 ± 3) and 28 patients (age: 50 ± 16) who underwent pelvic MRI for gynecologic diseases. MRI was performed at 1.5T scanner (MAGNETOM Symphony) utilizing a multi-

Table 1: Visual evaluation

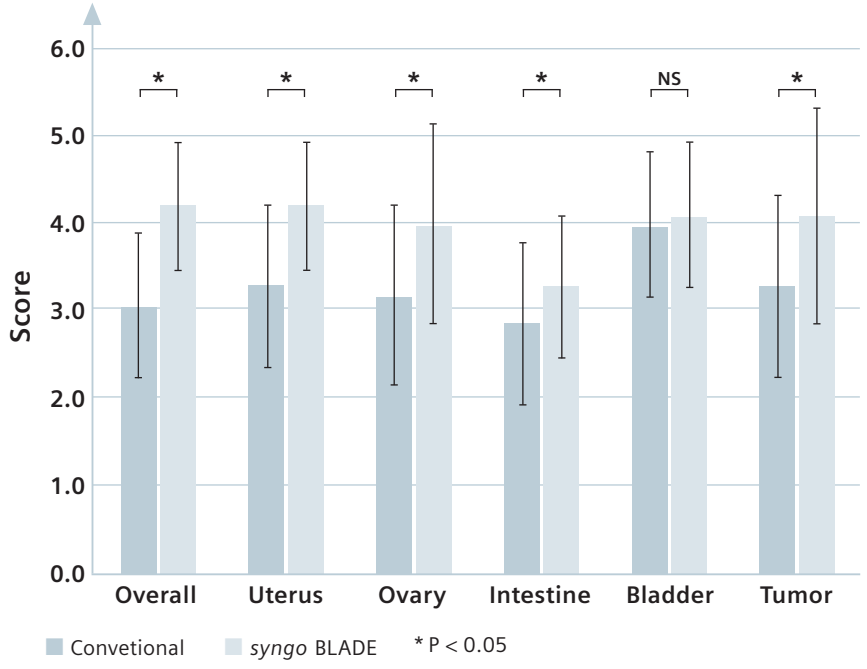

This graph represents the results of visual evaluation. The overall image quality, delineation of the **pelvic organs** including the uterus, the ovary, the intestines and tumors were superior in BLADE-T2WI compared with conventional T2WI, **except for the bladder.**

	syngo BLADE	Conventional	P Value*
Overall (n = 34)	4.1 ± 0.7	3.0 ± 0.8	< 0.001
Uterus	4.1 ± 0.7	3.2 ± 0.9	< 0.001
Ovary	3.9 ± 1.1	3.1 ± 1.0	0.001
Intestine	3.2 ± 0.8	2.8 ± 0.9	0.009
Bladder	4.0 ± 0.8	3.9 ± 0.8	0.395
Tumor	4.0 ± 1.2	3.2 ± 1.0	0.001

*Calculated by Wilcoxon's signed-rank test. P < 0.05 was considered statistically significant.

channel phased array coil. Sequence protocols other than TR, TE were identical in both T2-weighted scanning; FoV of 260 mm, slice thickness of 5 mm, interslice gap of 0.9–1.5 mm and matrix of 320. All MR images were independently evaluated by two radiologists using a 5-point scale, regarding the overall image quality, the sharpness of the configuration of the intestine, uterus, bladder and tumor, if present. The presence and type of artifacts in each sequence were also described. The results of MR image evaluation were compared in each subject.

The results of the evaluation of MR images are summarized in Table 1. T2WI with *syngo* BLADE provided better overall image quality and less ghosting artifacts, which were always present in T2WI with conventional turbo spin echo technique. The delineation of the pelvic organs and tumors in T2WI with BLADE was superior to T2WI with conventional turbo spin echo, except for the bladder. In one patient with cervical carcinoma, T2WI with *syngo* BLADE could successfully depicted tumor that was hardly recognizable on conventional T2WI (Fig. 1). On the otherhand, T2WI with BLADE was associated with some minor but unique artifacts, including fine linear artifacts in the intestine (n = 34) and bladder roof (n = 12), faint sunburst like radiating lines from the body in all, wrap around artifacts (n = 20), sharp lines at the corner of the FoV (n = 14). The fine linear artifacts around the bladder roof may result from motions associated with urine influx and intestinal peristalsis. The unique sunburst-like artifact may represent a kind of wrap around artifact, resulting from rotating data acquisition. However, these artifacts were

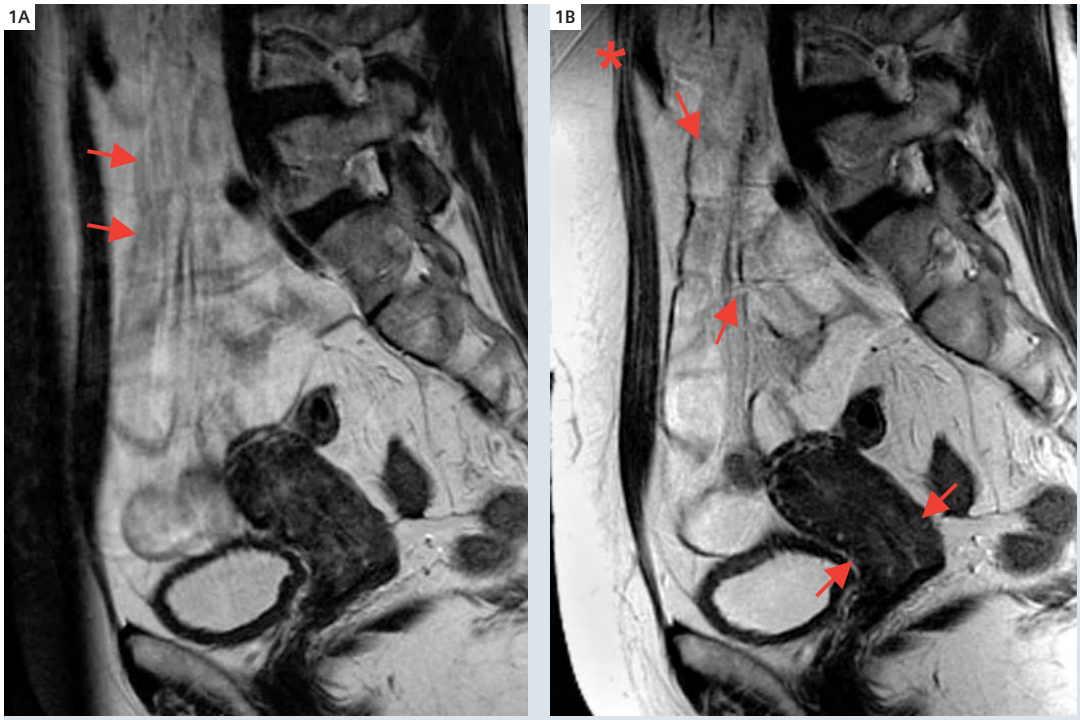

Conventional TSE

syngo BLADE

1 Uterine Cerviacal Cancer
Sagittal T2-weighted images with *syngo* BLADE provide better overall image quality and clearer delineation of the uterus and intestine by reducing ghosting and blurring caused by motion artifacts (A arrows), and demonstrates uterine cervical carcinoma (B arrowheads) that is hardly recognizable on conventional T2-weighted image. Nonetheless, the T2-weighed image with *syngo* BLADE has fine linear artifacts in the small intestine (B arrows) and sharp lines at the corners of FoV (B asterisk).

Conventional TSE

T2-weighted image with *syngo* BLADE

2 Pregnant Woman
A case of a pregnant* woman. Ghosting artifact is eliminated in the T2-weighted image with *syngo* BLADE, but delineation of the uterus, the placenta, and the fetus is severely degraded by prominent linear artifacts.
*The safety of imaging fetuses/infants has not been established.

only minor, and did not significantly degrade the overall image qualities, except in one pregnant* woman. In one of three pregnant women in our series, artifacts from fetal motion severely degraded T2-weighted images with *syngo* BLADE. In summary, T2-weighted images with *syngo* BLADE can provide better image quality and clearer delineation of the organs in the female pelvis by eliminating the ghosting artifacts, compared with T2-weighted images with conventional acquisition.
We believe that T2-weighted images with *syngo* BLADE have high potentials to improve image quality of T2-weighted images in other body regions.

*The safety of imaging fetuses/infants has not been established.

Table 2: artifacts evaluation

N = 35	Conventional	PROPELLER
Motion artifact	35	0
Fine linear artifacts	0	35(intestine) 12(bladder)
Sharp lines at the corner of FOV	0	20
Wrap-around artifact	0	14

Regarding the artifacts, motion artifacts (which are) seen in all conventional technique were successfully eliminated in BLADE-T2W images. However, in BLADE images, there were several minor artifacts including fine linear artifacts in the intestine and the bladder, sharp lines at the corner of FOV and unique wrap-around artifacts.

References
1 Wintersperger, B.J., Runge, V.M., Biswas, J. et al., Brain magnetic resonance imaging at 3 Tesla using BLADE compared with standard rectilinear data sampling. Invest Radiol, 2006. 41(7): p. 586-92.
2 Seo H, Masui T, Katayama M, et al, Comparison of PROPELLER Fast Spin Echo,Respiratory-Triggered Fast Spin Echo and Single-Shot Fast Spin Echo Sequences for Transverse T2-Weighted Magnetic Resonance Imaging of the Female Pelvis. 13th Scientific Meeting and Exhibition ISMRM 2005. 5 Miami Beach.
3 Pipe; Motion Correction With PROPELLER MRI: Application to Head Motion and Free-Breathing Cardiac Imaging; MRM 1999; 42; 963-969.

3D MR Cholangiopancreatography and Volume Rendering: a Perfect Liaison

Tobias Baumann, M.D.; Arnd-Oliver Schäfer, M.D.; M. Langer, M.D.

Department of Diagnostic Radiology, University Hospital Freiburg, Germany

Background

Complaints arising from diseases of the biliary tract are a common cause of hospital admissions throughout the world. From an epidemiological point of view, the vast majority of biliary symptoms are usually caused by cholecystolithiasis or cholecystitis and are met by straightforward diagnosis and treatment. However, very complex diseases like biliary and pancreatic neoplasms or congenital disorders require sophisticated diagnostic work-up and a custom-tailored therapeutic approach.

Endoscopic retrograde cholangiopancreatography (ERCP) is the central clinical method that allows imaging of the biliary and pancreatic ducts as well as the collection of tissue samples for histopathological examination. The possibility of removing concrements or place stents additionally renders ERCP a therapeutic technique.

As an invasive procedure ERCP is afflicted by a morbidity of 1–7% and a mortality of 0.2–1% and can be hindered by postoperative conditions like choledochojejunostomy or liver transplantation and high-grade stenosis [1].

Although ERCP as an endoluminal technique will in many cases provide accurate diagnosis and offer therapeutic alternatives within the biliary tract, it must be kept in mind that it can never see beyond the wall into the surrounding tissue.

The staging of malignant tumors inside or around the biliary tract in particular, however, requires comprehensive assessment of the biliary tract itself and its adjacent tissue.

Therefore, MR cholangiopancreatography has evolved as a competitive adjunct or even replacement for invasive imaging techniques in a wide variety of pancreatic and bilary applications. The capability of MRI to visualize the ductal structures, the surrounding tissue, neoplastic tissue, and the involved vasculature in one examination underlines the direct influence of the radiologist's report on therapeutical decision making and surgical planning.

MR Techniques

The ability of MRI to directly visualize the biliary tract relies on the presence of barely moving fluid with long T2-relaxation times [2]. Three different types of strongly T2-weighted sequences with long echo times are generally applied to MR cholangiopancreatography (MRCP):

- RARE (rapid acquisition with relaxation enhancement),
- HASTE (half-Fourier acquisition single shot turbo spin echo), and
- 3D-TSE (3D turbo spin echo).

RARE – The RARE sequence is based on a single 90° excitation pulse and a long echo-train of up to 256 echos [3]. A single thick slab acquired in only a few seconds creates a projection-like image, comparable to images obtained during ERCP. Several slabs are subsequently acquired in paracoronal projections oriented along the relevant structures. The strength of MRCP with RARE is the fast acquisition that even provides diagnostic image quality in severely ill patients who find difficulty in holding their breath for more than just a few seconds. The projection-like image characteristic, however, offers neither three-dimensional information nor visualization of the surrounding tissue. Furthermore, the superposition of other fluid collections in the stomach, duodenum or the peritoneal cavity can remarkably reduce image quality in RARE MRCP.

HASTE – As the whole data for one slice is also acquired after a single excitation pulse, HASTE can be considered a variant of RARE [4]. The acquisition of thinner slices instead of large slabs in combination with depiction of the surrounding tissue, however, allows a much better anatomical correlation and avoids impairment by overlaying fluid collections. The incomplete acquisition of k-space data ("Half-Fourier)" in combination with a single-shot approach reduces signal-quality for high frequency image information and can thus lead to blurring of sharp edges. Although it is possible to cover the desired field-of-view (FoV) within two or three breathholds of approximately fifteen seconds each, unsteady breathing can lead to displacement between adjacent slices, known as "serious misregistration artifact". This drawback can in most cases be encountered by mutliplanar imaging or navigator-techniques.

3D-TSE – In contrast to the above mentioned techniques, 3D imaging uses two phase-encoding directions that allow for imaging of an anatomical slab with very high through-plane resolution and improved signal-to-noise ratio (SNR) [5]. As the acquisition time for 3D-TSE is

much longer than for 2D single-shot sequences, free-breathing with navigator technique has to be applied. When steady breathing can be accomplished by the patient, a high-resolution dataset is obtained in 3–6 minutes and, if parallel imaging is employed, even faster. A technical highlight of 3D sequences for MRCP is the use of a restore pulse. When the last echo during a turbo-spin acquisition has been recorded, another 180° pulse is used to refocus the remaining transverse magnetization, but instead of acquiring the echo, a subsequent 90° pulse is used to flip the transverse magnetization back to the z-axis. Thus the magnetization is restored much faster than relying on the natural T1-relaxation. After an interval of several repetition times, a steady state of longitudinal magnetization is established with net enhancement of the long T2-components. In this manner, signals from fluid can be enhanced dramatically in these images [6]. Although the rather long acquisition of 3D-TSE sequences renders them susceptible for motion artifacts, according to our experiences, images of excellent quality can be obtained in the vast majority of patients. It is the combination of high spatial resolution and a high contrast-to-noise ratio for fluids that make these images the ideal starting point for advanced post-processing and visualization.

Post-processing

It is the ongoing evolution of hardware and software that brings highly sophisticated post-processing techniques from the ivory tower of high performance computer labs to our everyday working place. The combination of reconstructed image stacks and interactive visualization gives us the possibility of exploring complex datasets and define and optimize the presentation of regions-of-interest and different image characteristics after the examination has been completed. The standard post-processing tools that are available on a variety of workstation and server-client solutions mainly comprise multiplanar-reformation (MPR), maximum intensity projection (MIP), and volume rendering techniques (VRT). Although originally applied to CT data, the ability of MRI to create images with high resolution and uniformly high contrast for vessels or other distinct anatomical structures now allows for a combination of both techniques.

Image Gallery

In our optinion, MRCP – especially the use of volume rendering and perspective volume rendering – opens up a new way of looking at MRI data that not only fascinates the clinician but also allows a comprehensive visualization of the examination for the radiologist, sometimes indicating changes that could have been missed on source images. It has to be kept in mind, however, that this kind of post-processing will always lead to a reduction of information compared to the source data. Therefore a thorough review of these images cannot be omitted.
All presented images were acquired with a 1.5T scanner (MAGNETOM Avanto, Siemens, Erlangen, Germany) and post-processed on a dedicated workstation.

Case 1: Gallstones

A 58-year-old male patient was referred for MRI of the liver and biliary tract after experiencing an episode of severe upper abdominal pain. Liver enzymes were slightly elevated. Ultrasonography was initially performed and showed cholecystolthiasis, but clear visualization of the wall of the gallbladder and the neighboring tissue could not be achieved due to superimposing structures. Although acute cholecystitis was already suspected, MRCP was performed to exclude other causes of enzyme elevation.
(A) An axial HASTE image shows sludge (arrowhead) three stones (arrow) in the gallbladder. A thickened wall can be noted as a sign of the acute inflammation.
(B) A coronal source image from the 3D TSE sequence shows a section through the gallbladder with sludge (inhomogeneous low signal) and two stones (arrow). The intrahepatic and extrahepatic bile ducts appear normal.
(C) A paracoronal MPR of the 3D TSE shows stones and sludge in the neck of the gallbladder, but the cystic duct remains free of concrements.
(D and E) MIP (D) and VRT (E) of the 3D TSE sequence nicely depict the biliary and pancreatic ducts. The sludge and stones can be recognized as filling defects of the gallbladder, but differentiation between stones and sludge is impossible due to the low signal of both entities. Image orientation represents a posterior view.
(F) Shows a planning image for perspective VRT. A set of three perpendicular MPR images (only one shown here) is used to place a camera-like point on which the ray-tracing paths are centered to create a virtual endoscopy view.
(G and H) Two virtual views using perspective VRT from the top of the gallbladder onto the sludge and the stones rising above this level, as icebergs in the sea.

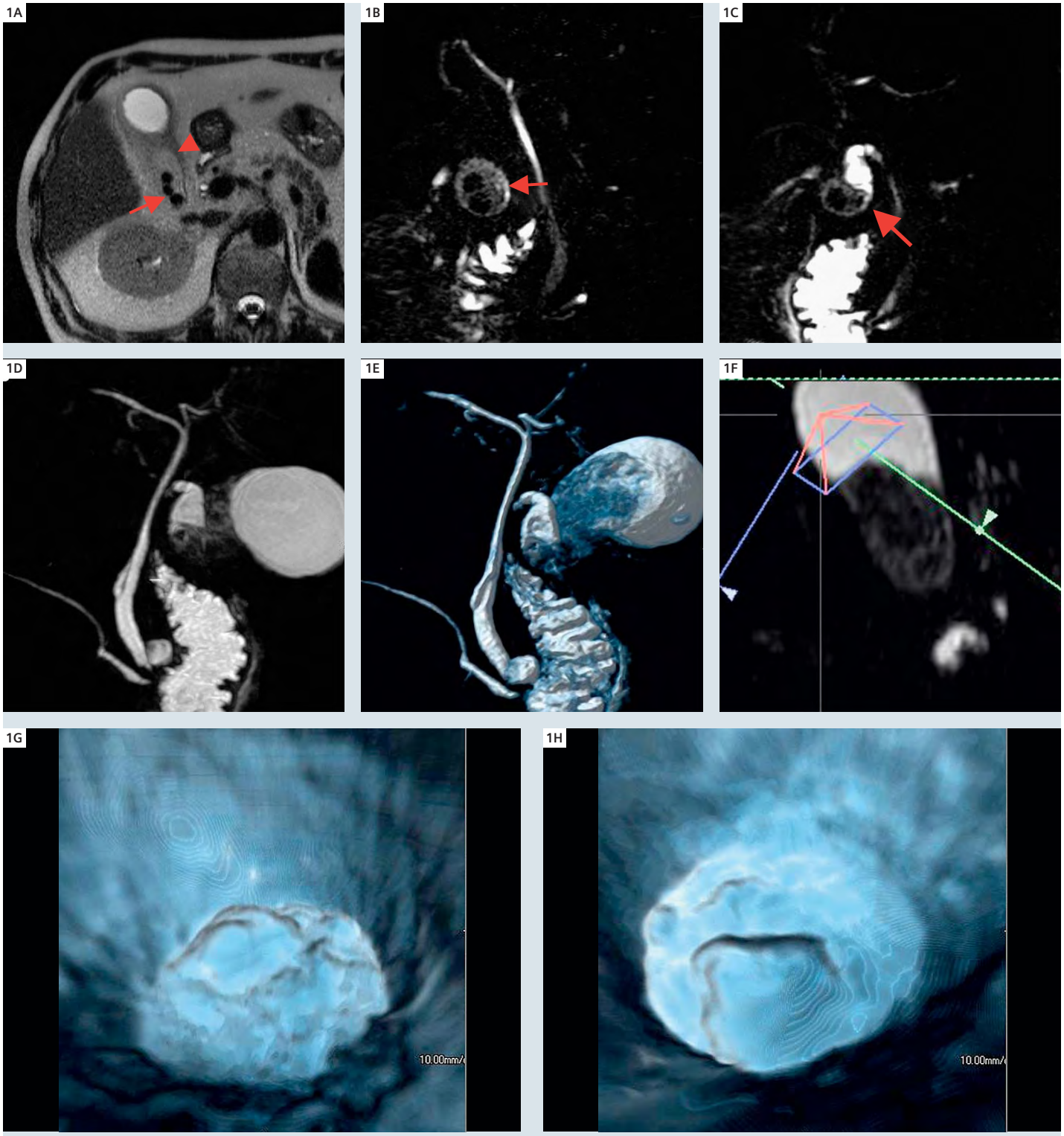

1 Case 1: Gallstones

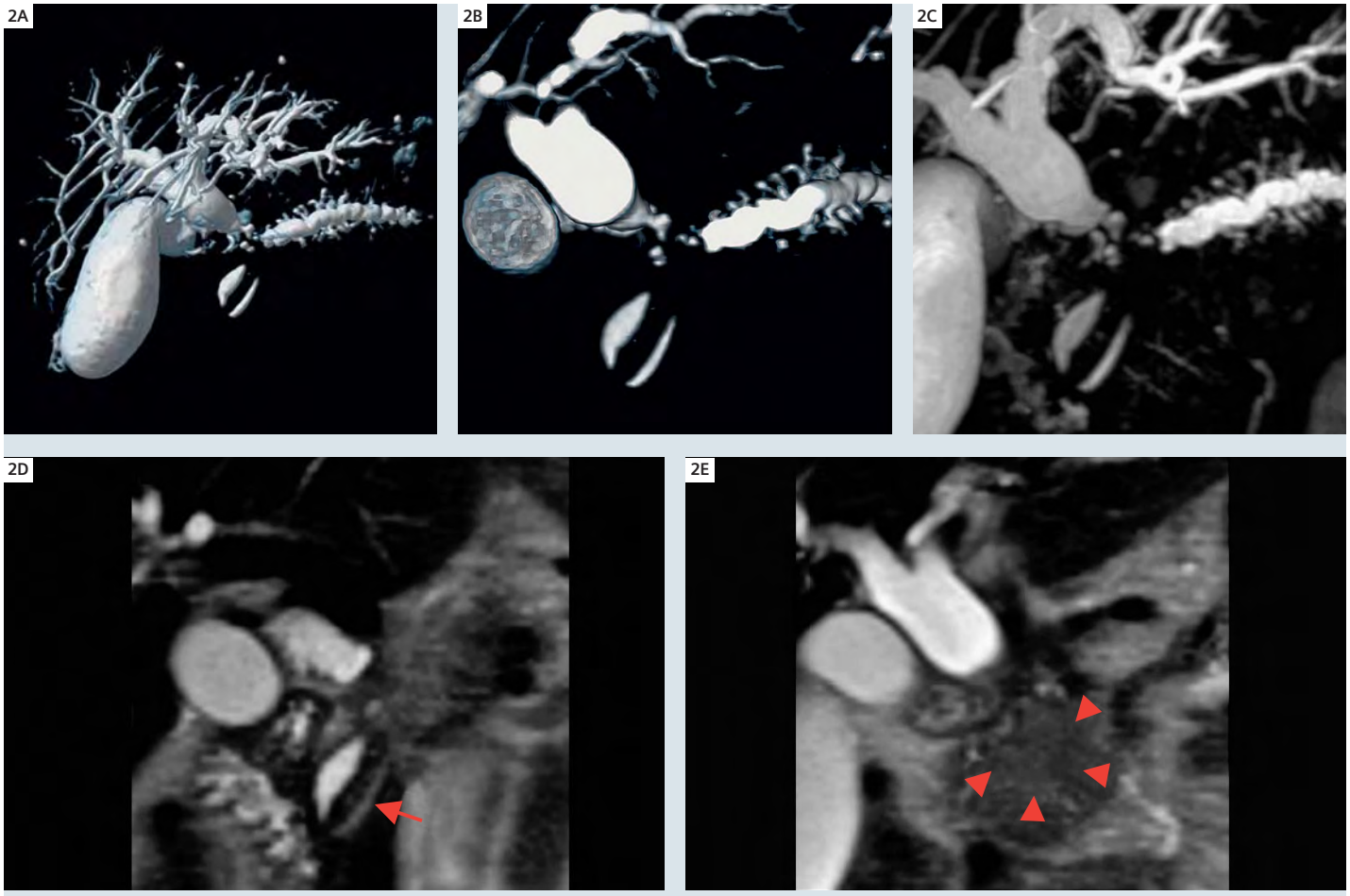

2 Case 2: Pancreatic cancer

Case 2: Pancreatic cancer

A 65-year-old female patient was referred to our oncology department due to weight-loss and recently developed jaundice. Ca19-9 as a tumor marker for e.g. pancreatic carcinoma was elevated over 3000 U/ml. She received an MRI scan of the pancreas and biliary tract in search of a pancreatic neoplasm.
(A) A VRT of the 3D TSE sequence shows markedly dilated intrahepatic and pancreatic ducts. Distal to the cystic duct in the upper part of the pancreatic head both biliary and pancreatic ducts almost completely terminate. Shortly below this area both ducts can again be delineated with normal caliber down to the papilla.
(B) An enlarged view of the defect of both ducts with a coronal cut-plane through the proximal part of the common bile duct and the pancreatic duct shows the conic stump of the bile duct and the tremendous dilation of both systems with even the small side-branches of the pancreatic duct being clearly visible down to third order branches.
(C) A MIP image in the same orientation as (B) depicts the findings with even higher clarity and resolution but with a weaker 3-dimensional impression.
(D and E) Coronal HASTE images parallel to the cut-plane in (B). In (D) the distal parts of both ducts can be seen (arrow). In (E), two slices dorsal to (D), a neoplasm in the pancreatic head can be noted (arrowheads) that abuts the duodenum and the biliary tract.

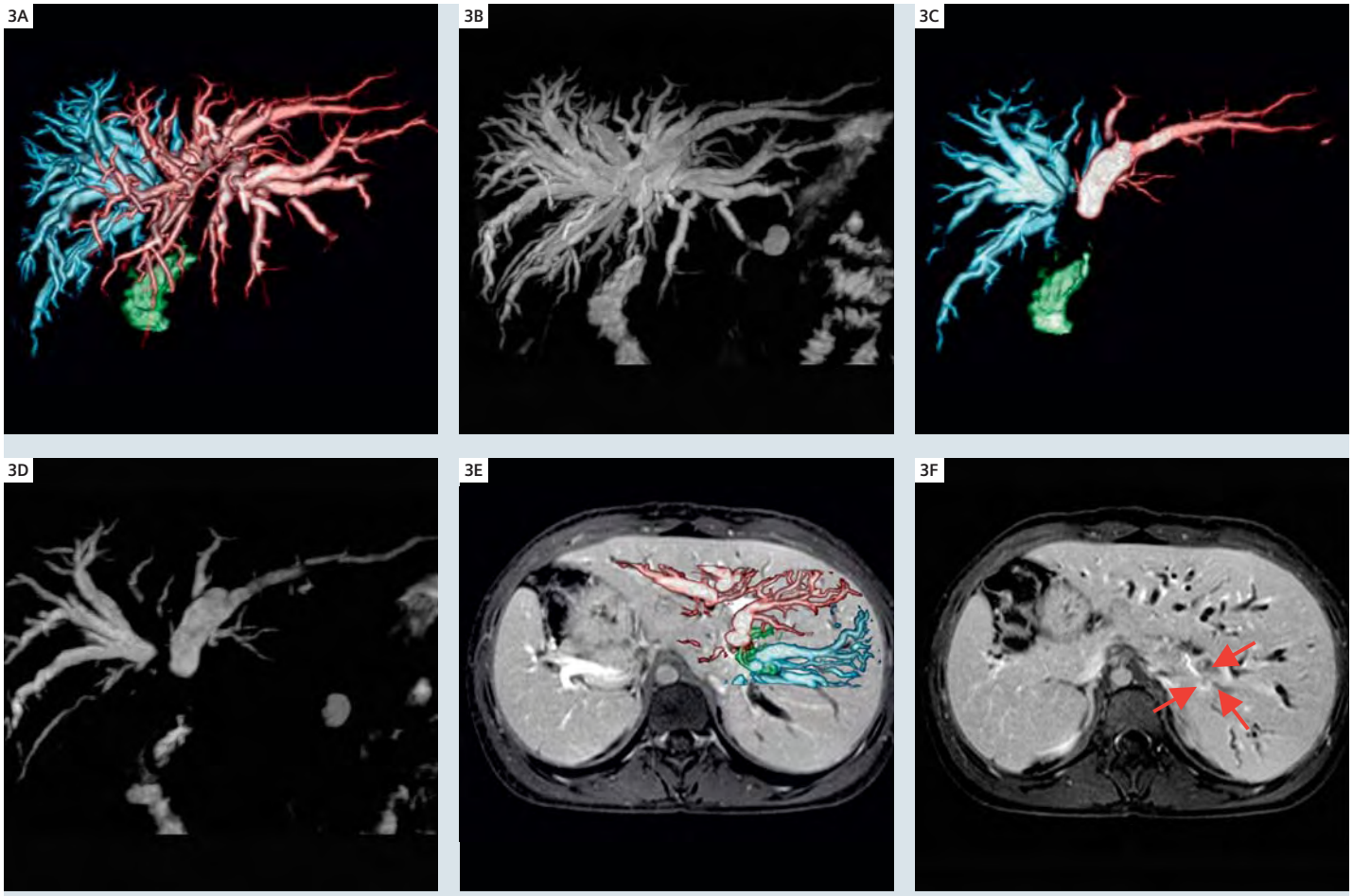

3 Case 3: Klatskin tumor

Case 3: Klatskin tumor

A 22-year-old female patient with jaundice and no upper abdominal pain. MRI of the upper abdomen was conducted as part of a thorough work-up.
(A and B) VRT (A) and MIP (B) images reconstructed from the 3D TSE sequence. For the VRT manual segmentation were used in the source slices to idntifiy right and left hepatic duct system as well as the remaining parts of the extrahepatic system. Segmentation information was combined with different color-coded transfer functions (right = blue; left = red; extrahepatic = green), allowing better identification of the anatomy when slabs and cut-planes are used (see C to F). All intrahepatic bile ducts show marked dilation.
(C and D) Same images as (A) and (B), but with a paracoronal cut-plane (A) or a paracoronal slab selection (B; 1.5 cm) to gain better view of the central parts of the biliary tree. Note the conic abrogation of both hepatic ducts proximal to the common bile duct. Remnants of the common bile duct and the gallbladder are present more distally.
(E) Here we manually superimposed an axial slab from the color-coded VRT with an axial contrast-enhanced gradient-echo sequence. The image orientation of the axial sequence was mirrored to maintain a "view from above", as is normally used with VRT instead of the classic radiological view of slice data. The correlation with anatomic information further strengthens the localization of the stenoses in the region were left and right hepatic system normally join to form the common bile duct.
(F) An image from the same series of contrast enhanced images as in (E) just two slices lower. In the region of the ductal stenoses a hypointense lesion with rim-enhancement can be delineated (arrowheads). After histological sampling the diagnosis of a Klatskin tumor could be confirmed. Unfortunately resection was considered impossible as the MRI showed gross involvement of the left and right biliary systems.

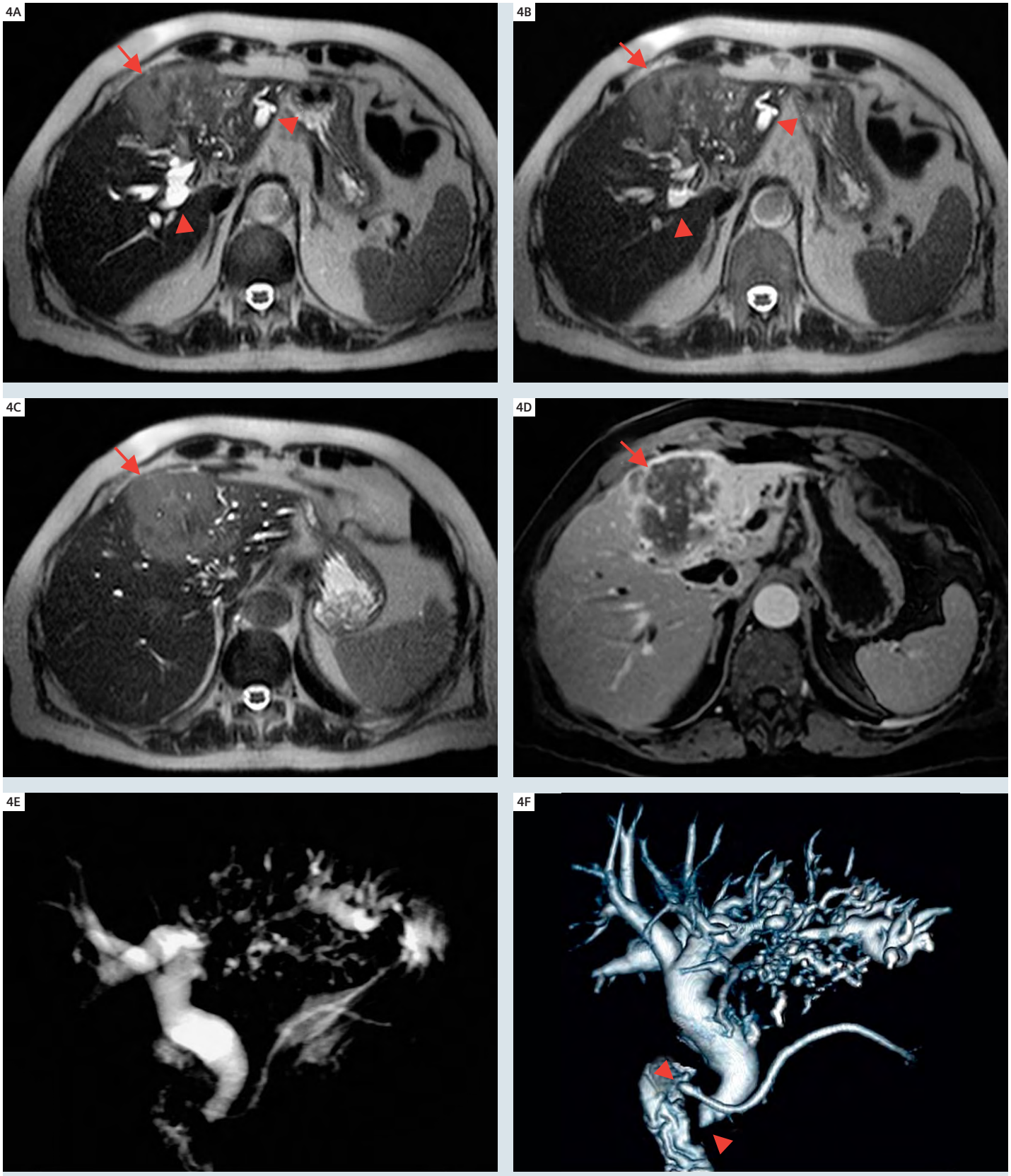

4 Case 4: Intrahepatic cholangiocarcinoma

4G

4H

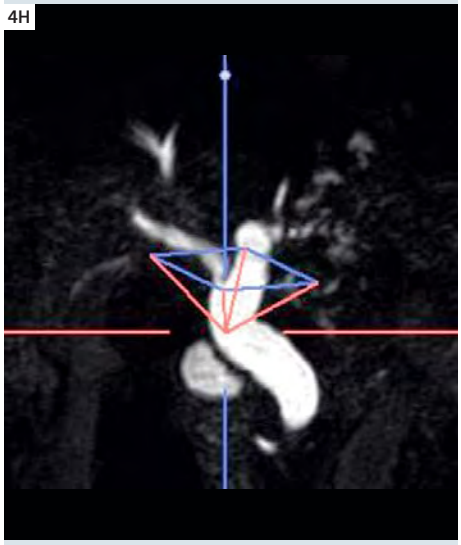

4I

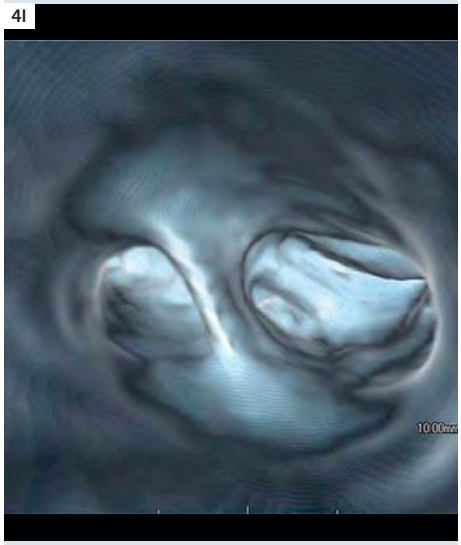

4 Case 4: Intrahepatic cholangiocarcinoma

Case 4: Intrahepatic cholangiocarcinoma

An 80-year-old male patient was referred to our department after repeated episodes of hepatolithiasis and a suspected mass in the left liver lobe.

(A–C) Three consecutive slices from an axial HASTE sequence show a large hyperintense and ill-defined mass (arrow) arising from the left liver lobe causing dilation of the adjacent ductal structures (arrowheads). Whereas slice A and B can clearly be delinaeted as consecutive images, slice C represents a markedly different anatomic position. Due to this offset in position the bile ducts and other anatomic structures cannot easily be traced in through-plane direction. This offset in image position is known as "serious misregistration artifact" and represents a major drawback of breath-hold HASTE imaging.

(D) Shows a image from an axial contrast-enhanced gradient-echo sequence. The large tumor can be identified as a hypointense multilobulated structure with rim-enhancement. Histological work-up confirmed the diagnosis of an intrahepatic cholangiocarcinoma.

(E-G) RARE (E) and 3D-TSE images as VRT (F) and MIP (G) all nicely show the disruption of the intrahepatic bile ducts in the left lobe concomitant with dilation of the residual ducts. The presence of a pancreas divisum with the common bile duct and the pancreatic duct opening to different papillae can, although visible in all images, best be identified in the VRT (arrowheads). The MIP also shows the actual finding, but does not provide further depth-information. The MRCP image is impaired by fluid overlay from the stomach and duodenal bulb.

(H and I) A manually angulated MPR of the 3D-TSE images in a paracoronal orientation (H) shows a section through the common bile duct in a comparable position to images E-G. This image is use to plan the "camera position" for the virtual VRT (I) that shows an endoluminal view on the main branching of the bile duct.

References

1 Rosch T, Meining A, Fruhmorgen S et al. A prospective comparison of the diagnostic accuracy of ERCP, MRCP, CT, and EUS in biliary strictures. Gastrointest Endosc 2002 ; 55: 870–876.

2 Wallner BK, Schumacher KA, Weidenmaier W, et al. Dilated biliary tract: evaluation with MR-cholongiography with a T2-weighted contrast enhanced fast sequence. Radiology 1991; 181: 805–808.

3 Hennig J, Nauerth A, Friedburg H. A fast imaging method for clinical MR. Magn Reson Med 1986; 3:823-833.

4 Wallnoefer AM, Herrmann KA, Beuers U, et al. Comparison of 2D and 3D sequences for MRCP. Clinical value of the different techniques. Radiologe 2005; 45(11): 996-1003.

5 Bley TA, Pache G, Saueressig U, et al. State of the Art 3D MR-Cholangiopancreatography for Tumor Detection. In vivo 2007; 21(3).

6 Augui J, Vignaux O, Argaud C, et al. Liver: T2-weighted Imaging with Breath-hold Fast-Recovery Optimized Fast Spin-Echo Compared with Breath-hold Hald-Fourier and Non-Breath-hold Respiratory-triggered Fast Spin-Echo Pulse Sequences. Radiology 2002; 223(3):853-9.

Both Morphological and Functional Assessments of Congenital Urinary Tract Abnormality using 3D Sequences

Nicole Nicaise, M.D.[1]; Roger Demeure, Ph.D.[2]; Christian Delcour, M.D.[1]

[1] ISPPC Charleroi, Service d'Imagerie Médicale, Charleroi, Belgium, [2] Siemens Medical Solutions, Brussels, Belgium

Patient history

26-year-old woman with right lumbar pain. **Sonography:** Right located horse-shoe kidney. **Scintigraphy:** No left kidney and normal right kidney.

MRI protocol

Images were acquired after IV furosemide diuretic stimulation on a MAGNETOM Symphony, A Tim System.

Morphological evaluation was based on both source and MIP (maximum intensity projection) images which were generated from:

a) Respiratory-triggered (PACE) heavily T2-weighted SPACE pulse sequence (TR/TE/ETL: 1800/678/129, 40 slices, voxel size: 1.5 mm³) (Fig. 2).

b) The first acquisition (arterial time) and the latest acquisitions of a 10 s dynamic contrast-enhanced T1-weighted 3D-FLASH pulse sequence (TR/TE/ : 3.6/1.5/60°, 32 slices, voxel size: 2.5 mm³, acquisition protocol: every 15 s during 5 min, every 30 s during the following 3 min, and every minutes until 20 min after contrast IV bolus (0.2 mmol/kg, 2.5 ml/sec). The linearity of signal intensity versus contrast agent concentration (ranging from 0 to 4.5 mmol/l) was previously asserted by test-object (R = 0.995) (Fig. 3).

Functional analysis was based on time-intensity curves generated from regions of interest (ROIs) drawn over the aorta, the long axis parenchyma (Figs. 4A, B), and the collecting system (Figs. 5A, B). Cortical intake, transit time were computed and urinary excretion was evaluated.

Conclusion

This MR procedure provides an accurate all-in-one assessment of the urinary tract. Accordingly, MR is a technique of choice especially when considering laparoscopic surgery.

1

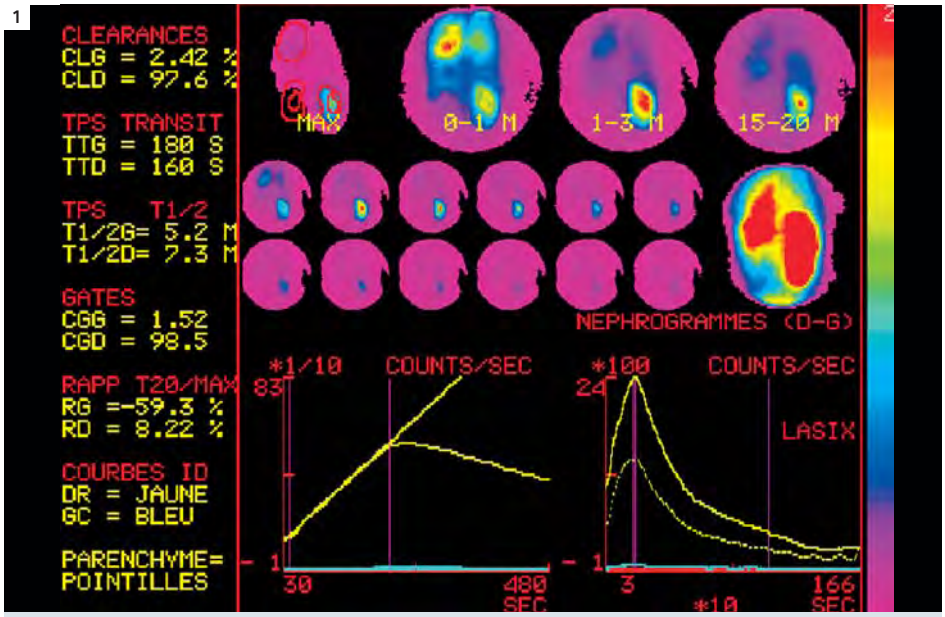

1 Scintigraphy showed no left kidney and normal right kidney.

2

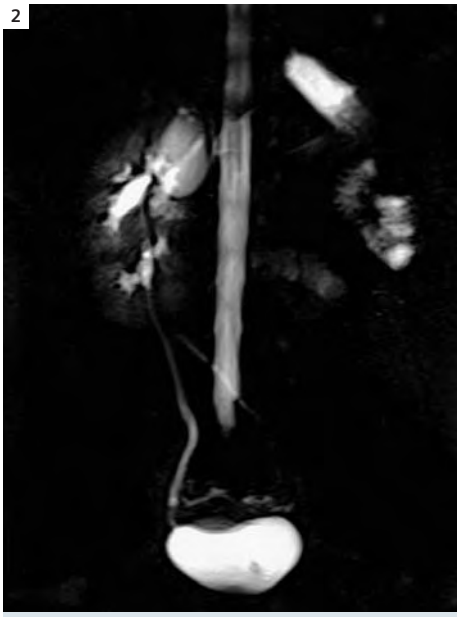

2 On this RARE image, crossed renal ectopia is suspected but left renal ureter is not very well delineated.

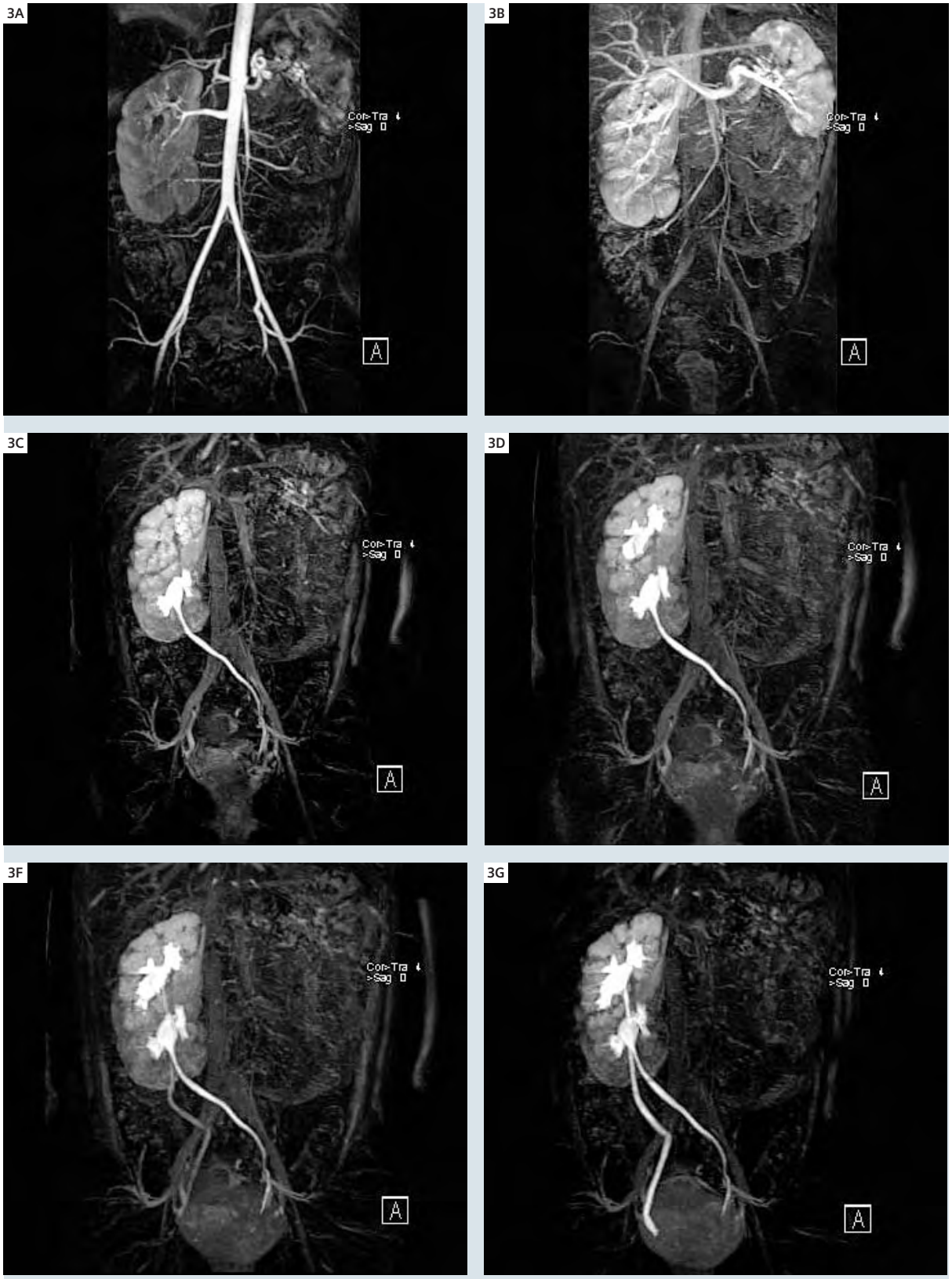

3 MIPs generated from the dynamic sequences. On the first arterial MIP, an inferior accessory renal artery is depicted and the crossed renal ectopia is nicely delineated.

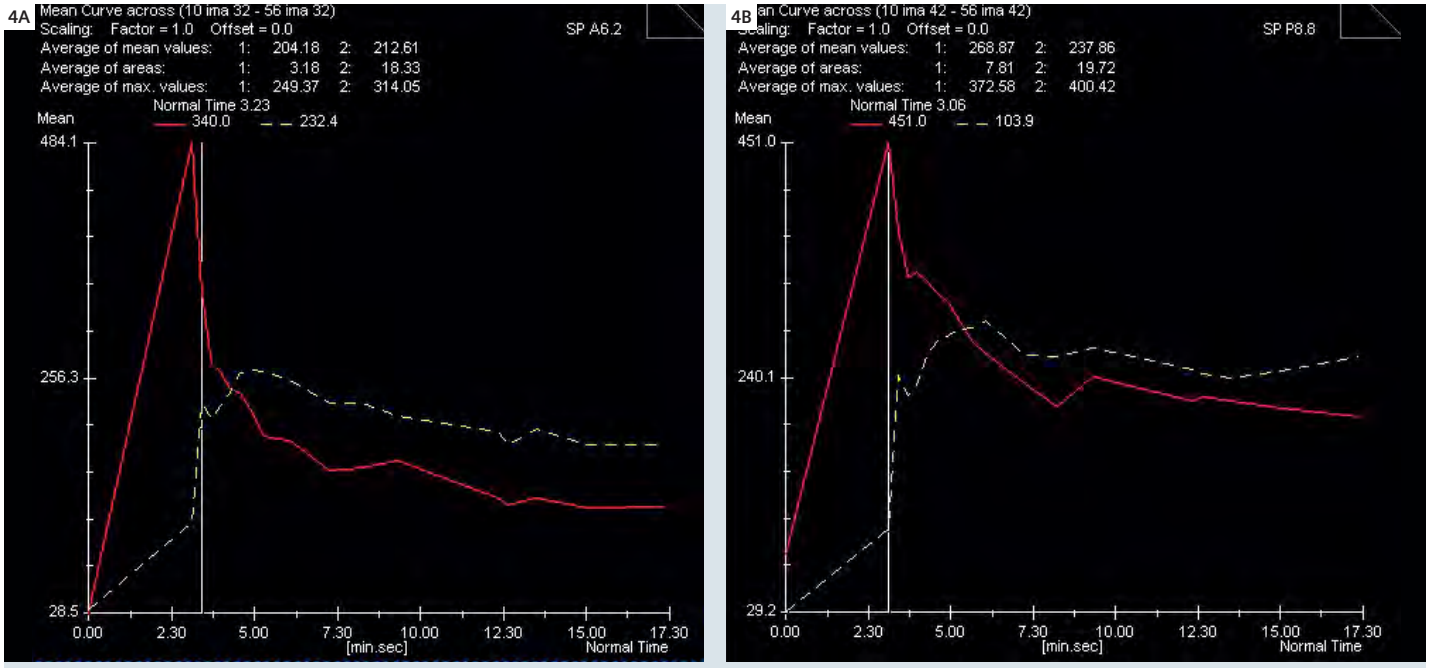

4 Time/Intensity curves of the upper **(A)** and lower **(B)** parts of the renal parenchyma (yellow) compared to the aorta (red). Cortical intakes are similar.

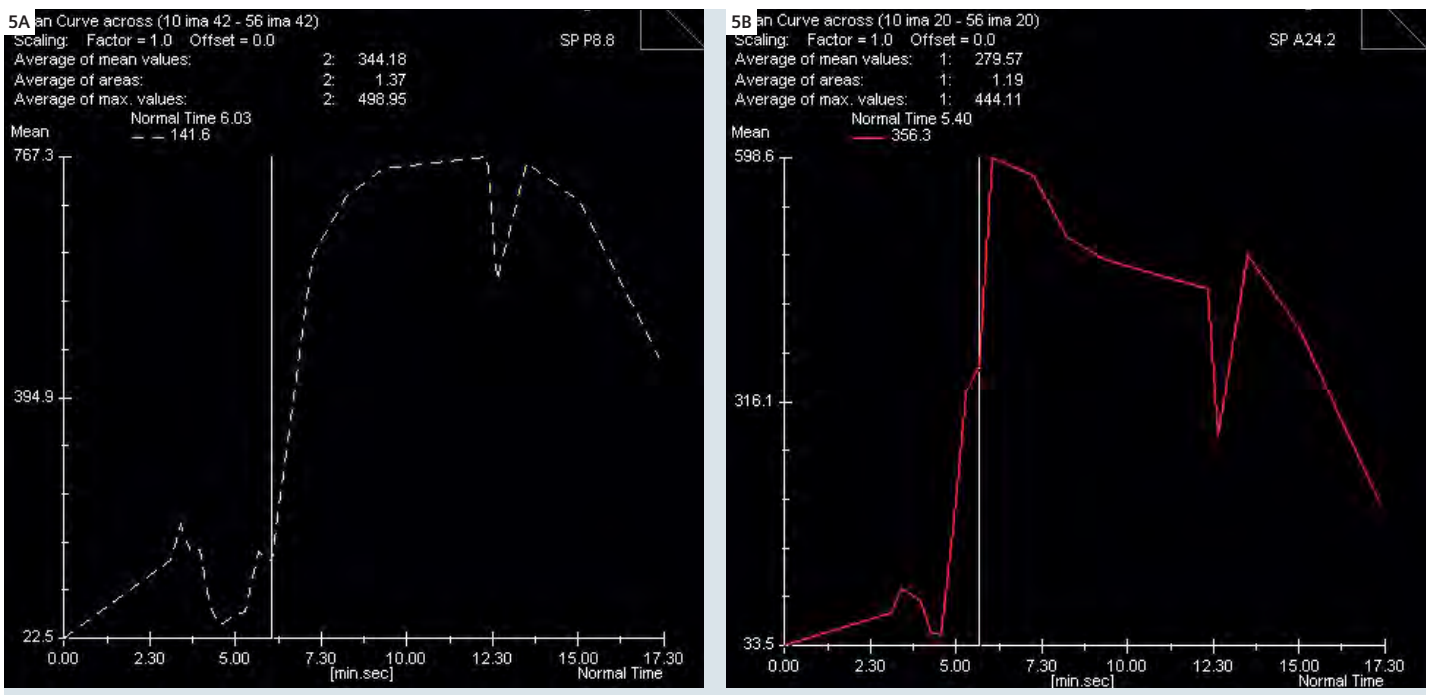

5 Compared Time/Intensity curves of the upper and lower collecting system, also similar.

* WIP – Works in progress. This information about this product is preliminary. The product is under development and not commercially available in the U.S., and its future availablility cannot be ensured.

How can we meet her expectations?

With Breast Care Solutions: A comprehensive approach – covering every step of the way.

About every 10th woman will be diagnosed with breast cancer in her life. That's why we have bundled our strengths to help fight breast cancer worldwide: You receive everything you need from one source, so you can offer outstanding quality of care. For women. For health. For life. **www.siemens.com/healthcare +49 69 797 6420**

Answers for life.

SIEMENS

CC-Z1059-2-7600

Clinical Applications of Diffusion Tensor Imaging

Tammie L. S. Benzinger, M.D., Ph.D.[1]; Robert C. McKinstry III, M.D., PhD.[2]; Chin-I Chen, M.D[1]; Agus Priatna, Ph.D.[3]

[1]*Mallinckrodt Institute of Radiology, Washington University School of Medicine, St Louis, Missouri, USA*
[2]*St. Louis Children Hospital, Mallinckrodt Institute of Radiology, Washington University School of Medicine, St Louis, Missouri, USA*
[3]*Siemens Medical Solutions, Malvern, PA, USA*

Introduction

Diffusion tensor imaging (DTI) is an emerging method for clinical neuroradiology. DTI allows for quantitative evaluation of the rate and direction of water motion within a voxel. In the brain, the axons of neurons form fiber tracts which impose directionality (anisotropy) on measurements of water diffusion. The aggregate diffusion of water within these tracts is quantified at each point by the diffusion tensor (D) [Stejskal and Tanner, 1965]. Multiple parameters can be derived from the diffusion tensor, including the „trace", Tr(D)= 1 + 2 + 3 = 3 × ADC (apparent diffusion coefficient), the relative anisotropy (RA, defined as the standard deviation of the three eigenvalues, normalized by the ADC), and the fractional anisotropy (FA, which is the standard deviation of the three eigenvalues normalized to the magnitude of the diffusion tensor). These secondary parameters are independent of the frame of reference and are very sensitive to white matter pathology [Alexander et al., 2007; Melhem et al., 2002].

Until recently, DTI required extensive off-line calculations to generate the tensor (D) and related parameter maps. However, using the current DTI packages available on the Tim (Total imaging matrix) platforms, DTI can now be performed as part of a routine clinical brain MRI, with Inline calculation of the D, ADC, and FA, and rapid off-line calculation of additional parameter maps as needed. We have developed a 25-direction DTI protocol with 25 b-values which can be run with isotropic 1 mm voxels at 3 Tesla in 4 minutes. We now include this as part of the standard imaging routine for pediatric and adult brain MRIs at St. Louis Children's Hospital and Washington University Medical Center.

Method

Imaging was performed at 3 Tesla MAGNETOM Trio, A Tim System or 1.5 Tesla MAGNETOM Symphony, A Tim System with Quantum gradient system using 12-channel Head Matrix coils. A single shot spin-echo echo planar imaging (EPI) was used for DTI acquisition at the Tim Trio with the following parameters: 60 slices without a gap, FoV = 190 mm, phase FoV = 100 %, slice thickness = 2 mm, base resolution = 96, phase resolution = 100 (that makes voxel size = 2 x 2 x 2 mm), phase partial Fourier = 6/8, TR = 9900 msec, TE = 102 msec, average = 1, b-value = 1400 sec/mm^2, bandwidth = 1080 Hz, EPI factor = 96, echo spacing = 1 msec. A similar protocol was setup for the Tim Symphony with 2.5 x 2.5 x 2.5 mm isotropic voxel. Average ADC map, trace weighted map, FA map, and tensor data were created inline. Post-processing was performed with Neuro 3D application package. The package has the capability of processing directional color encoded fractional anisotropy map (blue = SI direction, green = AP direction, and red = RL direction), tensor map, aligned tensor and anatomy data, aligned tensor and fractional anisotropy data, texture diffusion that maps the overall fiber tracts within the slices, and tractography.

Clinical cases

The following cases are some of the examples of the clinical applications of diffusion tensor imaging in pediatrics and adults which we have encountered in the course of routine clinical practice.

Case 1: Septo-optic dysplasia

A 14-year-old boy was admitted to the hospital with severe, chronic headaches. MRI shows absence of the septum pellucidum is consistent with his clinical diagnosis of septo-optic dysplasia. Moderate hydrocephalus and thinning of the corpus callosum were found. DTI show marked diminution, with significant reduction in the visual fiber tracts of the optic radiations but with persistent anisotropy (Fig. 1). These findings are concordant with his clinical presentation of intact visual function and are also in accordance with reports in the literature [Polizzi et al., 2006; Schoth et al., 2004]. Septo-optic dysplasia consists of a heterogenous deficits of midline brain structures which include absence or dysplasia of septum pellucidum, optic nerve and pituitary-hypothalamic dysfunction. In addition, the lesions may associate cerebral development malformations such as schizencephaly and polymicrogyria. A HESX1 gene mutation has been identified in familial septo-optica dysplasia. Clinical manifestations include diminished visual acuity, color blindness, nystagmus, microphthalmia, mental retardation, and endocrine disturbance.

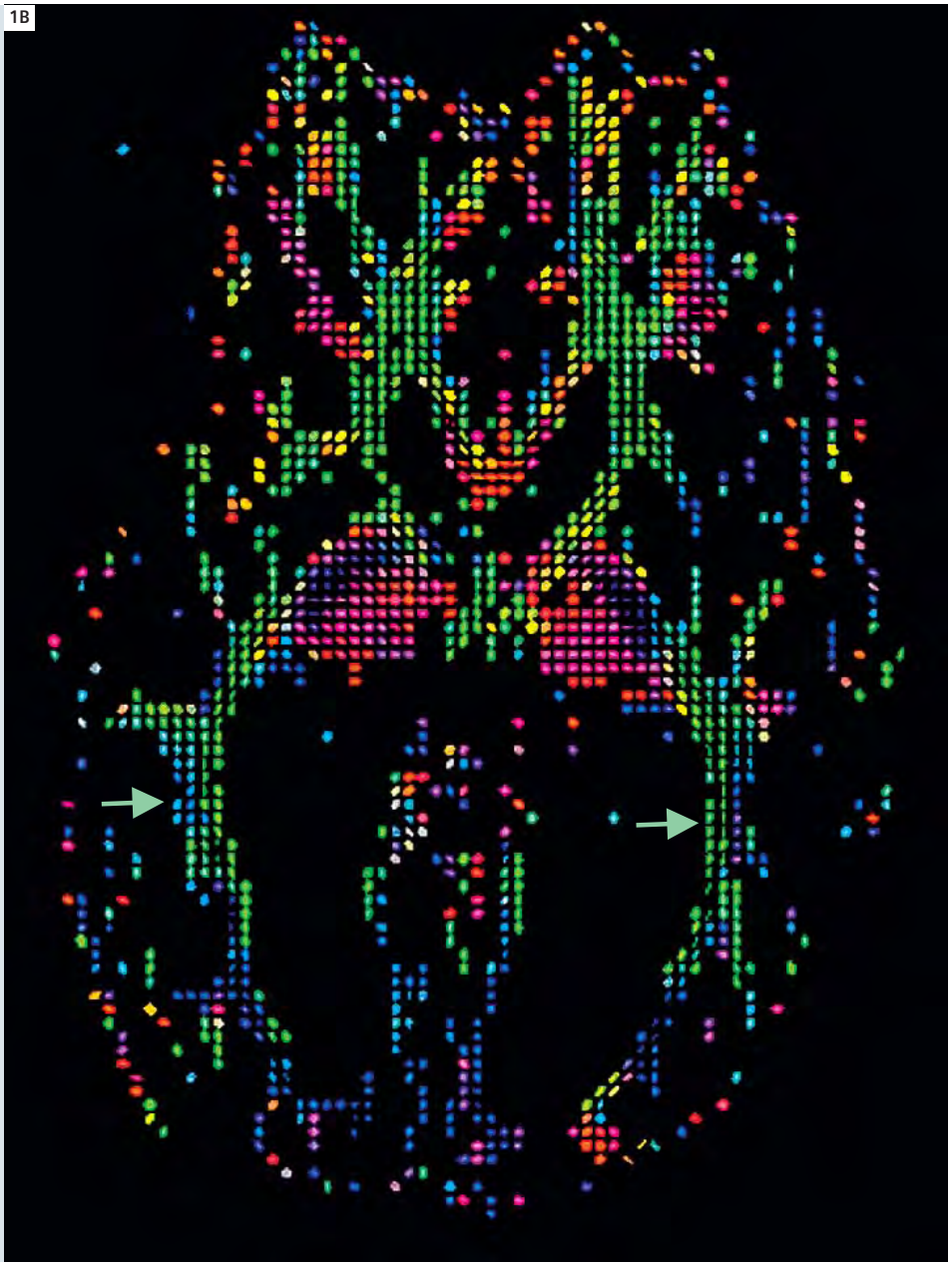

1 Septo-optic dysplasia. MR examinations were performed at 3T MAGNETOM Trio, A Tim System: **(A)** T1-weighted (MPRAGE) anatomic image demonstrating enlargement of the ventricles and absence of the septum pellucidum (arrow). **(B)** Tensor diagram computed from a 4 minute DTI scan performed with isotropic 2 mm voxels at 3 Tesla. The shape and color of the ellipsoids corresponds to the orientation of the white matter tract (anterior-posterior is green, transverse is red, and cranio-caudal is blue). The optic radiations (arrowheads) adjacent to the lateral ventricles are thin but intact.

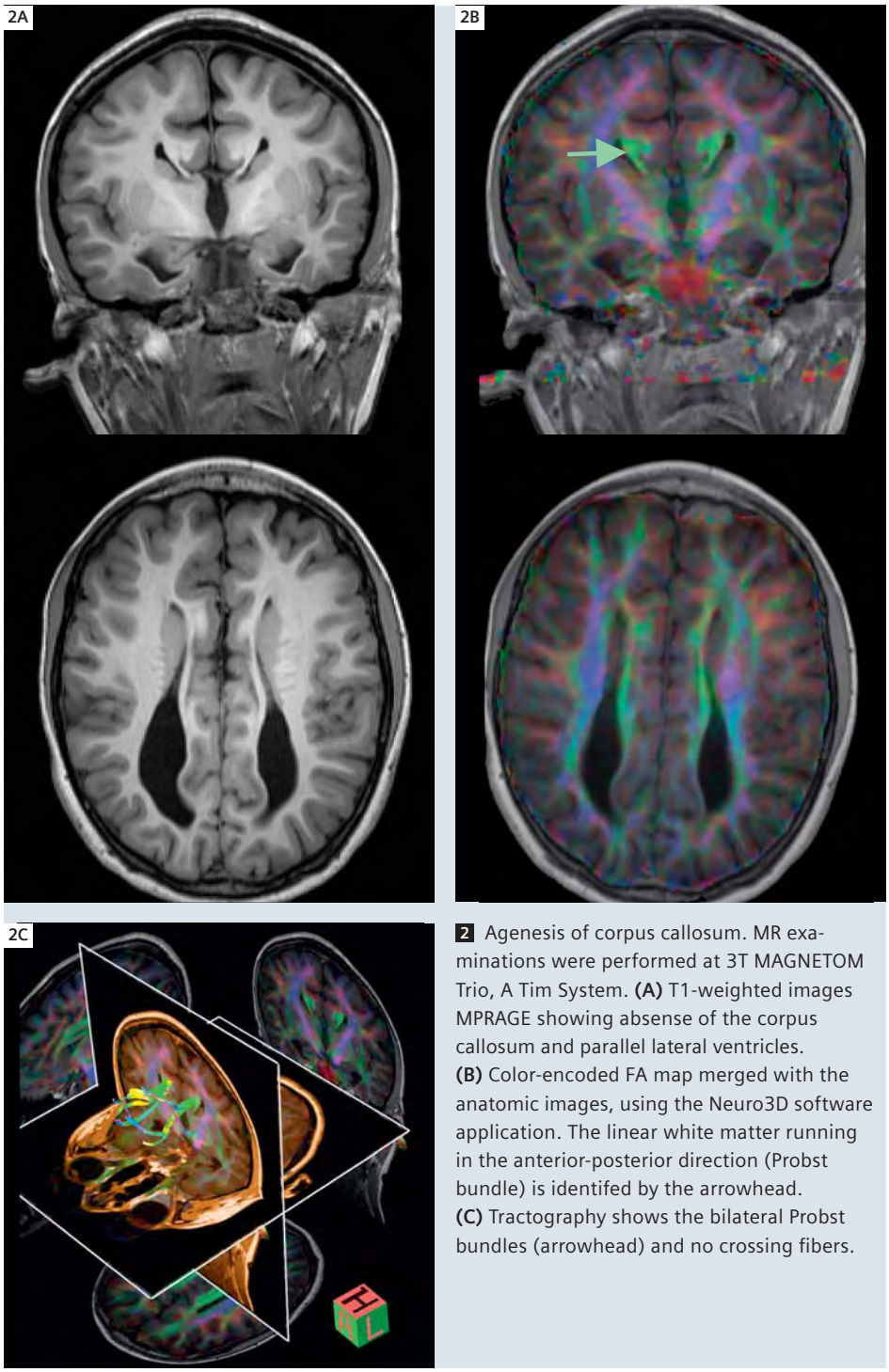

2 Agenesis of corpus callosum. MR examinations were performed at 3T MAGNETOM Trio, A Tim System. **(A)** T1-weighted images MPRAGE showing absense of the corpus callosum and parallel lateral ventricles. **(B)** Color-encoded FA map merged with the anatomic images, using the Neuro3D software application. The linear white matter running in the anterior-posterior direction (Probst bundle) is identifed by the arrowhead. **(C)** Tractography shows the bilateral Probst bundles (arrowhead) and no crossing fibers.

Case 2: Agenesis of corpus callosum

A 9-year-old girl was diagnosed with developmental delay and intractable seizures. MRI shows colpocephaly, parallel lateral ventricles, and agenesis of the corpus callosum. DTI shows no crossing fibers in the expected region of the corpus callosum (Fig. 2). With tractography, the orientation of the parallel Probst bundles are clearly identified. Tractography has recently been described as a useful imaging approach to callosal agenesis and dysgenesis [Tovar-Moll, 2007]. Agenesis of corpus callosum is a failure to develop the large bundle of fibers that connect the cerebral hemispheres. The complex disorder can result from any one of the multiple steps of callosal development, such as cellular proliferation and migration, axonal growth or glial patterning at the midline. Its subjacent mechanisms are still unknown. Patients can show variable presentations ranging from no symptoms to severe cognitive impairment [Paul et al., 2007].

Case 3: Schizencephaly

A 4-year-old girl has a past history of seizures. MRI (Fig. 3) shows a major malformation of cortical development involving the left motor strip, dorsal lateral premotor region, frontal operculum, frontal polar region, orbital frontal and lateral frontal regions, parietal operculum, and posterior temporal lobe. An associated left-sided schizencephaly is identified. The left lateral ventricle is mildly dilated. There is abnormal configuration of the central sulcus on the left. DTI shows diminished anisotropy of the underlying white matter region in subjacent to the malformation of cortical development [Eriksson et al., 2001; Trivedi, et al., 2006]. Schizencephaly presents a cleft in the cerebral cortex unilaterally or bilaterally, usually located in the frontal area. Associated septum pellucidum deficits are often found, suggesting that schizencephaly may share similar genetic mechanisms with septo-optic dysplasia. Mutation in the EMX2 gene can lead to schizencephaly. Clinical symptoms include seizures and mental impairment [Tanaka et al., 2000].

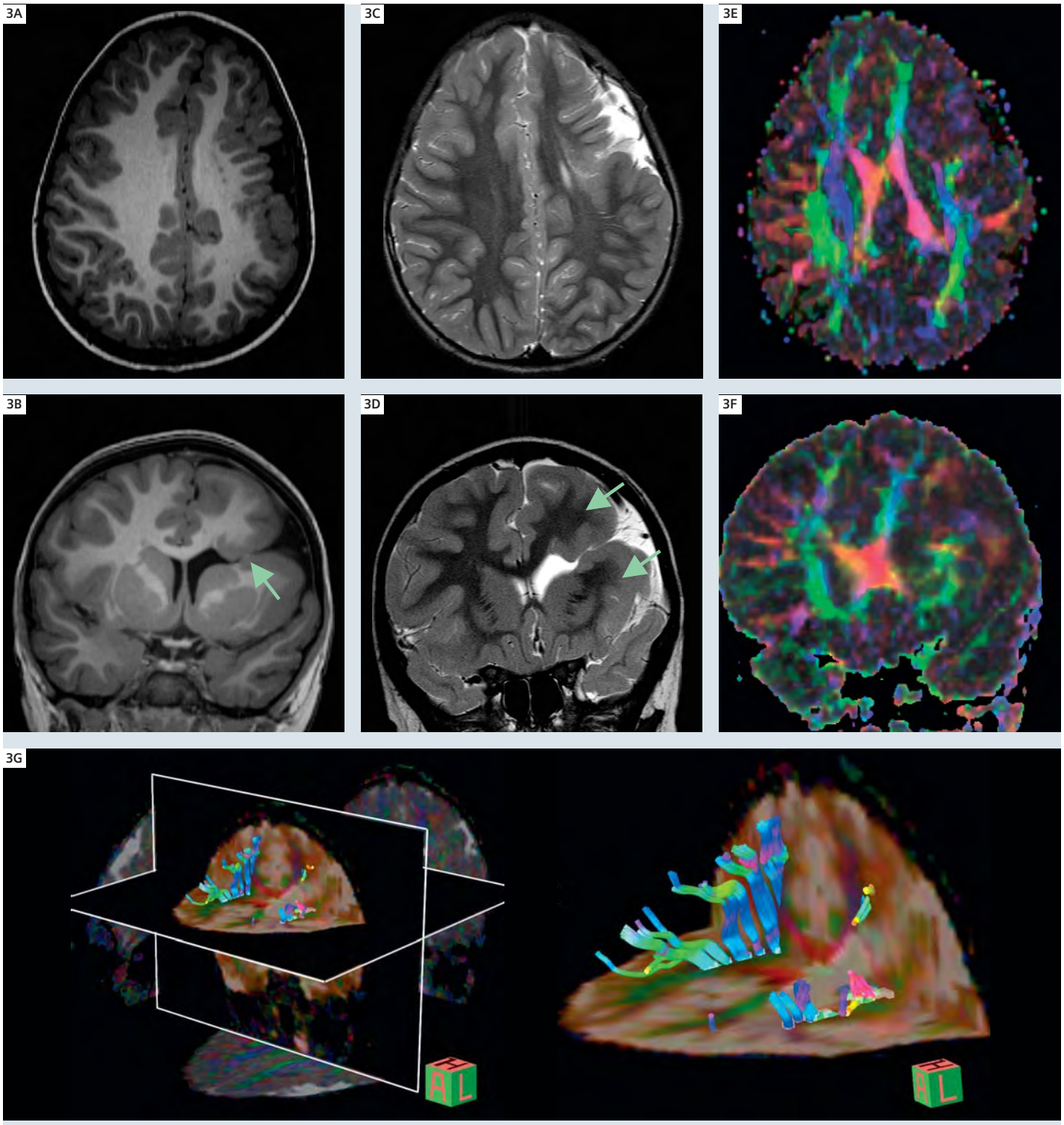

3 Schizencephaly. MR examinations were performed at 3T MAGNETOM Trio, A Tim System. T1 **(A, B)** and T2-weighted **(C, D)** transverse **(A,C)** and coronal images **(B, D)** demonstrating a large schizencephalic cleft in the left cerebral hemisphere (arrow). Accompanying this is an extensive malformation of cortical development (arrowheads). Although the white matter underlying the abnormal cortex appears normal on the clinical T1 and T2-weighted images, when the directional encoded FA map is superimposed on the anatomic images **(E, F)** there is complete loss of the normal (green and red) anisotropy in this white matter. **(G)** Tractography images show the tortuous fibers which do not cross the schizencephalic cleft.

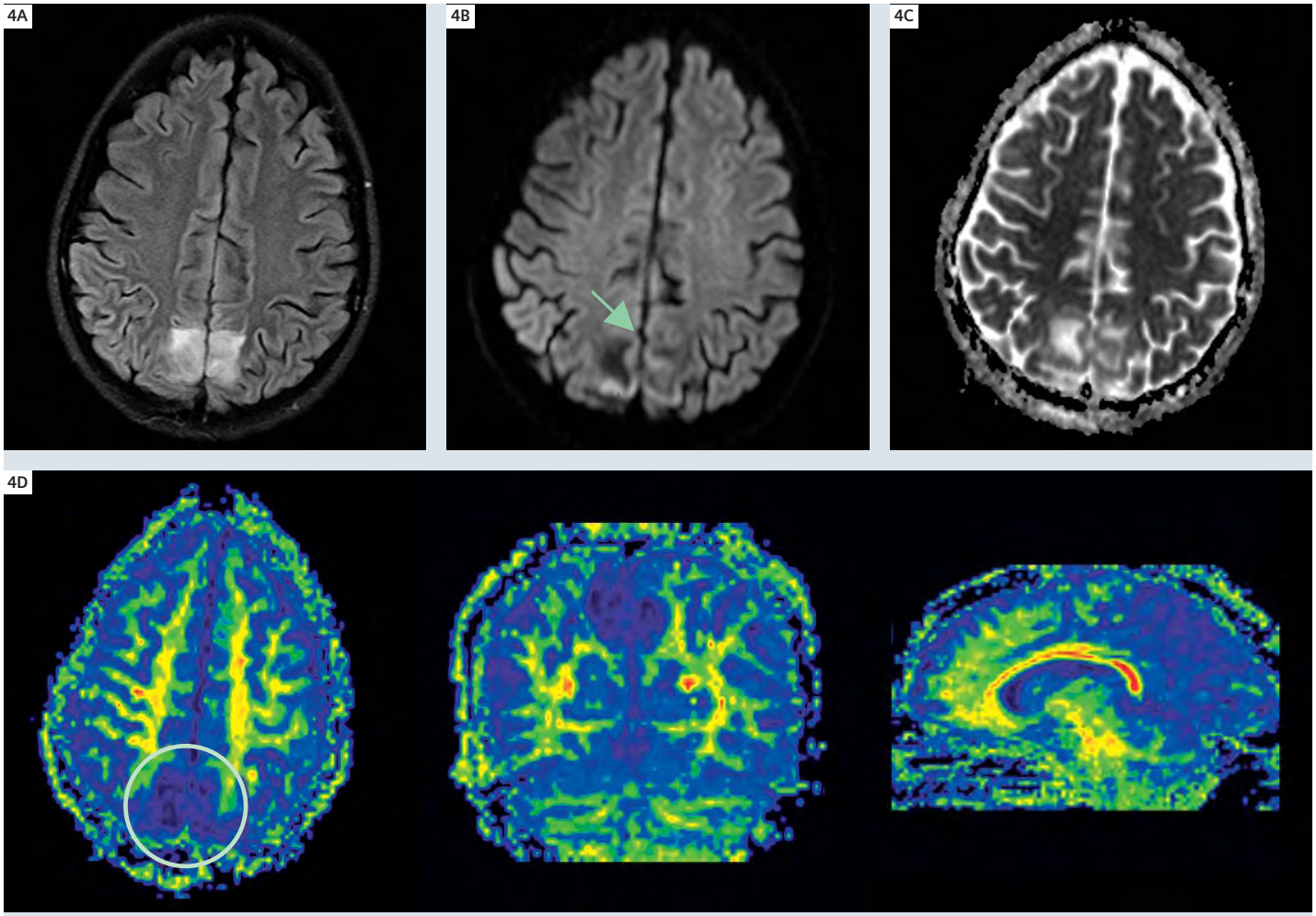

4 Reversible Posterior Leukoencepalopathy Syndrome (RPLS). MR examinations were performed at 3T MAGNETOM Trio, A Tim System: **(A)**, **(B)**, and **(C)** are the DarkFluid T2-weighted TSE, b = 0 image, and ADC map shows the area of restricted diffusion. **(D)** Fractional anisotropy, reformatted in transversal, coronal, and sagittal orientations shows loss of anisotropy in the right parietal lobe extending beyond the areas of T2 hyperintensity.

Case 4: Reversible Posterior Leukoencepalopathy Syndrome (RPLS)

A 13-year-old girl who with a past medical history of hypertension and end stage renal disease was transferred to pediatric ICU because of hypertensive seizure. MRI shows bilateral posterior parietal-occipital areas of T2 hyperintensity, with a focal area of reduced diffusion in the right parietal lobe. The FA parameter map derived from DTI demonstrates an area of abnormal anisotropy in the right parietal lobe which extends beyond the area of T2 hyperintensity (Fig. 4). Although restricted diffusion can has been reported in RPLS, the FA changes in the surrounding white matter have not previously been examined. Incorporating DTI into the routine clinical protocol will allow for larger research studies to be generated to further evaluate this finding [Mukherjee et al., 2001]. RPLS is a clinicoradiological entity which appears as reversible white matter edema predominantly involving the parietal and occipital lobes. The syndrome has been associated with a spectrum of disorders, including hypertensive encephalopathy, eclampsia, thrombotic thrombocytopenic purpura, acute renal failure, hemolytic-uremic syndrome, acute intermittent porphyria, and immunosuppressive drugs. The eitiology of RPLS is believed to be due to a breakdown of the blood-brain barrier with transudation of fluid and protein into the extravascular space resulting in cerebral edema [Min et al., 2006; Doelken et al., 2007].

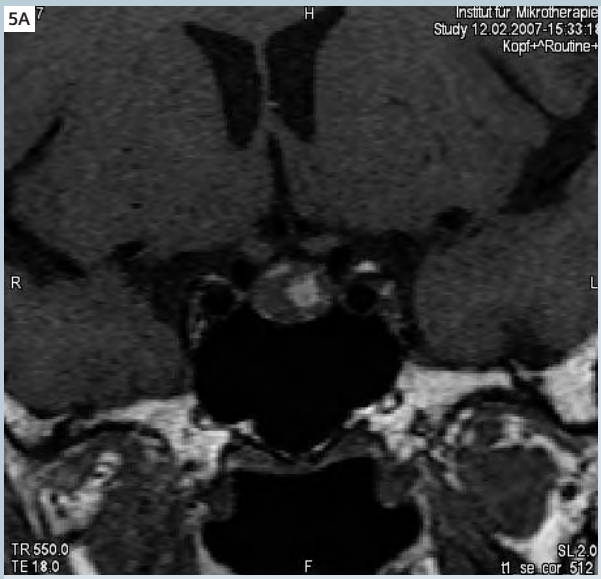

5A Coronal SE, TA = 5:21 min.

5B Sagittal SE, TA = 5:25 min.

6 Coronal T2-weighted TSE, TA = 3:25 min.

Conclusion

By using fast acquisition times, it is possible to obtain useful images due to better positioning. These images allow for highly exact planning with fewer slices and reduced voxel size. This leads to an overall reduction in examination time. However, we have applied part of the time gained to image resolution in order to increase the image quality. This method is not limited to examinations of the skull. It can be used for all types of examinations. It is desirable that the patient remains in the scanner for an additional minute. During this time, the faster sequences can be applied instead of looking at a 5-minute measurement time and realizing that the planning was not successful which means that the measurement has to be repeated.

Neuro 3D – A Clinical Exam

Jeff Zimmers, BSRT(R) (MR) ARRT

Advanced Clinical Education Specialist, Siemens Medical Solutions, USA

Many new tools are available for imaging the brain for surgical planning. Neuro 3D in the lastest *syngo* MR B15 software provides a comprehensive diagnostic tool that utilizes cutting-edge imaging techniques such as BOLD (Blood Oxygen Level Dependent) and Diffusion Tensor Imaging (DTI). These imaging techniques have been mostly research in the past, but now they are clinical reality with new imaging techniques and post processing BOLD imaging with DTI was performed

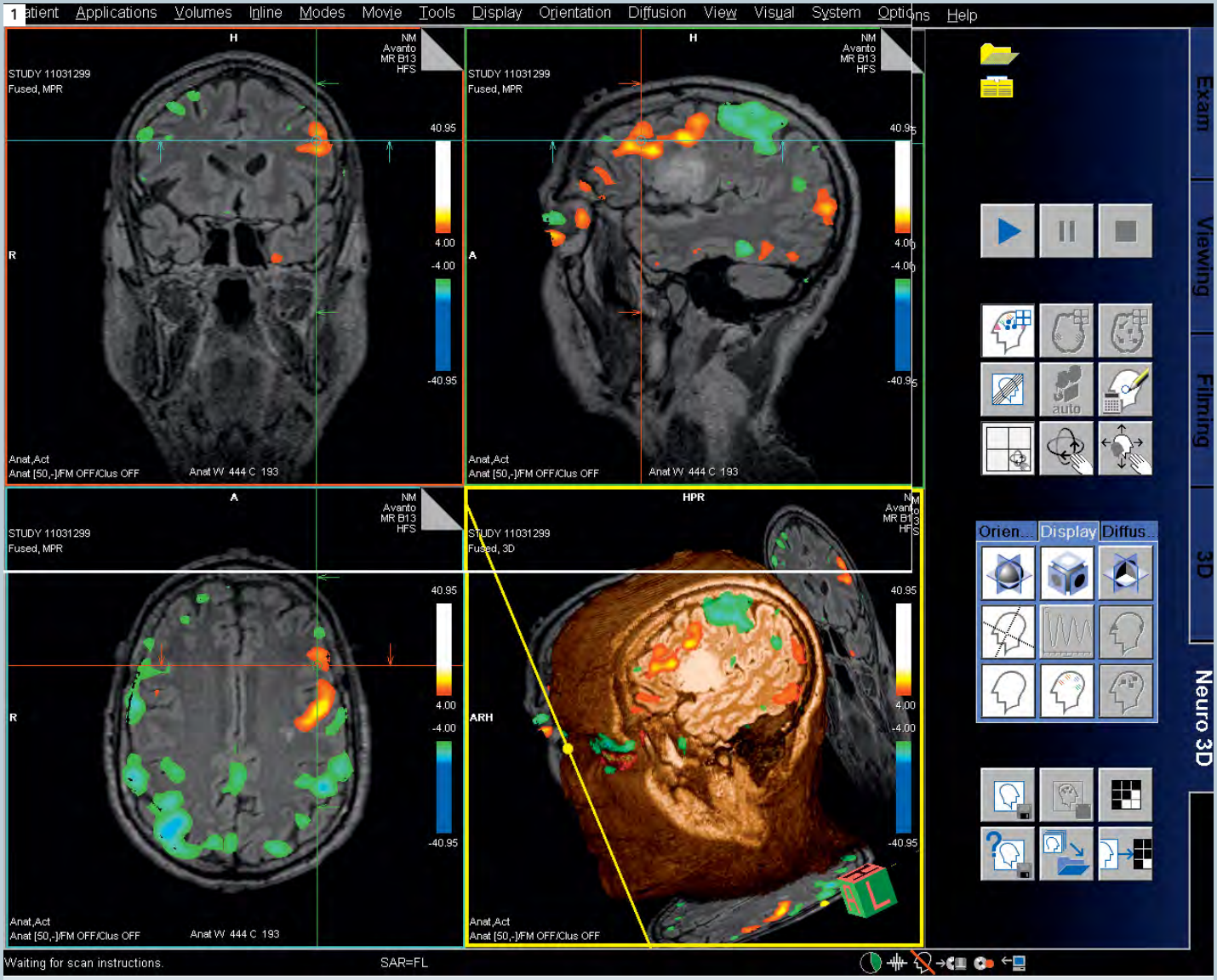

1 These images were reviewed by the neurosurgeon and radiologist in a matter of minutes. Surgical planning was changed dramatically due to the BOLD activation superiorly to the lesion. More advanced post processing was then done to take a look at fractional anisotropy (FA) and tractography. New for *syngo* MR B15 is the texture FA. This involves a simple click of the texture icon (Fig. 2A).

on a patient with a known lesion in the left hemisphere to assess a surgical approach. The neurosurgeon was concerned that damage would be done to the patients motor skills. The first important imaging technique is a 3D sequence loaded into Neuro 3D. In this case, a SPACE DarkFluid sequence was used to define tumor borders. *syngo* SPACE provides high isotropic resolution in a very short period of time using iPAT (integrated Parallel Acquisition Techniques). Next the GLM (General Linear Model) was loaded into Neuro 3D that was acquired from our 3D PACE epi bold sequence. The GLM was calculated inline with Inline BOLD imaging, so no post processing was needed to get the GLM. Next, the tensor data was loaded into Neuro 3D. This too was calculated inline, with Inline diffusion. With *syngo* MR B15 software, this can also be calculated offline. This will allow for older data to be used with Neuro 3D as in this case. The functional information is automatically displayed as well as an FA (fraction anisotropy) map superimposed on the SPACE images. The BOLD experiment was done with bilateral finger tapping to activate the motor stripe. Excellent protocols for these techniques can be found in the new clinical libraries in the Siemens protocol tree on *syngo* MR B15 software.

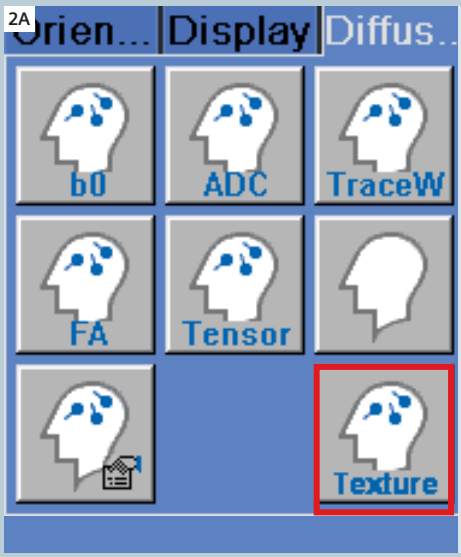

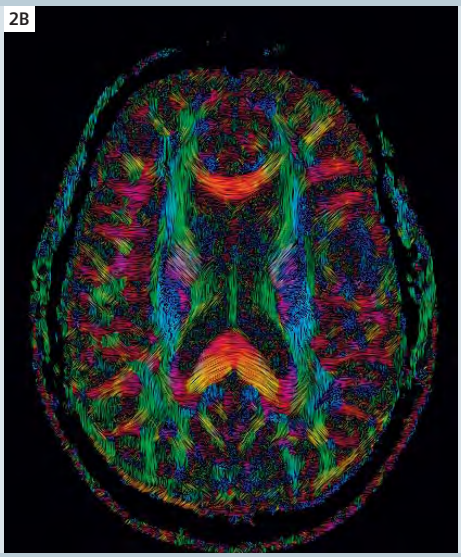

2 Texture diffusion is a fast way to get a quick impression of possible tracts. The image shows anisotropic diffusion as flow patterns across the entire image. The FA image shows the absence and deviation of tracts.

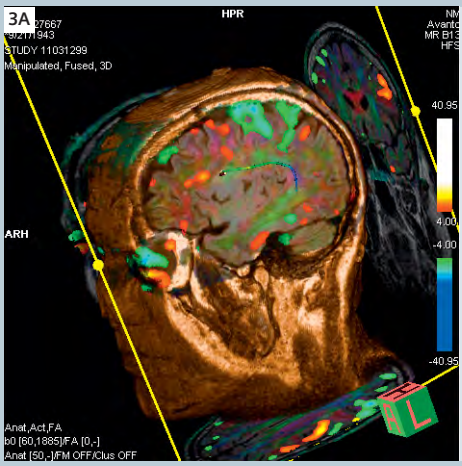

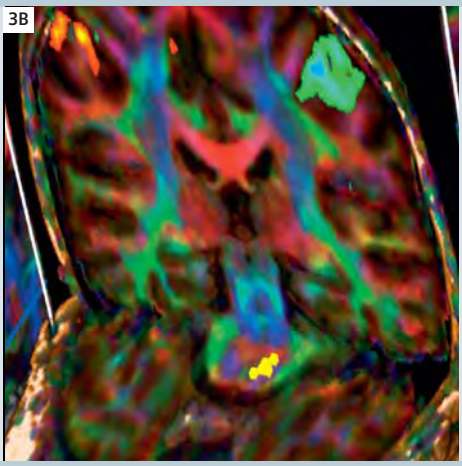

3 Quick Tract is another very useful new tool. By selecting the pixel lens, tracts can be instantly seen. This can be done by pressing the shift button while selecting the left mouse in fusion mode on the 3D data set **(A)**. Quick track can also be used in Diffusion Mode with a left mouse click via pixel lens **(B)**.

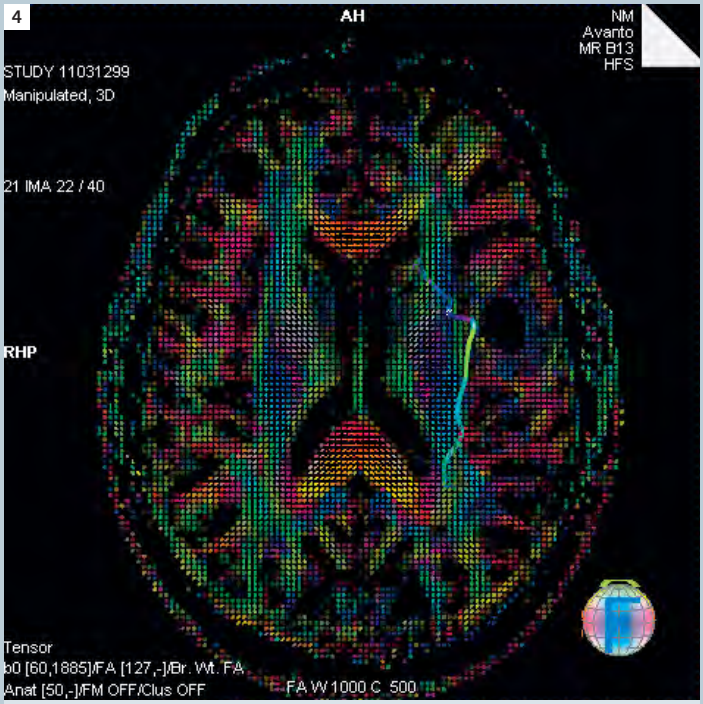

4 Quick Tract is a great starting point for the next step in the process. By selected the "ctrl" key and using the left mouse, seed points can be defined along the areas where the tracts are shown.

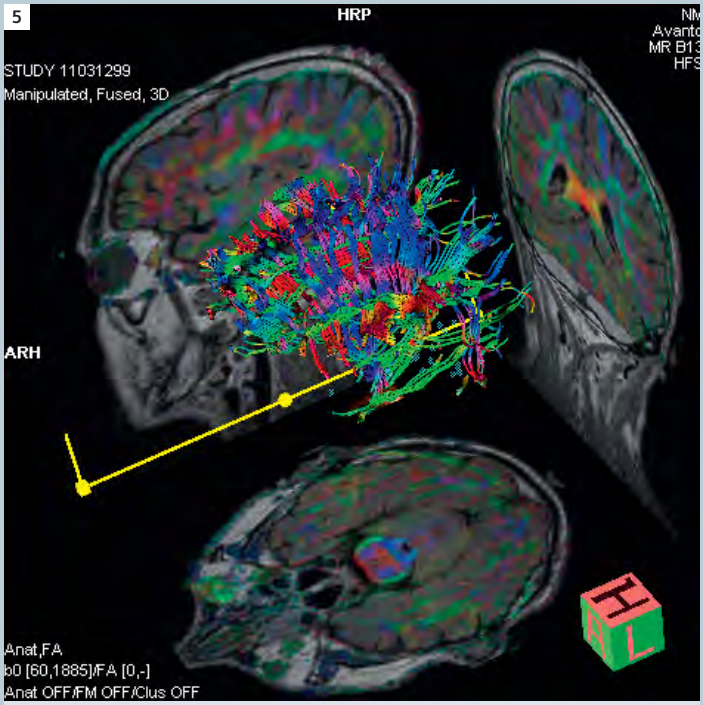

5 Once seed points are created tracts can be generated with a left mouse menu and selecting "start tractography". Several seed groups can be created and tracts generated between seed groups. Colored tracts are displayed in 3D. Color denotes direction of the tracts.

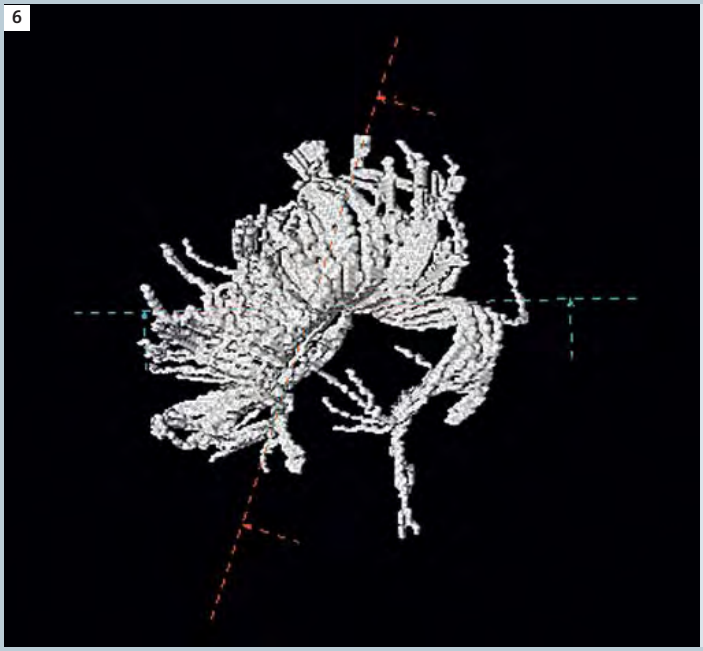

6 Both the seed points can be saved and exported to be processed offline. Tractography can be saved as a color image. There is also a "save tracts as volume" option. This produces a 3D monochrome image that can be exported to other systems for surgical planning. The data can also be used on the 3D card to produce MPR and volume rendered images (VRT).

In conclusion, Neuro 3D, along with SPACE, BOLD and DTI, produced a comprehensive imaging protocol for surgical planning for this case. With Siemens Inline technology, very little processing time was needed. These powerful tools are available on *syngo* MR B15 software.

Can you believe 70 cm at 3T?

Were they reading our minds?

Siemens introduces MAGNETOM Verio
Delivering 3T + 70 cm + Tim

No mind reading required. We just made your wish list our To Do list. Siemens combined a 70 cm Open Bore at 3T with Tim™ (Total imaging matrix) in one feature-rich system. MAGNETOM® Verio will help you accomodate more types of patients, offer more applications, and enhance your workflow. If you're thinking about adding 3T, MAGNETOM Verio is the answer.
www.siemens.com/healthcare +49 69 797 6420

Answers for life.

SIEMENS

MR-Z1050-2-7600

Fat Suppression in the Abdomen

Wilhelm Horger

Siemens Medical Solutions, Erlangen, Germany

Introduction

Due to the different chemical environment, hydrogen nuclei in water- and in fat-tissue have different values for some MRI-relevant parameters, mainly being the relaxation time and the resonance frequency (chemical shift).
These differences can be used to selectively suppress/reduce the signal of fat bound protons.
Thus relaxation-dependant and chemical shift-dependant methods can be used for fat suppression.

Inversion Recovery (STIR = Short TI Inversion Recovery)

This technique is based on the different relaxation behavior of water- and fat tissue. Fat has a much shorter T1 relaxation time than other tissues.
Prior to the excitation pulse of the sequence an inversion pulse ($\alpha = 180°$) is applied which inverts the spins of all tissues. The tissues perform T1 relaxation.
By choosing TI such that the longitudinal magnetization of fat at that time is zero, fat spins will not contribute to the MR signal.

STIR images have an inverted T1 contrast: Tissue with long T1 appears brighter than tissue with short T1.

Advantages:
- Insensitive to B_0 inhomogeneities.

Disadvantages:
- Additional inversion pulse increases minimal TR and total measurement time or reduces maximum number of slices.
- Tissue contrast is affected.

Applications:
Detection of metastasis in the abdominal region.

1

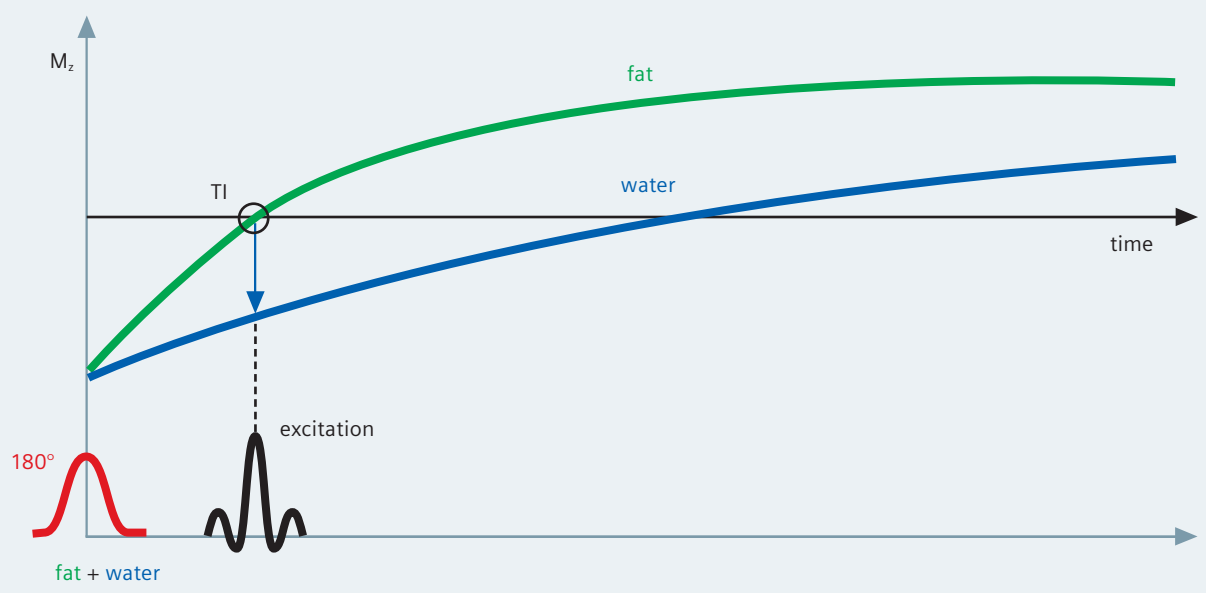

1 Short TI Inversion Recovery (STIR).

SPAIR technique (SPAIR = Spectrally Adiabatic Inversion Recovery)

SPAIR is an alternative to the conventional methods spectral fat saturation or water excitation.
A spectrally selective adiabatic inversion pulse excites only fat spins, thus no STIR like contrast is created. With gradient spoiling the transverse magnetization is destroyed.
The inversion time TI_{null} is such that the longitudinal magnetization of fat at that time is zero, so fat spins will not contribute to the MR signal.

SPAIR Mode: Strong/Weak is available for SE-type sequences.

Advantages:
- Insensitive to B_1 inhomogeneity.
- Tissue contrast is not affected.
- Quick FatSat can be applied for increased performance (VIBE).

Disadvantages:
- Increased minimal TR or reduced maximal number of slices due to more complex preparation pulse (partially compensated by Quick FatSat).
- Slightly reduces the overall signal intensity in single shot sequences (*syngo* REVEAL).

Applications:
- Abdominal breath-hold applications with TSE, SPACE, HASTE, VIBE.
- Fast T1-weighted applications in breath-hold based on the VIBE sequence (with proper setting of the parameter "Lines per shot").

2

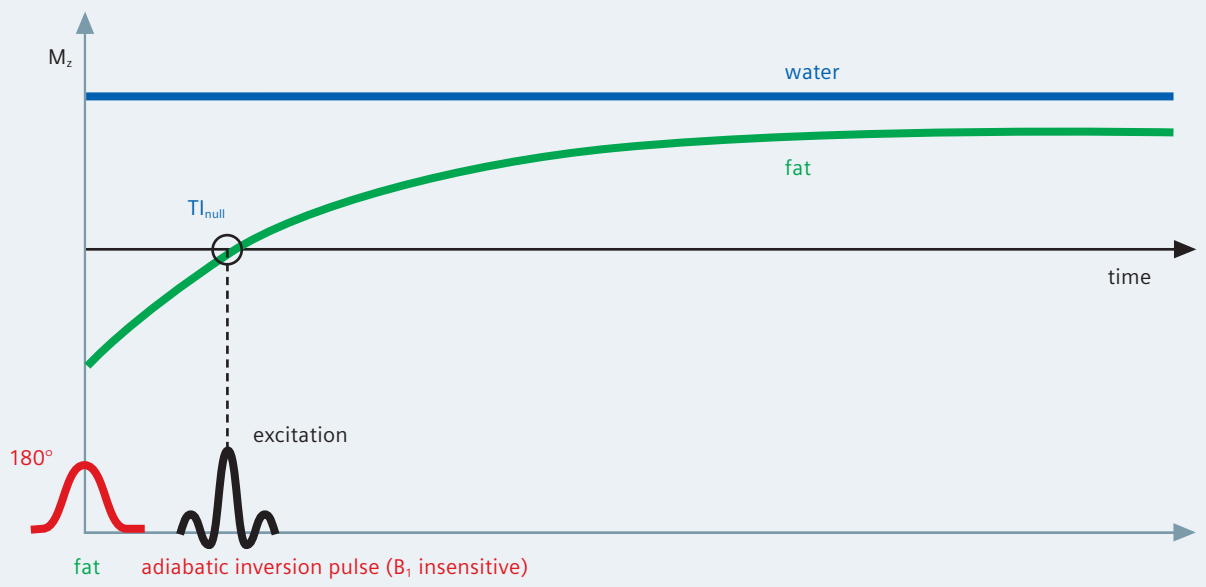

2 Spectrally Adiabatic Inversion Recovery (SPAIR).

3

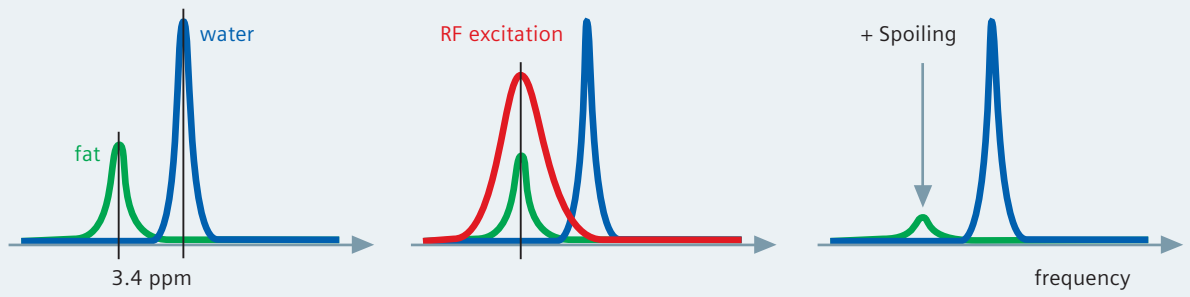

3 Spectral fat saturation.

Spectral Fat Saturation

This technique is based on the chemical shift (3.4 ppm) i.e. the difference in resonance frequencies between fat- and water-bound protons.
Applying a narrow band frequency selective RF pulse, mainly fat-bound protons are excited. This transversal magnetization is destroyed afterwards by spoiler gradients, thus no fat magnetization is left for imaging.

Setting *Quick FatSat* not every slice excitation is preceded by a preparation pulse, thus:

- a shorter TR possible
- breath-hold examinations possible (e.g. VIBE, recommended 40 lines/shot)

Two *FatSat Mode's (strong/weak)* are available.

Advantages:

- Tissue contrast is not affected.
- Quick FatSat can be applied for increased performance.

Disadvantages:

- Sensitive to B_0 and B_1 inhomogeneities.
- Additional preparation pulse increases minimal TR and total measurement time or reduces maximum number of slices (partially compensated by Quick FatSat).

Applications:

- T2-weighted abdominal applications with Fat Saturation based on the sequences TSE, HASTE and SPACE.
- Fast T1-weighted applications in breath-hold with Quick FatSat based on the sequences FLASH-2D and VIBE.

Water Excitation

This technique is based on the chemical shift i.e. the difference in resonance frequencies between fat- and water-bound protons.
No additional preparation pulse is necessary, instead a special excitation pulse (binomial pulse) is used with the spectral excitation profile as shown below (minimum excitation of fat bound protons, maximum excitation of water-bound protons):

Advantages:

- Insensitive B_1 inhomogeneities.

Disadvantages:

- Increased min TE, TR and total measurement time or reduced maximum number of slices.

Applications:

- Frequently used on low field systems where spectral fat suppression is inapplicable.
- Axial TurboFLASH applications with breath-hold or PACE (**P**rospective **A**cquisition **C**orr**E**ction) free breathing.
- *syngo* REVEAL applications in breath-hold technique.

4

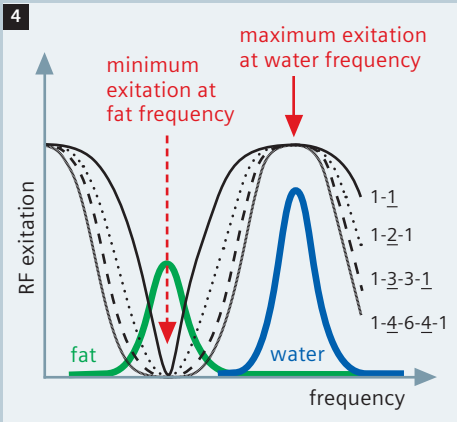

4 Water Excitation.

Dixon Technique

The Dixon technique is based on the chemical shift i.e. the difference in resonance frequencies between fat- and water-bound protons. With this technique two images are acquired. In the first image the signal from fat-protons and from water-protons are "in phase", in the second they are "opposed phase". By additional computations a separate fat- and water-image can be calculated. The Dixon method is integrated into the VIBE sequence.

Dixon delivers up to 4 contrasts in one measurement: in-phase, opposed-phase, water and fat images.

Advantages:

- Insensitive to B_0 and B_1 inhomogeneities.
- 4 contrasts delivered in one measurement.

Disadvantages:

- Increases minimal TR because in- and opposed phase data must be acquired (partially compensated by using integrated Parallel Acquisition Techniques (iPAT)).

Applications:

- Robust fat / water imaging in abdominal applications.
- Fat quantification measurements.

5A

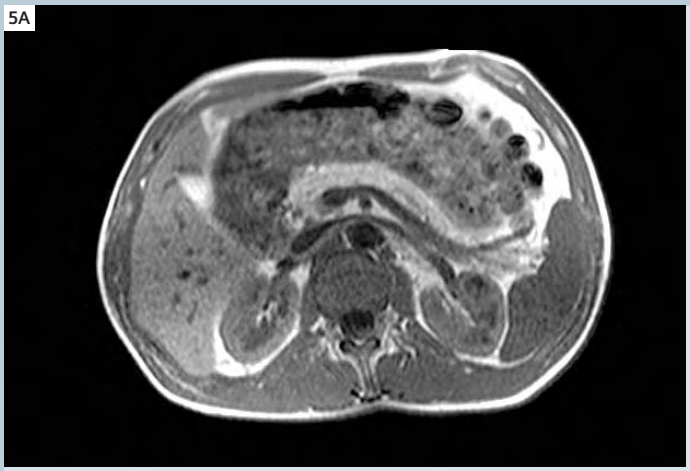

5A In-phase image.

5B

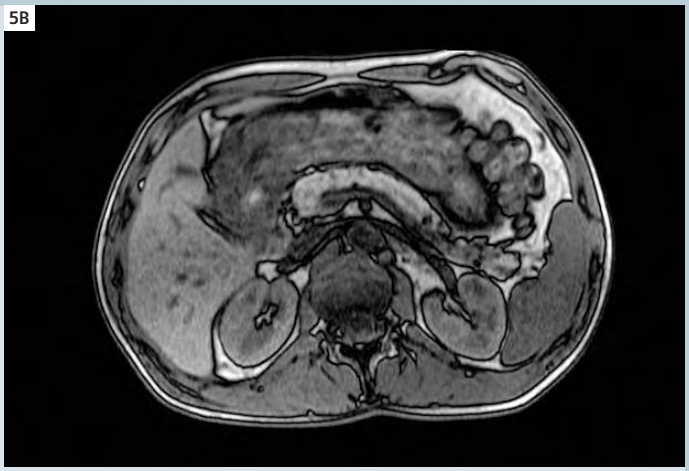

5B Opposed-phase image.

5C

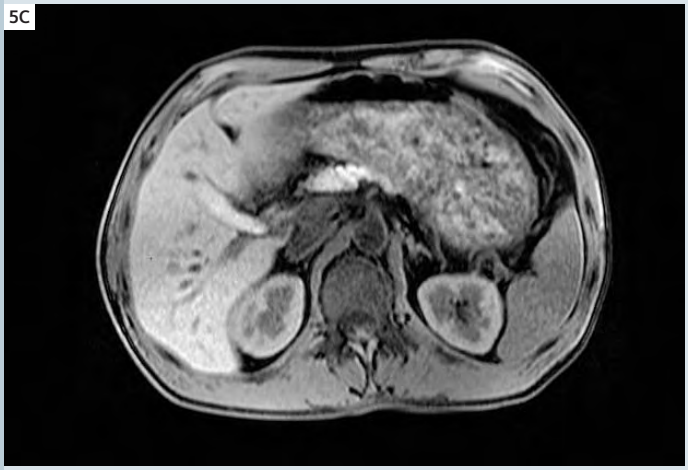

5C Water image.

5D

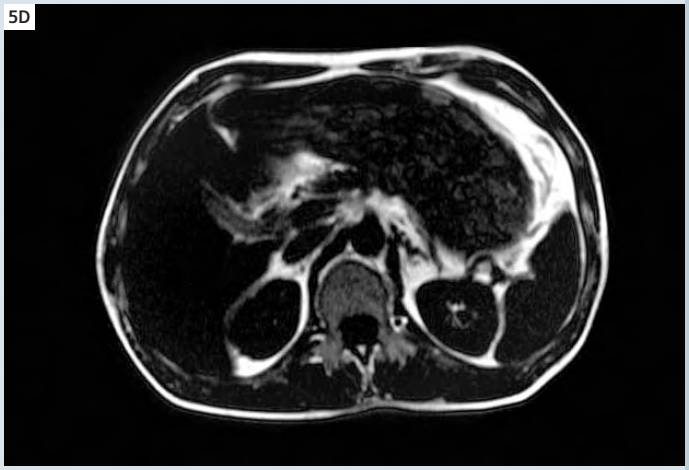

5D Fat image.

STIR-Example

6 STIR PACE free breathing.

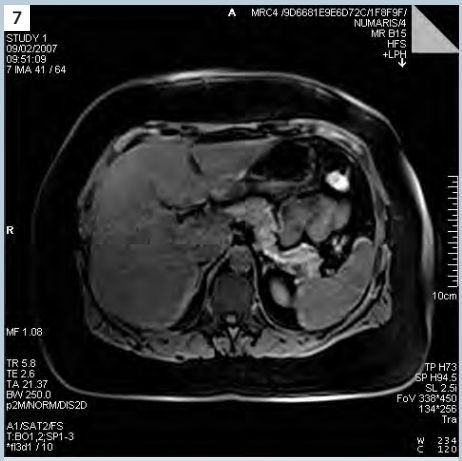

7 T1-weigthed VIBE
Quick FatSat with breathhold.

Water Exitation Examples

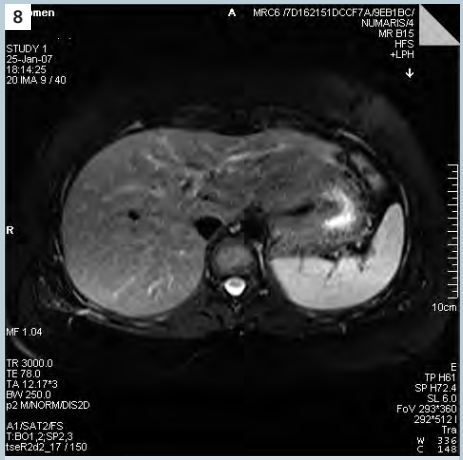

8 T2-weighted TSE SPAIR
with multi-breathhold.

9 T1-weighted VIBE SPAIR breathhold.

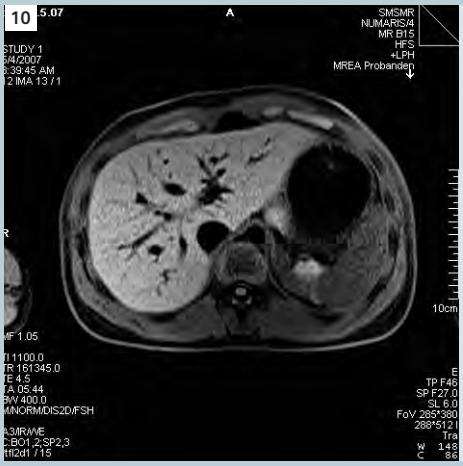

10 T1-weighted TurboFLASH
with Water Excitation
and PACE free breathing.

Overview: Sequences used in abdominal imaging with recommended fat/water selective techniques

	FatSat		SPAIR		STIR	Water Exitation	Dixon
	std	**Mode: strong/weak**	**std**	**Mode: weak/strong**			
TSE/SE	✓	✓	✓	✓	✓	–	–
HASTE	✓	✓	✓	✓	✓	–	–
SPACE	✓	✓	✓	✓	✓	–	–
FLASH-2D	✓ *	✓ **	–	–	–	–	–
VIBE	✓ ***	–	✓ ****	–	–	✓	✓
Reveal	✓	–	✓	–	✓	✓	–
TurboFLASH	–	–	–	–	–	✓	–
TrueFISP	✓	–	–	–	–	✓	

*both FatSat and Quick FatSat available, **only with Quick FatSat, ***with Quick FatSat "Lines per shot" are selectable, **** "Lines per shot" are selectable

Overview: Advantages / Disadvantages of different Fat Suppression techniques

	FatSat	SPAIR	STIR	Water Exitation	Dixon
Insensitive to B_1 inhomogeneities	✓	✓	–	✓	✓
Insensitive to B_0 inhomogeneities	✓	–	✓	–	✓
High performance (quick mode)	✓	✓	–	–	–
Multiple contrasts generated	–	–	–	–	✓
Timing changes	TR, TA	TR, TA	TR, TA	TE, TR	TR
Contrast not affected	✓	✓	✓	✓	✓

70 cm Bore in Clinical Practice: Why It Works

Anne Sheehan, Marketing Manager MAGNETOM Espree

Siemens Medical Solutions, Inc., Malvern, USA

The first MAGNETOM Espree Open Bore system was installed at the Mayo Clinic in Jacksonville, Florida, USA in August 2004.

Patients accept Open Bore

Mayo Clinic presented a poster at the 2005 RSNA Scientific session: "Open-Bore MRI: Patient Acceptance and Image Quality", in which they surveyed patients on their experience with the 70 cm bore. Over 70% of patients previously scanned on a vertical field open found it more comfortable, while 27% found it equivalent. Over 90% indicated that they would agree to another scan on the Espree. Jeffrey Towers, MD of University of Pittsburgh Medical Center (UPMC) presented additional data to support patient tolerance of the open bore at the 2006 MAGNETOM World Summit in San Diego. St. Margaret's (one of multiple Esprees installed in the UPMC network) previously scheduled 4 sedations per week (on two traditional bore MRIs), each sedation requiring 5 hours of personnel time (scheduling, same day admission, nursing, radiologist, and anesthesia standby). Scan time took 1 ½ hours – but had a failure rate of 30%. After installing the MAGNETOM Espree next to the traditional bore systems, patients were redirected to the open bore system. St. Margaret's was able to eliminate outpatient IV sedations, and schedule claustrophobics on arrival. Tim Gutsie, R.T., Manager of Hazelton Radiology Associates in Hazelton, PA, USA replaced a traditional 60 cm bore magnet with the Open Bore Espree and reduced patient rejections from 5 per week to only 1, which results in over $75,000 in revenue gains per year.

Obesity epidemic requires Open Bore + Tim technology

Historically, larger patients that could not fit into traditional 60 cm bores were directed to vertical field open systems. However, these systems still underserved obese patients in four ways.
Firstly, it is already challenging to obtain sufficient signal-to-noise (SNR) when imaging obese patients and to achieve an image quality equivalent to that in thinner patients. Since the vast majority of tradi-

1

"Compared to your scan on vertical field open, the Espree was ..."

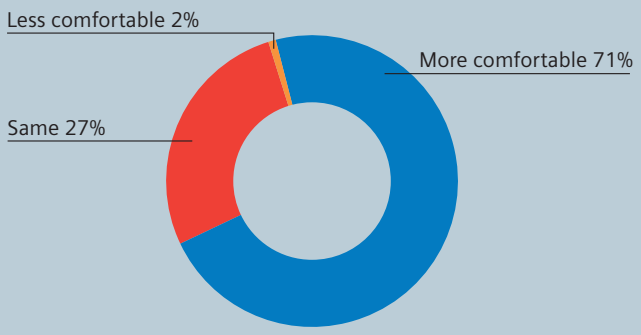

*RSNA Scientific poster presentation at the 2005 RSNA "Open-Bore" MRI Patient Acceptance and Image Quality courtesy Mayo Clinic Jacksonville

1 MAGNETOM Espree's proven patient acceptance. 71% of patients found their experience with the 70 cm bore more comfortable than a previous scan on a vertical field open system.

2

"Would you have another scan on the Espree?"

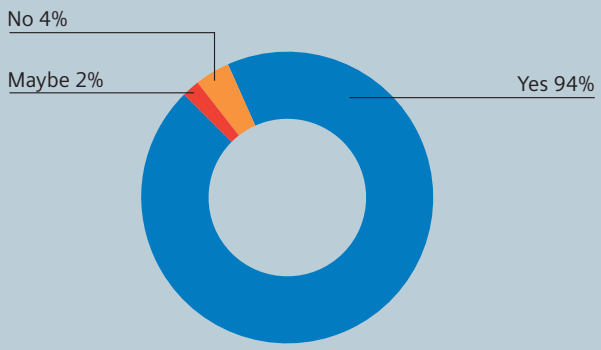

*RSNA Scientific poster presentation at the 2005 RSNA "Open-Bore" MRI Patient Acceptance and Image Quality courtesy Mayo Clinic Jacksonville

2 Over 90% of patients indicated that they would agree to another scan on the MAGNETOM Espree.

3

3 MAGNETOM Espree at the University of Pittsburgh, PA, USA.

tional opens were 0.2–0.3 Tesla, MR images of obese patients were further signal-starved. Their routine scan times simply needed to be lengthened.
Secondly, the vertical gap on many opens is below 45 cm (with patient table), which precludes access for certain large patients.
Thirdly, diseases associated with obesity (peripheral vasculature disease, cardiac disease, liver and pancreatic disease) are typically imaged with high performance sequences at high resolution.
Lastly, the coils that are both used to image obese patients on low field vertical magnets are both difficult to position and difficult to optimize for patients of different body habitus, once again limiting SNR which is so necessary to do good quality exams for these patients.
The MAGNETOM Espree delivered improvements to all four areas mentioned above. The 1.5 Tesla field strength gave a boost of up to four times the SNR over traditional vertical field opens. The distance from table top to magnet cover (55 cm) was also greater than all vertical field opens on the market – to accommodate even larger patients. The Espree now offered the obese patients access to more high field applications: diffusion, pMRA, cardiac and abdominal studies (Figs. 4–6).
Tim Matrix coil technology not only made patient positioning easier, but also offered creative solutions to those patients who could not fit into rigid coils. For instance, the Body Matrix coil can be draped over the largest knees (Figs. 7A, B). Elements are then selected from both the Spine and Body Matrix coils to create a bariatric knee coil, producing high image quality.

4

4 MAGNETOM Espree, 240 kg (530 lb) uncooperative patient. *syngo* BLADE (T2-weighted). Visualizes pituitary mass that was obscured by motion in the original scan.

Courtesy of Mayo Clinic, Jacksonville, Florida, USA.

5

5 MAGNETOM Espree, 250 kg (550 lbs) patient with acute panniculitis, unable to be scanned in any other MR system. Coronal and sagittal images were obtained (1.5 s per slice). Scan confirmed there was no abscess, avoiding surgery for the patient.

Courtesy of Laurel Highlands Advanced MRI, Johnstown, PA, USA.

6

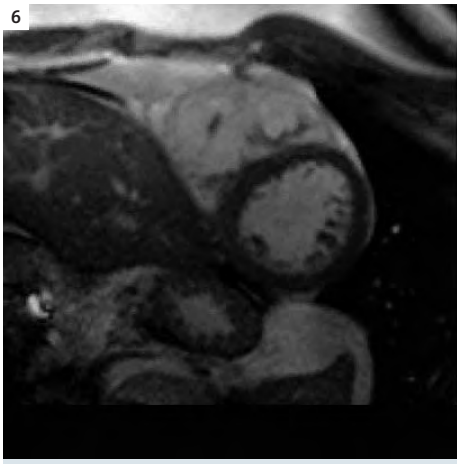

6 MAGNETOM Espree, 198 kg (438 lbs) cardiac patient.

Courtesy of Suburban Hospital, NIH, Bethesda, MD, USA.

7A

7A MAGNETOM Espree, build your own coil with Tim: Body Matrix coil + Spine Matrix coil.

7B

7B Tim technology offers unique benefits in imaging of larger patients, the Tim Body Matrix coil can, for example, be draped over the largest knees: 167 m (5'5"), 204 kg (450 lbs) patient.

Open Bore brings benefits beyond obesity and claustrophobia
As more open bore MAGNETOM Espree systems were installed, customers found novel ways to use the 70 cm diameter to solve diagnostic challenges.

Positioning on the side: unique to Open Bore
There are various clinical situations that, in order to complete the MR scan, a patient might need to lie on his/her side. But, as most adult patients would not fit in any other magnet lying on their side, this is a relatively new application.

Positioning on the side for respiratory issues
One example was sent in by Stephen Cool R.T. (R) (N) (MR), Technical Director, Oregon Advanced Imaging, Medford, Oregon, USA. A claustrophobic patient with respiratory issues was referred for a lumbar spine exam. He very was very clear: "You need to get me out in 15 minutes!" Advanced Imaging was able to scan the patient on his side, with the Body Matrix coil wrapped around his back (Fig. 8A); This allowed him to breathe comfortably. Using the high SNR and integrated Parallel Acquisition Techniques (iPAT) capabilities of the Tim Matrix coils, the site was able to meet the patient's needs, as well as deliver excellent image quality (Fig. 8B).

Positioning on the side for isocenter imaging
Another example was presented by Robert Prost, Ph.D. of Froedert Memorial Lutheran Hospital, Milwaukee, WI, USA. This patient, also claustrophobic, needed her wrist and digits scanned. Positioning on the side allowed the head of this 1.64 m (5'1") patient to be outside the back of the magnet (Fig. 9), easing her fears, but also delivered the best homogeneity for excellent FatSat and highest SNR for best resolution.

8A Special positioning for special needs. Patient positioned on his side with the Body Matrix coil wrapped around his back.

8B MAGNETOM Espree, PAT 2, 4 mm slices, 28 cm, TA 1:17. Scoliosis, kyphosis.

Image courtesy of Advanced Oregon Imaging, Medford, OR, USA.

9 1.64 m (5'1") tall patient has head out of magnet!

11 MAGNETOM Espree with ancillary equipment.

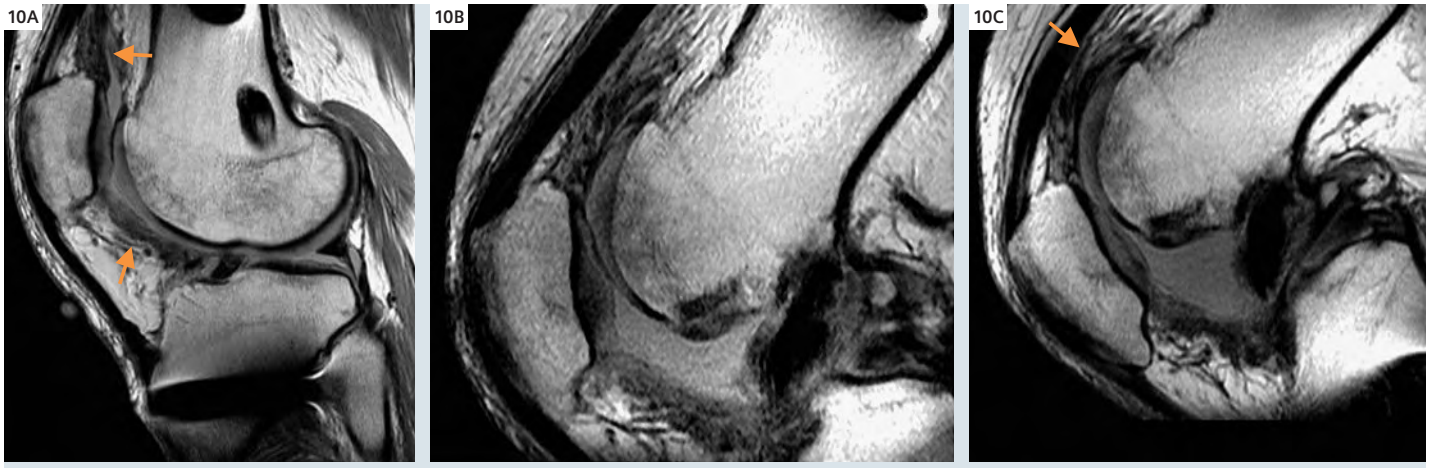

10 MAGNETOM Espree: Knee flexion with Arthrofibrosis. Post op ACL, limited range of motion.

Courtesy of University of Pittsburgh Medical Center, Pittsburgh, PA, USA.

Positioning on the side for knee flexion studies

Dr Towers of University of Pittsburgh Medical Centers has studied the knee in the flexed position in the 70 cm bore. The patient lies on the side, with the affected knee on the Spine Matrix coil. The Body Matrix (or 4-channel flex) coil is draped over the patient, and elements are selected from both to create a "Tim Flexion" coil (Fig. 10).

Room for ancillary support equipment

The 70 cm bore also provides extra room for ancillary equipment – vital for intra-operative installations (Fig. 11).

Get creative with the 70 cm bore!
Mayo Clinic, Rochester, MN, USA discovered a novel way to use the bore: the "recliner".
The "recliner", uses the standard system cushions to prop the patient up in the 70 cm bore. The Body Matrix or Neck Matrix coil is placed between the patient and the cushion, and images are scanned in this semi recumbent position (Fig. 12). Patients with lower back pain can also lie with knees up during lumbar spine scan, thereby reducing discomfort and maximizing image quality (Fig. 13).

Conclusion

70 cm Open Bore has set a new standard in MRI. 70 cm Open Bore offers high quality, high-field diagnostic scans to patient populations underserved before, increases patient comfort, increases image quality and opens the door to new applications such as kinematic studies and intervention.

12A

12A „Recliner" imaging: Propped up patient in the 70 cm bore.

12B

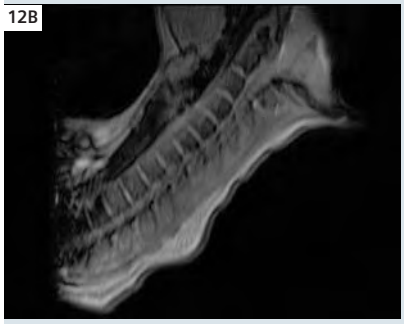

12B Semirecumbent cervical spine.
Courtesy of Mayo Clinic, Rochester, MN, USA.

12C

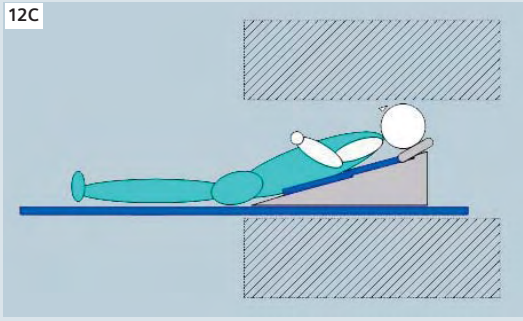

12C Propped up patient in the 70 cm bore.

13

13 Patient with lower back pain in the MAGNETOM Verio's 70 cm Open Bore.

MAGNETOM Verio, delivering the most exciting equation in MRI

Siemens has set a new benchmark in MRI again.
The significance of Open Bore MR in patient care is so great that Siemens applied the innovations necessary to be able to offer 70 cm at two field strengths! By bringing the benefits of Open Bore to 3T, Siemens has set a new benchmark in MRI.
3T field strength + 70 cm Open Bore + Tim (Total imaging matrix) together in one powerful system, MAGNETOM Verio. With the first Open Bore system introduced in 2004, at 1.5T it is only appropriate that Siemens innovations make it possible at 3T. Regardless of the clinical demand of 1.5T or 3.0T now 70 cm is available and can serve patients:

More space puts your patients at ease
- Limit claustrophobic rejections.
- Sedate fewer patients.
- Capture sharper images due to less anxiety-related movement.

Accommodate patients with special needs and conditions
- Pain and mobility issues.
- Respiratory problems.
- Kyphosis.

Expand your care to a wider range of patients
- Obese population.
- Claustrophobic patients.
- Pediatric and elderly patients.
- ICU patients or those dependent upon medical equipment.

Broaden your clinical possibilities
- Easy access in interventional MRI.
- Opportunities to perform more kinematic studies.

Chronology of the Open-Bore MR systems

1983: In the beginning
At the commercial introduction of MR systems in the early nineteen-eighties, there was a wide variety of magnets available: permanent, resistive or superconducting designs. By 1984 field strengths choices ranged from 0.2 to 1.5 Tesla. All MR systems were relatively large and "boxy". By 1988 1.5 Tesla machines had established market dominance with 45% of sales.

1988: Paradigm shift
During this decade, the MR referral mix evolved from patients with life altering neuro-based diseases (brain tumors, multiple sclerosis, disk herniations, etc.) to orthopedic injuries (meniscal, cartilage and ligament injuries of the knee, shoulder, wrist and ankle).

1990s: Comfort is king
By 1993, the market began to recognize the need for patient cooperation. Vertical field open systems not only appealed to patient comfort, but also the burgeoning referrals for obese patients who could not be scanned in traditional 60 cm horizontal bore magnets.
The market share of vertical field open MR systems (typically 0.2 – 0.35 Tesla) rose dramatically from 15% in 1993 to 43% in 1997, surpassing even 1.5 Tesla systems, which represented only 33% during that year.

1999: Return of high field
But even as vertical field open magnet sales surged, MR applications at high field were making strides. MR Angiography (MRA) was being performed throughout the body to visualize pathology formally diagnosed only by digital angiography. Early changes in brain anatomy brought on by stroke could now be visualized in seconds by Diffusion techniques. Breast MR was starting to be recognized as a tool that could provide valuable diagnostic information. New strategies to diminish or avoid motion artifacts (breath-holding, 2D PACE) allowed 1.5 Tesla systems to better handle abdominal studies.
In 1997 the 1.5 Tesla MAGNETOM Symphony was introduced. Not only did the Symphony provide access to high end applications, but its compact design was a departure from the former "boxy" high field designs, making it more patient friendly. The new Integrated Panoramic Array (IPA) design also addressed an area all but ignored by most MR manufacturers: streamlining patient handling by minimizing coil changes.
By 1999, the market had once again reversed: 1.5 Tesla sales now passed vertical field open sales.

2000: "Higher-field" opens
The market wanted the best of both worlds: the comfortable environment associated with vertical field opens and 1.5 Tesla applications, image quality and throughput. A higher field vertical open seemed to be the answer, and several 0.7 Tesla products hit the market between the years 2000 – 2001.

2004: Open Bore concept: CT-like comfort, advanced applications
Siemens delivered the first 1 Tesla vertical field open, the MAGNETOM Rhapsody. But despite the acceptance of these systems by the first installations, there were several inherent limitations associated with any 1 Tesla vertical field open. Firstly, the 1 Tesla market had diminished to less than 5% of new sales – 1.5T was the standard and preferred field strength worldwide. Secondly, project costs (equipment + siting) would exceed that of horizontal bore 1.5T systems. Thirdly, the new Tim (Total imaging matrix) technology, introduced in 2003 on the MAGNETOM Avanto, would not be able to be implemented.
Computed Tomography (CT) systems with 70 cm bores never experienced the same wave of patient discomfort or inability to accommodate larger patients that MR did. It stood to reason that if Siemens could design a horizontal bore 1.5 Tesla MR that more closely resembled a CT, then patients would accept and fit into it. Additionally the boost in signal-to-noise would also better serve the obese patient by providing better image quality, reduced exam times and more advanced applications than low field, vertical opens. Tim technology could be implemented in a horizontal bore design. Enter a new concept: the Open Bore MR.

2005 – 2007 Open Bore proof of concept
The Open Bore design incorporated CT's 70 cm bore diameter with a magnet length of 125 cm – only a piece of paper longer than a CT system. When scanned feet first, the patient's head would remain outside of the magnet for a majority of scans (lumbar spine to ankles). The 70 cm bore also provided a foot (30 cm) of space above the patient's face – about twice that of vertical field opens.

Listen – Discuss – Share
6th MAGNETOM World Summit

May 29 – June 1, 2008 in Munich, Germany

We invite you to join our community of Siemens MR users worldwide to the 6th MAGNETOM World Summit in Munich, Germany.
The positive feedback from 5 previous events is proof that the meeting is an ideal opportunity to meet other members of the MAGNETOM World, to develop contacts and to exchange valuable information.

You can attend a wide spectrum of presentations to help keep you on the edge of new trends in MR.

- Hear about best practices and clinical trends from the world's leading experts
- Learn advanced techniques and innovative solutions
- Exchange ideas and knowledge with other MAGNETOM users

The MAGNETOM World Summit will take place at the Sofitel Hotel Bayerpost, right next to the central railway station in the middle of Munich.
Even though Munich, the capital city of Bavaria, is Germany's third largest city, it is called *"Weltstadt mit Herz"* (metropolis with a heart). Located on the river Isar north of the Alps it is right in the middle of some of the most beautiful scenery in Europe. The city features beautiful architecture and a cultural scene that is second to none. World famous however, is its annual Oktoberfest, *d'Wiesn* as the locals call it.
Munic is home to everything quintessentially Bavarian. Besides its breweries it is well-known for *Weißwurst*, a breakfast sausage, *Schweinsbraten mit Knödeln und Kraut* (roased pork with dumplings and cabbage) or *Leberkässemmeln* (an untranslatable specialty you will have to try.) These delicacies are often served in the beergardens. During the evening events we will present to you the traditional Munich as well as the modern city that is celebrating its 850th birthday this year.

We look forward to seeing you there!

For more information and to register, please visit

www.siemens.com/magnetom-world

Munich, Germany

The 6th MAGNETOM World Summit is sponsored in part by Bayer Schering Pharma AG, Berlin, Germany and by IMRIS, Manitoba, Canada.

Bayer HealthCare
Bayer Schering Pharma

IMRIS

Tim Proves to be a Total Improvement

J. Dehem, M.D.

Jan Yperman Ziekenhuis, Ieper, Belgium

The first impressions of my Tim (Total imaging matrix) upgrade: What is most significant to me is the overall improvement in image quality, especially the dramatic gain in signal intensity and homogeneity. The following side-by-side comparisons of routine cases – scanned before and after the Tim upgrade – demonstrate this striking enhancement in image quality.

The MAGNETOM Symphony, A Tim System comes with new coils. The CP Head, CP Neck Array, CP Spine Array and CP Body Array coils are exchanged for Matrix coils, each one containing multiple "clusters" of 3 coil elements which yield more signal. The advantages of the new coils are shown in a side-by-side comparison of the same volunteer with the CP Head coil on the MAGNETOM Symphony and the Head Matrix coil on the MAGNETOM Symphony, A Tim System. Additionally, if you combine the signal and quality gain from the RF system with the signal and quality gain of the new coils, you get even more improvement.

MAGNETOM Symphony, A Tim System

Several coil plugs on the patient table with the Tim system allow the combination of multiple coils. These coil combinations are indeed 'seamless' and offer major advantages in orthopedic, breast and angiographic imaging. Especially the light weight and flexibility of the Body Matrix coil is highly appreciated by both the patients and technologists.

Multiple coil combinations allow for extensive use of parallel imaging. Since the patient is covered by multiple coil elements, iPAT (integrated Parallel Acquisition Technique) is used in all 3 directions. And in 3D imaging the combination of iPAT in both the phase and slice directions is possible (iPAT²). The extensive use of higher PAT factors (PAT 3), combined with iPAT² imaging (PAT 2 x PAT 2 = PAT 4), takes advantage of the increased signal to scan faster with equal or even better image quality, but at shorter scan times.

Prior to the installation of the Tim upgrade we used a (rare) spare moment on the last day of our MAGNETOM Symphony to scan volunteers. After the installation of our new MAGNETOM Symphony, A Tim System (same magnet, same gradients, same volunteer, but new RF system, new Body coil, new computers and software), we repeated for the sake of comparison the same sequences with exactly the same scan parameters (using Phoenix technology).

Again, most striking is the signal gain and the homogeneity of the image, especially when looking at the edges of the images on all sequences.

Below are some of the cases from this before and after comparison. Do I even need to mention that the upper rows of images are from the MAGNETOM Symphony, A Tim System?

Adding light and resolution

Case 1

The Head Matrix coil allows for iPAT, which further reduces the image distortion artifact due to the long EPI-readout. This is demonstrated in the follow-up examination (follow-up carotid aneurysm) of this patient. 3D TOF (Time of Flight) has also markedly improved leading to depiction of smaller branches.

MAGNETOM Symphony, A Tim System

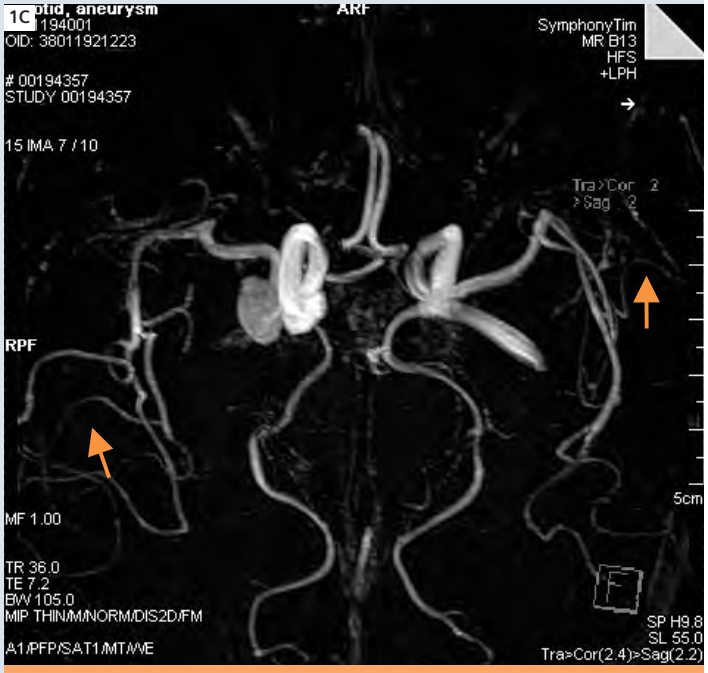

MAGNETOM Symphony, A Tim System

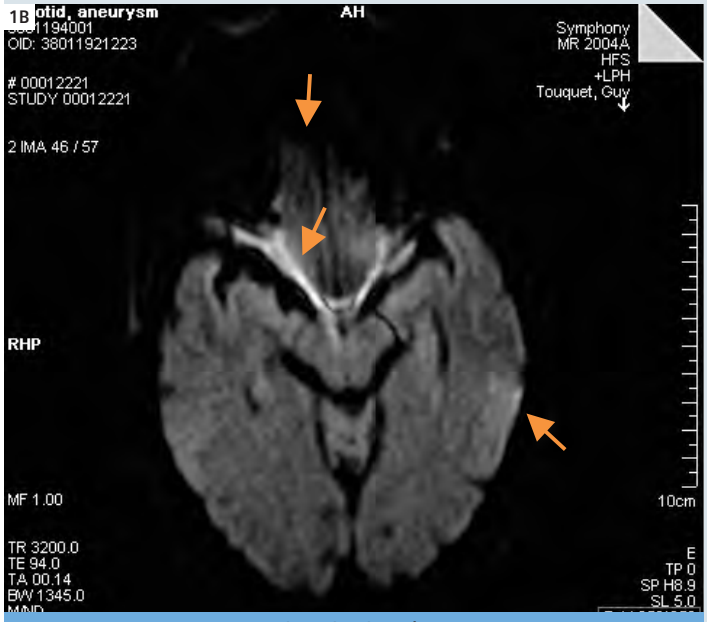

MAGNETOM Symphony

MAGNETOM Symphony

Case 2

In this cirrhotic liver patient we see a boost in image quality in the follow-up examination on the Tim system. In a slightly shorter breathhold time we have thinner slices (4 mm → 2.4 mm) and a nice delineation of e.g. the right adrenal. The shorter breathhold allows the patient to cooperate more. Now we can easily identify 2 HCC lesions on the VIBE arterial phase acquired on the Tim system (upper row of images). In the previous examination, we cannot see the large one as well and, in retrospect, may only suspect the small one.

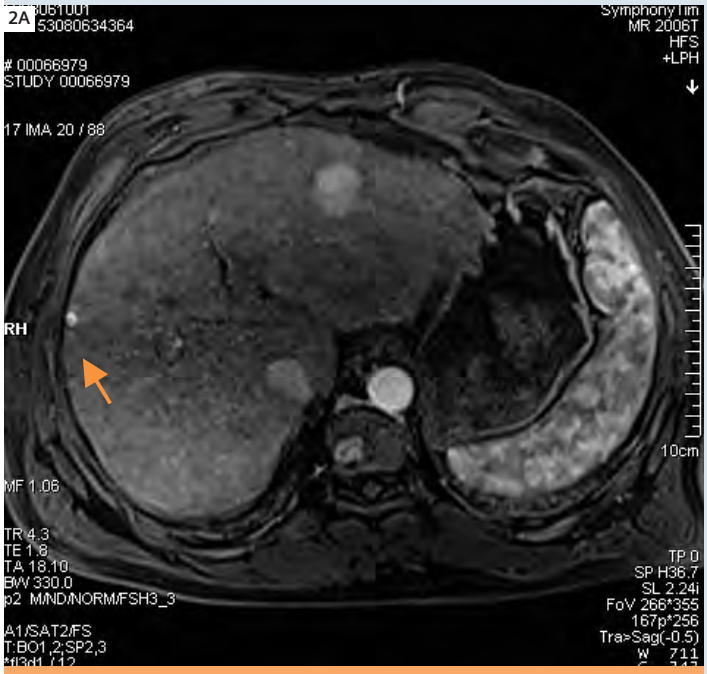

MAGNETOM Symphony, A Tim System

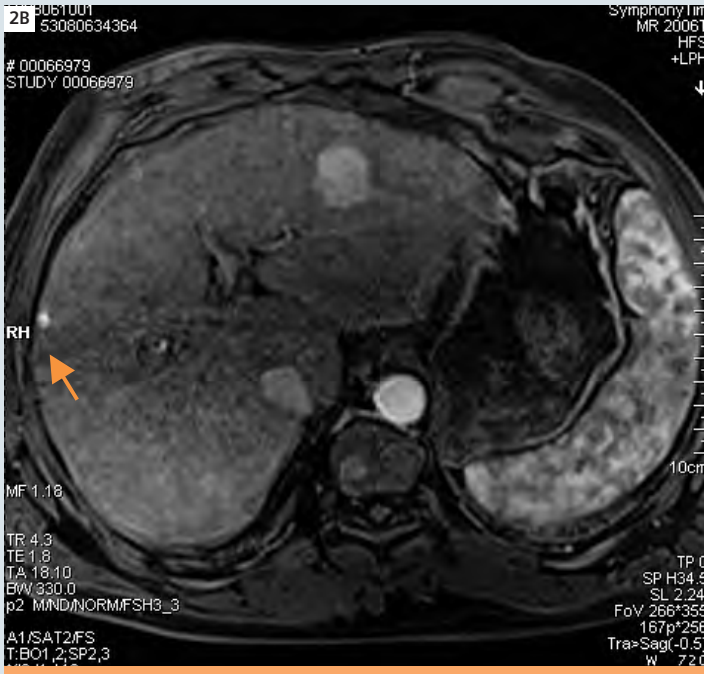

MAGNETOM Symphony, A Tim System

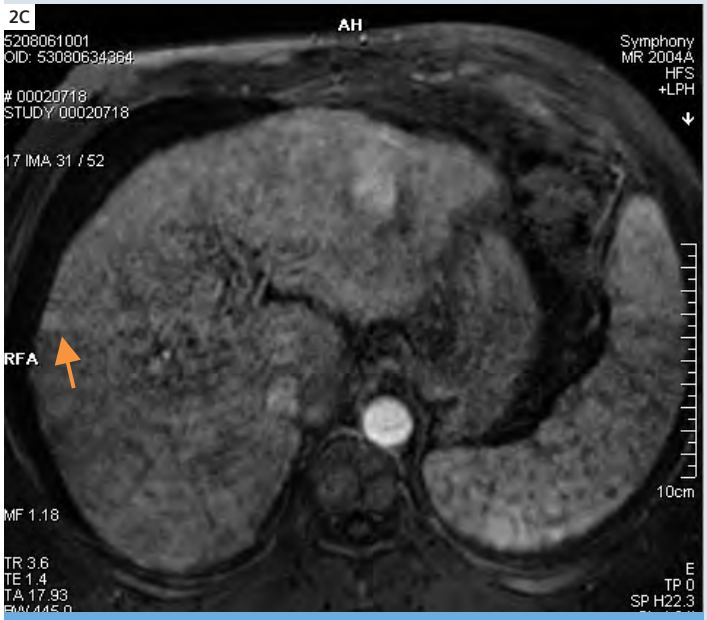

MAGNETOM Symphony

MAGNETOM Symphony

Case 3

The signal gain can be used to significantly (3-fold) speed up acquisition and still enhance image quality.
This case is a follow-up examination for avascular necrosis as a complication of chemotherapy treatment (lymphoma).

The AVN and the sciatic nerve are better delineated.
There is signal in the lower part of the image. And the scan time dropped dramatically from 4.26 → 1.30 min for the same resolution at better signal-to noise ratio (SNR)!

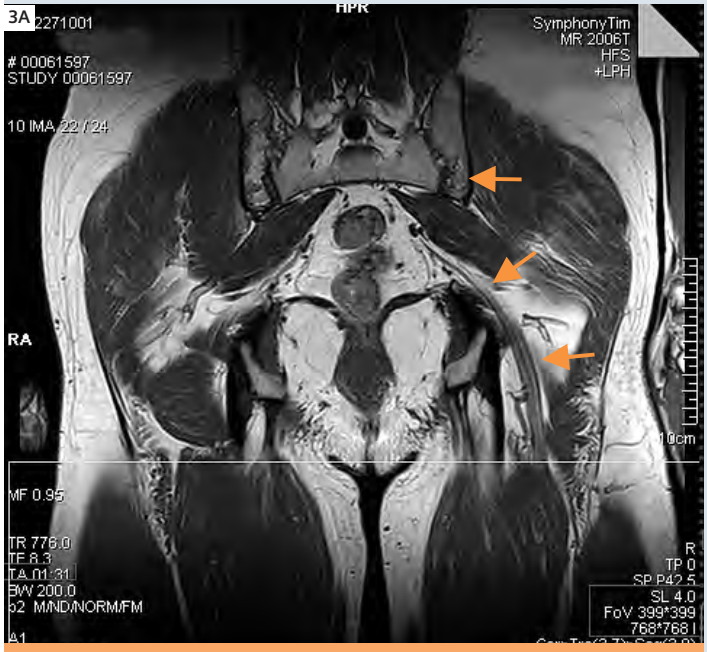

MAGNETOM Symphony, A Tim System

MAGNETOM Symphony, A Tim System

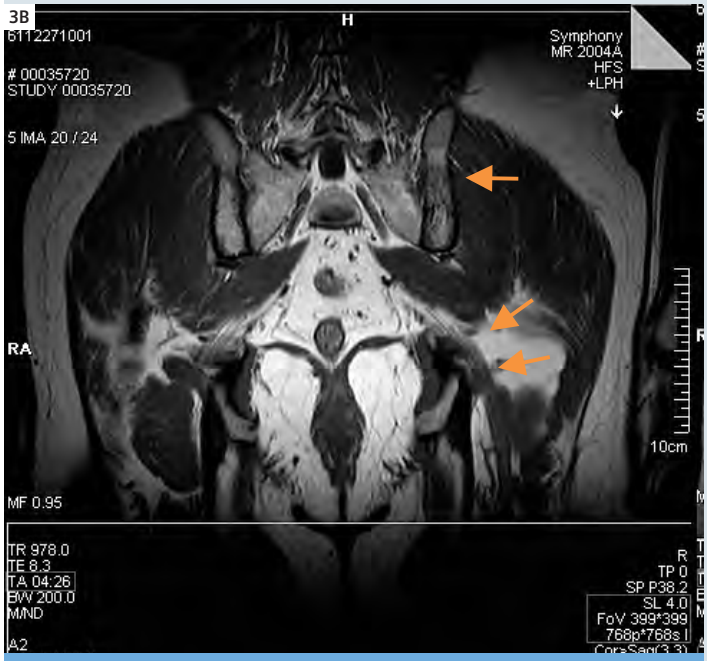

MAGNETOM Symphony

MAGNETOM Symphony

Case 4

A follow-up study of plexus invasion demonstrates the seamless integration of Matrix coils on the MAGNETOM Symphony, A Tim System. Combining posterior elements of the Head Matrix, the upper row of the Spine Matrix and the Neck Matrix coils results in better image quality compared to the MAGENTOM Symphony images. Recurrent breast cancer invades the left brachial plexus.

The same scan settings using a combination of the CP Spine Array and CP Neck Array coils on the MAGNETOM Symphony, and the Head Matrix, Spine Matrix and Neck Matrix coils in the follow-up exam on the MAGNETOM Symphony, A Tim System. Overall there is better SNR and a more homogeneous image. Pay particular attention to the edges of the image: e.g. note much better depiction of AC joints and brain.

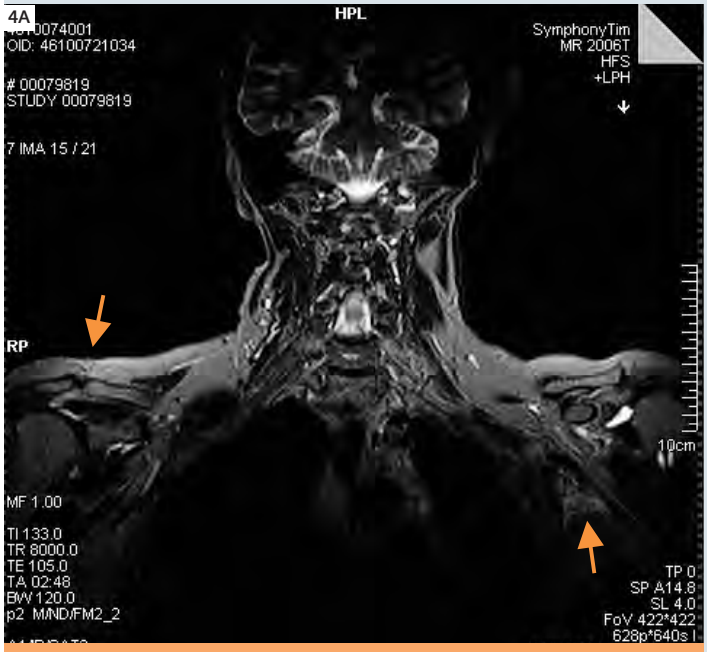

MAGNETOM Symphony, A Tim System

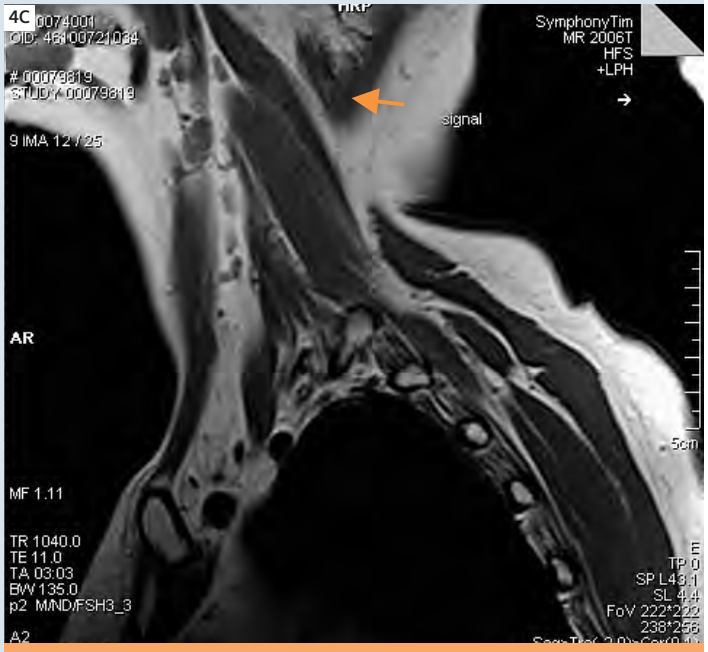

MAGNETOM Symphony, A Tim System

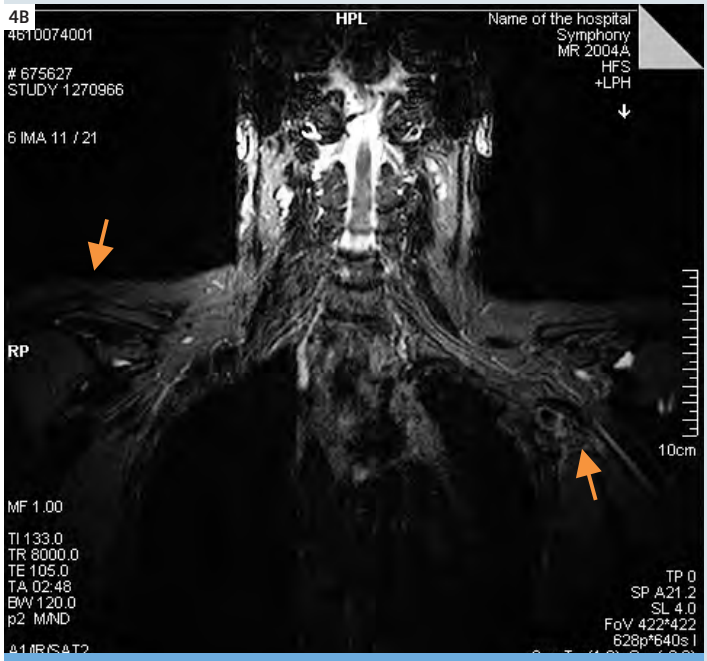

MAGNETOM Symphony

MAGNETOM Symphony

Case 5

Of course it is also possible to set-up alternative and inventive coil combinations. For example, combining the Body Matrix coil with the Breast Matrix coil opens up the axillae. Shown here is a follow-up examination in a patient with multiple benign lesions: The field of view (FoV) has almost doubled and overall homogeneity has improved. There is a better depiction of the focal lesions.

MAGNETOM Symphony, A Tim System

MAGNETOM Symphony, A Tim System

MAGNETOM Symphony

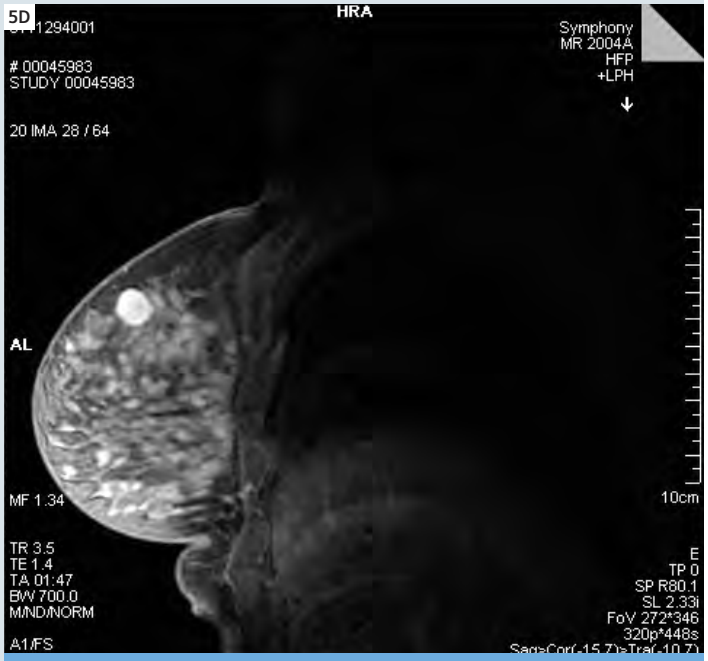

MAGNETOM Symphony

Higher speed and better FoV with MAGNETOM Symphony, A Tim System

Case 6

The more conventional and frequent combination of the Body Matrix coil and the spine coil is shown here in an examination of the thoracic and abdominal region, e.g. dorsal and lumbar spine, where a large FoV is important. This patient was actually sent to us for an examination of the lumbar spine with clinically obvious S1 pathology. The dorsal hernia was rather unexpected. Note the fast scan time of the T2-weighted scan (1:36 s) with high resolution (512 matrix) and a PAT factor of 3.

MAGNETOM Symphony, A Tim System

MAGNETOM Symphony, A Tim System

Case 7

Combining the coils enables iPAT resulting in excellent image quality and fast acquisition times. For example if you want to do an additional coronal series of the sacroiliac joints, it takes only 46 seconds for high resolution thin slices! This middle-aged female repeatedly complained of right-sided lower back pain. MRI of the lumbar spine was uneventful. One coronal series of the sacro-iliac joints and 46 seconds later we have the diagnosis. These are 46 seconds that will change her life!

MAGNETOM Symphony, A Tim System

MAGNETOM Symphony, A Tim System

Case 8

The same holds true for this patient in a follow-up for a benign liver lesion: Axial VIBE and coronal HASTE. Better Fat Saturation results in pencil lined delineation of e.g. the skin, the adrenal gland and the focal fatty liver in segment IV. We used the same in-plane resolution, but reduced slice thickness from 3.3 → 2 mm. Also note excellent homogeneous Fat Sat and sharp delineation of e.g. skin or adrenal gland. Reducing the echo train length (iPAT) reduces the blur in the HASTE images. And slice thickness went down from 7mm → 5 mm.

MAGNETOM Symphony, A Tim System

MAGNETOM Symphony, A Tim System

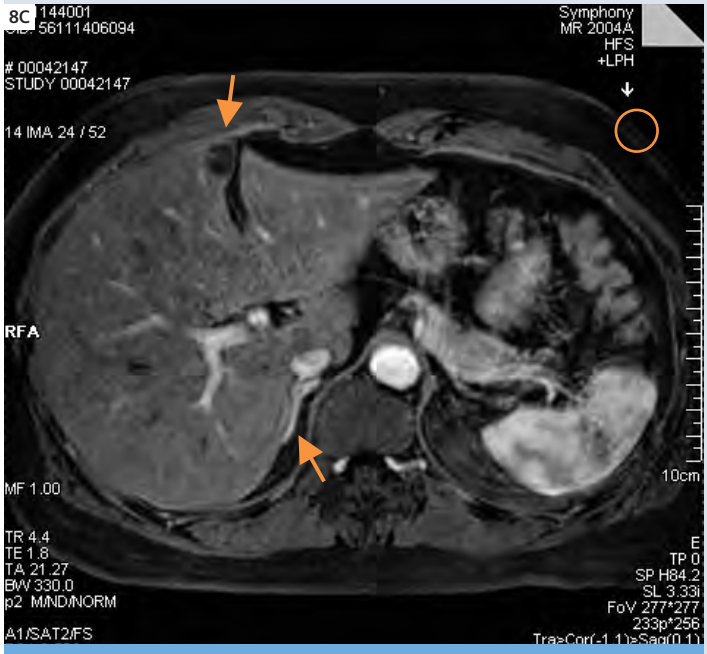

MAGNETOM Symphony

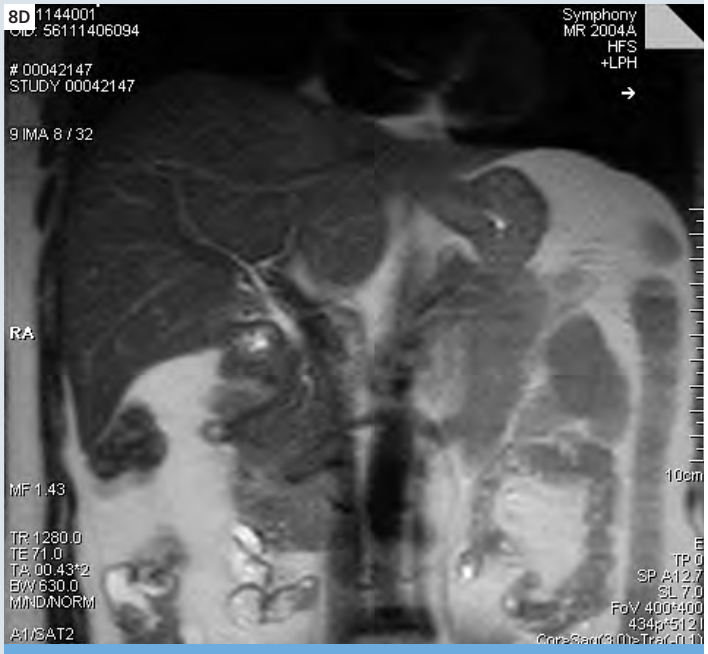

MAGNETOM Symphony

New applications show the power of the new MAGNETOM system

Routine applications improved with our Tim upgrade, and many new ones became possible.

Diffusion-Weighted Imaging (DWI)
DWI proves to be a decisive tool for detection of (recurrent) cholesteatoma with the Single Shot SE DWI revealing the diffusion restriction in a cholesteatoma in contrast to the surrounding inflammation-fibrosis as depicted in this young girl. SE DWI allows a reduction in slice thickness down to 2.5 mm as compared to the 5 mm slice thickness of the EPI DWI. Moreover, SE DWI effectively removes all the susceptibility artifacts that obscure the EPI DWI images in the temporal bone.

MAGNETOM Symphony, A Tim System

MAGNETOM Symphony, A Tim System

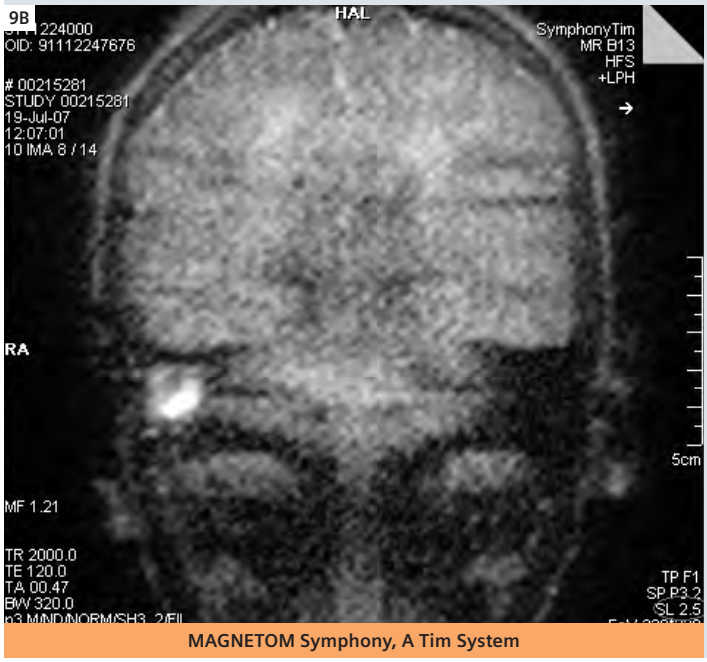

MAGNETOM Symphony, A Tim System

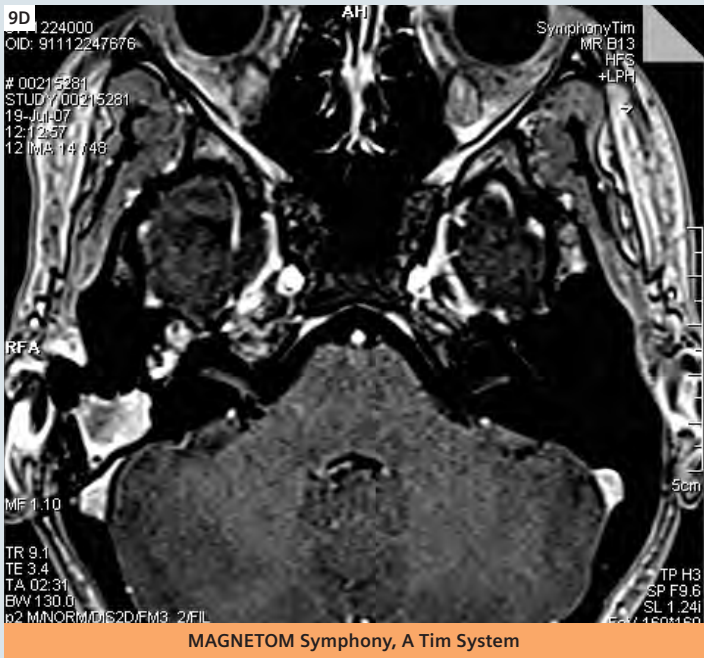

MAGNETOM Symphony, A Tim System

***syngo* SPACE**

This patient has a tumor relapse after a partial liver resection for cholangiocarcinoma. Single shot MRCP (MR Colangiopancreatography) images are not satisfactory due to superposition of ascites.

Triggered 3D SPACE acquisition helps to demonstrate and understand the altered biliary anatomy. Reconstructions on the isotropic dataset eliminate the need for invasive imaging.

MAGNETOM Symphony, A Tim System

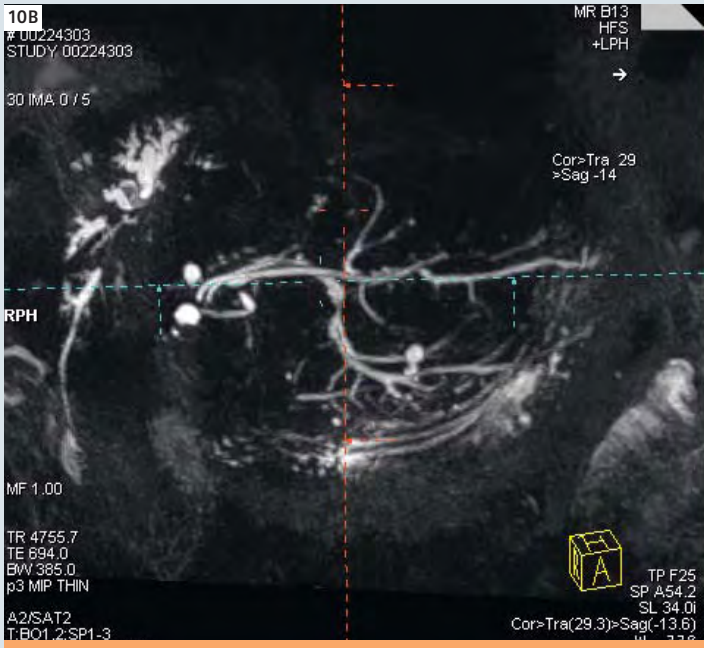

MAGNETOM Symphony, A Tim System

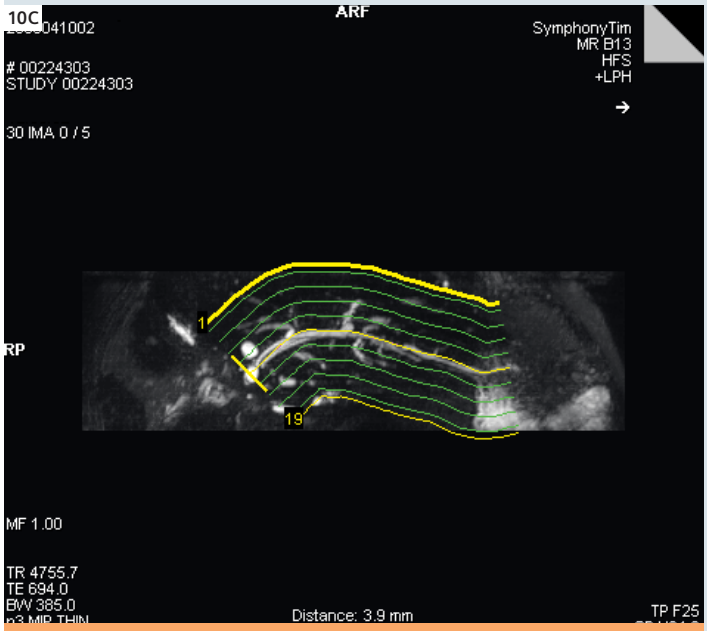

MAGNETOM Symphony, A Tim System

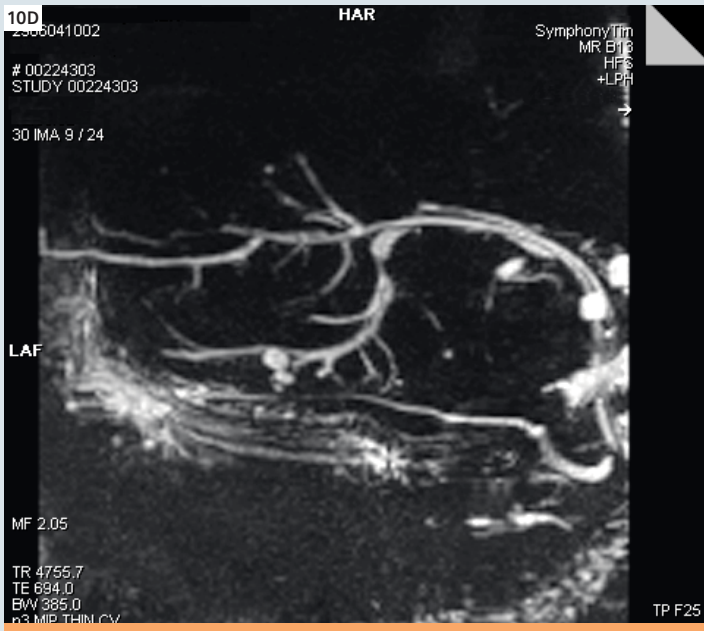

MAGNETOM Symphony, A Tim System

***syngo* Composing**

Separate regions can be composed in a single series of images, e.g. a vascular roadmap for the surgeon or an overview of the total spine for the oncologist.

Vascularly-compromised patient with a history of more than 30 years of vascular interventions (but still smoking) presents with cold leg. History of high amputation on the right side, aorto-femoral graft (> 15 years) and femoro-tibial graft (6 months ago). Cold leg since previous night.

Occluded femoro-tibial bypass directly visible on the MinIP (minimum Intensity Projection) of composed native pre-contrast images.

Occluded left superficial femoral artery on the left side with distal filling in fibular artery is easily depicted on the composed post contrast MIP (Maximum Intensity Projection) image. Occluded proximal anastomosis is also directly visible (stump).

MAGNETOM Symphony, A Tim System

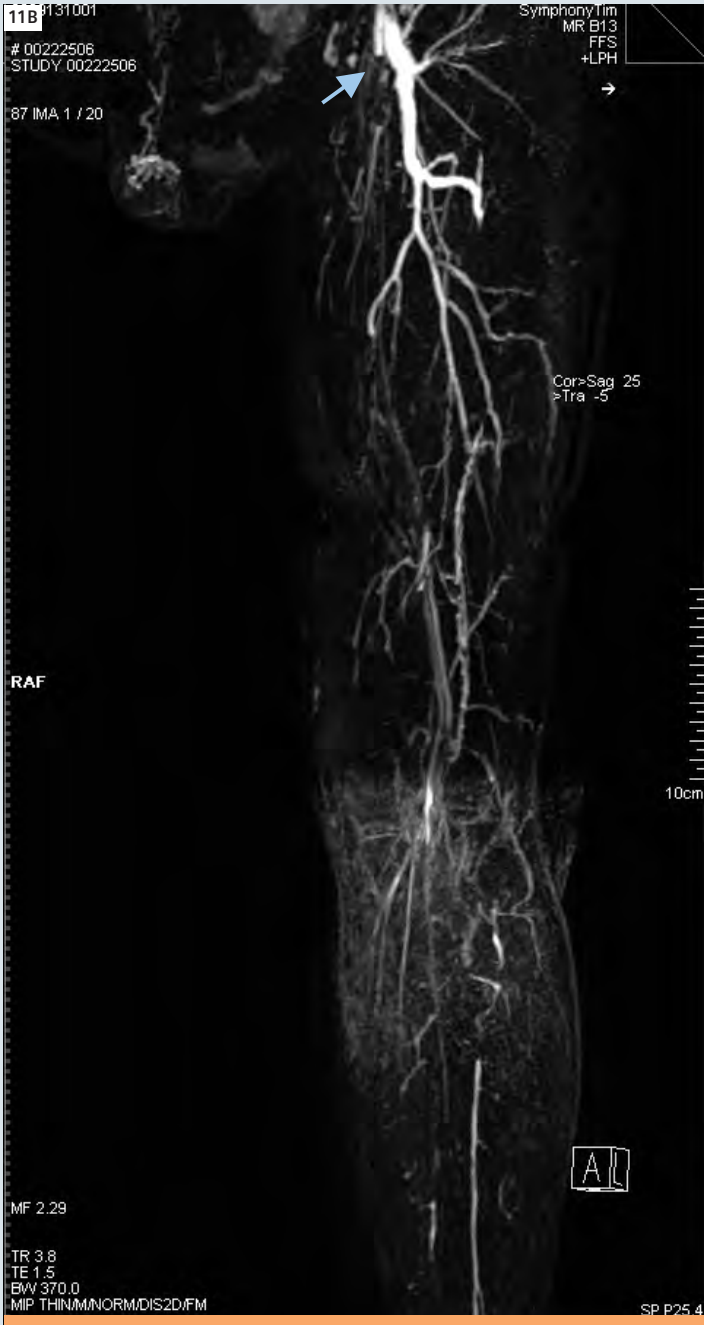

MAGNETOM Symphony, A Tim System

Diagnosis at a glance – and a surgical roadmap for free

MAGNETOM Symphony, A Tim System

MAGNETOM Symphony, A Tim System

***syngo* Perfusion**

The Neuro Suite and the *syngo* Perfusion software* enables intuitive post processing of perfusion datasets as in this case depicting a perfusion/diffusion mismatch.

*Please note that the Neuro Perfusion software is only for tumor evaluation and not for stroke evaluation.

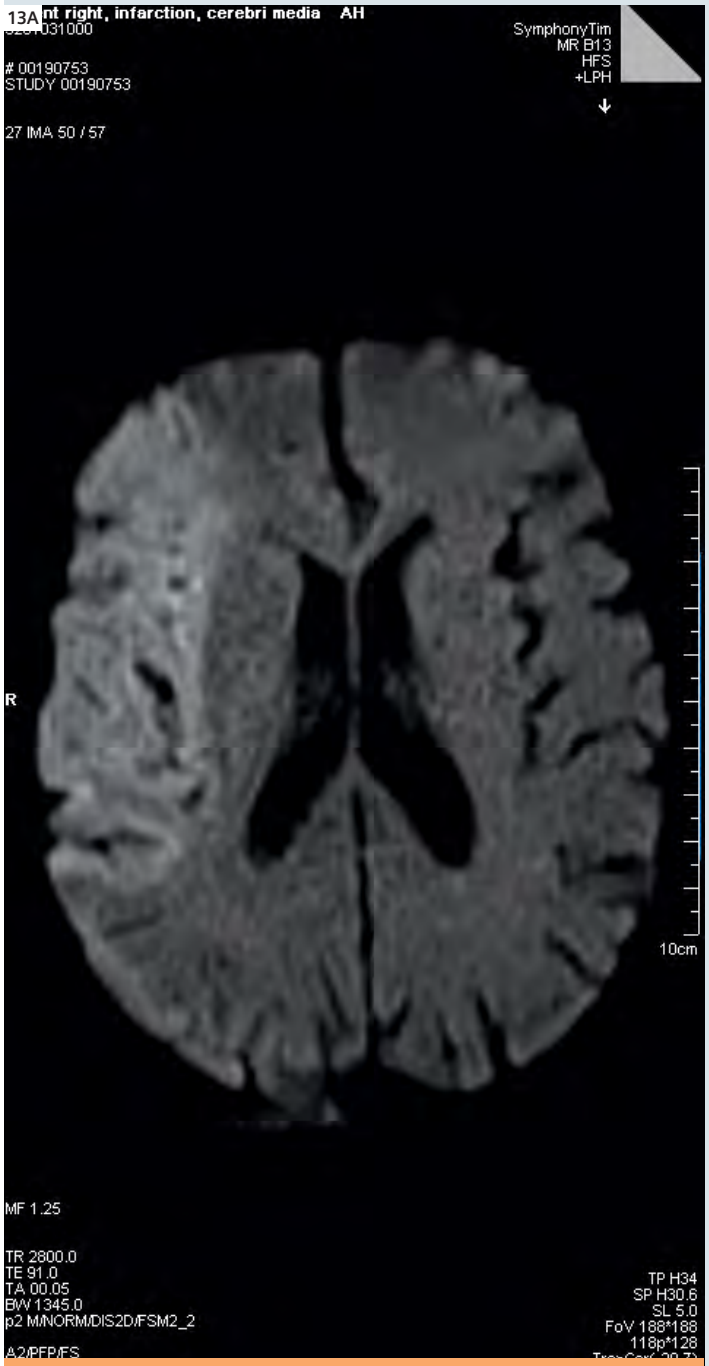

MAGNETOM Symphony, A Tim System

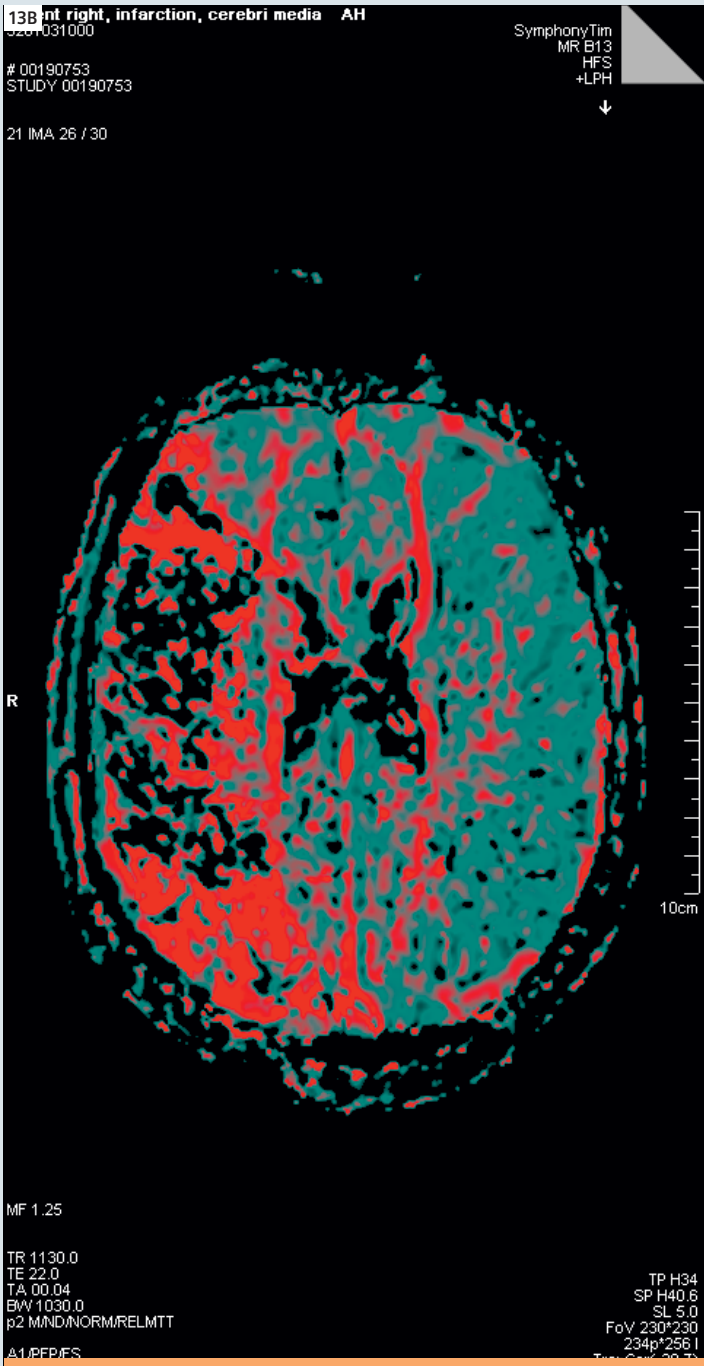

MAGNETOM Symphony, A Tim System

***syngo* TWIST**

Increased speed, up to real time, during angiographic acquisition is possible with *syngo* TWIST. This can be used when you need dynamic information, for example in the evaluation of collateral circulation. Or you can use it to speed up the examination, for example in critical care stroke patients.

For carotid arteries we scan 4 sub-millimeter datasets in 50 seconds. The resulting images have a good resolution and signal as demonstrated in this patient with a critical high grade stenosis on the left internal carotid and a high grade stenosis on the right internal carotid. The patient is less than 5 minutes on table including localisers and planning!

MAGNETOM Symphony, A Tim System

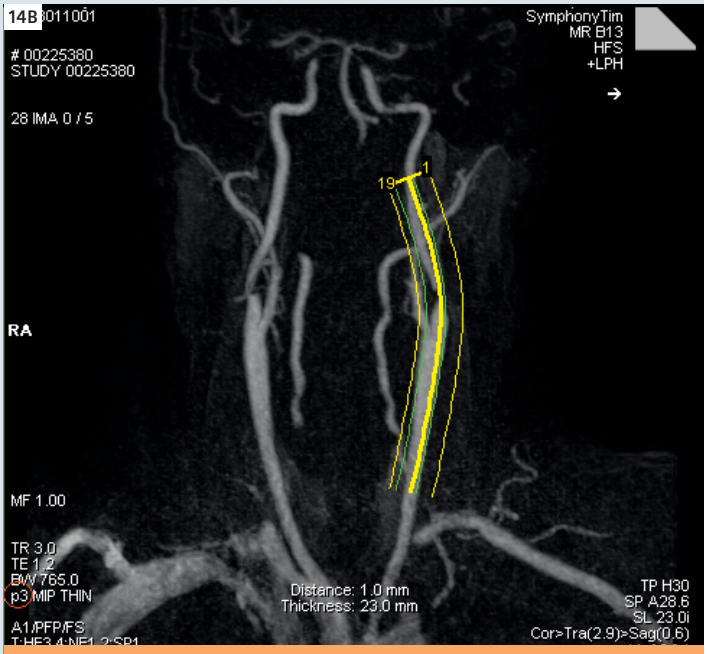

MAGNETOM Symphony, A Tim System

MAGNETOM Symphony, A Tim System

MAGNETOM Symphony, A Tim System

TWIST is also convenient for providing functional anatomy as in this patient, examined for thoracic outlet syndrome in the supine position while performing Addson manoeuver. In high-resolution (1.1 x 1.3 mm) a slice thickness of 8 mm was achieved. You see the contrast arrival, pulmonary phase and early and late arterial phase at a temporal resolution of 3 seconds!

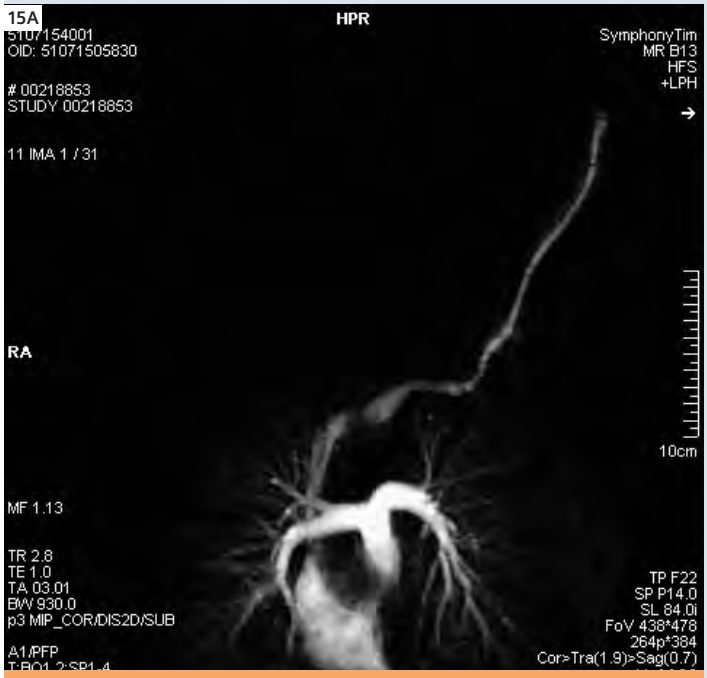

MAGNETOM Symphony, A Tim System

MAGNETOM Symphony, A Tim System

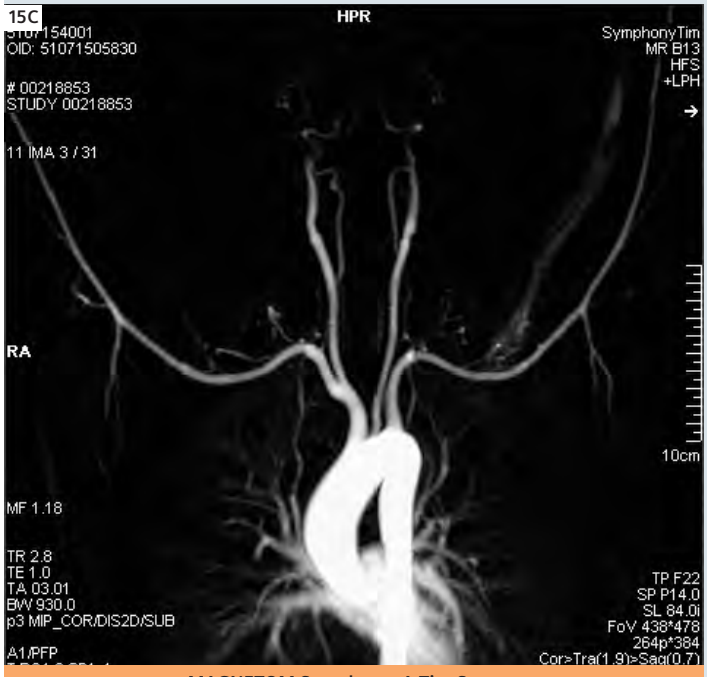

MAGNETOM Symphony, A Tim System

MAGNETOM Symphony, A Tim System

syngo MR B13 brings improved planning software
Iso-positioning and automatic coil selection: The operator simply selects the region of interest and the AutoCoil Select feature guarantees the activation of the appropriate coils. The table automatically moves the center of the region of interest (ROI) to the center of the magnet, thus ensuring the best magnetic field homogeneity.

This becomes even more important since we routinely use large fields of view. In this example you see how we scan an elbow by combining the Spine Matrix and Body Matrix coils. High resolution and high speed, scanned at the isocenter of the magnet!

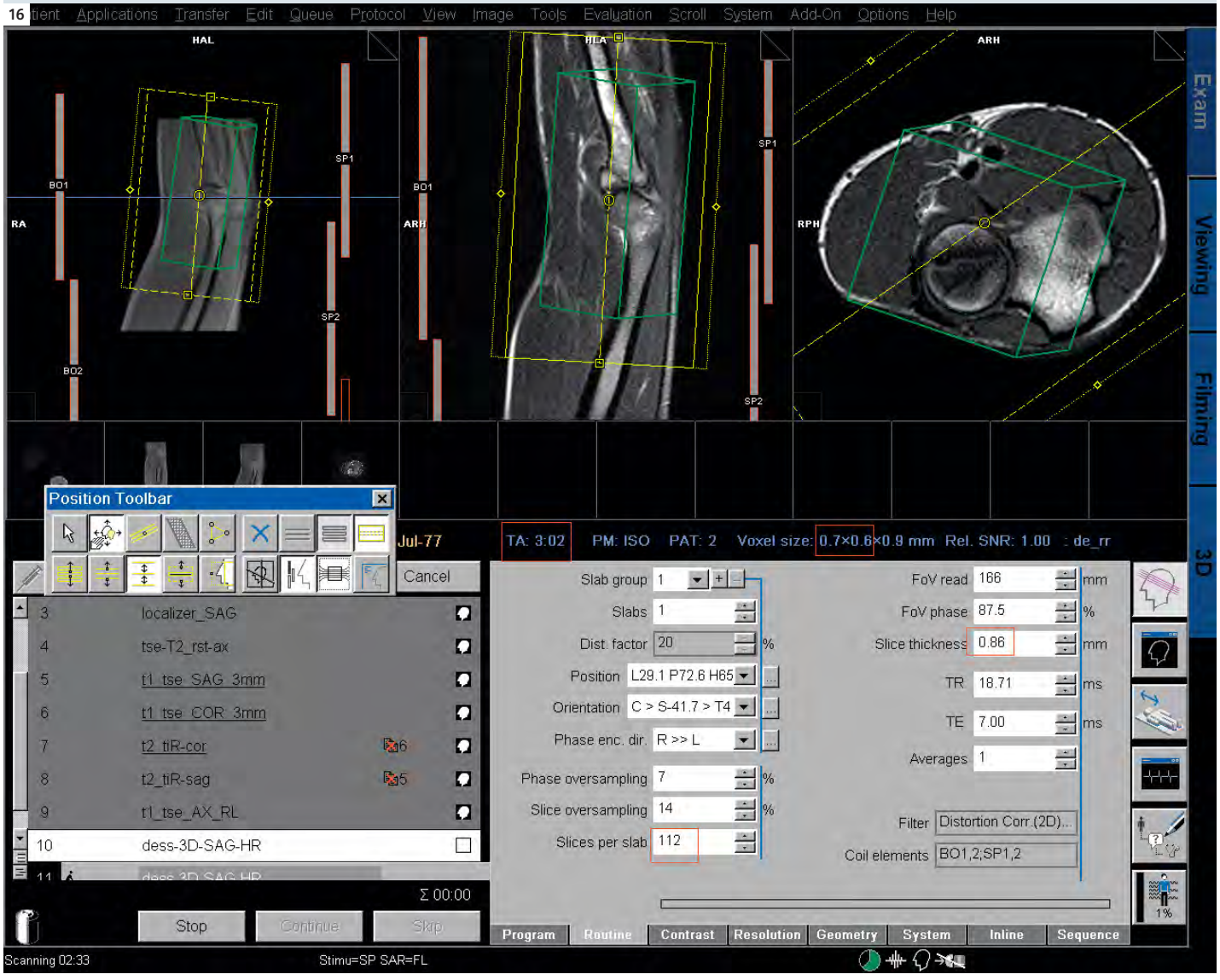

More throughput in the same time

Data acquired with Siemens' Utilization Management tool was used to determine the change in productivity after a Tim upgrade. The upgrade was done at X-Leme Clinic in Brazil (Dr. Heraldo Mello Neto) in November 2006, where a MAGNETOM Symphony with Quantum gradient system had been used since 2001 to offer a complete range of MR examinations. With the MAGNETOM Symphony, A Tim System, productivity increased on average by nearly 40% (comparing the two months prior to the upgrade with the four months following it). Less scan time, more patients, and a fast return on investment. More patients per month in the same number of working hours.

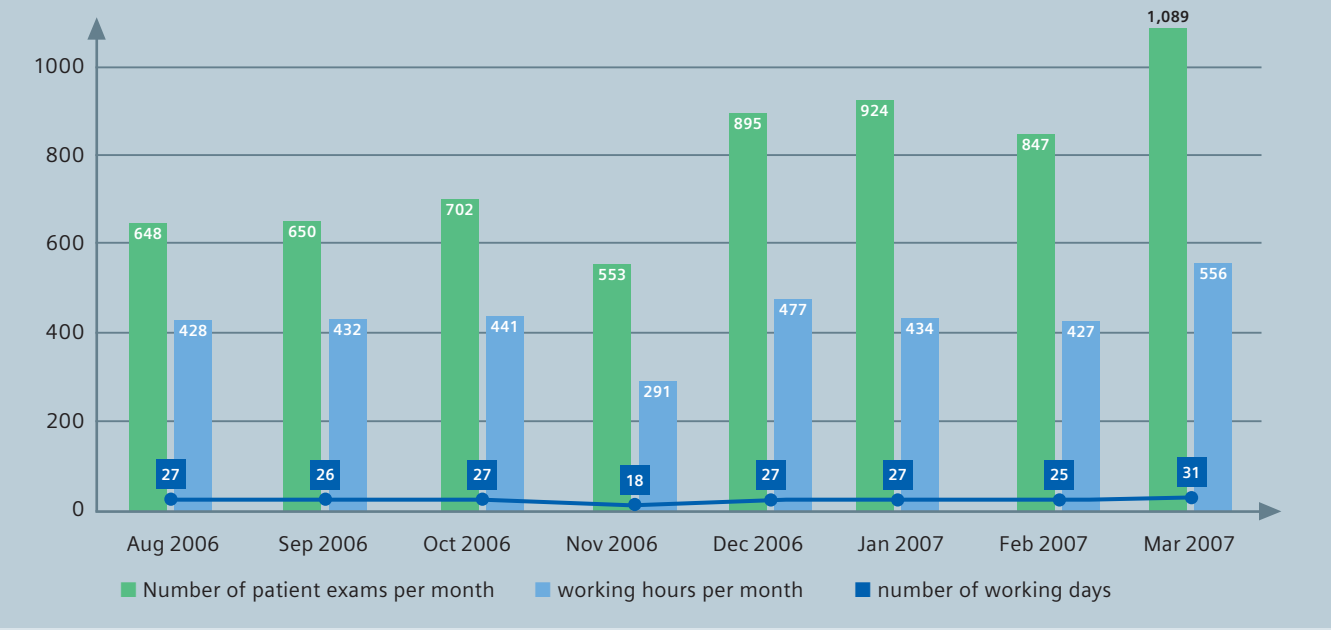

Faster scan times mean more patients per day

The productivity improvement can also be seen in the figure below. Due to faster scan times, study durations are significantly shorter and the number of patients per day increased in practically the same number of working hours: For example, between September 2006 and January 2007, the average study duration decreased by nearly 8 minutes (-25%) with the same or even better image quality, thus the average number of patients per day increased significantly (from 25 in September to 34.1 in January 2007). The majority of this improvement was due to faster average scan time per patient.

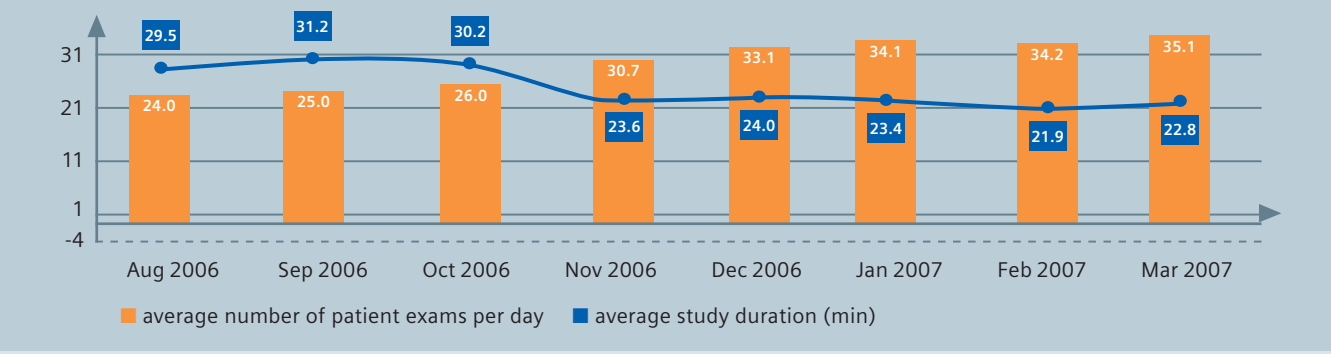

Dr. Heraldo Mello Neto
X-Leme Clinic, Brazil

"... after the Tim Upgrade we reduced scan times from 30 minutes to 20 minutes ...."

"Although Tim stands for Total imaging matrix, after experiencing the MAGNETOM Symphony with Tim myself I have decided that Tim stands for Total improvement."

Dr. Johan Dehem
VZW Jan Yperman,
Belgium

7T Musculoskeletal (MSK) Imaging (initial results)

Prof. Siegfried Trattnig[1]; Dr. Oliver Bieri[2]; Prof. Klaus Scheffler[2]; Tallal Charles Mamisch[3]; Timothy Hughes[4]; Willi Horger[4]

[1]*Department of Radiology, Medical University Vienna, Austria*
[2]*MR Physics, University Basel, Switzerland*
[3]*Department of Orthopedic Surgery, University Bern, Switzerland*
[4]*Siemens Medical Solutions, Erlangen, Germany*

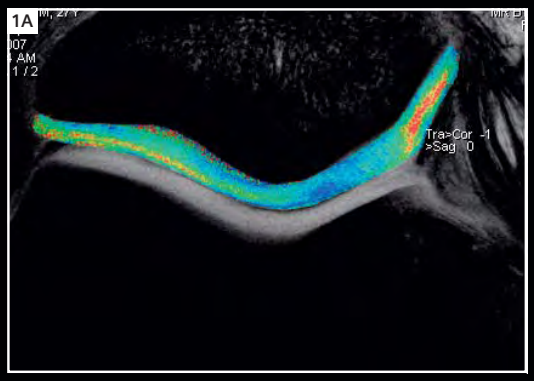

1 Ultra high resolution: MapIt 0.1 x 0.1 x 3 mm (A) From morphological to (B) biochemical imaging

2 Ultra high resolution: 0.1 x 0.1 x 3 mm (A) Cartilage surface (B) Cartilage ultra structure

3 Ultra high resolution: 0.2 x 0.2 x 1 mm

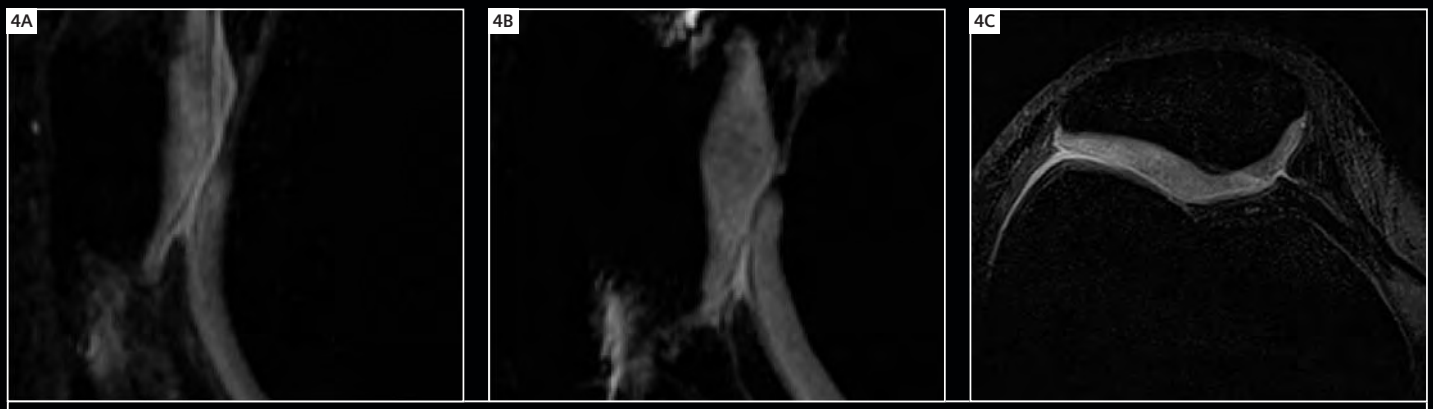

4 Ultra high resolution: Isotropic imaging using 3D, Isotropic 0.3 x 0.3 x 0.3 mm resolution

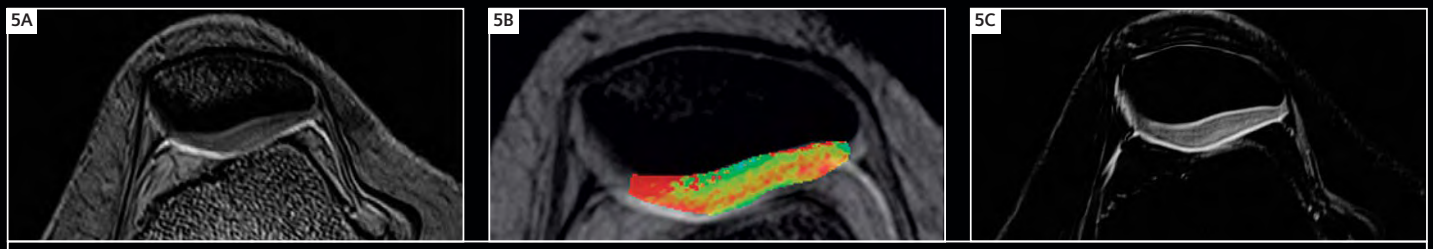

5 *syngo* MapIt: MTC and T2-weighted measurement, T2-map

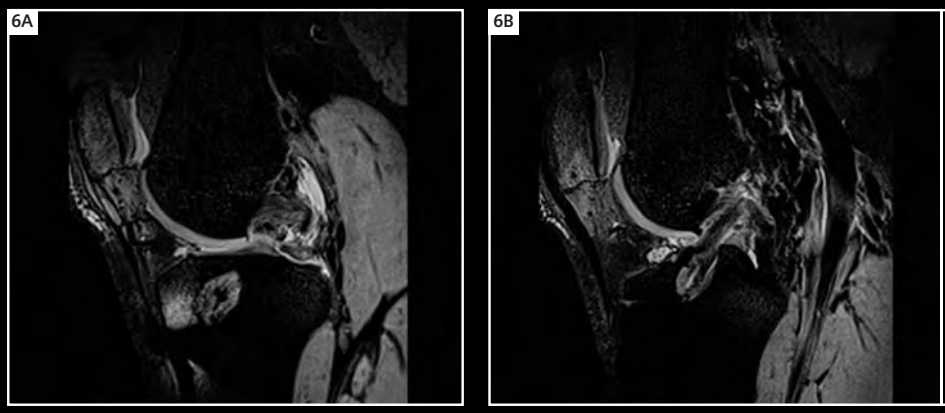

6 Robust imaging:
3D SPACE with metal implants.
Isotropic 0.64 x 0.64 x 0.64 mm resolution

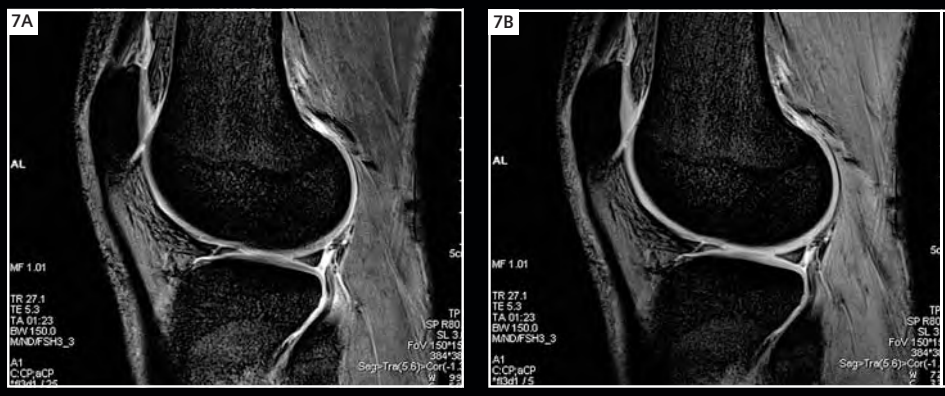

7 *syngo* MapIt: T1-weighted measurement using 3D VIBE (2 different flip angles)

The setting: Philadelphia, Pennsylvania, USA

Innovations ’07: Siemens Annual Education Symposium for Technologists and IT Customers

Rosemary Fisher, MR Clinical Education Development Specialist

Siemens Medical Solutions, Pleasanton, CA, USA

Nearly 1,200 customers met recently in Philadelphia, Pennsylvania, USA for Innovations ’07, Siemens Medical Solutions annual education symposium. Customers from across the US and other countries gathered to maximize their use of Siemens solutions, learn about new enhancements and technologies, meet with Siemens product experts, and share real-life experiences with their colleagues — perhaps one of the most valuable aspects of the program. General sessions and a multitude of breakout sessions included imaging modality sessions on Angiography, Computed Tomography (CT), Molecular Imaging (MI), Magnetic Resonance (MR), Radiography and Women’s Health alongside the IT topics.

The meeting opened with an uplifting General Session with Christopher Gardner whose story inspired the movie “The Pursuit of Happyness,” starring Will Smith. There were more than 250 education sessions in 29 tracks, and attendees were

A view overlooking the ballroom where breakfast and lunch were offered for the 1,200 attendees of Innovations '07.

given complimentary access to more than 1,300 online courses available from the Siemens Medical Academy in the e.Learning Center. Presented by Dr. Richard Carmona, the 17th Surgeon General of the United States, CEO of Canyon Ranch Health, and President of the Canyon Ranch Institute, the closing General Session, which highlighted the importance of disease prevention and health literacy, capped off a very successful educational symposium.

Attendees earned Category A continuing education credits from the American Society of Radiologic Technology (ASRT) for each modality session. The MR education program featured the following topics.

- Renal Disease, Gadolinium-based MR Contrast Agents and Nephrogenic Systemic Fibrosis (NSF) by Dr. Emanuel Kanal from the University of Pittsburgh
- Technical Considerations of Breast MR Imaging was given by Michael Coles from First Hill Diagnostic Imaging in Seattle, WA
- A Comparison of Cardiac CT and Cardiac MR was presented by Dr. Ricardo Cury, the director of Clinical Cardiac MR at Massachusetts General Hospital and Harvard School of Medicine in Boston, MA
- Positioning and Imaging Tips – Going the Extra Mile by Candi Roth of Imaging Education Associates
- The Effects of Tim (Total imaging matrix) and Parallel Imaging in Clinical Practice offered insights and real-life experience from Dr. Ulrich Rassner of the University of Utah Health Care in Salt Lake City, UT
- Protocol Optimization at 3T, also presented by Dr. Ulrich Rassner
- The Future of MR•PET by Nealie Hartman, MR Clinical Marketing from Siemens Medical Solutions USA

Feedback from this year's attendees indicates that, once again, Innovations '07 was a successful conference – due, in large part, to the participation of customers like you.

Innovations '08 is scheduled for July 28–31 at the Mandalay Bay Resort in Las Vegas, Nevada. Plan ahead to take advantage of this opportunity to learn about the solutions and applications that can be used to improve your daily clinical practice, and network with colleagues and Siemens experts. See you in Las Vegas!

Visit us at www.siemens.com/magnetom-world to see some of the presentations held at Philadelphia.

“ars intrinsica” – MR images in another setting

63-year-old Günter Kohout in front of the whole-body MR images that depict the former bodybuilder.

St. Florian monastary near Linz in Austria.

On August 3, 2007, the "ars intrinsica" exhibition opened for 2 months in St. Florian outside Linz in Austria. Professor Franz Fellner, head of radiology at the AKH Linz, provided the public with a new setting for MR and CT images in the baroque staircase of the Augustinian Abbey of the monastery. Different images from inside the human body or lifeless objects were digitally post-processed with programs such as 3D Neuro, Volume Rendering, and Image Fusion. Structures were emphasized in color and presented as an artistic whole. The works were reproduced in large format as well as excellent quality. Two of the creations were produced in cooperation with the contemporary Austrian painter, Anatole Ak.

The pre-opening was held in the baroque marble gallery of the monastery. The welcoming speech was held by F. Reisinger, the Dean of the monastery, and C. Dolezal, the vice mayor of the City of Linz, with an introduction by Professor Fellner.

The main speech that evening was given by Professor W. Seipl, the Director of the Museum of Art History in Vienna. In his presentation, he connected the antique understanding of anatomy to Renaissance depictions, and continued with painters of the Netherlands up to the possibilities of diagnostic imaging with X-ray images, CT and MR. Ars Intrinsica – a new look inside the human body.

Because the event was such a success, the exhibition has been moved to the Musikschule Linz (music school). Here, visitors can experience first hand how computed tomography (CT) and magnetic resonance imaging (MRI) systems not only deliver vital medical information, but also broaden the scope of creativity in modern art.

Siemens Medical Solutions – Customer Magazines

Our customer magazine family offers the latest information and background for every healthcare field. From the hospital director to the radiological assistant – here, one can quickly find information relevant to their needs.

Medical Solutions
Innovation and trends in healthcare. The magazine, published three times a year, is designed especially for members of the hospital management, administration personnel, and heads of medical departments.

AXIOM Innovations
Everything from the worlds of interventional radiology, cardiology, fluoroscopy, and radiography. This semi-annual magazine is primarily designed for physicians, physicists, researchers and medical technical personnel.

MAGNETOM Flash
Everything from the world of magnetic resonance imaging. The magazine presents case reports, technology and product news and "How I do it" sections. It is primarily designed for physicians, physicists, and medical technical personnel.

SOMATOM Sessions
Everything from the world of computed tomography. With its innovations, clinical appli-cations, and visions, this semi-annual magazine is primarily designed for physicians, physicists, researchers, and medical technical personnel.

For details and to order the magazines please visit us at **www.siemens.com/medical-magazine**

Listen – Discuss – Share
6th MAGNETOM World Summit

May 29 – June 1, 2008
in Munich, Germany

We invite you to join our community of Siemens MR users worldwide to the 6th MAGNETOM World Summit in Munich, Germany.
The positive feedback from 5 previous events is proof that the meeting is an ideal opportunity to meet other members of the MAGNETOM World, to develop contacts and to exchange valuable information.

We look forward to seeing you there!

Please don't forget to register:

www.siemens.com/magnetom-world

MAGNETOM Flash – Imprint
© 2008 by Siemens AG, Berlin and Munich,
All Rights Reserved

Publisher:
Siemens AG
Medical Solutions
Business Unit Magnetic Resonance,
Karl-Schall-Straße 6, D-91052 Erlangen,
Germany

Editor in Chief: A. Nejat Bengi, M.D.

Associate Editior: Antje Hellwich
(antje.hellwich@siemens.com)

Editorial Board: Dagmar Thomsik-Schröpfer, Ph.D.; Cécile Mohr, Ph.D.; Heike Weh; Bernhard Baden; Peter Kreisler, Ph.D.; Milind Dhamankar, M.D.; Kathleen Giannini; Gary R. McNeal; Sunil Kumar S.L., M.D.

Production: Norbert Moser, Siemens AG, Medical Solutions

Layout: independent Medien-Design
Widenmayerstrasse 16, D-80538 Munich

Printers: Farbendruck Hofmann, Gewerbestraße 5, D-90579 Langenzenn, Printed in Germany

MAGNETOM Flash is also available on the internet:
www.siemens.com/magnetom-world

Note in accordance with § 33 Para.1 of the German Federal Data Protection Law: Despatch is made using an address file which is maintained with the aid of an automated data processing system.
MAGNETOM Flash with a total circulation of 25,000 copies is sent free of charge to Siemens MR customers, qualified physicians, technologists, physicists and radiology departments throughout the world. It includes reports in the English language on magnetic resonance: diagnostic and therapeutic methods and their application as well as results and experience gained with corresponding systems and solutions. It introduces from case to case new principles and procedures and discusses their clinical potential.
The statements and views of the authors in the individual contributions do not necessarily reflect the opinion of the publisher.
The information presented in these articles and case reports is for illustration only and is not intended to be relied upon by the reader for instruction as to the practice of medicine. Any health care practitioner reading this information is reminded that they must use their own learning, training and expertise in dealing with their individual patients. This material does not substitute for that duty and is not intended by Siemens Medical Solutions to be used for any purpose in that regard. The drugs and doses mentioned herein are consistent with the approval labeling for uses and/or indications of the drug. The treating physician bears the sole responsibility for the diagnosis and treatment of patients, including drugs and doses prescribed in connection with such use. The Operating Instructions must always be strictly followed when operating the MR system. The sources for the technical data are the corresponding data sheets. Results may vary.
Partial reproduction in printed form of individual contributions is permitted, provided the customary bibliographical data such as author's name and title of the contribution as well as year, issue number and pages of MAGNETOM Flash are named, but the editors request that two copies be sent to them. The written consent of the authors and publisher is required for the complete reprinting of an article.
We welcome your questions and comments about the editorial content of MAGNETOM Flash. Please contact us at magnetomworld.med@siemens.com. Manuscripts as well as suggestions, proposals and information are always welcome; they are carefully examined and submitted to the editorial board for attention. MAGNETOM Flash is not responsible for loss, damage, or any other injury to unsolicited manuscripts or other materials. We reserve the right to edit for clarity, accuracy, and space. Include your name, address, and phone number and send to the editors, address above.

Subscription

Please enter your business address

Institution

Department

Title

Name

Street

Postal Code

City

State

Country

MR System used

Please include me in your mailing list for the following Siemens Healthcare customer magazine(s):

- ☐ Medical Solutions
- ☐ MAGNETOM Flash
- ☐ SOMATOM Sessions
- ☐ AXIOM Innovations

Stay up to date with the latest information Register for:

- ☐ the e-Newsletter

E-mail

- ☐ Yes, I consent to the above information being used for future contact regarding product updates and other important news from Siemens.
- ☐ unsubscribe from info service

Please print clearly!

SUBSCRIBE NOW!

– and get your free copy of future MAGNETOM Flash! Interesting information from the world of magnetic resonance – gratis to your desk. Send us this postcard, or subscribe online at **www.siemens.com/MAGNETOM-World**

MAGNETOM Flash

Siemens AG
Medical Solutions
Magnetic Resonance
Antje Hellwich – Marketing
P.O. Box 32 60
D-91050 Erlangen
Germany

© 04.2008, Siemens AG
Order No.
A91MR-1000-46C-7600
Printed in Germany
CC MR 01000 ZS 040815.

www.siemens.com/healthcare-magazine

On account of certain regional limitations of sales rights and service availability, we cannot guarantee that all products included in this brochure are available through the Siemens sales organization worldwide. Availability and packaging may vary by country and is subject to change without prior notice. Some/All of the features and products described herein may not be available in the United States.

The information in this document contains general technical descriptions of specifications and options as well as standard and optional features which do not always have to be present in individual cases.

Siemens reserves the right to modify the design, packaging, specifications and options described herein without prior notice.
Please contact your local Siemens sales representative for the most current information.

Note: Any technical data contained in this document may vary within defined tolerances. Original images always lose a certain amount of detail when reproduced.

Siemens AG
Wittelsbacherplatz 2
80333 Muenchen
Germany

Headquarters

Siemens AG, Medical Solutions
Magnetic Resonance
Henkestr. 127
91052 Erlangen
Telephone: +49 9131 84-0

Contact Addresses

Asia/Pacific:
Siemens Medical Solutions
Asia Pacific Headquarters
The Siemens Center
60 MacPherson Road
Singapore 348615
Telephone: +65 9622-2026

Canada:
Siemens Canada Limited
Medical Solutions
2185 Derry Road West
Mississauga ON L5N 7A6
Canada
Telephone: +1 905 819-5800

Europe/Africa/Middle East:
Siemens AG, Medical Solutions
Henkestr. 127,
91052 Erlangen
Germany
Telephone: +49 9131 84-0

Japan:
Siemens-Asahi
Medical Technologies Ltd.
Takanawa Park Tower 14 F
20-14, Higashi-Gotanda 3-chome
Shinagawa-ku
Tokyo 141-8644
Japan
Telephone: +81 35 42 38 489

Latin America:
Siemens S.A., Medical Solutions
Avenida de Pte. Julio A. Roca No 516, Piso 7
C1067ABN Buenos Aires
Argentina
Telephone: +54 11 4340 8400

USA:
Siemens Medical Solutions U.S.A., Inc.
51 Valley Stream Parkway
Malvern, PA 19355-1406
USA
Telephone: +1-888-826-9702